

Safety Analysis Report DN30 Package

0023-BSH-2016-002-Rev1


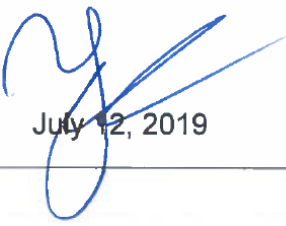
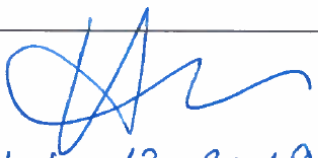
Prepared	Checked	Released
M. Hennebach	Y. van Wijk	F. Hilbert
 July 11, 2019	 July 12, 2019	 July 12, 2019

TABLE OF CONTENTS

Table of Contents	2
List of Revisions.....	6
List of Abbreviations.....	9
List of Tables	10
List of Figures.....	13
Literature.....	19
PART 1	21
1.0 Preface	22
1.1 List and status of documents pertaining to this SAR	22
1.2 Administrative Information	23
1.2.1 Name of Package.....	23
1.2.2 Identification of Package Designer	23
1.2.3 Type of Package Design	23
1.2.4 Criticality Safety Index.....	23
1.2.5 Package Design Identification and Restrictions.....	23
1.2.6 Modes of Transport for which the Package is Designed	24
1.2.7 Lowest Transport Temperature for which the Package is Designed	24
1.2.8 Maximum normal Operating Pressure	24
1.2.9 Reference to Applicable Regulations and Standards	24
1.3 Specification of the Radioactive Contents	26
1.3.1 General Specification	26
1.3.1.1 Permissible mass of UF_6	26
1.3.1.2 Purity of UF_6	26
1.3.1.3 Permissible conditions for repeated use	26
1.3.1.4 Non-fissile and fissile material.....	26
1.3.1.5 Total radioactivity	26
1.3.1.6 Definition of the permissible contents	27
1.3.2 Physical and chemical state.....	28
1.3.3 Special form or low dispersible radioactive material	28
1.3.4 Nature and characteristics of the radiation emitted	28
1.3.5 Limitation of the heat generation rate of the content	29
1.3.6 Mass of fissile material and nuclides	29
1.3.7 Other dangerous properties	29
1.3.8 Contents not permitted.....	29
1.4 Specification of the packaging.....	30
1.4.1 List of all packaging components and complete design drawings	30
1.4.1.1 30B cylinder	31
1.4.1.2 DN30 PSP.....	33
1.4.2 Description of the DN30 packaging	38
1.4.2.1 30B cylinder	38
1.4.2.2 DN30 PSP.....	38
1.4.2.3 Design safety features of the DN30 packaging	40
1.4.2.4 Handling features of the DN30 packaging	41
1.4.2.5 Tie-down features of the DN30 packaging.....	44
1.4.3 The components of the packaging relevant for the containment system	46

1.4.4	The components of the packaging relevant for shielding	46
1.4.5	The components of the packaging relevant for the confinement system	46
1.4.6	The components of the packaging relevant for thermal protection	46
1.4.7	The components of the packaging relevant for heat dissipation	46
1.4.8	The protection against corrosion	47
1.4.9	The protection against contamination	47
1.4.10	The shock absorbing components of the packaging	47
1.4.11	The transport concept	47
1.5	Package performance characteristics	48
1.5.1	Main design principles	48
1.5.2	Performance characteristics	48
1.5.2.1	<i>Performance characteristics under RCT</i>	48
1.5.2.2	<i>Performance characteristics under NCT</i>	48
1.5.2.3	<i>Performance characteristics under HAC</i>	48
1.5.3	Assumptions used for the safety analysis	49
1.5.3.1	<i>Containment function</i>	49
1.5.3.2	<i>Dose rates</i>	49
1.5.3.3	<i>Criticality safety</i>	49
1.6	Compliance with regulatory requirements	50
1.6.1	Definitions, general provisions, activity limits and classification	50
1.6.2	Requirements and controls for transport	51
1.6.3	General requirements for all packagings and packages	52
1.6.4	Requirements for packages containing uranium hexafluoride	53
1.6.5	Requirements for type A packages	54
1.6.6	Requirements for type B packages (relevant for thermal and containment analysis)	55
1.6.7	Requirements for packages containing fissile material	56
1.6.8	Test procedures	58
1.7	Operation	60
1.7.1	Testing requirements and controls before first use	60
1.7.2	Testing requirements and controls before each transport	60
1.7.2.1	<i>Inspection of the 30B cylinder</i>	60
1.7.2.2	<i>Inspection of the DN30 PSP</i>	61
1.7.3	Handling and tie down requirements	62
1.7.4	Loading procedures for the 30B cylinder and the DN30 PSP	62
1.7.4.1	<i>Loading and unloading of UF₆ content into the 30B cylinder</i>	62
1.7.4.2	<i>Loading of the 30B cylinder into the DN30 PSP</i>	63
1.7.4.3	<i>Unloading of the 30B cylinder from the DN30 PSP</i>	63
1.7.5	Supplementary equipment and operational controls	63
1.7.6	Precautions and measures due to the other dangerous properties of the content	64
1.8	Inspection	65
1.8.1	Annual Inspection requirements for the DN30 PSP	65
1.8.2	5-year inspection requirements for the 30B cylinder and the DN30 PSP	65
1.9	Management system	67
1.9.1	Design, SAR, documentation and records	67
1.9.1.1	<i>General</i>	67
1.9.1.2	<i>Design</i>	67
1.9.1.3	<i>Documents and Records</i>	68
1.9.2	Manufacturing and testing	68
1.9.2.1	<i>Manufacturing of 30B cylinders</i>	68
1.9.2.2	<i>Manufacturing of serial DN30 PSPs</i>	68
1.9.2.3	<i>Testing of samples and prototypes</i>	68
1.9.3	Operation	69
1.9.4	Maintenance and repair	69
1.9.5	Compliance of any activity with the SAR	70
1.9.6	Deviations	70

1.9.7	Safety elements	70
1.10	Package illustration	72
PART 2	74
2.1	Common provisions for all technical analyses	75
2.1.1	Package design.....	75
2.1.1.1	Content.....	75
2.1.1.2	30B cylinder	76
2.1.1.3	DN30 PSP.....	76
2.1.1.4	Summary of the material characteristics used for the technical analyses	77
2.1.2	Acceptance criteria and design assumptions.....	79
2.1.2.1	Mechanical design	79
2.1.2.2	Thermal design	80
2.1.2.3	Containment system design.....	80
2.1.2.4	External dose rate assessment.....	80
2.1.2.5	Criticality safety assessment.....	80
2.1.3	Description and justification of analysis methods	81
2.1.3.1	Structural analysis.....	81
2.1.3.2	Thermal analysis	83
2.1.3.3	Containment design analysis	85
2.1.3.4	External dose rate analysis	89
2.1.3.5	Criticality safety analysis	90
2.1.4	Results of physical testing of specimens and prototypes	90
2.1.4.1	Overview of the physical tests.....	90
2.1.4.2	Deviations between prototype and series	91
2.2	Technical analyses.....	101
2.2.1	Structural analysis.....	101
2.2.1.1	Basic assumptions for the calculations	101
2.2.1.2	Handling	112
2.2.1.3	Ability to withstand RCT	132
2.2.1.4	Ability to withstand NCT	143
2.2.1.5	Ability to withstand HAC.....	148
2.2.1.6	Analysis of stresses caused by temperature influences	228
2.2.2	Thermal analysis	230
2.2.2.1	Objective of verification	230
2.2.2.2	Results of the thermal tests of specimens and prototypes	238
2.2.2.3	Results of the thermal analysis	251
2.2.2.4	Proof for the package DN30 to meet the requirements of [10CFR71].....	268
2.2.2.5	Summary.....	269
2.2.3	Containment design analysis	270
2.2.3.1	Objective of verification	270
2.2.3.2	Calculation method	270
2.2.3.3	Package data used for the analysis	271
2.2.3.4	Radioactive inventory, releasable radioactive inventory and activity concentration in the cavity atmosphere	271
2.2.3.5	Permissible standard Helium leakage rates.....	271
2.2.3.6	Measured standard Helium leakage rates after the regulatory tests	272
2.2.3.7	Summary and evaluation of results.....	272
2.2.4	External dose rates analysis	273
2.2.4.1	Objective of verification	273
2.2.4.2	Assumptions for the calculations	274
2.2.4.3	Calculation method, its verification and validation	275
2.2.4.4	Gamma and neutron source terms	275
2.2.4.5	Model Specification	278
2.2.4.6	Dose rate profiles	279
2.2.4.7	Verification of compliance with the dose rate limits	281
2.2.4.8	Summary and evaluation of results.....	284

2.2.5	Criticality safety analysis	285
2.2.5.1	Objective of verification	285
2.2.5.2	Assumptions for the proof of criticality safety.....	285
2.2.5.3	Calculation method, verification and validation.....	287
2.2.5.4	Model Specification	288
2.2.5.5	Proof of criticality safety	290
Appendix 1.1 (List of Applicable Documents)		299
Appendix 1.3 (Radioactivity).....		300
Appendix 1.4.1 (Drawings).....		301
Appendix 1.4.2 (Material Data PIR Foam)		302
Appendix 1.4.3 (Material Data Intumescent Material).....		303
Appendix 1.4.4 (Material Data Microtherm Overstitched 1000R HY).....		304
Appendix 1.4.5 (Absence of Halogen in Intumescent Material).....		305
Appendix 1.7.1 (Handling Instruction)		306
Appendix 1.7.2 (Contamination and Dose Rate Measurements).....		307
Appendix 1.8.1 (Periodical Inspections)		308
Appendix 1.8.2 (Inspection Criteria).....		309
Appendix 1.9.1 (IMS)		310
Appendix 1.9.2 (Manufacturing Specification)		311
Appendix 1.9.3 (Quality Assurance Program)		312
Appendix 2.2.1.1 (Drop Test Program).....		313
Appendix 2.2.1.2 (Drop Test Reports).....		314
Appendix 2.2.1.3 (Structural Analysis of the DN30 Package under NCT and HAC).....		315
Appendix 2.2.2.1 (Thermal Test Program)		316
Appendix 2.2.2.2 (Thermal Test Report)		317
Appendix 2.2.2.3 (Thermal Analysis)		318
Appendix 2.2.3.1 (Containment Analysis).....		319
Appendix 2.2.3.2 (Uranium Hexafluoride DEWITT 1960).....		320
Appendix 2.2.4 (Dose Rate Analysis).....		321
Appendix 2.2.5 (Criticality Safety Analysis)		322

LIST OF REVISIONS

Revision	Date of revision	Modifications
0	08.02.2018	Original
1	29.03.2019	<p>Content changes from Rev. 0 are given below for each report section. For modifications due to NRC Requests for Additional Information (RAIs), the number of the RAI is indicated. All content changes are marked by a line on the right of the page.</p> <p>Throughout the report, U.S. codes and standards have been provided in addition to international standards (RAI 1.3).</p>

SAR section	Modifications in Rev. 1
1.0	Complete revision; updated information on French license and more detailed explanation of compliance with the US Code of Federal Regulations. (RAI 1.3)
1.2.9	Reordered references, stronger emphasis on [10CFR71] and [49CFR173]. (RAI 1.3)
1.4.1.1	Clarification on applicable standards for 30B cylinders. Table 5: Additional material specification for the plug (hex or socket head)
1.4.1.2	Addition of list of main drawings Inclusion of substitute materials in Table 6 (RAI 1.2)
1.4.2.1	Clarification on applicable standards for 30B cylinders.
1.4.2.2	Table 11: Additional data for maximum gross weight
1.4.2.3	New subsection 1.4.2.3.1 (Pressure envelope of the DN30 package). Addition of thermal plugs in 1.4.2.3.3 (Thermal protection system)
1.4.2.5	Clarification for tie-down for higher accelerations added; removal of heels cylinders for tie-down using straps.
1.4.5	Addition of DN30 PSP steel shells to the confinement system (RAI 6.3).
1.5.3.3	Indication of the maximal amount of water ingress (RAI 6.2). Addition of DN30 PSP steel shells to the confinement system (RAI 6.3).
1.6.3	Indication of minimum safety factor of three against yielding (RAI 2.3)
1.6.5	More detailed demonstration of compliance with tie-down requirements (RAI 2.6)
1.6.6	New subsection: Type B requirements applicable due to fissile content
1.6.7	Indication of the maximal amount of water ingress (RAI 6.2).
1.7.2	Complete revision; thorough explanation of testing requirements for both DN30 PSP and 30B cylinder (RAI 1.1)
1.7.4	Sections 1.7.4 and 1.7.5 from Rev. 0 have been merged; no content changes to the (new) subsections 1.7.4.2 and 1.7.4.3 (RAI 1.1).

SAR section	Modifications in Rev. 1
1.8	Complete revision; clarifications and addition of 5-year inspection requirements (periodical recertification) for 30B cylinders (RAI 1.1).
2.1.1	Additional information on UF ₆ surrogate material for structural analysis (RAI 2.1). DN30 PSP steel shells are taken into account in the criticality analysis (RAI 6.3).
2.1.2.1	Complete revision; detailed listing of acceptance criteria for the mechanical design (RAIs 2.3 and 2.6), evaluation of material failure in the FEM model (RAI 2.15).
2.1.2.2	New admissible 30B cylinder temperature under HAC of 131 °C (RAI 3.6).
2.1.2.5	DN30 PSP steel shells are taken into account in the criticality analysis (RAI 6.3).
2.1.3.3	New section 2.1.3.3.1 on leakage tests results and methodology (RAI 4.2).
2.1.4.2.6.2	New admissible 30B cylinder temperature under HAC of 131 °C (RAI 3.6).
2.2.1.1.1.2	Table 18: Updated values for accelerations.
2.2.1.1.2	Complete revision; detailed explanation for substitute materials and addition of applicable US standards (RAI 1.2).
2.2.1.2.3	Revised analysis for the lifting lugs (RAI 2.3) and the forklift pockets.
2.2.1.3	Complete revision; updated analysis with accelerations from 10 CFR 71 (RAI 2.6), fatigue analysis for all tie-down features.
2.2.1.4.3	Complete revision; detailed analysis of compression test (RAI 2.13).
2.2.1.5.1	Replacement of qualitative descriptions with quantitative information in several instances throughout this section (RAI 2.16).
2.2.1.5.3.1	Revision with clear references to the internal pressure analysis (RAI 3.10).
2.2.1.6	New section with analysis of thermal stresses (RAIs 2.11 and 3.5).
2.2.2.1	Removal of verification for type B(U) packages. Complete revision of subsection 2.2.2.1.4 on admissible temperatures (RAI 3.6).
2.2.2.2.1.4	Updated to improve clarity and comprehensibility (RAI 3.1).
2.2.2.3.2.4	Total radiation coefficient of 0.9 for the fire phase (RAI 3.2). Justification of the pool fire gas velocity (RAI 3.4). New Table 60 with convective heat transfer coefficients (RAI 3.3).
2.2.2.3.3	Replacement of qualitative descriptions with quantitative information in two instances in this section (RAI 2.16).
2.2.2.3.4.2	Complete revision; additional calculation results for partially filled and empty 30B cylinders (RAI 3.8)
2.2.2.3.5	Recalculated temperatures with a total radiation coefficient of 0.9 (RAI 3.2). New subsection 2.2.2.3.5.2 for pressure build-up under HAC (RAI 3.10).

SAR section	Modifications in Rev. 1
2.2.2.4.2	Complete revision; new summary of pressure build-up calculations with references to subsections 2.2.2.1.4 and 2.2.2.3.5.2 (RAI 3.10).
2.2.5.1	Updated calculational bias, reference to the new technical report with additional validation calculations (RAI 6.3).
2.2.5.2.2	Additional explanation of the amount of water ingress (RAI 6.2).
2.2.5.3.2	Updated calculational bias, reference to the new technical report with additional validation calculations (RAI 6.3).
2.2.5.5.3.4	Updated evaluation of the calculation result for bare 30B cylinders (RAI 6.3).
Appendices 1.7.1 1.8.1 1.8.2	Changed from proprietary to non-proprietary (RAI 7.1).

LIST OF ABBREVIATIONS

BAM	<i>German Federal Institute for Material Research and Testing</i>
CSI	<i>Criticality Safety Index</i>
FEM	<i>Finite Element Method</i>
HAC	<i>Hypothetical Accident Conditions</i>
IMS.....	<i>Integrated Management System</i>
MNOP	<i>Maximum Normal Operating Pressure</i>
MTSP	<i>Manufacturing and Test Sequence Plan</i>
NCT.....	<i>Normal Conditions of Transport</i>
PDSR	<i>Package Design Safety Report</i>
PSP.....	<i>Protective Structural Packaging</i>
RCT.....	<i>Routine Conditions of Transport</i>
SAR.....	<i>Safety Analysis Report</i>

LIST OF TABLES

Table 1:	Content of enriched commercial grade UF ₆ complying with [ASTM C996] ¹⁾²⁾	27
Table 2:	UF ₆ properties (extract from [USEC 651])	28
Table 3:	Heat generation rate of 2277 kg UF ₆ with the composition given in Table 1	29
Table 4:	Materials of the pressure envelope of the 30B cylinder (excerpt from [ANSI N14.1])	31
Table 5:	Materials of the valve and the plug of the 30B cylinder (excerpt from [ANSI N14.1])	32
Table 6:	Material specification of the DN30 PSP	33
Table 7:	Properties of RTS 120 and RTS 320 (according to the technical data sheets)	34
Table 8:	Properties of Promaseal®	35
Table 9:	Properties of MICROTHERM® OVERSTITCHED 1000R HY	35
Table 10:	Summary of the mechanical tests with PIR foam samples	35
Table 11:	Main data of the 30B cylinder	38
Table 12:	Main data of the DN30 PSP	39
Table 13:	Safety elements	71
Table 14:	Mechanical properties used for the static analyses	77
Table 15:	Thermal properties used for the analyses	78
Table 16:	Leak rates before and after each test	88
Table 17:	Load assumptions for handling	102
Table 18:	Load assumptions for RCT	103
Table 19:	Load assumptions for NCT	104
Table 20:	Load assumptions for HAC	105
Table 21:	Material data for plates of material No. 1.4301 (Type 304)	106
Table 22:	Material data for plates of material No. 1.4307 (Type 304L)	107
Table 23:	Material data for plates of material No. 1.4541 (Type 321)	108
Table 24:	Material data for shapes of material No. 1.4541 (Type 321)	109
Table 25:	Material data for shapes of material No. 1.4571 (Type 316Ti)	110
Table 26:	Material data for bars of material No. 1.4542 (Type 630)	110
Table 27:	Material data for plates of material No. 1.4462 (Type 2205)	111
Table 28:	Nominal stresses in the lifting lugs at the feet	114
Table 29:	Stress amplitudes in the lifting lugs at the feet	117
Table 30:	Material 1.4307 for the FEM analysis	119
Table 31:	Reaction forces obtained from the FEM analysis	121
Table 32:	Stress amplitudes in the left welding seam of the lifting lugs at the feet	123
Table 33:	Stress amplitudes in the lower welding seam of the lifting lugs at the feet	123
Table 34:	Settings for implicit LS-DYNA solver	145
Table 35:	Deviations of the FEM model from the design of the DN30 package and their justification	149

Table 36:	Mesh statistics.....	151
Table 37:	Deformation and remaining dimensions calculated for the drop onto the valve corner	159
Table 38:	Deformations and remaining dimensions measured for the drop onto the valve corner in sequence 1 and sequence 7	170
Table 39:	Deformations and remaining dimensions measured for the drop onto the valve corner (ambient temperature) and comparison with calculated values at RT	171
Table 40:	Deformations and remaining dimensions calculated for the drop onto the plug corner	175
Table 41:	Deformations and remaining dimensions measured for the drop onto the plug corner (ambient temperature) and comparison to calculated values	180
Table 42:	Deformation and remaining dimensions calculated for the flat drop onto the valve side.....	184
Table 43:	Deformations and remaining dimensions measured for the flat drop onto the valve side (ambient temperature) and comparison with calculated values	191
Table 44:	Measured impressions for the flat drop onto the closure system at RT and comparison to calculated values	199
Table 45:	Deformations and remaining dimensions calculated for the flat drop onto the top	204
Table 46:	Measured distances (penetrations) for the slap-down at RT and comparison to calculated values	213
Table 47:	Material specification of the closure device	220
Table 48:	Convergence study	221
Table 49:	Vapor pressure of UF ₆ extracted from [WITT 1960].....	231
Table 50:	Required wall thickness for the cylinder for internal pressure	234
Table 51:	Required wall thickness for the dished heads for internal pressure	235
Table 52:	Admissible component temperatures of the package DN30	237
Table 53:	Temperatures at the 30B cylinder at the end of the fire (Benchmark 1) ...	246
Table 54:	Temperatures at the 30B cylinder at the end of the fire (Benchmark 2) ...	246
Table 55:	Maximal temperatures at the 30B cylinder in the thermal test (Benchmark 1).....	250
Table 56:	Maximal temperatures at the 30B cylinder in the thermal test (Benchmark 2).....	250
Table 57:	Factors used for the calculation of the heat generation of the foam.....	253
Table 58:	Solar insolation data	254
Table 59:	Ambient temperature	254
Table 60:	Heat transfer by radiation at the surface of the DN30 package.....	254
Table 61:	Heat transfer coefficients for the convective heat transfer	255
Table 62:	Comparison of measured and calculated maximum temperatures during the test with the prototype of the DN30 package – Benchmark 1	258

Table 63:	Comparison of measured and calculated maximum temperatures during the test with the prototype of the DN30 package – Benchmark 2.....	264
Table 64:	Temperatures at the DN30 package loaded with an empty, a partially filled and a filled 30B cylinder under RCT and NCT	266
Table 65:	Maximum temperatures at the DN30 package loaded with an empty, partially filled and filled 30B cylinder.....	267
Table 66:	Package data used for the containment design analysis under NCT	271
Table 67:	Radioactive inventory, releasable radioactive inventory and activity concentration in the cavity atmosphere	271
Table 68:	Permissible standard Helium leakage rates	271
Table 69:	Measured standard Helium leakage rates after the regulatory tests for HAC	272
Table 70:	Nuclides and associated daughter nuclides considered for the determination of the source intensities.....	276
Table 71:	Maximal dose rates at 1 m distance from the external surface of the DN30 package under RCT loaded with a 30B cylinder containing UF₆.....	281
Table 72:	Maximal total dose rates at the surface of the DN30 package loaded with a 30B cylinder containing UF₆ or heels of UF₆	281
Table 73:	Maximal total dose rates at the external surface of a vehicle loaded with DN30 packages loaded each with 30B cylinders containing UF₆ or heels of UF₆.....	282
Table 74:	Maximal total dose rates at 2 m distance from the external surface of a vehicle loaded with DN30 packages loaded each with 30B cylinders containing UF₆ or heels of UF₆	282
Table 75:	Composition of the polyisocyanurate rigid foam.....	290

LIST OF FIGURES

Figure 1:	Lifting of the DN30 package by using the 4 lifting lugs	42
Figure 2:	Lifting of the DN30 package by using a forklift	43
Figure 3:	Lifting of the empty DN30 PSP by using slings	43
Figure 4:	Lifting of the top half of the DN30 packaging.....	44
Figure 5:	General tie-down method for the DN30 package / DN30 PSP	45
Figure 6:	Tie-down of the DN30 PSP without a cylinder using straps.....	45
Figure 7:	DN30 PSP overview.....	72
Figure 8:	DN30 PSP bottom half.....	73
Figure 9:	Example of dummy 30B cylinder used during the drop and fire test for testing the leakage rate: a) outside, valve side (upside down), b) inside, valve side (empty), c) inside valve side (filled with concrete)	86
Figure 10:	Pump creating a vacuum inside the 30B cylinder.....	86
Figure 11:	Leak detector unit	87
Figure 12:	Helium cage around the cylinder	88
Figure 13:	Rotation preventing device: a) DN30 PSP prototype b) DN30 PSP.....	93
Figure 14:	Reinforcement plate: a) DN30 PSP prototype b) DN30 PSP	94
Figure 15:	Forces in the handling means of the loaded DN30 package when lifted using the lifting lugs	114
Figure 16:	Geometry of the lifting lug for calculation.....	115
Figure 17:	Geometry of the lifting lug for the FEM analysis.....	118
Figure 18:	Mesh of the lifting lug used for the FEM analysis.....	120
Figure 19:	Boundary conditions for the FEM analysis	121
Figure 20:	Forces in the handling means when lifting the top half.....	126
Figure 21:	Geometry of the lifting lug for calculation of the handling of the top half.....	126
Figure 22:	Mechanical model for the welding seams between the feet and the outer shell.....	134
Figure 23:	Axial accelerations during RCT.....	137
Figure 24:	Lateral accelerations during RCT.....	137
Figure 25:	Calculation model of the foot of the DN30 PSP.....	138
Figure 26:	FEM model of the DN30 package for the compression test	146
Figure 27:	Compression test – Results of the von Mises stress	146
Figure 28:	Compression test – Results of the effective plastic strain.....	147
Figure 29:	Mesh of the DN30 package, outer shell and feet.....	152
Figure 30:	Mesh of the DN30 package, foam parts	153
Figure 31:	Mesh of the DN30 package, inner shells.....	153
Figure 32:	Mesh of the 30B cylinder	154
Figure 33:	Mesh of the DN30 package, content of the 30B cylinder.....	154
Figure 34:	Material properties of PIR foam RTS 120 used for the FEM-model.....	155
Figure 35:	Material properties of PIR foam RTS 320 used for the FEM-model.....	156
Figure 36:	Material properties of stainless steel No. 1.4307 / 1.4301 used for the FE-model	157
Figure 37:	Measured distances in sequence 1	161

Figure 38: Deformed structure after the 1.2 m free drop test at RT onto the valve corner	161
Figure 39: Deformed structure after the 9.0 m drop test at RT onto the valve corner	161
Figure 40: Deformed structure in the valve area after the test sequence at RT onto the valve corner	162
Figure 41: Comparison of the deceleration in the valve area during the 9.0 m drop in sequence 1 at 60 °C and 20 °C – low-pass filtered (SAE, 20 Hz cut-off) ...	163
Figure 42: Comparison of the deceleration in the valve area during the 9.0 m drop in sequence 1 at 60 °C and 20 °C – low-pass filtered (SAE, 584 Hz cut-off) .	163
Figure 43: Comparison of the deceleration in the valve area during 9.0 m drop in sequence 1 at -40 °C and 20 °C – low-pass filtered (Butterworth, 584 Hz cut-off).....	164
Figure 44: Comparison of the deceleration in the valve area during 9.0 m drop in sequence 1 at -40 °C and 20 °C – low-pass filtered (Butterworth, 584 Hz cut-off).....	165
Figure 45: Sequence 1 - Deformation after the 1.2 m drop.....	166
Figure 46: Sequence 1 - Deformation after the 9.0 m drop.....	166
Figure 47: Sequence 1 - Deformation after the drop onto a bar from 1.0 m.....	167
Figure 48: Sequence 1 – Deformation and cracks of the top half, inner shell	167
Figure 49: Sequence 1 – Deformation of the bottom half, inner shell	168
Figure 50: Deformations of the DN30 PSP after sequence 7.....	169
Figure 51: Qualitative comparison of the deformations in simulation and experiment	172
Figure 52: Comparison of simulation and experiment – deceleration in the valve area during 9.0 m drop in sequence 1 – low-pass filtered (SAE, 20 Hz cut-off)	173
Figure 53: Comparison of simulation and experiment – deceleration in the valve area during 9.0 m drop in sequence 1 – low-pass filtered (SAE, 584 Hz cut-off)	173
Figure 54: Measured distances in sequence 2.....	175
Figure 55: Deformed structure after the 1.2 m free drop onto the plug corner.....	176
Figure 56: Deformed structure after the 9 m drop onto the plug corner	176
Figure 57: Deformed structure after the test sequence onto the plug corner	176
Figure 58: Sequence 2 - Deformation after the 1.2 m drop.....	177
Figure 59: Sequence 2 - Deformation after the 9.0 m drop.....	178
Figure 60: Sequence 2 - Deformation after the drop onto a bar from 1.0 m.....	178
Figure 61: Sequence 2 – Deformation of the bottom half, inner shell	179
Figure 62: Qualitative comparison of the deformations in simulation and experiment	181
Figure 63: Comparison of simulation and experiment – deceleration in the plug area during 9.0 m drop in sequence 2 – low-pass filtered (SAE, 20 Hz cut-off)	182
Figure 64: Comparison of simulation and experiment – deceleration in the plug area during 9.0 m drop in sequence 2 – low-pass filtered (SAE, 584 Hz cut-off)	182

Figure 65:	Measured distances in sequence 3.....	184
Figure 66:	Deformed structure after the 1.2 m free drop flat onto the valve side	185
Figure 67:	Deformed structure after the 9.0 m drop flat onto the valve side	185
Figure 68:	Deformed structure after the test sequence flat onto the valve side.....	185
Figure 69:	Deceleration in the plug area during 9.0 m drop in Sequence 3 at -40 °C compared to sequence 3 at 20 °C – low-pass filtered (SAE, 20 Hz cut-off)	186
Figure 70:	Deceleration in the plug area during 9.0 m drop in Sequence 3 at -40 °C compared to sequence 3 at 20 °C – low-pass filtered (SAE, 584 Hz cut-off)	187
Figure 71:	Sequence 3 - Deformation after the 1.2 m drop.....	188
Figure 72:	Sequence 3 - Deformation after the 9.0 m drop.....	188
Figure 73:	Sequence 3 - Deformation after the drop onto a bar from 1.0 m.....	189
Figure 74:	Sequence 3 – Deformation of the bottom half, inner shell	189
Figure 75:	Qualitative comparison of the deformations in simulation and experiment	192
Figure 76:	Comparison of simulation and experiment – deceleration in the plug area during 9.0 m drop in sequence 3 – low-pass filtered (SAE, 20 Hz cut-off).....	193
Figure 77:	Comparison of simulation and experiment – deceleration in the plug area during 9.0 m drop in sequence 3 – low-pass filtered (SAE, 584 Hz cut-off)	193
Figure 78:	Undeformed initial state of the DN30 package for sequence 4	195
Figure 79:	Deformed structure after the test sequence onto the closure system: a) bottom half b) top half (section view)	196
Figure 80:	Sequence 4 - Deformation after the 1.2 m drop.....	197
Figure 81:	Sequence 4 - Deformation after the 9.0 m drop.....	197
Figure 82:	Sequence 4 - Deformation after the drop onto a bar from 1.0 m.....	198
Figure 83:	Numbering of the measured depths of impression at the welding seams of the closure devices for the 1.2 m and 9.0 m drop in sequence 4.....	199
Figure 84:	Qualitative comparison of the deformations in simulation and experiment	200
Figure 85:	Comparison of simulation and experiment – deceleration in the valve area during drop I in sequence 4 – low-pass filtered (SAE, 20 Hz cut-off)	201
Figure 86:	Comparison of simulation and experiment – deceleration in the valve area during drop I in sequence 4 – low-pass filtered (SAE, 584 Hz cut-off)	202
Figure 87:	Measured distances for the free drop test and drop I of sequence 8	204
Figure 88:	Deformed structure after the 1.2 m free drop flat onto the top	205
Figure 89:	Deformed structure after the drop test sequence flat onto the top	205
Figure 90:	Absolute values of the deceleration in the valve area during the 9.0 m drop test in sequence 8 – low-pass filtered (Butterworth, 584 Hz cut-off)	206
Figure 91:	Absolute values of the deceleration in the valve area during the 9.0 m drop test in sequence 8 – low-pass filtered (Butterworth, 584 Hz cut-off)	206

Figure 92:	States with maximal deformation of the DN30 package during the free drop test in sequence 5: a) First impact on the plug side b) Secondary impact on the valve side	209
Figure 93:	State with the maximal deformation of the DN30 package in sequence 5210	
Figure 94:	Sequence 5 - Deformation after the 1.2 m drop.....	211
Figure 95:	Sequence 5 - Deformation after the 9.0 m drop.....	211
Figure 96:	Sequence 5 - Deformation after the drop onto a bar from 1.0 m.....	212
Figure 97:	Measurement points in sequence 5	213
Figure 98:	Qualitative comparison of the deformations in simulation and experiment	214
Figure 99:	Comparison of simulation and experiment – deceleration in the valve area during the 9.0 m slap down drop in sequence 5 – low-pass filtered (SAE, 20 Hz cut-off)	215
Figure 100:	Comparison of simulation and experiment – deceleration in the valve area during the 9.0 m slap down drop in sequence 5 – low-pass filtered (SAE, 584 Hz cut-off).....	215
Figure 101:	Closure device – comparison between CAD a) and FEM model b).....	216
Figure 102:	Generated mesh for each part of the closure device: a) Lower part b) Upper part c) Pin d) Pin front view	217
Figure 103:	Boundary conditions for the static FEM simulation of the closure device	218
Figure 104:	Evaluation of the maximal tensile force at the section plane during the 9 m slap-down drop in Sequence 5.....	219
Figure 105:	Contact interfaces: a) Between the pin and the lower part b) Between the pin and the upper part.....	220
Figure 106:	Deformation of the Pin: a) Total deformation (Scale factor 14) b) Equivalent plastic strain	222
Figure 107:	Equivalent plastic strain: a) Lower part b) Upper part.....	223
Figure 108:	Thermal test prototype for Benchmark 2 after drop test sequence 7	239
Figure 109:	Bottom half of the DN30 PSP before the thermal test.....	239
Figure 110:	DN30 prototype for Benchmark 2 coated for the thermal test.....	242
Figure 111:	DN30 prototype for Benchmark 1 in heating jacket propped up at fire test location	243
Figure 112:	DN30 prototype for Benchmark 2 in heating jacket	243
Figure 113:	Picture of the fire test showing the full flame engulfment of the DN30 prototype for Benchmark 2.....	244
Figure 114:	Gases escaping from the DN30 prototype for Benchmark 1 during the cooling phase	245
Figure 115:	Gases escaping from the DN30 prototype for Benchmark 2 during the cooling phase	245
Figure 116:	30B cylinder inside the DN30 PSP after the thermal test with expanded intumescent material (Benchmark 1)	247
Figure 117:	30B cylinder inside the DN30 PSP after the thermal test (Benchmark 2)	247
Figure 118:	Expanded intumescent material inside the plug protecting device (Benchmark 2)	248

Figure 119: Expanded intumescent material inside the bottom half of the DN30 PSP (Benchmark 2)	248
Figure 120: 30B cylinder after the thermal test inside the bottom half (Benchmark 1)	249
Figure 121: 30B cylinder valve after the thermal test (Benchmark 2).....	249
Figure 122: Geometry of the calculation model for the DN30 package, full view	252
Figure 123: Measured and calculated temperatures at the prototype of the DN30 package for Benchmark 1 – fire phase and 5 hours cooling down.....	257
Figure 124: Measured and calculated temperatures at the prototype of the DN30 package for Benchmark 1 – fire phase and 5 hours cooling down; detail view	258
Figure 125: Temperature distribution at the DN30 package for Benchmark 1 at fire end (t = 1810 s).....	259
Figure 126: Temperature distribution at the DN30 package for Benchmark 1 around the time of maximal valve temperature (t = 11720 s).....	259
Figure 127: Remaining foam concentration after the fire test for RTS 120 for the Benchmark 1 calculation	260
Figure 128: Remaining foam concentration after the fire test for RTS 320 for the Benchmark 1 calculation	260
Figure 129: Remaining foam after the prototype fire test for Benchmark 1 for RTS 120 mantle side, top shell	261
Figure 130: Remaining foam after the prototype fire test for Benchmark 1 for the valve side, bottom shell	261
Figure 131: Measured and calculated temperatures at the prototype of the DN30 package for Benchmark 2 – fire phase and 5 hours cooling down.....	263
Figure 132: Measured and calculated temperatures at the prototype of the DN30 package for Benchmark 2 – fire phase and 5 hours cooling down; detail view	264
Figure 133: Temperature distribution at the DN30 package for Benchmark 2 at fire end (t = 1930 s).....	265
Figure 134: Temperature distribution at the DN30 package for Benchmark 2 around the time of maximal valve temperature (t = 5720 s).....	265
Figure 135: Total gamma energy release rates for initially 1 g of the uranium isotopes U-232, U-234, U-235, U-236, U-238 and the fission product Tc-99 in MeV/s over a period of 10 years	276
Figure 136: Total neutron source intensities for initially 1 g of the uranium isotopes U-232, U-234, U-235, U-236, U-238 in n/s over a period of 10 years	277
Figure 137: Gamma dose rate profile for the package DN30 loaded with a 30B cylinder completely filled with UF6 (normalized source strength)	279
Figure 138: Axial gamma dose rates for two packages DN30 positioned face to face (normalized source strength) – possible transport configuration	280
Figure 139: Axial gamma dose rates for four packages DN30 positioned side by side (normalized source strength) – standard transport configuration	280

Figure 140: Comparison between DN30 package loaded with 30B cylinders containing heels, contact with the inner shell at 6 o'clock position (left side) and at 12 o'clock position (right side)	284
Figure 141: Longitudinal section of the calculation model used for RCT and NCT	292
Figure 142: Cross section of the calculation model used for RCT and NCT.....	292
Figure 143: Longitudinal section of the calculation model used for HAC.....	293
Figure 144: Cross section of calculation model for the hexagonal array for HAC	296
Figure 145: Cross section of the arrangement of two cylinders with impurity sphere for corner-to-corner orientation (plane through center of spherical arrangements)	297
Figure 146: Longitudinal section of the arrangement of two cylinders with impurity sphere for corner-to-corner orientation (plane through center of spherical arrangements)	297

LITERATURE

[10CFR71]	Code of Federal Regulations Title 10 Part 71 "Packaging and Transportation of Radioactive Material"
[49CFR173]	Code of Federal Regulations Title 49 Part 173 "Shippers - General Requirements for Shipments and Packagings"
[ANSI N14.1]	Uranium Hexafluoride – Packaging for Transport, ANSI N14.1- 2012
[ANSYS]	ANSYS®, Release 19.0, Help System, ANSYS, Inc
[ASME BPVC]	ASME Boiler and Pressure Vessel Code, 2017 Edition
[ASTM C996]	Standard Specification for Uranium Hexafluoride enriched to less than 5 wt. % 235U
[BEGUE 2013]	Begue L., Milin M., Caplin G., Evo S., Nuclear Criticality Safety of Enriched UF6 cylinders, PATRAM 2013
[CONNOR 2013]	O'Connor G., Regulatory Criticality Safety Review of Uranium Hexafluoride Transport Package Applications, PATRAM 2013
[DAHER 2019-1]	DAHER NT, Technical Note on Structural RAIs for the DN30 Package, 0023-BBR-2019-004, Revision 1, Hanau, 2019
[DAHER 2019-2]	DAHER NT, Additional Validation of Criticality Calculations for the DN30 Package, Technical Note 0023-BBR-2019-003, Hanau, 2019
[DIN EN 10028-3]	Flat products made of steels for pressure purposes - Part 3: Weldable fine grain steels, normalized, October 2017
[DIN 25478]	Application of computer codes for the assessment of criticality safety, July 1994
[DIN EN 10088-1]	Stainless steels - Part 1: List of stainless steels, December 2014
[DIN EN 10088-2]	Stainless steels - Part 2: Technical delivery conditions for sheet/plate and strip of corrosion resisting steels for general purposes, December 2014
[DIN EN 10088-3]	Stainless steels - Part 3: Technical delivery conditions for semi-finished products, bars, rods, wire, sections and bright products of corrosion resisting steels for general purposes, December 2014
[FKM 2012]	Rechnerischer Festigkeitsnachweis für Maschinenbauteile aus Stahl, Eisenguss- und Aluminiumwerkstoffen (Translation: Proof of strength by calculation for machine parts made of steel, cast iron and aluminum materials), FKM-Richtlinie (Guideline), VDAM Verlag, 2012
[Harris Sn50]	Technical Information Sheet, 50/50 Tin Lead Solder, The Harris Products Group, 2017
[IAEA 2012]	Regulations for the Safe Transport of Radioactive Material, 2009 Edition, SSR-6, IAEA, Vienna, 2012

[ISO 12807]	Safe transport of radioactive materials – Leakage testing on packages, ISO 12807, 1996
[ISO 7195]	ISO 7195, Nuclear Energy – Packaging of uranium hexafluoride (UF ₆) for transport, Second edition, September 2005
[LS-DYNA 2015]	LS-DYNA. Keyword User's Manual – Volume I, LS-DYNA R8.0, 2015
[LS-PREPOST]	http://www.lstc.com/lsp (25.11.2016)
[MILIN 2016]	Milin M., Rannou J., Viaulle L., Caplin G., Evo S., Hydration of uranium residues contained in enriched UF ₆ cylinders, PATRAM 2016
[NEA 2008]	International Handbook of Evaluated Criticality Safety Benchmark Experiments, NEA Nuclear Science Committee, September 2008 Edition, NEA/NSC/DOC(95)03
[PATRAM86]	M.H. Burgess; Heat transfer boundary conditions in pool fires; PATRAM 1986
[PATRAM92]	G. Wieser, B. Droste: Thermal test requirements and their verification by different test methods, PATRAM 1992
[PDSR 2014]	Technical Guide, Package Design Safety Reports for the Transport of Radioactive Material, European PDSR Guide ISSUE 3 (December 2014)
[REZGUI 2013]	Rezgui S., Hilbert F., Criticality Analyses of Enriched Uranium-Hexafluoride Containing Impurities, PATRAM 2013
[ROLOFF 2017]	Wittel, H., Jannasch, D., Voßiek, J., Spura, C.; Roloff/Matek Maschinenelemente: Normung, Berechnung, Gestaltung; 23. Auflage; Springer Vieweg Verlag, 2017
[SCALE 2009]	SCALE 6, A Modular Code System for Performing Standardized Computer Analyses, ORNL/TM-2005/39, Version 6, Oak Ridge National Laboratory, 2009
[SCALE 2011]	SCALE 6.1, Comprehensive Modeling and Simulation Suite for Nuclear Safety Analysis and Design ORNL/TM-2005/39, Version 6.1, Oak Ridge National Laboratory, 2011
[SSG-26]	Advisory Material for the IAEA Regulations for the Safe Transport of Radioactive Material (2012 Edition), Specific Safety Guide No. SSG-26, IAEA, Vienna, 2012
[SWIFT 1952]	H.W. Swift: Plastic instability under plane stress, Journal of Mechanics and Physics of Solids, Volume 1, Issue 1, October 1952
[USEC 651]	The UF ₆ Manual – Good Handling Practices for Uranium Hexafluoride, Rev. 9, USEC, 2006
[WITT 1960]	R. DeWitt, Uranium Hexafluoride: A Survey of the Physico-Chemical Properties, Goodyear Atomic Corporation, Portsmouth, Ohio, GAT-280 Chemistry General, 1960
[YOUNG 1998]	Warren C. Young, Roark's Formulas for Stress and Strain, Sixth Edition, Mc.Graw Hill, 1998

PART 1

1.0 PREFACE

This safety analysis report (SAR) demonstrates the compliance of the type AF package DN30 with the requirements of [10CFR71] and [49CFR173] as well as the international requirements stipulated in [IAEA 2012] for the transport of radioactive material.

The DN30 package has been developed in Europe with its first application for package approval in France. The application in France included a type AF, a type IF and a type B(U)F package design approval to allow the transport UF₆ containing commercial grade as well as reprocessed uranium, whereas the application in the USA includes UF₆ containing commercial grade uranium, only. The French certificates of package approval have already been issued end of 2018. The certificate nos. are F/420/AF, F/420/IF and F/420/B(U)F. The certificate F/420/AF was submitted to DOT for validation.

The French certificates are based on the Package Design Safety Report (PDSR) no. 0023-BSH-2016-001 which was written in compliance with the requirements of the European PDSR Guide [PDSR 2014]. The SAR no. 0023-BSH-2016-002 for the application for package approval of the DN30 in the USA is derived from this original PDSR. Accordingly, the structure reflects the requirements of [PDSR 2014].

The major changes made to the original PDSR are as follows:

- References to [IAEA 2012] were amended by references to the respective chapters of [10CFR71] and [49CFR173]
- Chapter 1.6 shows the compliance with the requirements of [10CFR71] and [49CFR173] and provides a cross-reference to [IAEA 2012]
- Additional requirements from [10CFR71] and [49CFR173] are taken into account in the SAR
- Those parts of the original PDSR referring to a type IF or a type B(U)F package and/or to reprocessed uranium have been removed
- A quality assurance plan that demonstrates compliance with the requirements from Subpart H of Title 10, part 71 of the CFR has been added as Appendix 1.9.3 (Quality Assurance Program)

The appendices to the original PDSR were not revised, partly because they contain external documents, partly in order to preserve consistency of the technical documentation for different DN30 license applications. As such, they contain no references to [10CFR71] and [49CFR173] but the cross-reference list in chapter 1.6 can be used to link these appendices to [10CFR71] and [49CFR173]. In the cases where they contain information on reprocessed uranium, this is noted when they are referenced in this SAR.

1.1 LIST AND STATUS OF DOCUMENTS PERTAINING TO THIS SAR

The list of applicable documents and their status pertaining to this SAR is included in Appendix 1.1 (List of Applicable Documents).

1.2 ADMINISTRATIVE INFORMATION

1.2.1 NAME OF PACKAGE

The package is designated: **DN30**

1.2.2 IDENTIFICATION OF PACKAGE DESIGNER

The DN30 package designer and license holder is:

DAHER NUCLEAR TECHNOLOGIES GmbH
Margarete-von-Wrangell-Straße 7
D-63457 Hanau
Germany

Principal contact:

Name: Mr. Franz Hilbert
Tel: +49 6181 501-232
Fax: +49 6181 501-266
E-mail: f.hilbert@daher.com

In this report, DAHER NUCLEAR TECHNOLOGIES GmbH will be designated as “DAHER NT”.

1.2.3 TYPE OF PACKAGE DESIGN

The DN30 packaging loaded with the allowable content as described in section 1.3 fulfils the requirements according to [10CFR71] and [49CFR173] as well as [IAEA 2012] for a package of:

- Type AF for UF₆ containing commercial grade uranium in less or equal to A₂ quantities, and an enrichment of not more than 5 wt.% U-235 in uranium

1.2.4 CRITICALITY SAFETY INDEX

For the DN30 package the criticality safety index is

$$\text{CSI} = 0$$

1.2.5 PACKAGE DESIGN IDENTIFICATION AND RESTRICTIONS

A unique manufacturing serial number is assigned to each DN30 packaging valid for the whole usage lifetime. This number is stamped on the nameplate under the entry “manufacturers serial No.”.

The serial number is in this form:

XX-YYYY-ZZZZ

Where:

XX = designation of the fabricator (abbreviation assigned by DAHER NT)

YYYY = year of manufacturing

ZZZZ = sequential number

The list of all serial numbers is managed and filed by DAHER NT. All users of the DN30 packaging will be requested to update the status of the individual packaging after completion of the regular periodical inspections. Packagings with overdue periodical inspections (more than 1-year overdue) will be marked in that list as “not in use”.

Each individual package may be marked with an owner serial number different from the manufacturer serial number. This owner serial number may be marked on the nameplate under the entry “owner’s serial No.” or on an additional nameplate attached to the DN30 PSP. The owner serial number may change whenever required by the owner.

1.2.6 MODES OF TRANSPORT FOR WHICH THE PACKAGE IS DESIGNED

- 1) The DN30 package is designed for transport by road, rail, sea and inland waterways.
- 2) Transport by air is not permitted.

Hump shunting of the wagons transporting the DN30 packages is not allowed.

1.2.7 LOWEST TRANSPORT TEMPERATURE FOR WHICH THE PACKAGE IS DESIGNED

The lowest temperature allowed for the transport of the DN30 package is -40 °C.

1.2.8 MAXIMUM NORMAL OPERATING PRESSURE

The maximum normal operating pressure for the DN30 package is defined as the pressure at the triple point of UF₆ (see Table 2):

MNOP = 152 kPa

Remark: the MNOP of the 30B cylinder is specified in [ANSI N14.1] and [ISO 7195] with 1.38 MPa. This definition applies to the use of the 30B cylinder in the enrichment and fuel fabrication process and not for its use as part of the DN30 packaging.

1.2.9 REFERENCE TO APPLICABLE REGULATIONS AND STANDARDS

The safety proof of the DN30 PSP is based on following regulations and standards:

- [10CFR71] Code of Federal Regulations Title 10 Part 71
“Packaging and Transportation of Radioactive Material”
- [49CFR173] Code of Federal Regulations Title 49 Part 173
“Shippers - General Requirements for Shipments and Packagings”
- [ANSI N14.1] American National Standard, For Nuclear Materials – Uranium Hexafluoride – Packagings for Transport, ANSI N14.1-2012
- [ASTM C996] Standard Specification for uranium Hexafluoride Enriched to Less than 5 % ²³⁵U
- [IAEA 2012] Regulations for the Safe Transport of Radioactive Material, 2012 Edition, SS-R-6, IAEA, Vienna, 2009

- [ISO 7195] ISO 7195, Nuclear Energy – Packaging of uranium hexafluoride (UF₆) for transport, Second edition, 2005-09-01

The safety proof is based on [10CFR71] and [49CFR173] or [IAEA 2012] (see chapter 1.0). Compliance with the relevant requirements from [10CFR71] and [49CFR173] is shown in chapter 1.6.

1.3 SPECIFICATION OF THE RADIOACTIVE CONTENTS

The UF_6 is contained in the primary packaging 30B cylinder according to [ANSI N14.1] and [ISO 7195]. The DN30 PSP accommodates the 30B cylinder and provides mechanical and thermal protection during RCT, NCT and HAC.

1.3.1 GENERAL SPECIFICATION

The 30B cylinders are filled with uranium in the chemical composition Uranium Hexafluoride (UF_6).

1.3.1.1 Permissible mass of UF_6

- The permissible mass of UF_6 is between 0 kg and 2277 kg for non-heels fillings.
- The permissible mass of UF_6 including all other chemical compositions is between 0 kg and 11.4 kg for heels fillings.

1.3.1.2 Purity of UF_6

- The UF_6 concentration shall not be less than 99.5 g UF_6 per 100 g. This is corresponding to an atomic number ratio H/U of not more than 0.088.

1.3.1.3 Permissible conditions for repeated use

Cylinders complying with [ANSI N14.1] and [ISO 7195] and within the valid recertification period specified in these standards may be refilled with uranium complying with [ASTM C996] enriched commercial grade UF_6 ¹.

1.3.1.4 Non-fissile and fissile material

The uranium is classified as fissile material:

- Enriched uranium with a max. enrichment of 5.0 wt. % U-235 from uranium with natural isotopic composition

1.3.1.5 Total radioactivity

The uranium has a total radioactivity less or equal to A_2 .

¹ commercial natural UF_6 , or depleted natural UF_6 are included

1.3.1.6 Definition of the permissible contents

The permissible contents are based on the composition of commercial grade uranium as given in [ASTM C996] and listed in Table 1.

Table 1: Content of enriched commercial grade UF₆ complying with [ASTM C996]¹⁾²⁾

Radionuclides	Weight percent max. (wt. %)
U-232	1.0×10^{-8}
U-234	5.5×10^{-2}
U-235	5.0×10^0
U-236	2.5×10^{-2}
U-238	rest
Tc-99	1.0×10^{-6}

¹⁾ commercial natural UF₆, or depleted natural UF₆ are included

²⁾ impurities from multiple refilling of a cylinder containing heels of UF₆ complying with Table 1 are permissible

1.3.2 PHYSICAL AND CHEMICAL STATE

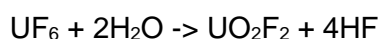
During transport, the UF₆ contained in the DN30 package is in solid form. Table 2 shows some properties of UF₆.

Table 2: UF₆ properties (extract from [USEC 651])

Property	Value
Density in solid state (20 °C)	5.1 g/cm ³
Density in liquid state (64.1 °C)	3.6 g/cm ³
Density in liquid state (121 °C)	3.3 g/cm ³
Sublimation point	56.6 °C (101 kPa)
Triple point	64.1 °C (152 kPa)
Heat of sublimation (64.1 °C)	135 kJ/kg
Heat of fusion (64.1 °C)	56 kJ/kg
Heat of vaporization (64.1 °C)	81 kJ/kg
Critical pressure	4.61 MPa
Critical temperature	230.2 °C
Specific heat, solid (27 °C)	477 J/(kg·K)
Specific heat, liquid (72 °C)	544 J/(kg·K)

Concerning the chemical properties, UF₆ reacts slightly with most metals (Nickel, Monel, Copper, and Aluminum) to create a fluoride of the metal and other uranium compounds. It reacts heavily with hydrocarbons, hence the absence of hydrocarbons in empty cylinders before filling with UF₆ is essential.

UF₆ does not react with Nitrogen, Oxygen, Carbon Dioxide or dry air. However, UF₆ reacts strongly with water and water vapor in the air producing HF-H₂O fog. This fog is highly harmful if inhaled.



The UF₆ could contain some impurities due to chemical reactions. These impurities, like HF or UO₂F₂·5.5H₂O, are also taken into account in the safety criticality analysis, see section 2.2.5.

1.3.3 SPECIAL FORM OR LOW DISPERSIBLE RADIOACTIVE MATERIAL

The radioactive content in the DN30 package is not in special or low dispersible form.

1.3.4 NATURE AND CHARACTERISTICS OF THE RADIATION EMITTED

The radiation emitted by the content of the DN30 package is mainly gamma radiation with a very small contribution of neutron radiation.

1.3.5 LIMITATION OF THE HEAT GENERATION RATE OF THE CONTENT

Table 3 shows the heat generation rate of 2277 kg of UF₆ with the composition given in Table 1 complying with [ASTM C996]. The most significant contribution is from U-234 with a concentration of 0.055 wt% in U. For the thermal analysis, a heat generation rate of 3 W is assumed, safely covering the actual heat generation rate of the content. The contribution to the thermal power from the traces of fission products and other actinides is negligible.

Table 3: Heat generation rate of 2277 kg UF₆ with the composition given in Table 1

Nuclide	Composition g/gU	Heat generation rate (W)
U-232	1.00E-10	1.00E-04
U-234	5.50E-04	1.52E-01
U-235	5.00E-02	4.56E-03
U-236	2.50E-04	6.73E-04
U-238	9.49E-01	1.24E-02
Total	1.00E+00	1.72E-01

1.3.6 MASS OF FISSILE MATERIAL AND NUCLIDES

The maximum mass of the fissile material is calculated from

Maximum total mass of UF₆ = 2277 kg

Maximum enrichment in U-235 = 5 wt.%

$$m_{\text{fiss}} = 2277 \times 0.05 \times 238 / (238 + 6 \times 19) = 77 \text{ kg U-235}$$

1.3.7 OTHER DANGEROUS PROPERTIES

UF₆ is also classified as 'CORROSIVE' and 'POISON' in accordance with Title 49, §172.505(b) of the CFR.



1.3.8 CONTENTS NOT PERMITTED

All contents not complying with the definitions in this chapter 1.3 are not permitted.

1.4 SPECIFICATION OF THE PACKAGING

1.4.1 LIST OF ALL PACKAGING COMPONENTS AND COMPLETE DESIGN DRAWINGS

The DN30 packaging consists of the DN30 Protective Structural Packaging (PSP) and the 30B cylinder specified in [ANSI N14.1] or [ISO 7195]. The DN30 PSP provides both mechanical and thermal protection for the 30B cylinder and its radioactive content and is designed to meet RCT, NCT, and HAC as required by [10CFR71] and [49CFR173] or [IAEA 2012].

The main packaging components are:

- 30B cylinder specified in [ANSI N14.1] or [ISO 7195] and with installed valve and plug,
- Bottom half with two feet welded to the outer structure for tie-down during transport incorporating four handling attachment points to be used for the loaded package and two forklift pockets for handling the empty and loaded packaging,
- Top half with two handling attachment points for handling of the top half,
- Valve protecting device attached to the bottom half by means of hinges,
- Plug protecting device mounted in the bottom half,
- Rotation preventing devices consisting of two pins mounted in the bottom half,
- Closure system consisting of in total six steel blocks welded to the top half and six steel blocks welded to the bottom half forming mortise-and-tenon style joints connected by steel pins,
- Steel blocks welded to the top and bottom half for sealing the package.

1.4.1.1 30B cylinder

The DN30 PSP may be loaded with any standard 30B cylinder in compliance with [ANSI N14.1] or [ISO 7195] or any previous editions of these standards. The complete part list and drawings of the 30B cylinder are specified in [ANSI N14.1] or [ISO 7195]. The following specifications for the pressure envelope as well as the valve and the plug are an excerpt from [ANSI N14.1]. Any changes in materials for components in previous editions are admissible.

1.4.1.1.1 Pressure envelope

The materials of the pressure envelope are specified in Table 4.

Table 4: Materials of the pressure envelope of the 30B cylinder (excerpt from [ANSI N14.1])

Item	Applicable standards
Shells	<p>The following are acceptable materials:</p> <ul style="list-style-type: none"> a) normalized steel conforming to ASTM A516/A516M:2004, grade 55, 60, 65 or 70, meeting heat treatment and supplementary requirements S5 b) coil steel meeting all requirements of ASTM A516/A516M material, c) steel conforming to grade P275NL1 or P355NL1
Heads and skirts	<p>The following are acceptable materials:</p> <ul style="list-style-type: none"> a) normalized steel conforming to ASTM A516/A516M:2004, grade 55, 60, 65 or 70, meeting heat treatment and supplementary requirements S5 b) steel conforming to grade P275NL1 or P355NL1
Seal loops	Steel conforming to ASTM A36/A36M or from steel conforming to EN 10025:1990, grade S235 JRG2/11
Valve and plug couplings	Forged steel conforming to ASTM A105/A105M:2003 or ASTM A106-A:2004b, grade C

1.4.1.1.2 Valve and plug

The materials of the valve and the plug are specified in Table 5.

Table 5: Materials of the valve and the plug of the 30B cylinder (excerpt from [ANSI N14.1])

Item	Applicable standards
Valve body	Forging, aluminium bronze alloy UNS C63600 (CDA alloy 636)
Port cap	The following are acceptable materials: a) bar aluminium bronze alloy UNS C63600 (CDA alloy 636) b) nickel-copper alloy conforming to ASTM B164:2003 N04400, c) bar aluminium bronze UNS C61300
Packing nut	The following are acceptable materials: a) nickel-copper alloy conforming to ASTM B164:2003 N04400, b) bar aluminium bronze UNS C61300
Packing follower and packing ring	The following are acceptable materials: a) bar aluminium bronze alloy UNS C63600 (CDA alloy 636) b) bar aluminium bronze UNS C61300
Stem	Nickel-copper alloy bar conforming to ASTM B164:2003, class A or B
Packing and port cap gasket	Teflon, 100 % virgin TFE unfilled
Fluorinated lubricant	Occidental-Hooker HO-125 or valve-buyer approved equivalent
Hex head plug or socket head plug.	Hex head plug: Bar, upset forged, extruded or extruded and drawn, aluminum bronze (UNS C61300) ASTM B150. Socket head plug (these plugs may be used in lieu of hex head plugs): a) Shall conform to hex head plug or b) Bar, upset forged, extruded or extruded and drawn, aluminum bronze D (UNS C61400, with a tin content restricted to 0.2-0.5%) ASTM B150 or c) Plate, chemical composition as specified in a) or b) and conforming to ASTM B171.
Solder	Tin-lead conforming to ASTM B32 or to ISO 9453 and having a minimum tin content of 45 %, such as alloy ASTM B32 SN50.

1.4.1.2 DN30 PSP

The DN30 PSP is defined in following main drawings:

- 0023-ZFZ-1000-000 “DN30 PSP complete”
- 0023-ZFZ-1000-100 “Closure device complete”
- 0023-ZFZ-1100-000 “Bottom half complete”
- 0023-ZFZ-1200-000 “Top half complete”

Appendix 1.4.1 (Drawings) contains proprietary drawings and parts lists of the individual parts of the DN30 PSP.

The materials of the DN30 PSP are specified in Table 6. The material properties, according to the manufacturer, of the PIR foam used as shock absorbing and thermal insulating material are listed in Table 7. The summary report of the tests performed on these materials as well as the results is given in Appendix 1.4.2 (Material Data PIR Foam). The material properties of Promaseal® and MICROTHERM® OVERSTITCHED 1000R HY are listed in Table 8 and Table 9, respectively.

Table 6: Material specification of the DN30 PSP

Item	Applicable EU standards	Applicable US standards
Inner and outer steel shells	[DIN EN 10088-2], 1.4301, 1.4307, 1.4541	ASME SA-240, Type 304 (UNS S30400) ASME SA-240, Type 321 (UNS S32100)
Inner structure	[DIN EN 10088-2], 1.4301, 1.4307, 1.4541	ASME SA-240, Type 304 (UNS S30400) ASME SA-240, Type 321 (UNS S32100)
Feet	[DIN EN 10088-2], 1.4301, 1.4307, 1.4541	ASME SA-240, Type 304 (UNS S30400) ASME SA-240, Type 321 (UNS S32100)
Lifting lugs of the feet	[DIN EN 10088-2], 1.4462	ASME SA-240, Type 2205 (UNS S31803)
Steel structure of valve protecting device	[DIN EN 10088-2], 1.4301, 1.4307, 1.4541	ASME SA-240, Type 304 (UNS S30400) ASME SA-240, Type 321 (UNS S32100)
Rotation preventing device	[DIN EN 10088-2], 1.4301, 1.4307, 1.4541	ASME SA-240, Type 304 (UNS S30400) ASME SA-240, Type 321 (UNS S32100)
Plug protecting device	[DIN EN 10088-2], 1.4301, 1.4307, 1.4541	ASME SA-240, Type 304 (UNS S30400) ASME SA-240, Type 321 (UNS S32100)
Closure device	[DIN EN 10088-3] ([DIN EN 10088-2]), 1.4541	ASME SA-479 (SA-240), Type 321 (UNS S32100)

Item	Applicable EU standards	Applicable US standards
	[DIN EN 10088-3] ([DIN EN 10088-2]), 1.4571	ASME SA-479 (SA-240), Type 316Ti (UNS S31635)
Body of the pin	[DIN EN 10088-3], 1.4542	ASME SA-564, Type 630 (Alloy 17-4 PH, UNS S17400)
Head of the pin	[DIN EN 10088-3], 1.4541 [DIN EN 10088-3], 1.4571	ASME SA-479, Type 321 (UNS S32100) ASME SA-479, Type 316Ti (UNS S31635)
Securing bolt	Nitronic 50	ASME SA-193, Type XM-19 (UNS S20910)
Washers	NL16-254SMO ([DIN EN 10088-2], 1.4547)	ASME SA-240M, Alloy 254 (UNS S31254)
Gaskets	EPDM	
Foam	Polyisocyanurate rigid foam (PIR foam) conforming to the specifications RTS 120 and RTS 320	
Thermal insulation (intumescent material)	Promaseal-PL®	
Thermal insulation	MICROTHERM® OVERSTITCHED 1000R HY	
Thermal plugs	Polyamide	
Pads	Silicone	

Table 7: Properties of RTS 120 and RTS 320 (according to the technical data sheets)

Item	Standards	Units	Foam type	
			RTS 120	RTS 320
Density	EN 1602 / ASTM D1622	kg/m ³	120 ± 10	320 ± 20
Static compression strength - parallel	EN 826 / ASTM D1621	MPa	1.68 ± 0.16	7.50 ± 0.40
Static compression strength - perpendicular	EN 826 / ASTM D1621	MPa	1.50 ± 0.20	7.40 ± 0.40
Thermal conductivity (10 °C)	EN 12667 / ASTM C518	mW/mK	28.0	49.0
Operating temperature		°C	-180/+120	-196/+120
Closed cells	EN ISO 4590/ASTM D6226	%min	92	95
Fire reaction (maximum extent of the burnt area)	EN ISO 3582	mm	<30	<60
Fire reaction (extinguishing time)	EN ISO 3582	sec	<60	<120

Table 8: Properties of Promaseal®

Item	Reference	Units	Promaseal®
Density (25.4 °C)	See Appendix 1.4.3 (Material Data Intumescent Material)	kg/m ³	1000
Thermal conductivity (20 °C) nominal thickness not expanded		W/(m·K)	0.19
Specific heat capacity (30 °C)		J/(kg·K)	1232
Max. operating temperature		°C	470
Intumescent temperature		°C	184
Expansion ratio dV/V ₀		-	9.5 - 20

Table 9: Properties of MICROTHERM® OVERSTITCHED 1000R HY

Item	Standards / measured by	Units	MICROTHERM® OVERSTITCHED 1000R HY
Density (room temperature)	Appendix 1.4.4 (Material Data Microtherm Overstitched 1000R HY)	kg/m ³	260
Thermal conductivity 200 °C		mW/mK	26
Specific heat capacity 200 °C		J/(kg·K)	920
Max. operating temperature		°C	1000

1.4.1.2.1 Static and dynamic mechanical tests with samples of the technical foam

The static and dynamic tests with samples of the technical foam used for the DN30 PSP are documented in section 3 of Appendix 1.4.2 (Material Data PIR Foam). Table 10 gives a summary of the mechanical tests carried out with foam samples.

Table 10: Summary of the mechanical tests with PIR foam samples

Temperature °C	Orientation with respect to foaming	Test condition	Impact velocity m/s
-40 °C	parallel	quasi-static	
-40 °C	perpendicular	quasi-static	
-20 °C	parallel	quasi-static	
-20 °C	perpendicular	quasi-static	
+20 °C	parallel	quasi-static	
+20 °C	perpendicular	quasi-static	
+50 °C	parallel	quasi-static	
+50 °C	perpendicular	quasi-static	
+80 °C	parallel	quasi-static	

Temperature °C	Orientation with respect to foaming	Test condition	Impact velocity m/s
+80 °C	perpendicular	quasi-static	
-40 °C	parallel	dynamic	13
-40 °C	perpendicular	dynamic	13
-20 °C	parallel	dynamic	13
-20 °C	perpendicular	dynamic	13
+20 °C	parallel	dynamic	13
+20 °C	perpendicular	dynamic	13
+50 °C	parallel	dynamic	13
+50 °C	perpendicular	dynamic	13
+80 °C	parallel	dynamic	13
+80 °C	perpendicular	dynamic	13

The results of these tests were used to calibrate the material model being used in the dynamic FEM simulations of the DN30 packaging under NCT and ACT, see section 4.4.4 of Appendix 2.2.1.3 (Structural Analysis of the DN30 Package under NCT and HAC).

The summary of the results is:

- The deformation force is depending on the temperature
- The deformation force is depending on the test conditions: for dynamic test conditions the deformation force is higher than for quasi-static tests conditions
- There is almost no dependency on the foaming orientation

1.4.1.2.2 Thermal tests with samples of RTS 120 and RTS 320

The thermal tests with samples of the technical foam used for the DN30 PSP are documented in section 4 of Appendix 1.4.2 (Material Data PIR Foam).

The tests carried out were:

- A thermos-gravimetric test by heating samples up to 800 °C
- Measurement of thermal diffusivity, thermal expansion, heat capacity and density up to about 300 °C
- Gas analysis of the gases produced when the foam disintegrates at higher temperatures

The summary of the results is:

- Thermal properties of the foam can be determined up to approx. 250 °C; beyond that temperature the foam disintegrates
- During disintegration, no dangerous gases are produced

The results of these tests with samples were used for the thermal analyses of the DN30 packaging under RCT, NCT and ACT, see section 6.4.4 of Appendix 2.2.2.3 (Thermal Analysis).

1.4.1.2.3 Thermal tests with samples of Promaseal-PL®

The thermal tests with samples of the intumescent material used for the DN30 PSP are documented in Appendix 1.4.3 (Material Data Intumescent Material).

Following tests were carried out:

- A thermo-gravimetric test by heating samples up to 800 °C
- Measurement of heat capacity up to about 300 °C
- Measurement of thermal expansion up to more than 800 °C
- Measurement of the thermal conductivity for non-expanded and expanded samples
- Measurement of the force of expansion during increase of temperature

The results of these tests with samples were used for the thermal analyses of the DN30 packaging under RCT, NCT and ACT as well as for the analysis of the reaction forces on the 30B cylinder during the thermal test, see section 6.4.5 of Appendix 2.2.2.3 (Thermal Analysis).

1.4.2 DESCRIPTION OF THE DN30 PACKAGING

The DN30 packaging consists of

- the 30B cylinder specified in [ANSI N14.1] or [ISO 7195],
- the DN30 protective structural packaging (PSP).

1.4.2.1 30B cylinder

The 30B cylinder is specified and described in [ANSI N14.1] or [ISO 7195]. The main data are extracted from there and listed in Table 11 for completeness of the SAR.

The 30B cylinders permissible for the transport in DN30 PSPs are in full compliance with the latest [ANSI N14.1] or [ISO 7195] standard or any previous edition of these standards.

Table 11: Main data of the 30B cylinder

Item	Value
Nominal diameter:	760 mm
Nominal length:	2060 mm
Wall thickness:	13 mm
Nominal tare weight:	635 kg
Max net weight:	2277 kg
Minimum volume:	0.736 m ³

1.4.2.2 DN30 PSP

The DN30 PSP consists of

- The bottom half with integrated feet, handling attachment points suitable for the loaded package, valve protecting device, plug protecting device, rotation preventing device and bottom half of the closure device
- The top half with integrated handling attachment points suitable for the top half and the top half of the closure device.

The main data are listed in Table 12.

Table 12: Main data of the DN30 PSP

Item	Value
Nominal diameter	1216 mm
Nominal height	1329 mm
Nominal length:	2437 mm
Nominal tare weight:	1100 kg
Nominal gross weight:	4012 kg
Maximum gross weight:	4100 kg
Minimum volume:	0.736 m ³

1.4.2.2.1 Bottom half of the DN30 PSP

The body of the bottom half is made of an inner and outer shell of stainless steel, both in the form of a tub, which are connected at the top by a flange. The cavity between inner and outer shell and flange is filled with the PIR foam types RTS 120 and RTS 320, with a layer of 10 mm MICROTHERM® as thermal insulation between the inner shell and the RTS 120 foam. At the side the thickness of the inner shell is 2 mm and of the outer shell 3 mm. At the ends the thickness of the inner shell is 10 mm and of the outer shell 4 mm.

At the bottom side there are two feet of stainless steel welded to the outer shell at each end of the PSP. The feet have a base plate made of 2 x 10 mm thick stainless steel which contains at each side two holes for tie-down to an adapted flat-rack (the arrangement and size of these holes is compatible with existing PSP designs).

At the side of each of the feet there is an eyelet welded to the side plate of the foot. These eyelets are designed to be used for lifting the loaded DN30 package.

At the top side of the bottom half of the DN30 PSP there are the lower halves of the mortise-and-tenon closure system welded to the outer shell three per side. Adjacent to one of these parts of the closure device the sealing block is welded to the outer shell.

At the inside of the bottom half there is the valve protecting device attached by hinges to the flange at one end. The valve protecting device consists of a casing of stainless steel filled with PIR foam RTS 320 and a protecting housing, with its inner walls covered with intumescent material.

On the other end there is the plug protecting device in the form of a pot welded into the inner shell and with its walls covered with intumescent material.

At the inner sides of the flange there are two rotation preventing devices welded to the flange. These devices consist of a pin, which is withdrawn into the flange during loading and inserted during transport into the two holes in the skirt of the 30B cylinder.

All the surfaces of the inner shell of the bottom half are covered with a layer of 2.6 mm intumescent material.

1.4.2.2.2 Top half of the DN30 PSP

The body of the top half is similar to the bottom half. It is made of an inner and outer shell of stainless steel, both in the form of a tub, which are connected at the bottom by a flange. The cavity between inner and outer shell and flange is filled with the PIR foam types RTS 120 and RTS 320, with a layer of 10 mm MICROTHERM® as thermal insulation between the inner shell

and the RTS 120 foam. At the side the thickness of the inner shell is 2 mm and of the outer shell 3 mm. At the ends the thickness of the inner shell is 10 mm and of the outer shell 4 mm.

At the top there are two eyelets welded to the outer shell one on each side. These eyelets are designed to be used for lifting the top half only.

At the bottom side of the top half of the DN30 PSP there are the upper halves of the mortise-and-tenon closure system welded to the outer shell three per side. Adjacent to one of these parts of the closure device the sealing block is welded to the outer shell.

At the inside of the top half there is a recess to accommodate the valve protecting device.

In the flange of the top half there is an elastomeric gasket to prevent inleakage of water during routine conditions of transport.

All the surfaces of the inner shell of the top half are covered with a layer of 2.6 mm intumescent material.

1.4.2.3 Design safety features of the DN30 packaging

1.4.2.3.1 Pressure envelope of the DN30 package

The 30B cylinder including its valve and plug is the pressure retaining component of the DN30 package.

The DN30 PSP is not designed as pressure retaining component. Due to its design, a pressure difference between the ambient and the DN30 PSP can be excluded.

For pressure release during HAC, the DN30 PSP is equipped with fusible plugs which will release any pressure induced by the decomposition of the foam parts.

1.4.2.3.2 Mechanical protection system

The mechanical protection system consists of the stainless steel/foam structure of the bottom and top half of the DN30 PSP. It prevents excessive mechanical impacts onto the 30B cylinder during RCT, NCT and HAC.

1.4.2.3.3 Thermal protection system

The thermal protection system consists of the stainless steel/foam structure of the bottom and top half of the DN30 PSP, each fitted with nine thermal plugs screwed into the outer steel shells, the MICROTHERM® layer between the RTS 120 foam and the inner steel shell, and the intumescent material at the inner surfaces of the DN30 PSP. It prevents excessive thermal impacts onto the 30B cylinder and its valve and plug during RCT, NCT and HAC.

1.4.2.3.4 Closure system

The two halves of the DN30 PSP are connected by the closure system consisting of 6 robust mortise-and-tenon like devices and the flange.

The two parts of each mortise-and-tenon system have four teeth each with a hole in the center. When closed, the two halves are connected by a pin inserted into these holes. This pin is secured by a bolt. The design of the mortise-and-tenon system is such that neither the connecting pin nor the securing bolt are exposed to mechanical impacts but protected by the massive body of the system. The system prevents excessive relative movements of top and bottom half in vertical direction in RCT, NCT and HAC.

The flange is shaped like an upside-down U. It prevents excessive relative movements of top and bottom half in all horizontal directions in RCT, NCT and HAC. Furthermore, in flat drop orientations the flange will be deformed in such a way that top and bottom half are clamped together.

1.4.2.3.5 Valve protecting device

The valve protecting device consists of a stainless-steel housing filled with PIR foam. It is shaped like a U and encloses the valve of the 30B cylinder during transport. It is connected to the bottom half of the DN30 PSP by two hinges. In open condition, it is turned to horizontal position to allow loading and unloading of the cylinder. When the filled cylinder is loaded into the PSP, the device is turned by 90° to vertical orientation so that it is in contact with the cylinder head. The valve protecting device prevents contact of the valve with any part of the PSP or any other part the 30B cylinder except for its original point of contact (thread) during RCT, NCT and HAC.

A protecting housing is placed inside the U-shape of the valve protecting device. This housing is made of a thin stainless-steel sheet and the inside is covered with intumescent material.

1.4.2.3.6 Plug protecting device

The plug protecting device consists of a pot made of stainless steel welded to the inner shell of the bottom half of the PSP. This device allows the plug to move in axial direction without making contact with any part of the PSP during RCT, NCT and HAC. The inside of the pot is covered with intumescent material.

1.4.2.3.7 Rotation preventing system

The rotation preventing system consists of two rotation preventing devices installed at the sides of the inner flange of the bottom half of the PSP. The device consists of a stainless-steel pin accommodated in two sleeves, an internal sleeve in contact with the pin and an external sleeve which is welded to the flange. A lever is welded onto the steel pin to allow turning and lateral movements.

In open condition the steel pin is withdrawn into the flange so that the cylinder can be loaded and unloaded. In this condition the top half of the PSP cannot be put onto the bottom half as the position of the lever prevents the placement of the top flange onto the bottom flange. The connection of top and bottom half is only possible when the rotation preventing system is properly engaged. This excludes the possibility of the pin being withdrawn while the packaging is closed.

1.4.2.3.8 Sealing system

For sealing of the DN30 package there are two sealing blocks welded to the top and bottom half adjacent to a closure device. These blocks allow the use of high security seals compliant with ISO 17712:2010 / C-TPAT.

1.4.2.4 Handling features of the DN30 packaging

1.4.2.4.1 Lifting of the loaded DN30 package and empty DN30 PSP

The DN30 package can be lifted:

- By using the 4 lifting lugs welded to the upper part of the feet,

- By using a forklift,
- By using handling slings.

The handling of the empty DN30 PSP should be carried out in the same manner as for the loaded package.

1.4.2.4.1.1 Lifting by using the 4 lifting lugs

For lifting of the DN30 package by using the 4 lifting lugs welded to the upper part of the feet, shackles must be used and fixed to the lifting lugs. It is preferable to use lifting slings made from Polyester or Nylon.

The angle between the vertical axis of the lifting lugs and the slings/chains must not be greater than 30° (see Figure 1).

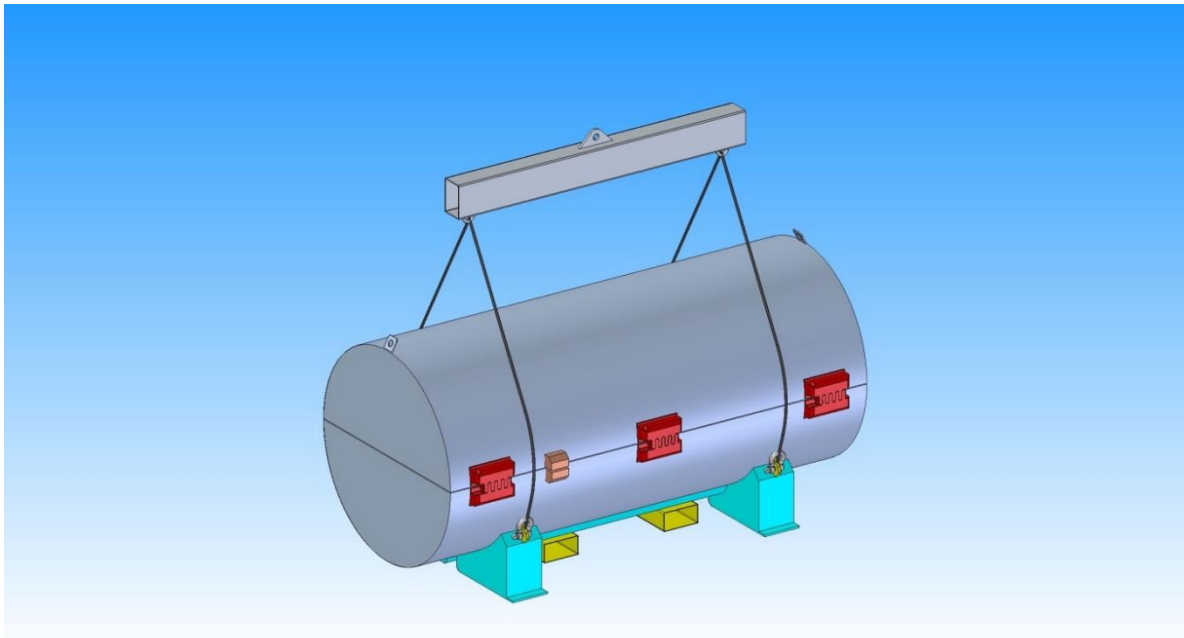


Figure 1: Lifting of the DN30 package by using the 4 lifting lugs

1.4.2.4.1.2 Lifting by using a forklift

The loaded DN30 package may be handled and lifted by using a forklift. For this purpose, there are two forklift pockets welded to the bottom half of the DN30 PSP (see Figure 2).

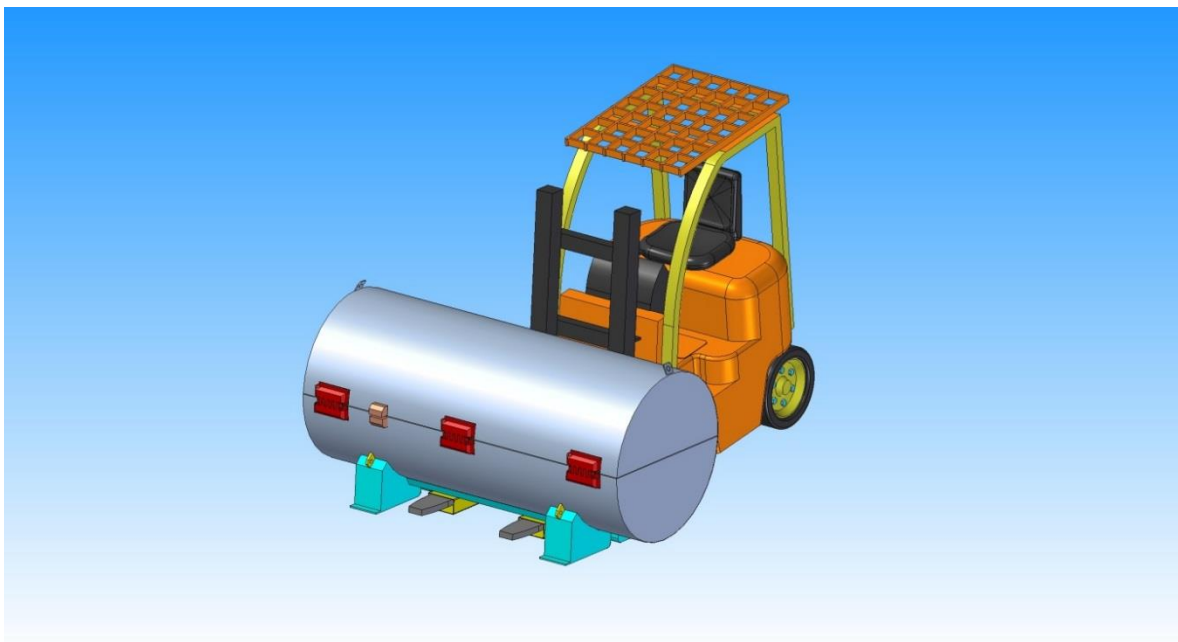


Figure 2: Lifting of the DN30 package by using a forklift

1.4.2.4.1.3 Lifting by using slings (only for empty PSP)

The empty DN30 packaging may be handled by slings attached to the bottom half of the DN30 package according to Figure 3.

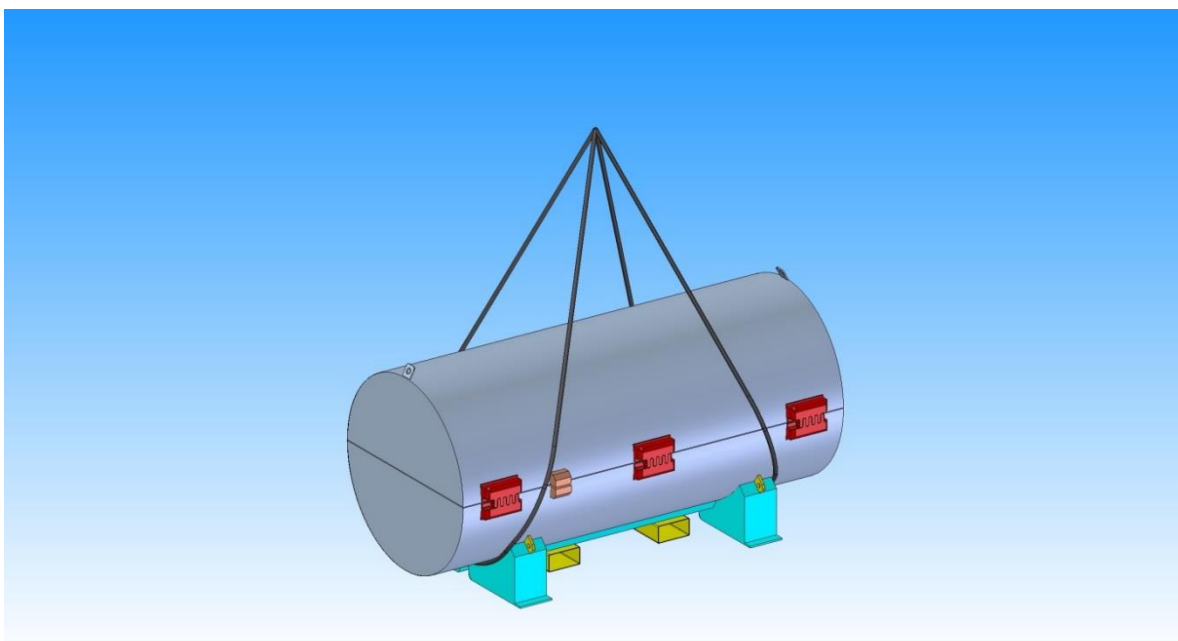


Figure 3: Lifting of the empty DN30 PSP by using slings

1.4.2.4.2 Lifting of the top half of the DN30 packaging

In general, the loaded DN30 package or the empty DN30 PSP is mounted with its feet to dedicated flatracks when transported. At the destination, only the top half needs to be removed for loading and unloading of the 30B cylinders from the DN30 PSPs.

For handling, see Figure 4, of the top half there are two lifting lugs, one at each end, welded to the outer shell of the DN30 PSP. These lifting lugs are only designed for the handling of the top half of the DN30 PSP. They must be blocked during transport to avoid inadvertent use of these attachment points for lifting of the loaded package, e.g. by inserting bolts.

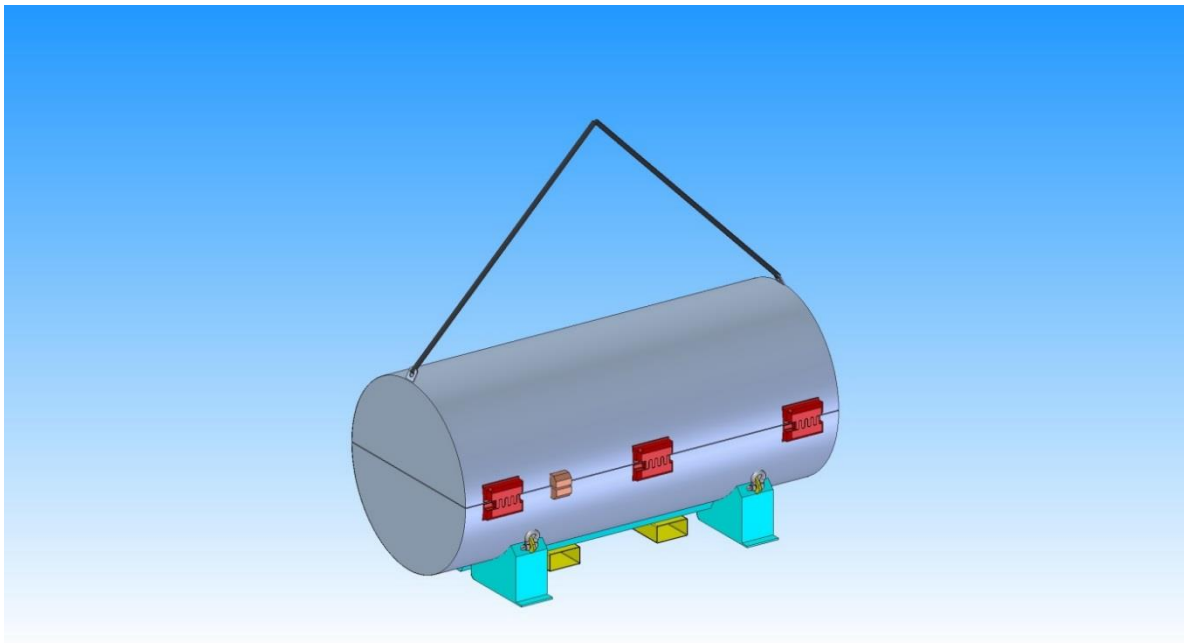


Figure 4: Lifting of the top half of the DN30 packaging

1.4.2.5 Tie-down features of the DN30 packaging

For tie-down, the DN30 PSP is equipped with two feet. The base plates of the feet consist of 2 x 10 mm thick stainless-steel sheets which contain two holes at each end. The dimension and placement of these holes is compatible with PSPs currently in use. During transport, the DN30 PSP is bolted to a dedicated flat-rack (see Figure 5).

According to international practice tie-down of the DN30 package on flat-racks by bolts is performed taking into account accelerations of 2 g in axial, 2 g in lateral and 2 g in vertical orientation. However, the tie-down features of the DN30 package are designed to withstand an acceleration of 10 g in axial, 5 g in lateral and 1 g +/- 2 g in vertical orientation (see section 2.2.1.3). For application of such tie-down parameters additional shocks or bumpers must be foreseen in the tie-down plan. However, this tie-down plan is not part of the application.

Only for the transport of DN30 PSP not loaded with a 30B cylinder and in case a dedicated flat-rack cannot be made available, tie-down by using straps according to Figure 6 is allowed. In that case, a tie-down plan has to be drawn up based on a tie-down calculation.

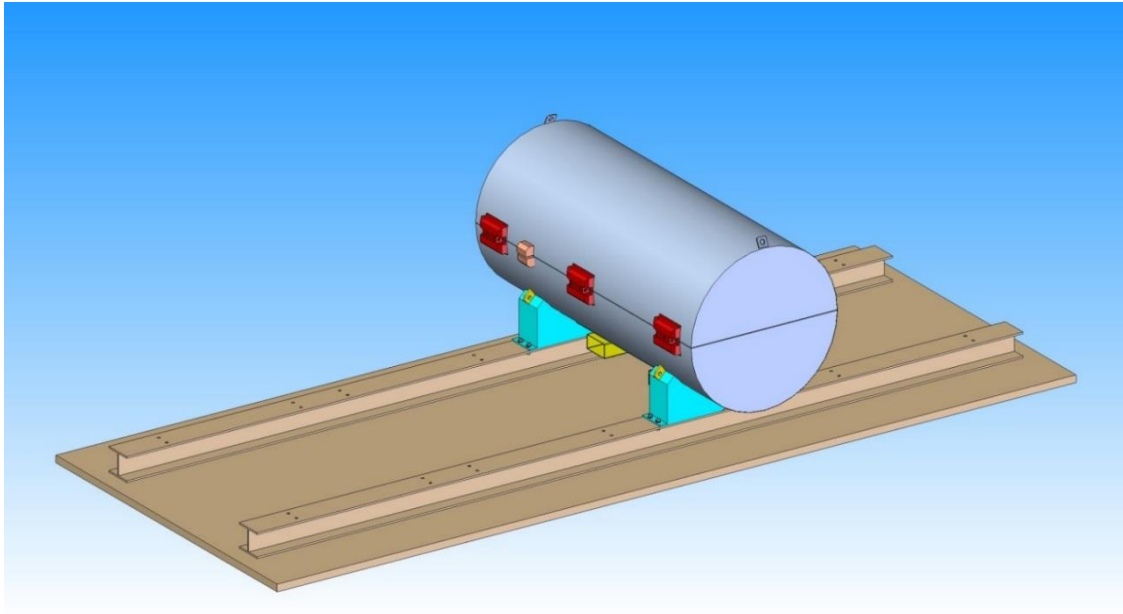


Figure 5: General tie-down method for the DN30 package / DN30 PSP

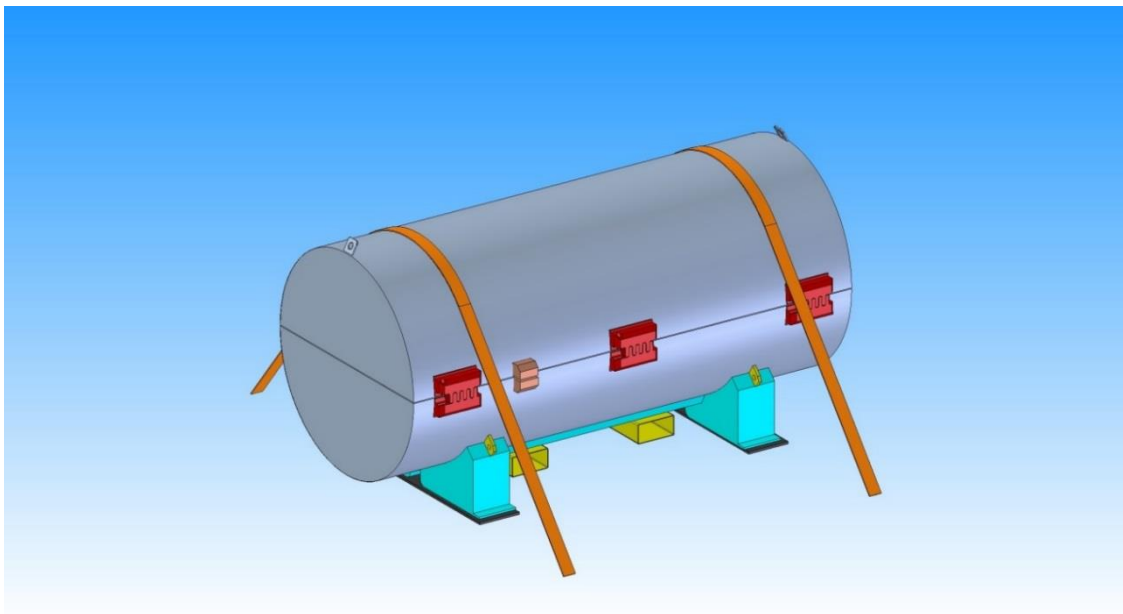


Figure 6: Tie-down of the DN30 PSP without a cylinder using straps

1.4.3 THE COMPONENTS OF THE PACKAGING RELEVANT FOR THE CONTAINMENT SYSTEM

The containment system consists of

- The 30B cylinder shell and heads together with the welding seams connecting the pressure envelope,
- The valve body and the stem, including the threaded connection between valve and cylinder body,
- The plug including the threaded connection between plug and cylinder body.

This containment system complies with the requirements defined in [ANSI N14.1] and [ISO 7195].

1.4.4 THE COMPONENTS OF THE PACKAGING RELEVANT FOR SHIELDING

The DN30 packaging has no components with shielding as the primary purpose. However, some level of shielding is provided by the shell of the 30B cylinder as well as the inner and outer shells of the DN30 PSP.

1.4.5 THE COMPONENTS OF THE PACKAGING RELEVANT FOR THE CONFINEMENT SYSTEM

The confinement system consists of

- The components of the containment system.
- The inner and outer steel shell of the DN30 PSP.

1.4.6 THE COMPONENTS OF THE PACKAGING RELEVANT FOR THERMAL PROTECTION

Following components of the DN30 PSP are relevant for thermal protection:

- The inner and outer shells
- The RTS 120 and RTS 320 foam
- The MICROTHERM® layer between inner shell and RTS 120 foam
- The intumescent material attached to the inside of the inner shell

1.4.7 THE COMPONENTS OF THE PACKAGING RELEVANT FOR HEAT DISSIPATION

Due to the very low level of thermal power there is no dedicated component for heat dissipation.

1.4.8 THE PROTECTION AGAINST CORROSION

All outer and inner surfaces of the DN30 PSP are made of austenitic stainless steel and are hence resistant to corrosion.

The 30B cylinder is generally coated with high quality paint preventing excessive corrosion.

Corrosion at the inside of the 30B cylinder is negligible. The long term and world-wide experience with this cylinder design proves that there is no excessive corrosion within the 5-year recertification period or when stored with UF₆ or heels, which could impair the safety functions of the cylinder.

There is no possibility of corrosion due to the interaction of the intumescent material or its glue, since the material is certified halogen-free (see Appendix 1.4.5 (Absence of Halogen in Intumescent Material)).

1.4.9 THE PROTECTION AGAINST CONTAMINATION

All outer and inner surfaces of the DN30 PSP are made of austenitic stainless steel and hence are easy to decontaminate.

The intumescent material is protected by an easy to decontaminate coating.

The 30B cylinder is generally coated with paint which can be easily decontaminated. In transport configuration, the surface of the 30B cylinder is not accessible from the outside.

1.4.10 THE SHOCK ABSORBING COMPONENTS OF THE PACKAGING

Following components of the DN30 PSP are relevant for shock absorption:

- The inner and outer shells
- The RTS 120 and RTS 320 foam
- The valve protecting device

1.4.11 THE TRANSPORT CONCEPT

Generally, the DN30 package is transported on dedicated flat-racks. A maximum of four DN30 packages can be mounted onto a 20' flat-rack by bolting them down via the holes in the feet. Alternatively, due to their low gross weight, for packages containing heels quantities individual transport is feasible by lashing the packages with straps to the transport means.

- The components of the packaging relevant for lifting are described in section 1.4.2.4.
- The components of the packaging relevant for tie-down are described in section 1.4.2.5.

1.5 PACKAGE PERFORMANCE CHARACTERISTICS

1.5.1 MAIN DESIGN PRINCIPLES

The packaging DN30 consists of the DN30 PSP which accommodates the 30B cylinder. The DN30 PSP is designed by DAHER NT whereas the design of the 30B cylinder is fixed and specified in [ANSI N14.1] and [ISO 7195].

The 30B cylinder is primarily designed to be used as a pressure vessel in enrichment and fuel manufacturing plants to accept enriched UF_6 from the enrichment process and to feed enriched UF_6 into the process at the fuel manufacturer's site. It acts as well as primary packaging for internal transports and as buffer storage on these sites. Hence, the 30B cylinder design provides the containment and the confinement function of the DN30 package.

For public transportation the 30B cylinder is protected by the DN30 PSP against mechanical and thermal impacts as defined in [10CFR71] and [49CFR173] or [IAEA 2012] so that the containment and confinement function of the 30B cylinder are maintained under NCT and HAC.

1.5.2 PERFORMANCE CHARACTERISTICS

1.5.2.1 Performance characteristics under RCT

Under RCT, the main performance characteristics are:

- Safe handling of the DN30 package,
- Safe tie-down of the DN30 package,
- Adequate design for accelerations and vibrations to be routinely expected,
- Easy handling operations under the environmental conditions to be routinely expected,
- Resistance to corrosion,
- Long term usability by taking into account temperatures and ambient conditions to be routinely expected.

1.5.2.2 Performance characteristics under NCT

Under NCT, the main performance characteristics are:

- Protection of the 30B cylinder against the mechanical conditions to be expected under NCT,
- Limitations of deformations to fulfill the requirement concerning dose rate increase.

1.5.2.3 Performance characteristics under HAC

Under HAC, the main performance characteristics are:

- Protection of the 30B cylinder against mechanical conditions to be expected under HAC,

- Protection of the 30B cylinder against the thermal conditions to be expected under HAC.

1.5.3 ASSUMPTIONS USED FOR THE SAFETY ANALYSIS

1.5.3.1 Containment function

The containment function is provided by the 30B cylinder and its installations valve and plug. With reference to [10CFR71] §71.55(b) and §71.55(g) or [IAEA 2012] para. 680 (b) it is assumed that the containment function is preserved if

- Following the tests prescribed in [10CFR71] §71.59(a)(2) or [IAEA 2012] para. 685 (b) there is no physical contact between the valve or plug and any other component of the packaging other than their original points of attachment,

And where, in addition

- Following the test prescribed in [10CFR71] §71.73(c)(4) or [IAEA 2012] para. 728 the valve and the plug remain leak tight.

1.5.3.2 Dose rates

The shielding function is provided by the shell of the 30B cylinder and the inner and outer shells of the DN30 PSP. For RCT and NCT the foam between inner and outer shell of the DN30 PSP is taken into account as well.

For the proof that the increase of the dose rate after the mechanical tests simulating NCT does not exceed the limits specified in the regulations, the reduction of the wall thickness of the DN30 PSP due to deformation is taken into account.

1.5.3.3 Criticality safety

The proof of criticality safety is based on the 30B cylinder. There are no requirements on the content, neither on its arrangement within the 30B cylinder nor regarding the distribution of impurities.

The containment function of the cylinder must be preserved according to section 1.5.3.1. The maximal amount of water ingress under HAC conditions is less than 3 g (see section 2.2.5.2).

The stainless-steel shells of the DN30 PSP are part of the confinement system. Neither the foam nor the distance between inner and outer shell need to be preserved as these parameters are not relevant for criticality safety. The closure system must assure that the top and bottom half of the DN30 PSP remain connected during RCT, NCT and HAC.

1.6 COMPLIANCE WITH REGULATORY REQUIREMENTS

In this section, the compliance of the type AF package design DN30 with the regulations for the transport of radioactive material is shown. The tables for each subsection are oriented along the paragraphs of the IAEA regulations [IAEA 2012] in column 1. In column 2 they reference the corresponding paragraphs from [10CFR71]. As the DN30 is a type A package containing uranium hexafluoride, references to [49CFR173] are also provided in column 3 where applicable. The subsections are:

- 1.6.1: Definitions, general provisions, activity limits and classification
- 1.6.2: Requirements and controls for transport
- 1.6.3: General requirements for all packagings and packages
- 1.6.4: Requirements for packages containing uranium hexafluoride
- 1.6.5: Requirements for type A packages
- 1.6.6: Requirements for type B packages (relevant for thermal and containment analysis)
- 1.6.7: Requirements for packages containing fissile material
- 1.6.8: Test procedures

1.6.1 DEFINITIONS, GENERAL PROVISIONS, ACTIVITY LIMITS AND CLASSIFICATION

IAEA SSR-6	10 CFR §71	49 CFR §173	Remarks
222	4 (<i>fissile</i>)	403 (<i>fissile</i>)	There is only the fissile nuclide U-235 present in the content.
306	Subpart H	-	The management system of DAHER NT is audited and certified by the German competent authority (see chapter 1.9). Appendix 1.9.3 (Quality Assurance Program) shows compliance of this system with requirements from Subpart H of [10CFR71] and contains the NRC approval.
417	15	453	See specification of contents in section 1.3.1.4; there are no exceptions by one of the provisions specified in this para.
418	31, 33, 35	-	The certificate of package approval is applied for based on this SAR (certificate of type AF package).
419	-	420(e)	For the DN30 package the UN number UN2977 shall be assigned.
420	-	420	The mass of UF ₆ contained in the DN30 PSP complies with the mass specified for the 30B cylinder in [ANSI N14.1] and [ISO 7195], see section 1.3.1.
428	4 (<i>Type A</i>)	-	See paras 429 and 430.
429	-	431(a)	The activity in a DN30 package licensed as type AF package is restricted to A ₂ , see section 1.3.1.6.

IAEA SSR-6	10 CFR §71	49 CFR §173	Remarks
430	Appendix A	433(d)	For mixtures of radionuclides the respective formula is applied, see section 1.3.1.6.

1.6.2 REQUIREMENTS AND CONTROLS FOR TRANSPORT

IAEA SSR-6	10 CFR §71	49 CFR §173	Remarks
501	85	-	The 30B cylinder as containment system is manufactured and tested before its first use to comply with [ANSI N14.1] and [ISO 7195]; before the first use of a packaging designed to contain fissile material, an inspection is carried out and recorded, see section 1.7.1.
502	87(a)	475 (a)	Administrative controls ensure that only the contents as specified in the certificate of package approval are loaded into the DN30 PSP, see section 1.7.2.
503	87(h)	-	The handling instructions defined in sections 1.7.3 and 1.7.4 take into account the respective measures.
507	-	2(a)	Other dangerous properties of UF ₆ are taken into account, see section 1.7.6.
508	87(i)	-	Contamination checks defined in section 1.7.2 take the specified limits into account.
526	47(a)	441(a)	The TI for all contents is below 10, see section 2.2.4.7.2.
527	47(a)	441(a)	The radiation level at the surface of each package is below 2 mSv/h under RCT and NCT, see section 2.2.4.7.4.
533	85(c)	-	The package mass is marked on the type plate, see Appendix 1.4.1 (Drawings)
566 (b)	47(b)	-	The radiation level of a conveyance of several packages is below 2 mSv/h at any point of the external surface and below 0.1 mSv/h at 2 m distance from the external surface, see section 2.2.4.
568	59(c)	-	The CSI of the DN30 package is in all cases 0; hence also for groups of DN30 packages the sum of the CSIs is 0.
569	59(c)(3)	-	Not applicable, see para. 568.
570	-	-	Not applicable, as the material defined in section 1.3.1.6 does not meet any of the provisions (a)-(f) in para. 417.
575	-	-	The radiation level at the surface of each package is below 2 mSv/h, see section 2.2.4.7.4.

1.6.3 GENERAL REQUIREMENTS FOR ALL PACKAGINGS AND PACKAGES

IAEA SSR-6	49 CFR §173*	Remarks
607	410(a)	The package can be easily and safely transported and properly secured during transport, see sections 1.4.2.4 and 1.4.2.5.
608	410(b)	The lifting attachments on the package are designed for their intended purpose with a minimum safety factor of three against yielding, see section 2.2.1.2.3.
609	410(b)	The attachments on the package which could be used for lifting are designed to support its mass, see section 1.4.2.4.1 and section 2.2.1.2.3.1; any other feature which could be used for lifting is rendered incapable, see section 1.4.2.4.2.
610	410(c)	The outer surfaces of the packaging consist of stainless steel and can be easily decontaminated, see section 1.4.2.
611	410(d)	The outer layer of the package prevents the collection and retention of water, see section 1.4.2.
612	410(e)	There are no features added to the package at the time of transport that could reduce its safety, see section 1.4.2.5.
613	410(f)	The package is designed to withstand effects of any acceleration, vibration or vibration resonance that may arise under RCT or NCT, see section 2.2.1.3.
614	410(g)	The materials of the packaging, mainly steel and technical foam, are physically and chemically compatible with each other; any part in contact with the radioactive content has been designed for such purpose, see section 1.4.2.
615	410(h)	The valve and the plug of the 30B cylinder are protected by the DN30 PSP during transport and cannot be operated unauthorized, see section 1.4.2.
616	-	The package is designed to comply with the requirements for fissile packages; it takes into account ambient temperatures and pressures that are likely to be encountered during RCT.
617	441(a)	Proof of shielding is contained in section 2.2.4.
618	2(a)	The other dangerous properties of UF ₆ are taken into account, see section 1.3.7.

* this section of the IAEA SSR-6 is very closely related to 49 CFR §173.410. Compliance with 10 CFR §71.43 (General standards) and other design specifications (lifting/tie-down in §71.45 and radiation limit in §71.47) are addressed in subsections 1.6.5, 1.6.6 and 1.6.8.

1.6.4 REQUIREMENTS FOR PACKAGES CONTAINING URANIUM HEXAFLUORIDE

IAEA SSR-6	49 CFR §173*	Remarks
631	420(a)(2)	The content of the DN30 PSP, UF ₆ , is packed and transported according to [ANSI N14.1] and [ISO 7195] and in compliance with the requirements of para. 632 and 633.
632	420(a)(3)	(a) The 30B cylinder compliant with [ANSI N14.1] and [ISO 7195] withstands the hydraulic test with a test pressure of 2.76 MPa (the DN30 PSP is not affected by this test). (b) The DN30 package withstands, without loss or dispersal of the UF ₆ , the free drop test simulating NCT, see section 2.2.3. (c) The DN30 package withstands without rupture of the containment system the thermal test simulating HAC, see chapter 7 of Appendix 2.2.3.1 (Containment Analysis).
633	-	The DN30 package has no pressure relief valves

* Packages containing uranium hexafluoride are not specifically addressed in 10 CFR §71.

1.6.5 REQUIREMENTS FOR TYPE A PACKAGES

IAEA SSR-6	10 CFR §71	49 CFR §173	Remarks
635	-	412	The DN30 package is designed to meet the requirements of paras 607-618 and 636-651.
636	43(a)	412(b)	The smallest overall dimension is not less than 10 cm, see section 1.4.
637	43(b)	412(a)	There is a sealing system at the outside of the package, see section 1.4.2.3.8.
638	45(b)	412(i)	Each tie-down device that is a structural part of the package withstands the acceleration forces required by 10 CFR §71.45(b) without generating stresses in any material of the package in excess of its yield strength, see section 2.2.1.3.1. Any other structural part of the package that could be used to tie down the package can be rendered inoperable for tying down the package during transport. Each tie-down device that is a structural part of a package is designed so that failure of the device under excessive load would not impair the ability of the package to meet other requirements of 10 CFR §71, see section 2.2.1.3.3.
639	43(g), 71	412(c)	The design of the packaging takes into account for the components of the packaging temperatures ranging from -40 °C to +70 °C, see section 1.4.1.
640	31(c)	-	The design and manufacturing techniques are in accordance with ISO and EN standards.
641	43(c)	412(d)	The containment system is defined in section 1.4.3; unintentional opening is not possible as the containment system is enclosed in the DN30 PSP during transport; and the containment system withstands a test pressure of 2.76 MPa, which is much higher than the internal pressure during RCT and NCT.
642	4 (special form)	412(d)	Not applicable
643	43(c)	412(d)	The valve and plug are positive fastening devices, see section 1.4.3 or [ANSI N14.1] and [ISO 7195].
644	43(d)	412(e)	The design of the 30B cylinder is standardized in [ANSI N14.1] and [ISO 7195]; this design is world-wide in use since decades.
645	71(c)(3)	412(f)	The pressure in the 30B cylinder during transport is below atmospheric pressure. As the 30B cylinder withstands a test pressure of 2.76 MPa, the containment is not affected by a reduction of the ambient pressure of 25 kPa or 60 kPa.
646	43(e)	412(g)	The 30B cylinder with its valve is enclosed by the DN30 PSP during transport.
647	43(c)	412(h)	The 30B cylinder is enclosed in the DN30 PSP which is securely closed by a positive fastening device, see section 1.4.2.

IAEA SSR-6	10 CFR §71	49 CFR §173	Remarks
648	43(f)	412(j)	The DN30 package is so designed that if it were subjected to the tests simulating NCT it would prevent (a) loss or dispersal of the UF ₆ , see section 2.2.3 (b) more than 20% increase in the maximum radiation level at any external surface of the package, see section 2.2.4.7.5
649	87(d)	412(k)(1)	During transport the physical state of UF ₆ is solid; however, to make provisions for filling effects the 30B cylinder is filled to about 60 % to take care of the expansion of UF ₆ during the phase change of solid to liquid in case the UF ₆ is liquefied during filling/emptying.
650	-	412(k)(2)	Not applicable as during transport the physical state of UF ₆ is solid.
651	-	412(l)	Not applicable as during transport the physical state of UF ₆ is solid.

1.6.6 REQUIREMENTS FOR TYPE B PACKAGES (RELEVANT FOR THERMAL AND CONTAINMENT ANALYSIS)

IAEA SSR-6	10 CFR §71	Remarks
656	73(a)(4)	The initial temperature, the fire temperature and the ambient in the cooling phase comply with the requirements of this paragraph (RAI 3.1).
657	71(c)	The solar insolation data specified in this para. were used for the thermal assessment of the package (RAI 3.7).
659	51	The requirement for type B packages is used to derive a leak tightness criterion for type A packages for the containment analysis under NCT.

1.6.7 REQUIREMENTS FOR PACKAGES CONTAINING FISSILE MATERIAL

IAEA SSR-6	10 CFR §71	Remarks
673	55 and 59	<p>Subcriticality of the DN30 package is proven in section 2.2.5 under RCT, NCT and HAC taking into account:</p> <ul style="list-style-type: none"> i. Leakage of water into the packages from operation and the water immersion test to the extent as restricted by para. 680 (b). The maximal water ingress amounts to 3 g, see section 2.2.5.2.2. ii. There are no built-in neutron absorbers or moderators. iii. Rearrangement of the contents within the package (inside the 30B cylinder); a loss from the package has not to be considered. iv. Reduction of spaces within or between the packages. v. Packages becoming immersed in water or buried in snow (surrounded by water of varying density). vi. Temperature changes (affecting the density of the UF₆). <p>Following requirements are met:</p> <ul style="list-style-type: none"> i. The smallest overall dimension is not less than 10 cm, see section 1.4. ii. The requirements prescribed elsewhere in this compliance matrix. iii. There is a sealing system at the outside of the package, see section 1.4.2.3.8. iv. See paras 676-686.
674	15	The exceptions specified do not apply to the DN30 package.
675	15(f)	The content specification of the DN30 package does not comprise any Plutonium.
676	55(b)	The chemical form of UF ₆ is well known. For the isotopic compositions, maximal values of the fissile nuclide U-235 are assumed. Physical form, mass, concentration of impurities, moderation ratio or density and geometrical configuration are varied to determine the maximum neutron multiplication factor. The variation calculations are documented in section 2.2.5.5 respectively Appendix 2.2.5 (Criticality Safety Analysis).
677	55(b)	UF ₆ is not considered irradiated nuclear fuel.
678	55(d)(4)	<p>The DN30 package after the tests simulating NCT:</p> <ul style="list-style-type: none"> (a) Preserves minimum overall outside dimension of at least 10 cm, see section 2.2.1. (b) Prevents the entry of a 10-cm cube, see section 2.2.1.
679	71(c)(1 and 2)	The package is designed for a temperature range of -40 °C (see section 1.2.7) and +38 °C (see section 2.2.1).

IAEA SSR-6	10 CFR §71	Remarks
680	55(b) 55(g)	<p>For the individual DN30 package in isolation, containing uranium hexafluoride only, with a maximum uranium enrichment of 5 wt. % in U-235, it is assumed, that</p> <ul style="list-style-type: none"> Following the tests prescribed in [10CFR71] §71.59(a)2 or [IAEA 2012] para. 685 (b) there is no physical contact between the valve or plug and any other component of the packaging other than their original points of attachment, <p>And where, in addition</p> <ul style="list-style-type: none"> Following the test prescribed in [10CFR71] §71.73(c)4 or [IAEA 2012] para. 728 the valve and the plug remain leak tight. <p>These conditions are verified in section 2.2.1 and 2.2.2 and proved in the tests documented in Appendix 2.2.1.2 (Drop Test Reports) and Appendix 2.2.2.2 (Thermal Test Report).</p> <p>In section 1.9 the high degree of quality management and control for manufacturing, inspection (section 1.8) and repair of packagings as well as operations (section 1.7) is specified.</p>
681	55(b)(3)	The analysis for an individual package in isolation assumes at least a layer of 20 cm water surrounding the DN30 package, see section 2.2.5.5.1.
682	55(d) 55(e)	<p>The DN30 package is analyzed consistent with</p> <ul style="list-style-type: none"> (a) RCT (b) NCT (c) HAC <p>See section 2.2.5.</p>
683	55(f)	The DN30 package shall not be transported by air.
684	59(a)(1)	The number N derived for the DN30 package is infinite. The proof of subcriticality for NCT is contained in section 2.2.5.
685	59(a)(2)	The number N derived for the DN30 package is infinite. The proof of subcriticality for HAC is contained in section 2.2.5.
686	59(b)	For the DN30 package the following applies: CSI = 0.

1.6.8 TEST PROCEDURES

General test procedures			
IAEA SSR-6	10 CFR §71	49 CFR §173	Remarks
701	41	461	For the demonstration of compliance, the following methods are used: <ul style="list-style-type: none"> Performance of tests, see section 2.2.1.5, Appendix 2.2.1.2 (Drop Test Reports), section 2.2.2.2.3, Appendix 2.2.2.2 (Thermal Test Report). Analysis and calculations, see sections 2.2.1.4, 2.2.1.5 and 2.2.2.3.
702	-	-	The prototypes used for the tests are assessed before and after the tests according to written procedures, see Appendix 2.2.1.2 (Drop Test Reports), Appendix 2.2.2.2 (Thermal Test Report).
713	-	462(a)	The specimens are inspected before each test according to a written procedure. The results of the inspection are documented. The inspection comprises at least: <ul style="list-style-type: none"> (a) Divergence from the design (b) Defects in manufacture (c) Corrosion and deterioration (d) Distortion of features The inspection procedures are specified in Appendix 2.2.1.2 (Drop Test Reports), Appendix 2.2.2.2 (Thermal Test Report).
714	-	462(c)	The 30B cylinder with its valve and plug is the containment system.
715	-	462(d)	The prototypes are marked with a serial no. and can be easily referenced, see Appendix 2.2.1.2 (Drop Test Reports), Appendix 2.2.2.2 (Thermal Test Report).
716	-	-	The results of the tests are recorded, documented and assessed with respect to influence on the integrity of the containment and confinement system, Appendix 2.2.1.2 (Drop Test Reports), Appendix 2.2.2.2 (Thermal Test Report).
717	71(c)(7) 73(c)(1)	465(c)(5)	The target for drop tests complies with the requirements of [SSG-26], para. 718.2, see Appendix 2.2.1.2 (Drop Test Reports).
718	-	-	The 30B cylinder complies with [ANSI N14.1] and [ISO 7195] and is tested hydraulically with a test pressure of 2.76 MPa.

Tests for normal conditions of transport			
IAEA SSR-6	10 CFR §71	49 CFR §173	Remarks
719	71(a)	465(a)	See paras 722-724.
720	71(a)	465(b)	The time interval between the water spray test and the subsequent tests is not relevant, see para. 721.
721	71(c)(6)	465(b)	The DN30 PSP is a fully closed and welded structure of stainless steel. Any influence of the water spray test on the properties of the DN30 package can be excluded.
722	71(c)(7)	465(c)	The free drop test is analyzed in section 2.2.1 and carried out on prototypes as documented in Appendix 2.2.1.2 (Drop Test Reports).
723	71(c)(9)	465(d)	The shape of the packaging prevents stacking; hence the stacking test is omitted.
724	71(c)(10)	465(e)	The DN30 package is tested to withstand accident conditions of transport. The drop test onto the bar required under HAC is much more severe than the penetration test defined in para. 724.
725	-	466	Not applicable as during transport the physical state of UF ₆ is solid.

Tests for hypothetical accident conditions of transport		
IAEA SSR-6	10 CFR §71	Remarks
726	73(a)	A prototype used for testing was subject to the cumulative effects of twice the mechanical tests specified in para. 722 and followed by twice the tests specified in para. 727 and finally followed by the thermal test specified in para. 728, see section 2.2.2.3.2.2 and Appendix 2.2.2.2 (Thermal Test Report).
727 (a)	73(c)(1)	As the mass of the DN30 package exceeds a mass of 500 kg, the 9-m drop test is carried out. The test results are documented and analyzed in 2.2.1 and Appendix 2.2.1.2 (Drop Test Reports).
727 (b)	73(c)(3)	It was determined in analyses, that the most damaging drop tests sequence is the 9-m drop followed by the drop onto the bar. The test results are documented and analyzed in 2.2.1 and Appendix 2.2.1.2 (Drop Test Reports).
727 (c)	73(c)(2)	As the mass of the DN30 package exceeds a mass of 500 kg, the dynamic crush test is not applicable.
728	73(c)(4)	The thermal test is carried out using a specimen which suffered the cumulative effects of twice the mechanical tests specified in para. 722 and followed by twice the tests specified in para. 727.
729	73(c)(6)	The water immersion test is analyzed in section 2.2.1.5.2; leakage of water during this test is taken into account for the criticality safety analysis, see section 2.2.5.5.
731	73(c)(5)	Under the provisions of para. 680 (b) water leakage into the 30B cylinder has been excluded.
732	-	The test conditions before the water leakage test comply with the test conditions required by para. 659 and 685.
733	73(c)(5)	The test conditions of the water leakage test defined here are less stringent than the test conditions defined in para. 729.

1.7 OPERATION

Operation is subdivided into four lifetime phases of the DN30 packaging:

1. Testing and controls before its first use,
2. Regular usage and testing and controls before each transport,
3. Periodical inspection in defined intervals,
4. Repairs to return the DN30 packaging to service.

All these phases are regulated in manufacturing specifications, handling and test instructions specified below. At the time of application of these specifications and instructions, the user must make sure that valid revisions of these specifications and instructions are available.

1.7.1 TESTING REQUIREMENTS AND CONTROLS BEFORE FIRST USE

The testing requirements and controls before the first use of the packaging are specified in

- [ANSI N14.1] or [ISO 7195] for the 30B cylinder.
- Specification No. 0023-SPZ-2016-001 for the DN30 PSP (see Appendix 1.9.2 (Manufacturing Specification)).

1.7.2 TESTING REQUIREMENTS AND CONTROLS BEFORE EACH TRANSPORT

The testing requirements and controls before each transport are described in

- [ANSI N14.1] or [ISO 7195] as well as [USEC 651] (or in equivalent plant specific instructions) for the 30B cylinder (see section 1.7.2.1 for details).
- Handling instruction No. 0023-HA-2015-001 (see Appendix 1.7.1 (Handling Instruction)) for the DN30 PSP (see section 1.7.2.2 for details).

For annual and 5-year inspection requirements as well as treatment of non-conformances and deviations, see section 1.8.

1.7.2.1 Inspection of the 30B cylinder

Before filling the 30B cylinder, inspections in accordance with [ANSI N14.1] or [ISO 7195] and at least as described in [USEC 651] (or in equivalent plant specific instructions) shall be carried out:

- The 30B cylinder shall be handled and filled in accordance with [ANSI N14.1] or [ISO 7195] and at least as described in [USEC 651].
- Any defective condition must be corrected before filling according to the requirements of [ANSI N14.1] or [ISO 7195]:
 - The 30B cylinder shall be routinely examined as received and prior to sampling, withdrawal, filling, or shipping to ensure that it remains in a safe and usable condition.
 - Leakage, cracks, excessive distortion, bent or broken valves or plugs, broken or torn skirts, or other conditions that may affect the safe use of the cylinder

shall warrant appropriate precautions, including removing the cylinder from service until the defective condition is satisfactorily corrected.

- Questionable conditions should be referred to a qualified inspector for evaluation and for recommendations concerning use, repair, or condemnation of the cylinder in question.
- Before filling, the cylinder is weighted to establish the net weight of the heels to ensure the fill limit will not be exceeded.
- To avoid overfilling, the 30B cylinder shall be weighted after being filled.

Before loading into the DN30 PSP, the inspection of the 30B cylinder should be carried out in accordance with [ANSI N14.1] or [ISO 7195], and at least as described in [USEC 651] (or in equivalent plant specific instructions):

- Before shipping, the 30B cylinder shall be inspected for leak-tightness, damage, as well as other unacceptable conditions.
- UF₆ shall be shipped only in its solid state and when the vapor pressure within the 30B cylinder is below atmospheric.
- The safe state of the 30B cylinder shall be recorded by the UF₆ supplier and the record shall be provided to the shipper.

Special care must be taken to ensure that the cylinder fulfills the leak-tightness criteria of [ANSI N14.1] or [ISO 7195] and the requirements of this SAR.

- The leak tightness of the valve seat of a filled cylinder shall be verified by leak rate testing of the pigtail before disconnection and after closing the cylinder valve seat.
- A leak rate larger than 1×10^{-4} Pa.m³/s SLR (Standardized Leakage Rate) shall not be permitted.
- The leak test method shall comply to the [ANSI N14.5] or [ISO 12807] standard.
- If air is used for a pressure drop test, the air supply should be clean, dry and free from oil. If it is not, or if the quality of the air supply is uncertain, the test should be performed with nitrogen to ensure reliable results.
- Alternatively, a vacuum test may be performed by attaching a pigtail to the closed cylinder valve and drawing a vacuum (Note: the cylinder's outer surface shall be approximately at ambient temperature and its vapor pressure below atmospheric pressure).

1.7.2.2 Inspection of the DN30 PSP

The DN30 PSP shall be inspected prior to loading according to handling instruction No. 0023-HA-2015-001. The inspection comprises:

- A visual inspection
- A functional test of all movable parts

Following observations shall be cause for further investigation, replacement of parts or rejection of the DN30 PSP as specified in detail in test instruction No. 0023-PA-2015-016 (see Appendix 1.8.2 (Inspection Criteria)):

- Structural changes of exterior or interior shells, like excessive deformations, cracks, holes, etc.
- Excessive damage of flange areas
- Missing or damaged marking of the DN30 PSP
- Missing or damaged thermal plugs
- Missing or damaged gasket
- Damage of the mortise-and-tenon closure system
- Damage of the valve protecting device as well as functional issues
- Damage of the rotation preventing device as well as functional issues
- Excessive wear and tear of the thermal protective material
- Damage to any welding seams like cracks, holes, excessive corrosion
- Excessive damage of handling devices

Test instruction No. 0023-PA-2015-016 contains in detail the inspection criteria and the measures in case of deviations. Measures could comprise cleaning, replacement of parts, minor repairs (on site), major repairs (to be carried out by the license holder or an authorized repair shop qualified for such repair).

1.7.3 HANDLING AND TIE DOWN REQUIREMENTS

Handling of the DN30 package and packaging and its parts is described in section 1.4.2.4. For the handling operations adequate means as described in the handling instruction No. 0023-HA-2015-001 have to be used.

Tie-down of the DN30 package and packaging is described in section 1.4.2.5. The procedures to be applied to ensure proper tie-down are specified in the handling instruction No. 0023-HA-2015-001.

1.7.4 LOADING PROCEDURES FOR THE 30B CYLINDER AND THE DN30 PSP

Before each use, the 30B cylinder and the DN30 PSP shall be inspected as described in section 1.7.2.1 and section 1.7.2.2, respectively.

1.7.4.1 Loading and unloading of UF₆ content into the 30B cylinder.

Filling of the 30B cylinder with UF₆ is described in the site specific operating handbooks, which are not part of this SAR. It must be assured that before transport the 30B cylinder was given ample time for cooling down such that the UF₆ is in solid state.

The testing and controls required in section 1.7.2 shall be performed and documented prior to loading a 30B cylinder into the DN30 package. Further any 30B cylinder filled with either UF₆ or heels from UF₆ should comply with the transport regulatory requirements for UF₆.

1.7.4.2 Loading of the 30B cylinder into the DN30 PSP

An overview of the safety related loading steps during loading of a 30B cylinder into the DN30 PSP is listed in the following. Details of the handling steps are specified in handling instruction No. 0023-HA-2015-001.

- 1) The lever of the rotation preventing devices are in position “open”.
- 2) The valve protecting device and its housing are in position “open”.
- 3) Lower the 30B cylinder in horizontal orientation with the valve in 12° o'clock position into the bottom half of the DN30 PSP.
- 4) When the lower rim of the cylinder skirt has passed the valve protecting device, rotate this valve protecting device towards the cylinder head by approx. 90° until it is in contact with the cylinder head. Then lower the cylinder until it rests on the inner shell of the bottom half of the DN30 PSP. Then push the housing in position “closed”.
- 5) Move the lever of the rotation preventing devices to position “closed”.
- 6) Lower the top half of the DN30 PSP onto the bottom half.
- 7) Insert the pins into the six mortise-and-tenon closure devices and fix the pins with the securing bolts.
- 8) Install the seals.

1.7.4.3 Unloading of the 30B cylinder from the DN30 PSP

In order to prevent damage of any safety related feature during unloading, the following general steps are required. Details are given in handling instruction No. 0023-HA-2015-001.

- 1) Check and remove the seals.
- 2) Loosen the securing bolts and remove the pins of the six mortise-and-tenon closure devices.
- 3) Lift off the top half of the DN30 PSP.
- 4) Move the lever of the rotation preventing devices to position “open”.
- 5) Pull the housing from the valve protecting device in position “open”.
- 6) Lift the 30B cylinder and rotate the valve protecting device by about 90° until it rests on the flange of the bottom half.
- 7) Lift the 30B cylinder out of the bottom half of the DN30 PSP.

1.7.5 SUPPLEMENTARY EQUIPMENT AND OPERATIONAL CONTROLS

No supplementary equipment except means for tie-down are used during transport of the DN30 package in any transport modes.

1.7.6 **PRECAUTIONS AND MEASURES DUE TO THE OTHER DANGEROUS PROPERTIES OF THE CONTENT**

No precautions and measures due to the other dangerous properties of the content are required except for the correct labeling according to the respective transport modes.

1.8 INSPECTION

1.8.1 ANNUAL INSPECTION REQUIREMENTS FOR THE DN30 PSP

The annual inspections of the DN30 PSP are described in test instruction No. 0023-PA-2015-015 (see Appendix 1.8.1 (Periodical Inspections)) and test instruction No. 0023-PA-2015-016 (see Appendix 1.8.2 (Inspection Criteria)), in which the criteria for the checks are defined and measures in case of non-conformances or deviations are specified.

In the case that non-conformances or deviations might affect the safety of the DN30 packaging the user of the packaging has to inform the owner of the certificate of package approval in writing about the non-conformance or deviation. It is then the decision of the owner of the certificate of package approval to undertake suitable measures to return the packaging to service in full compliance with the SAR and the certificate of package approval.

1.8.2 5-YEAR INSPECTION REQUIREMENTS FOR THE 30B CYLINDER AND THE DN30 PSP

The 5-year periodical inspections of the DN30 packaging are subdivided into the periodical recertification of the 30B cylinder and the periodical inspection of the DN30 PSP.

The 5-year inspection of the 30B cylinder shall be performed in accordance with [ANSI N14.1] or [ISO 7195] and at least as described in USEC 651 (or in equivalent plant specific instructions). This inspection includes, but is not limited to, the following:

- 30B cylinders, except those already filled at the 5-year expiration date, are to be periodically inspected and tested throughout their service life.
- 30B cylinders that have not been inspected and tested within the required 5-year period shall not be refilled until they are properly reinspected and retested. Prior to shipment, 30B cylinders that have not been recertified within the 5-year requirement shall be visually inspected for degradation of the cylinder wall. Any questionable conditions should be investigated. Details on the visual inspection are provided in attachment 2 of 0023-PA-2015-015 (see Appendix 1.8.1 (Periodical Inspections)).
- The 5-year periodic inspections and tests consist of the following:
 - An internal and external examination of the 30B cylinder by a qualified inspector.
 - A hydrostatic strength test as described in [ANSI N14.1] or [ISO 7195].
 - When a valve or plug change has occurred, a 100 psig pneumatic leak-test as described in [ANSI N14.1] or [ISO 7195] is required.
- After a 30B cylinder is tested, its outer shell may be cleaned and repainted. At each 5-year periodic inspection, the cylinder shall have the tare weight re-established.
- A 30B cylinder shall be removed from service (for repair or replacement) when it is found to contain leaks, corrosion, cracks, bulges, dents, gouges, defective valves, damaged skirts, or other conditions that, in the opinion of a qualified inspector, render it unsafe or unserviceable in its existing condition.
- A 30B cylinder shall no longer be used in UF₆ service when the shell thickness has decreased below 5/16 in.

The periodical inspections of the DN30 PSP are described in test instruction No. 0023-PA-2015-015 (see Appendix 1.8.1 (Periodical Inspections)) and test instruction No. 0023-PA-2015-016 (see Appendix 1.8.2 (Inspection Criteria)), in which the criteria for the checks are defined and measures in case of non-conformances or deviations are specified.

In case non-conformances or deviations might affect the safety of the DN30 packaging, the user of the packaging has to inform the owner of the certificate of package approval in writing about the non-conformance or deviation. It is then the decision of the owner of the certificate of package approval to undertake suitable measures to return the packaging to service in full compliance with the SAR and the certificate of package approval.

1.9 MANAGEMENT SYSTEM

The management system of company DAHER NUCLEAR TECHNOLOGIES GmbH (DAHER NT) is laid down in the Integrated Management Handbook (see Appendix 1.9.1 (IMS)).

The management system is certified according to

- DIN EN ISO 9001
- DIN EN ISO 14001
- OSHAS 18001
- KTA 1401
- BAM GGR 011
- 10CFR71 subpart H

covering design and development, manufacturing and operation of packagings for packages requiring approval by the competent authorities for the transport of radioactive material.

Appendix 1.9.3 (Quality Assurance Program) contains a description of the DAHER NT quality assurance program that demonstrates compliance with the specific requirements of Subpart H of [10CFR71]. The appendix also contains the NRC approval of this program.

1.9.1 DESIGN, SAR, DOCUMENTATION AND RECORDS

1.9.1.1 General

The 30B cylinder is specified in [ANSI N14.1] and [ISO 7195]. These standards define the design, manufacturing, inspection and controls before first use and operation including maintenance and periodical recertification of the 30B cylinder. No additional documents are provided by DAHER NT for this component of the DN30 package design.

DAHER NT is responsible for the design, development, safety analyses, manufacturer planning and surveillance, inspection and controls before first use and operation including maintenance and periodical recertification of the DN30 PSP.

All documents like drawings, calculations, specifications etc. are written, checked and released in accordance with the IMS of DAHER NT. The author and the examiner must be experienced in the respective field of technology whereas the person releasing the document must be authorized according to the organizational structure of DAHER NT. For each field of technology, the different roles of the employees of DAHER NT are described in the IMS.

Any design modifications including any revisions of specifications, drawings and instructions are carried out according to the processes laid down in the IMS and documented accordingly.

In case there are documents from suppliers, DAHER NT will check these documents according to the process laid down in the IMS.

1.9.1.2 Design

DAHER NT is responsible for the whole design process from establishing the requirements based on the applicable regulations and standards up to the completion of the drawings, safety analyses and the manufacturing specification. All individual steps necessary for the design process are stipulated in the IMS of DAHER NT.

Design modifications required due to the progress in carrying out the safety analyses or resulting from the outcome of physical tests with specimens or prototypes are introduced into the design process in compliance with the respective process described in the IMS of DAHER NT.

1.9.1.3 Documents and Records

Traceability of each document and record relevant during the design process is assured by the requirements of the IMS of DAHER NT with respect to a unique numbering and filing system.

For each document written and released by DAHER NT, the original workable document is stored together with the signed document as image. For documents and records of suppliers only the image of the document might be made available and stored.

During the design process the documents listed in section 1.0 are produced and filed.

1.9.2 MANUFACTURING AND TESTING

1.9.2.1 Manufacturing of 30B cylinders

Manufacturing of 30B cylinders is specified in [ANSI N14.1] and [ISO 7195].

1.9.2.2 Manufacturing of serial DN30 PSPs

Qualification and selection of the manufacturer as well as the requirements towards QA during material procurement, manufacturing and final inspection before first use are specified in manufacturing specification No. 0023-SPZ-2016-001 (see Appendix 1.9.2 (Manufacturing Specification)). This specification details among others the following requirements:

- Qualification of manufacturer,
- Scope of services and responsibilities of manufacturer,
- Responsibilities of DAHER NT,
- Requirements for materials including certification,
- Requirements concerning fabrication including welding,
- Requirements concerning final acceptance test,
- Treatment of non-conformances,
- Manufacturing test sequence plan (MTSP).

1.9.2.3 Testing of samples and prototypes

Manufacturing and testing of samples and prototypes is managed comparably to the standards specified for the serial DN30 PSPs.

Samples for mechanical and thermal testing of the foam used as shock absorbing material and thermal insulation are manufactured, certified and documented identically to the foam used in the prototypes and serial DN30 PSPs.

Samples for thermal testing of the thermal intumescent material are manufactured, certified and documented identically to the intumescent material used in the prototypes and serial DN30 PSPs.

The tests to determine the properties of foam and intumescent material are documented in the summary reports contained in Appendix 1.4. For these tests qualified institutes were involved:

- The Material Testing Institute, University of Stuttgart (MPA), for the mechanical tests.
- The institute for combustion and gas dynamics, University of Duisburg-Essen, for the analysis of the chemical composition of the foam under different thermal conditions.
- Company Influtherm, an independent society specialized in thermal measurements and services, for the measurement of the thermal properties of the foam and the intumescent material.
- Company Thermoconcept, an independent society specialized in thermal measurements and services, for the measurement of the thermal conductivity of expanded intumescent material.
- Company Mecanium, an independent society specialized in mechanical measurements and services, for the measurement of the expansion forces of the intumescent material.

Tests with prototypes were carried out by the BAM. For package approvals originating in Germany, BAM is one part of the German competent authorities and responsible for mechanical, thermal and containment analysis as well as QA.

1.9.3 OPERATION

The quality management requirements for operation are specified in the handling instruction No. 0023-HA-2015-001 (see Appendix 1.7.1 (Handling Instruction)).

In the case that the DN30 PSP is leased out for transports to a customer, the handling instruction will be provided to the respective customer and he has to confirm in writing that he will comply with the requirements stipulated there.

In case the DN30 PSP is sold to a customer, the handling instruction and the test instruction regulating regular and periodical inspections will be provided to the respective customer and he has to confirm in writing that he will comply with the requirements stipulated there.

1.9.4 MAINTENANCE AND REPAIR

The quality management requirements for periodical inspections of the DN30 PSP are described in test instruction No. 0023-PA-2015-015 (see Appendix 1.8.1 (Periodical Inspections)).

Both of these instructions, No. 0023-HA-2015-001 and No. 0023-PA-2015-015 refer to test instruction No. 0023-PA-2015-016 (see Appendix 1.8.2 (Inspection Criteria)), in which the non-conformances and deviations are described for which repair is required. In all cases where repair is required DAHER NT must be involved in the planning, authorization and execution of the repair measures.

For repair other than replacement of parts, the specification No. 0023-SPZ-2016-001 (see Appendix 1.9.2 (Manufacturing Specification)) must be complied with.

1.9.5 COMPLIANCE OF ANY ACTIVITY WITH THE SAR

Specification No. 0023-SPZ-2016-001 (see Appendix 1.9.2 (Manufacturing Specification)) ensures that during manufacturing and final acceptance test before first use the requirements of the SAR towards the design are met. In detail the following requirements are considered:

- Specification of the material properties in material data sheets to comply with the properties used throughout this SAR.
- Requirements for welders and welding to ensure the structural properties of the DN30 PSP as defined in this SAR.
- Specification of tests and documentation during manufacturing and before first use to ensure that the design of the DN30 PSP complies with the drawings.

Handling instruction No. 0023-HA-2015-001 (see Appendix 1.7.1 (Handling Instruction)) and test instruction No. 0023-PA-2015-015 (see Appendix 1.8.1 (Periodical Inspections)) together with the applicable secondary document test instruction No. 0023-PA-2015-016 (see Appendix 1.8.2 (Inspection Criteria)) ensure that during operation the DN30 is always kept in compliance with the SAR.

1.9.6 DEVIATIONS

Deviations concerning the safety elements listed in Table 13 are to be reported to the Competent Authority.

The corrective actions implemented are also to be reported to the Competent Authority.

1.9.7 SAFETY ELEMENTS

The safety elements of the DN30 Package are summarized in Table 13.

Table 13: Safety elements

Element of the package	Safety function	Parameters
Closure system	Mechanical protection	<ul style="list-style-type: none"> • Welds • Absence of structural defects • Completeness
Outer shell	Mechanical protection	<ul style="list-style-type: none"> • Welds • Absence of structural defects in the steel sheets
Foam	Mechanical protection	<ul style="list-style-type: none"> • Thickness • Density
Microtherm ®	Thermal protection	<ul style="list-style-type: none"> • Thickness • Thermal conductivity
Promaseal-PL®	Thermal protection	<ul style="list-style-type: none"> • Thickness • Completeness • Thermal conductivity
Inner shell	Mechanical protection	<ul style="list-style-type: none"> • Welds • Absence of structural defects in the steel sheets
Valve protecting device	Mechanical protection	<ul style="list-style-type: none"> • Welds • Absence of structural defects in the steel sheets • No unacceptable deformation of the housing • Completeness
Plug protecting device	Mechanical protection	<ul style="list-style-type: none"> • Welds • Absence of structural defects
Rotation preventing devices	Mechanical protection	<ul style="list-style-type: none"> • Welds • Absence of structural defects of the bolts • Completeness
30B cylinder	Containment	<ul style="list-style-type: none"> • Compliance with [ANSI N14.1] and [ISO 7195]

1.10 PACKAGE ILLUSTRATION

Figure 7 and Figure 8 show an illustration of the DN30 package. Appendix 1.4.1 (Drawings) contains the set of drawings for the DN30 PSP. The 30B cylinder is specified and shown in [ANSI N14.1] and [ISO 7195].

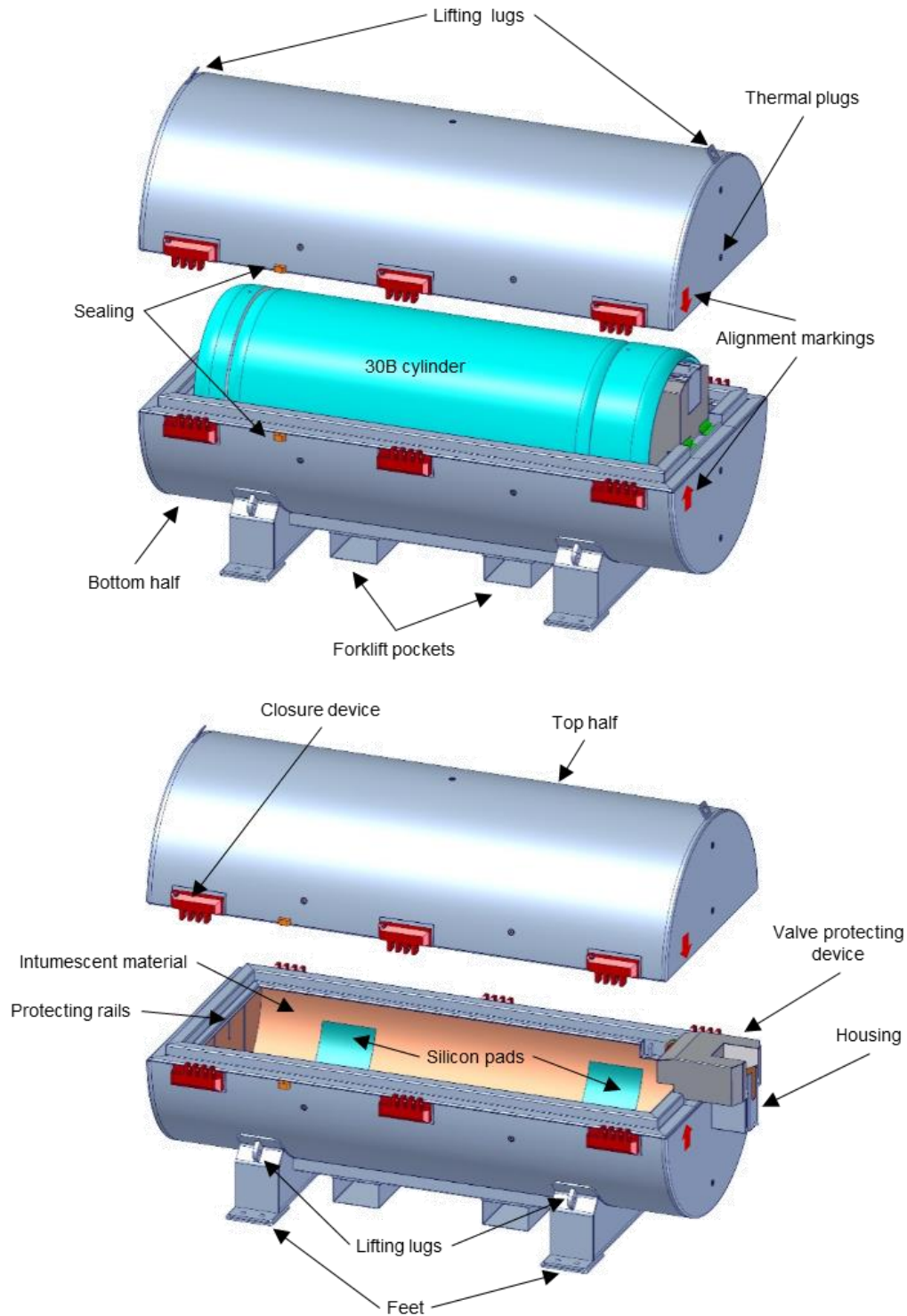


Figure 7: DN30 PSP overview

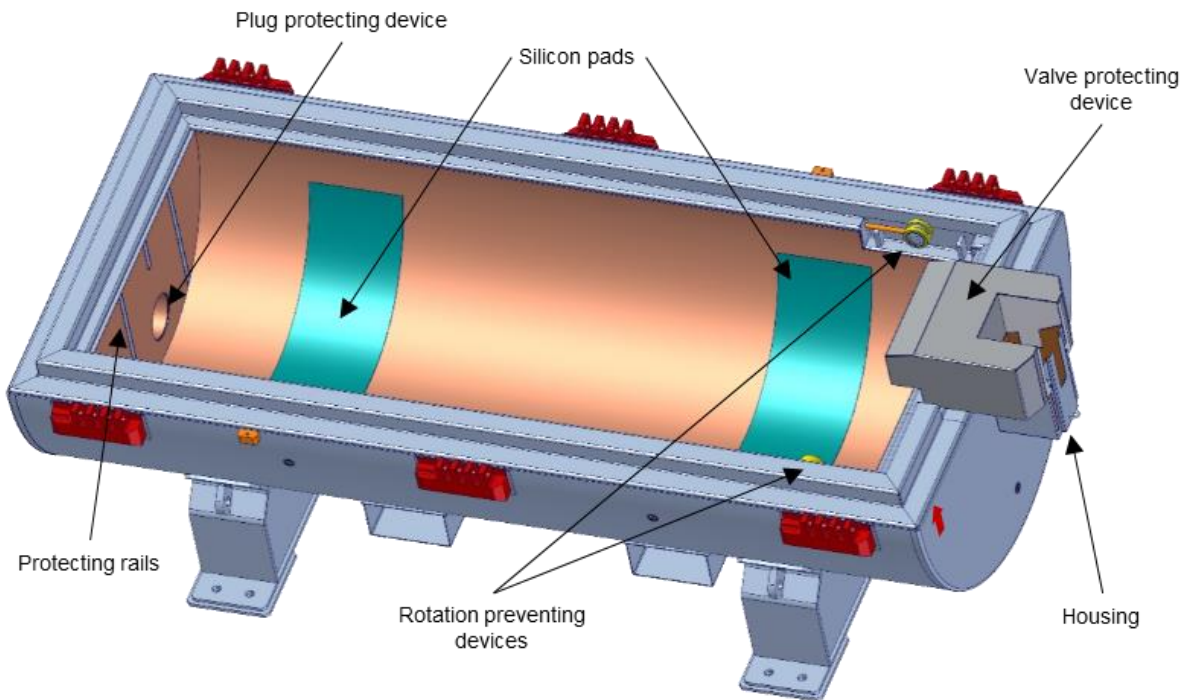


Figure 8: DN30 PSP bottom half

PART 2

2.1 COMMON PROVISIONS FOR ALL TECHNICAL ANALYSES

In this section, the common provisions valid for all technical analyses are described. For a better overview, the provisions of the respective technical analysis that might have an influence on other analyses are summarized as an extract from the detailed technical analysis.

2.1.1 PACKAGE DESIGN

The analyzed package design is described in section 1.3 (content) and in section 1.4 (30B cylinder and DN30 PSP).

2.1.1.1 Content

The content for all analyses is UF_6 . However, for the different analyses only a few properties of the material are relevant and taken into account:

- For the structural analysis, the density and the elastic-plastic material properties of the content are relevant. Because of its high toxicity, radioactivity and heavy reaction with water, performing tests with UF_6 is a difficult task and, thus, there is only limited information available on the mechanical properties of solid UF_6 . For this reason, a surrogate material is used to simulate the UF_6 content.

Heavy concrete has been proven to be an acceptable surrogate material for the structural analysis of the DN30 package. To comply with the density of solid UF_6 , the heavy concrete is mixed with steel shot. It is assumed that the heavy concrete fills about 60 % of the lower part of the 30B cylinder (standard transport configuration).

- For the thermal analysis, the relevant physical properties are the density, the thermal conductivity and the specific heat capacity. It is assumed that the UF_6 content fills about 60 % of the lower part of the 30B cylinder (standard transport configuration). Scenarios with a partially filled 30B cylinder are analyzed, too.
- For the containment analysis, the relevant physical property is the viscosity of gaseous UF_6 . For this analysis, the content configuration has no influence on results.

The source terms and physical properties of the radioactive contents (commercial grade UF_6) are specified in section 1.3.

- For the external dose rate analysis, the relevant physical properties are the density and the shielding properties of UF_6 . Conservatively, different filling ratios of the cylinder are considered up to a theoretically possible 100 % filled 30B cylinder, which exceeds the allowed maximal content mass of 2277 kg.

For cylinders containing heels, different configurations with a small amount of residues are analyzed. The configurations are heels forming a puddle at the lower side of the 30B cylinder or the homogeneous contamination of parts or the whole inner surface of the 30B cylinder shell with UF_6 .

The source terms and physical properties of the radioactive contents (commercial grade UF_6) are specified in section 1.3.

- For the criticality safety analysis, the relevant physical properties are the density, the purity (hydrogen impurities) and the nuclear physical properties of the nuclides present in UF_6 . A variety of configurations is analyzed comprising a 30B cylinder containing the maximal allowed 2277 kg UF_6 , a partially filled 30B cylinder, UF_6 forming a layer at the

inner surface of the 30B cylinder, grained structures and local concentrations of impurities.

2.1.1.2 30B cylinder

The 30B cylinder design is standardized and defined in [ANSI N14.1] or [ISO 7195].

- For the structural analysis, the nominal dimensions are assumed.
- For the thermal analysis, the nominal dimensions are assumed. For the material, standard physical properties are assumed.
- For the containment analysis, neither the dimensions nor the physical properties of the 30B cylinder are relevant.

However, the free volume inside the 30B cylinder is part of the analysis and for the evaluation of this parameter the nominal volume of the 30B cylinder reduced by the respective filling ratios is assumed. Furthermore, the design of the valve, especially the connection to the cylinder shell and the seat of the valve are taken into account based on the standards.

- For the external dose rate analysis, a simplified 30B cylinder with flat ends is assumed.
- For the criticality safety analysis, a simplified model with flat ends as well as a model with round ends are analyzed. Furthermore, dimensions and wall thickness are varied to assess the most reactive cases.

2.1.1.3 DN30 PSP

The design of the DN30 PSP is defined in the drawings specified in section 1.4.

- For the structural analysis, the nominal dimensions are assumed. The influence of temperature on the mechanical behavior of the package is analyzed in variation calculations. The maximum temperature of the package is evaluated in the thermal analysis. The minimum temperature of -40 °C is required by the transport regulations.
- For the thermal analysis under RCT and NCT, the nominal dimensions and standard physical properties are assumed.

For the thermal analysis under HAC, the standard dimensions and deteriorated physical properties are assumed. Furthermore, incineration of the foam as experienced in the thermal test is modelled.

- For the containment analysis the DN30 PSP is not taken into account.
- For the external dose rate analysis, the nominal dimensions and standard physical properties are assumed. For the analysis of the external dose rate under HAC the foam as well as the distance between inner and outer shell of the DN30 PSP are neglected.
- For the criticality safety analysis, only the stainless-steel shells of the DN30 PSP are taken into account. The foam material is neglected and the steel shells are compacted to a single layer of steel with a thickness of 5 mm, thereby minimizing the distance between adjacent packages.

2.1.1.4 Summary of the material characteristics used for the technical analyses

The mechanical and the thermal properties used in the technical analyses are summarized in Table 14 and Table 15.

Table 14: Mechanical properties used for the static analyses

Material	Grade	Mechanical properties at 20 °C	Reference
Steel*	1.4301	$R_{p0.2} = 220 \text{ MPa}$	See Table 21
		$R_m = 520 \text{ MPa}$	
		$E = 2.00E5 \text{ MPa}$	
	1.4541	$R_{p0.2} = 190 \text{ MPa}$	See Table 24
		$R_m = 500 \text{ MPa}$	
		$E = 2.00E5 \text{ MPa}$	
	1.4542	$R_{p0.2} = 720 \text{ MPa}$	See Table 26
		$R_m = 930\text{-}1100 \text{ MPa}$	
		$E = 2.00E5 \text{ MPa}$	
	1.4462	$R_{p0.2} = 460 \text{ MPa}$	See Table 27
		$R_m = 640 \text{ MPa}$	
		$E = 2.00E5 \text{ MPa}$	
Foam	RTS 120	Density = 120 kg/m^3	See section 4.4.4 of appendix 2.2.1.3
		$E = 1004 \text{ MPa}$	
		Poisson's ratio = 0.08	
		Tensile stress cut-off = 1.7 MPa	
	RTS 320	Density = 320 kg/m^3	See section 4.4.4 of appendix 2.2.1.3
		$E = 3000 \text{ MPa}$	
		Poisson's ratio = 0.08	
		Tensile stress cut-off = 6 MPa	
Intumescent material	PROMASEAL-PL®	**	**
Insulation	MICROTHERM®	**	**

* The mechanical properties given here are taken from [DIN EN 10088-2] and are used for the static analysis for handling and under RCT. The properties used for the dynamic analysis under NCT and HAC were taken from the properties of the different steel parts of the prototypes used for testing. These are given in Appendix 2.2.1.3 detailing the dynamic calculations.

** The intumescent and insulation material are used in the thermal analysis, but are not considered in the structural analysis.

Table 15: Thermal properties used for the analyses

Material	Grade	Thermal properties*	Reference
Stainless Steel	1.4301/ 1.4541/ 1.4542/ 1.4462	$\lambda = 14.9 \text{ W/(m}\cdot\text{K)}$	[BAILEY]
		$\rho = 7940 \text{ kg/m}^3$	[BAILEY]
		$c_P = 460 \text{ J/(kg}\cdot\text{K)}$	[BAILEY]
Carbon Steel	See Table 4	$\lambda = 50 \text{ W/(m}\cdot\text{K)}$	
		$\rho = 7821.2 \text{ kg/m}^3$	
		$c_P = 500 \text{ J/(kg}\cdot\text{K)}$	
Foam	RTS 120	$\lambda = 0.035 \text{ W/(m}\cdot\text{K)}$	See Appendix 1.4.2
		$\rho = 120 \text{ kg/m}^3$	See Appendix 1.4.2
		$c_P = 1323 \text{ J/(kg}\cdot\text{K)}$	See Appendix 1.4.2
	RTS 320	$\lambda = 0.049 \text{ W/(m}\cdot\text{K)}$	See Appendix 1.4.2
		$\rho = 320 \text{ kg/m}^3$	See Appendix 1.4.2
		$c_P = 1284 \text{ J/(kg}\cdot\text{K)}$	See Appendix 1.4.2
Intumescent material	PROMASEAL-PL®	$\lambda = 0.19 \text{ W/(m}\cdot\text{K)}$	See Appendix 1.4.3
		$\rho = 1000 \text{ kg/m}^3$	See Appendix 1.4.3
		$c_P = 1232 \text{ J/(kg}\cdot\text{K)}$	See Appendix 1.4.3
Insulation	MICROTHERM®	$\lambda = 0.026 \text{ W/(m}\cdot\text{K)}$	See Appendix 1.4.4
		$\rho = 260 \text{ kg/m}^3$	See Appendix 1.4.4
		$c_P = 920 \text{ J/(kg}\cdot\text{K)}$	See Appendix 1.4.4
Air (in gaps)	-	$\lambda = 0.0258 \text{ W/(m}\cdot\text{K)}$	
		$\rho = 0.8 \text{ kg/m}^3$	
		$c_P = 1000 \text{ J/(kg}\cdot\text{K)}$	
UF ₆	-	$\lambda = 0.519 \text{ W/(m}\cdot\text{K)}$	[WITT 1960]
		$\rho = 3093.8 \text{ kg/m}^3$	[WITT 1960]
		$c_P = 497 \text{ J/(kg}\cdot\text{K)}$	[WITT 1960]

* λ = Thermal conductivity, ρ = Density, c_P = Heat capacity; only the thermal properties for a temperature of approx. 20 °C are listed here, the complete thermal properties are listed in Appendix 2.2.2.3 (Thermal Analysis).

2.1.2 ACCEPTANCE CRITERIA AND DESIGN ASSUMPTIONS

2.1.2.1 Mechanical design

The acceptance criteria and design assumptions for the mechanical design are:

- Lifting attachments that are a structural part of a package are designed with a minimum safety factor of three against yielding when used to lift the package in the intended manner. Failure of any lifting device under excessive load does not impair the ability of the package to meet other requirements of [10CFR71].
- The tie-down devices that are a structural part of the package withstand, without generating stress in any material of the package in excess of its yield strength, a static force applied to the center of gravity of the package having a vertical component of 2 times the weight of the package with its contents, a horizontal component along the direction in which the vehicle travels of 10 times the weight of the package with its contents, and a horizontal component in the transverse direction of 5 times the weight of the package with its contents. Failure of the devices under excessive load does not impair the ability of the package to meet other requirements of [10CFR71].
- No physical contact of the 30B cylinder valve with any other packaging component except for the initial point of connection (thread).
- No physical contact of the 30B cylinder plug with any other packaging component except for the initial point of connection (thread).
- No failure of the 30B cylinder containment system. Any deformation of the 30B cylinder shell must be classifiable as acceptable damage according to [ANSI N14.1] or [ISO 7195].
- No failure of the DN30 closure system.

The evaluation of these design criterions for the DN30 package is possible without considering material damage or failure in the FEM model of the DN30 package, even if local deformations of the DN30 PSP shells above the uniform elongation occur. However, the following must be considered in this case:

- The material models for the steel parts cover the inelastic range up to the uniform elongation. For plastic strains above the uniform elongation, the discrepancy compared to the real material behavior increases successively because of the negligence of a damage and failure model. Thus, failure analysis of certain parts of the DN30 PSP shall be based on the experimental drop tests only.
- Locations with plastic strains above the uniform elongation and close to or above the elongation at fracture can be compared with the corresponding areas of the prototypes used for the experimental drop tests. If those locations match and failure occurred in the experimental drop tests, the exact value of the plastic strain is of no importance for the safety of the DN30 package because the fire test under HAC was passed with fractures in the inner and outer shells of the DN30 PSP.
- An analysis with previously introduced cracks in the inner shell of the DN30 FEM model, exceeding the cracks observed after the drop tests, proves that safety relevant simulation results are not sensitive to failure of the inner steel shells. The results of this sensitivity analysis are documented in chapter 5 of [DAHER 2019-1].

2.1.2.2 Thermal design

The acceptance criteria and design assumptions for the thermal design are:

- The temperatures at the 30B cylinder, including valve, plug and shell, should not exceed 131 °C (see section 2.2.2.1.4) during the thermal test simulating HAC for a package in the condition after the mechanical tests simulating NCT and HAC. The leakage rate after the test should be less than 1.0 E-4 Pa·m³/s after the test.
- No failure of the 30B cylinder containment system.

The thermal design takes into account different filling ratios between a full cylinder containing 2277 kg UF₆ and an empty cylinder containing heels.

2.1.2.3 Containment system design

The acceptance criteria and design assumptions for the containment system design are:

- Under NCT, the loss or dispersal of UF₆ must be prevented.
- The containment is the 30B cylinder with its valve and plug.
- The DN30 PSP has no containment function.

2.1.2.4 External dose rate assessment

The acceptance criteria and design assumptions for the external dose rate assessment are:

- The external dose rate limits for HAC, NCT and HAC as defined in [49CFR173] or [IAEA 2012] must not be exceeded.
- For the assessment of the dose rates, conservative assumptions with respect to the cylinder filling ratio and the shape of the 30B cylinder are used.
- For the assessment of the dose rate at the vehicle, two and four packages loaded side by side are considered, respectively.
- For the assessment of the dose rate increase after the tests simulating NCT, a permissible deformation is evaluated for filled cylinders (with respect to the limit of 20 % dose rate increase) and compared with the deformations calculated for NCT. Additionally, the dose rate increase is assessed for cylinders containing heels of UF₆ by taking into account conservative assumptions.

2.1.2.5 Criticality safety assessment

The acceptance criteria and design assumptions for the criticality safety assessment are:

- Criticality safety is ensured by the 30B cylinder and the steel shells of the DN30 PSP, which are compacted to a single layer of steel with a thickness of 5 mm, thereby minimizing the distance between adjacent packages.
- The foam is not a part of the confinement system.
- For RCT, NCT and HAC the criticality safety criterion is $k_{\text{eff}} + 3\sigma + \Delta k < 0.95$ (see section 2.2.5.1 for details).

2.1.3 DESCRIPTION AND JUSTIFICATION OF ANALYSIS METHODS

2.1.3.1 Structural analysis

2.1.3.1.1 Structural analysis for RCT

The structural analysis for RCT comprises

- Analysis of the lifting attachment points.
- Analysis of the features of the packaging used for tie-down.

These analyses are carried out by hand calculations using well established formulas for stress and strain.

2.1.3.1.2 Structural analysis for NCT and HAC

The structural analysis for NCT and HAC comprises the analysis of a sequence of the following tests:

Test 1: 1.2 m free drop test

Test 2: 9 m drop

Test 3: 1 m drop onto a bar

The structural analysis for NCT and HAC was carried out in three major steps:

- Pre-analysis of the behavior of the package by using proven FEM tools and selection of benchmarks for the real drop tests with prototypes.
- Real testing of prototypes by applying the selected benchmark test sequences.
- Refinement of the FEM model based on the results of the test results and complete analysis of the behavior of the DN30 package under NCT and HAC for the operating temperature range of -40 °C to +60 °C.

2.1.3.1.2.1 Pre-analysis

In the pre-analysis, the following sequences were considered:

- Test 1 – Test 2 – Test 3
- Test 1 – Test 3 – Test 2

The pre-analyses were carried out for all considerable orientations of the package before the experimental tests:

- Flat onto the valve side.
- Flat onto the plug side.
- Flat onto the closure system.
- Flat onto the top side.
- Inclined onto the valve side so that the line between center of gravity and point of impact is perpendicular to the target surface.

- Inclined onto the plug side so that the line between center of gravity and point of impact is perpendicular to the target surface.
- Inclined onto the closure system so that the line between center of gravity and point of impact is perpendicular to the target surface.
- Inclined onto the feet (slap-down).

The pre-analyses were carried using the FEM solver LS-DYNA. The results of the pre-analysis were used to set up the drop test sequences. The documentation of the pre-analysis is not part of the SAR.

2.1.3.1.2.2 Experimental drop tests

For the experimental drop tests, five sequences were selected:

- Flat onto the valve side.
- Inclined onto the valve side so that the line between center of gravity and point of impact is perpendicular to the target surface.
- Inclined onto the plug side so that the line between center of gravity and point of impact is perpendicular to the target surface.
- Inclined onto the closure system so that the line between center of gravity and point of impact is perpendicular to the target surface.
- Inclined onto the feet (slap-down).

These tests were carried out at the drop test facility of BAM.

2.1.3.1.2.3 Refinement of the calculation model and complete analysis for NCT and HAC

The experimental drop test results are used to refine the FEM model so that the simulation results agree with the results of the experimental drop tests. This “benchmarked” FEM model is used to perform a comprehensive analysis of the DN30 package under NCT and HAC taking into account the operating temperature range of -40 °C to +60 °C.

The calculations are documented in Appendix 2.2.1.3 (Structural Analysis of the DN30 Package under NCT and HAC).

2.1.3.1.3 Description of calculation programs used for the structural analysis

The results of the drop test simulations in this report are obtained by numerically solving the governing differential equations of structural mechanics, using the finite element method (FEM). Due to the highly dynamic nature of this kind of simulations, the FEM solver LS-DYNA (MPP S R8.0.0) [LS-DYNA 2015] of the software developer LSTC is used, which is integrated in ANSYS® Workbench 19.0 [ANSYS]. LS-DYNA is widely used for crash simulations by the automobile industry. Other applications include sheet metal forming and cutting in the manufacturing industry as well as bird strike, jet engine blade containment and structural failure in the aerospace industry.

As a pure FEM solver, LS-DYNA lacks any modeling features. Therefore, most of the modelling is performed in ANSYS Workbench, which provides several tools for geometry modifications and FEM modeling. The built-in software ANSYS DesignModeler is used for the geometry modifications, while the FEM model itself is developed in ANSYS Mechanical with the plugin “Explicit Dynamics (LS-DYNA Export)”. An input file for LS-DYNA is exported that is further

modified with the pre- and postprocessor LS-PrePost (V4.5) [LS-PREPOST] because the LS-DYNA plugin for ANSYS Mechanical only provides very basic features of LS-DYNA, especially concerning contact and material modelling. After the results are calculated, they are analyzed in LS-PrePost.

2.1.3.2 Thermal analysis

2.1.3.2.1 Thermal analysis for RCT and NCT

The thermal analysis for RCT and NCT comprises:

- Analysis of the DN30 package under an ambient temperature of 38 °C without solar insolation.
- Analysis of the DN30 package under an ambient temperature of 38 °C taking into account solar insolation.
- The steady-state and transient thermal analyses are carried out with ANSYS Workbench 19.0 [ANSYS].

2.1.3.2.2 Thermal analysis for HAC

The thermal analysis for HAC comprises:

- Analysis of the DN30 package under the conditions of the thermal test with an ambient temperature of 800 °C and an exposure time of 30 min.

2.1.3.2.2.1 Pre-analysis

In the pre-analysis the following conditions of the DN30 package specimen were considered:

- Condition of the DN30 PSP after an accumulation of a full drop test sequence inclined onto the valve side and a full drop test sequence inclined onto the plug side.
- Completely empty 30B cylinder to minimize the heat capacity of the 30B cylinder and content and, thus, maximize the temperature increase of the 30B cylinder and its components.

The results of the pre-analysis were used to set up the thermal test conditions. The documentation of the pre-analysis is not part of the SAR.

2.1.3.2.2.2 Experimental fire tests

The experimental fire tests performed for the thermal analysis were carried out with two DN30 package specimen that were:

- Pre-damaged by a full drop test sequence inclined onto the valve side followed by a full drop test sequence inclined onto the plug side.
- Contained an empty 30B cylinder.
- Heated up to a temperature of approximately 63 °C to take into account the initial conditions because of an ambient temperature of 38 °C and solar insolation.

2.1.3.2.2.3 Refinement of the calculation model and analysis for RCT, NCT and HAC

The experimental fire test results are used to refine the calculation model so that the simulation results agree with the results of the real thermal tests. This “benchmark” calculation model is used to perform a comprehensive analysis of the DN30 package under RCT, NCT and HAC.

The experimental fire test performed in November 2017 is designated “Benchmark 1”, the experimental fire test performed in September 2016 is designated “Benchmark 2”. The main difference between the two tests is that the prototype of the DN30 package used for Benchmark 2 does not include the Microtherm insulation layer.

2.1.3.2.3 Description of calculation programs used for the thermal analysis

The thermal analysis is carried out with ANSYS Workbench 19.0 [ANSYS]. ANSYS Workbench is a software environment for performing linear and non-linear structural, thermal and electromagnetic analyses using the finite element method (FEM). The capabilities of ANSYS Workbench encompass geometry creation or optimization, meshing, setting up the finite element model, solving and reviewing the results.

For thermal problems, ANSYS Workbench can solve steady-state as well as transient problems using two- or three-dimensional models. A model may include multiple materials and the thermal conductivity, density, and specific heat of each material may be temperature-dependent. Materials may undergo change of phase. Thermal properties of materials may be entered as data or may be extracted from a material properties library. The boundary conditions, which may be surface-to-environment or surface-to-surface, may be specified temperatures or any combination of prescribed heat flux, forced convection, natural convection and radiation. The boundary condition parameters may be time- and/or temperature dependent. General grey body radiation problems may be modelled with user-defined factors for radiant exchange. Heat-generation rates may be dependent on time and position, and boundary temperatures may be time- and position dependent.

Coupled-physics analysis are supported, e.g. structural-thermal, thermal-electric or thermal-diffusion. Additional functions that are not available via the Workbench user interface can be included in the model using APDL (ANSYS parametric design language) command scripts.

For the validation of the model, the results of two experimental fire test with DN30 prototypes are used:

- The DN30 prototype is modelled as described below in chapter 6.
- The thermal conductivity of the PIR foam is adjusted so that the temperatures at the 30B cylinder are close to the measured temperatures at the prototype.
- As the PIR foam of the prototype burned during the fire test and during the cooling phase it was assumed that the PIR foam acts as a thermal power source during that time. This thermal power is adjusted so that the maximal temperatures reached at the 30B cylinder and its components comply with the measured temperatures at the prototype.

The thermal analysis of the DN30 package is then carried out with the validated calculation model.

2.1.3.3 Containment design analysis

The containment analysis is performed for RCT and NCT. For all analyses, a maximal standard Helium leakage rate of $1.0 \text{ E-4 Pa} \cdot \text{m}^3 / \text{s}$ is assumed. This assumption is justified in the comprehensive drop test and thermal test program.

The containment design analysis is carried out according to [ISO 12807] in the following steps:

- Step 1:** Determination of the radioactive inventory (see Appendix 1.3 (Radioactivity))
- Step 2:** Determination of the activity releasable rate
- Step 3:** Specification of the permissible activity release rate
- Step 4:** Determination of the permissible activity release rate because of leakage
- Step 5:** Determination of the activity concentration
- Step 6:** Determination of the maximal volume leakage rate
- Step 7:** Determination of the equivalent capillary diameter
- Step 8:** Evaluation of the permissible standard leakage rate

The package has no elastomeric gaskets; hence there is no permeation activity release rate to be considered.

2.1.3.3.1 Leakage tests performed after the drop and fire tests

To prove that the standard Helium leakage rate of $1.0\text{E-4 Pa} \cdot \text{m}^3 / \text{s}$ used in the containment analysis is applicable not just for RCT and NCT, but even after HAC, the leakage rate of the 30B cylinders used for the DN30 prototypes was measured after the HAC drop and fire tests.

Special 30B cylinders were manufactured for this purpose: on the side of the valve, at 180° from the valve, a third orifice was added, through which the molecules inside the cylinder were vacuumed. This opening also consists of a tube inside the cylinder, so vacuum is possible even when the cylinder is filled with the concrete (see Figure 9); this is also the case for the plug.

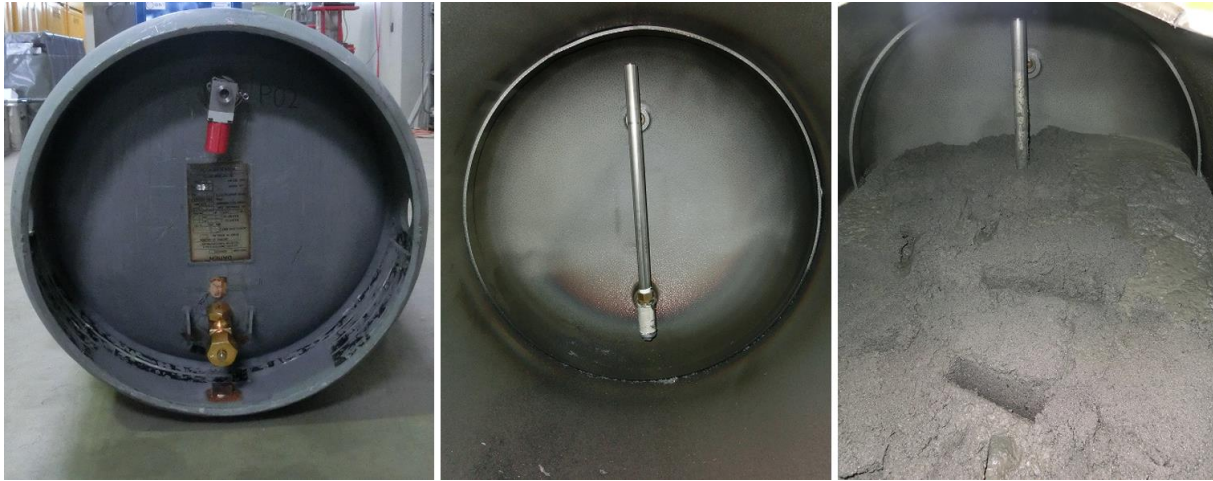


Figure 9: Example of dummy 30B cylinder used during the drop and fire test for testing the leakage rate: a) outside, valve side (upside down), b) inside, valve side (empty), c) inside valve side (filled with concrete)

The sealed orifice is connected to the pump (see Figure 10) that creates the vacuum inside the cylinder. From time to time, the tube is connected to the “leak detector unit” (see Figure 11), that measures the pressure inside a space, in this case inside the 30B cylinder.



Figure 10: Pump creating a vacuum inside the 30B cylinder



Figure 11: Leak detector unit

Once the pressure is below a certain point, a helium environment is created around the cylinder by enclosing the 30B cylinder in a closed box that is sealed with tape to the floor, and through which a source of helium is fixed.



Figure 12: Helium cage around the cylinder

Once the cage is filled with helium, the vacuum pump is turned on again to maybe move some helium molecules inside the 30B cylinder. Then, the tube is again connected to the device that measures the helium leakage rate of the 30B cylinder.

With this method, all three components of the 30B cylinder are being tested simultaneously: the valve, the plug and the welding seams.

Table 16 recaps the leak rate before and after the drop tests and the fire test.

Table 16: Leak rates before and after each test

Type of test	Leak rate before the test (Pa.m ³ /s)	Leak rate after the test (Pa.m ³ /s)
Drop sequence 1	5.67 x 10 ⁻⁸	4.94 x 10 ⁻⁹
Drop sequence 2	7.20 x 10 ⁻⁸	4.15 x 10 ⁻⁶
Drop sequence 3	2.86 x 10 ⁻⁸	3.19 x 10 ⁻⁸
Drop sequence 4	3.57 x 10 ⁻⁸	7.09 x 10 ⁻⁸
Drop sequence 5	5.08 x 10 ⁻⁸	1.37 x 10 ⁻⁸
Fire benchmark 1	5.54 x 10 ⁻⁸	3.40 x 10 ⁻⁵
Fire benchmark 2	6.58 x 10 ⁻⁸	6.63 x 10 ⁻⁹

2.1.3.4 External dose rate analysis

2.1.3.4.1 External dose rate analysis for RCT

The external dose rate analysis for RCT consists of:

- The analysis of the external dose rate at the surface of the DN30 package and at a distance of 2 m from the external surface of the DN30 package.
- The analysis of the external dose rate at a distance of 1 m from the external surface of the DN30 package to provide an estimate for the TI to be expected; the TI for transport will be determined in any case by measurement before transport.
- The analysis of the external dose rate at the surface of a standard vehicle routinely used for the transport of the DN30 package and in a distance of 2 m from the external surface of the vehicle; for this analysis, it is assumed that 20' flatracks are used for the transport of four DN30 packages side by side, so that the dose rates at the surface of the vehicle are identical to the dose rates at the front surfaces of the DN30 package; for the analysis of the external dose rate in 2 m distance from the vehicle, the influence of all four DN30 packages is taken into account.

2.1.3.4.2 External dose rate analysis for NCT

The external dose rate analysis for NCT consists of the comparison of the maximal dose rates for a non-damaged DN30 package complying with the manufacturing drawings and for a damaged DN30 package under NCT to prove that the increase in the maximal dose rate is not greater than 20 %.

2.1.3.4.3 Description of calculation programs used for the external dose rate analysis

The calculation of external dose rates at the DN30 package is carried out by means of the program system SCALE 6.1 [SCALE 2011].

In a first step, the gamma and neutron source terms are determined by means of the depletion analysis sequence ORIGEN-ARP. By considering a mass of 1 g of each nuclide individually, the decay of the involved nuclides is individually evaluated, and the respective neutron and gamma source terms are determined in the v7-27n-19g energy-group structure [SCALE 2011].

In a second step, the dose rates of 1 g of each radionuclide are calculated by means of the analysis sequence MAVRIC. The results used in the safety assessment are based on radial detectors, since calculations described in Appendix 2.2.4 (Dose Rate Analysis) show that for DN30 packages containing filled 30B cylinders the dose rates for radial detectors are always higher than the dose rates for axial detectors at the same distance from the surface of the package.

In a third step, the dose rates of 1 g of each radionuclide are multiplied by the concentration of the respective nuclide based on the content description in section 1.3 and by the mass of uranium modelled in the calculation model.

The second and third step are performed for each of the required calculations: 3 m distance from the unshielded material surface, surface of the DN30 package, 1 m distance from the DN30 package and 2 m distance from the vehicle.

2.1.3.5 Criticality safety analysis

2.1.3.5.1 General assumptions for the criticality safety analysis

Criticality safety analysis is based on the following assumptions

- For the single package in isolation and for the array of packages, flooding with water is excluded because of the results of analyses and drop tests described in the structural analysis in section 2.2.1.
- Criticality safety is not based on the effect of neutron absorbers inside the package.
- For all contents, the most reactive arrangement in the packaging is determined in all cases. Any credible rearrangement of contents in the package is taken into account in the analyses. Based on the results of analyses and drop tests described in the structural analysis, release of contents from the package needs not be assumed.
- A possible reduction of gaps in the package is analyzed. For arrays of packages, the distance between the packages is varied.
- Water around the package is considered in different layer thicknesses in the analysis of an array of packages.
- Temperature changes are taken into account by assuming a conservatively high density for UF_6 . In the analyses with theoretical maximal water density of 1 g/cm^3 , the particular optimal moderation for the arrangement is calculated. A decrease of water density caused by a temperature rise or freezing will lead to lower moderation that is less reactive.

2.1.3.5.2 Description of calculation programs used for the criticality safety analysis

All criticality safety calculations are performed by means of the sequence CSAS6 of the criticality safety code KENO VI. Both versions SCALE 6.0 [SCALE 2009] and SCALE 6.1.1 [SCALE 2011] are used for the analyses.

The most recent libraries, based on ENDB/BVII data, are used for the criticality safety calculations. This includes the library v7-238 being used for energy multi-group cross sections.

2.1.4 RESULTS OF PHYSICAL TESTING OF SPECIMENS AND PROTOTYPES

2.1.4.1 Overview of the physical tests

To support and benchmark the structural and thermal analyses, physical tests with specimens and prototypes were carried out:

- Static and dynamic mechanical tests with specimens of the technical foam used as shock absorbing material and thermal insulation (see Appendix 1.4.2 (Material Data PIR Foam)).
- Thermal tests with specimens of the technical foam used as shock absorbing material and thermal insulation (see Appendix 1.4.2 (Material Data PIR Foam) and Appendix 1.4.3 (Material Data Intumescent Material)).

- Drop tests with prototypes of the DN30 package loaded with a 30B cylinder containing surrogate material to simulate the maximal permissible mass of UF_6 (see Appendix 2.2.1.2 (Drop Test Reports)).
- A fire test with a prototype of the DN30 package loaded with an empty 30B cylinder; the DN30 PSP prototype had been pre-damaged by two consecutive HAC drop test sequences loaded with a 30B cylinder containing the maximal permissible mass of UF_6 (see Appendix 2.2.2.2 (Thermal Test Report)).

The results of the tests with prototypes and the comparison with the analyses are described in detail in section 2.2.1 and section 2.2.1.5.3.1 for the mechanical tests and in section 2.2.2 and in section 2.2.2.2 for the thermal tests.

2.1.4.2 Deviations between prototype and series

The feedback of users during the drop tests and the thermal tests as well as the result of some tests gave reason to certain design improvements of the DN30 PSP. These design improvements are described in the following sections. For each design improvement, the reason is specified and the impact on the results of the physical tests is evaluated.

2.1.4.2.1 Closure device

2.1.4.2.1.1 Description of the design modification

The pin of the closure system is secured by a bolt. In the prototype design, this bolt was a standard socket head screw with a length of 50 mm.

In the series design, the standard socket head screw is replaced by:

- A captive socket head screw with a length of 62 mm.
- Placement of a special washer between head and closure system body to prevent loosening of the bolt.

2.1.4.2.1.2 Justification of the design modification

The series design of the securing bolt ensures that the bolt remains connected to the closure system at all times during handling. To remove the bolt, the user has to pull the bolt and unscrew it at the same time. Removing the bolt from the closure system is not possible without simultaneously pulling the bolt.

The bolt could get lost because of vibrations during transport. The use of special washers securing the bolt ensures that it remains fixed during transport.

2.1.4.2.1.3 Impact on the results of the physical testing

2.1.4.2.1.3.1 Mechanical tests

The design of teeth and pin of the closure device of prototype and series DN30 PSP is identical. The design of the bolt has no influence on the results of the mechanical tests.

2.1.4.2.1.3.2 Thermal test

The design of the bolt of the closure device has no influence on the results of the thermal test.

2.1.4.2.2 Feet

2.1.4.2.2.1 Description of the design modification

During the drop test campaign, it was noticed that handling of the prototype of the DN30 package by using a forklift might cause damage to the lower part of the bottom half shell as the distance between the floor and bottom half was too small to allow the forks of the forklift to be inserted underneath the DN30 prototype.

Following modifications were introduced:

- The height of the feet was increased by 48 mm.
- The four individual parts of the feet are simplified to two individual parts.
- The number of subparts was reduced, and the thickness of sheets was adjusted to their function.
- Forklift pockets were added to improve safety during handling with a forklift.

2.1.4.2.2.2 Justification of the design modification

The design modification results in a safety improvement during handling of the DN30 package.

2.1.4.2.2.3 Impact on the results of the physical testing

2.1.4.2.2.3.1 Mechanical tests

The modifications of the design of the feet only have an impact on drop orientations onto the feet. The impact on the slap-down drop test is discussed in detail in Appendix 2.2.1.3 (Structural Analysis of the DN30 Package under NCT and HAC). There is no or only negligible impact on other drop orientations.

2.1.4.2.2.3.2 Thermal test

The design modification of the feet has no influence on the results of the thermal test.

2.1.4.2.3 Rotation preventing device

2.1.4.2.3.1 Description of the design modification

The design of the rotation preventing device as used in the prototypes is shown in Figure 13 a) and the design of the rotation preventing device as used in the series design is shown in Figure 13 b).

The prototype design is made of a pin that rests in a sleeve with a longitudinal and radial slit. The lever consists of a rectangular bar that is welded to the pin after the pin is inserted into the sleeve.

The series design is made of a pin that rests in an intermediate sleeve (the drive), which itself rests in an outer sleeve. The lever consists of a round bar that is screwed into the bolt and secured by a spot weld.

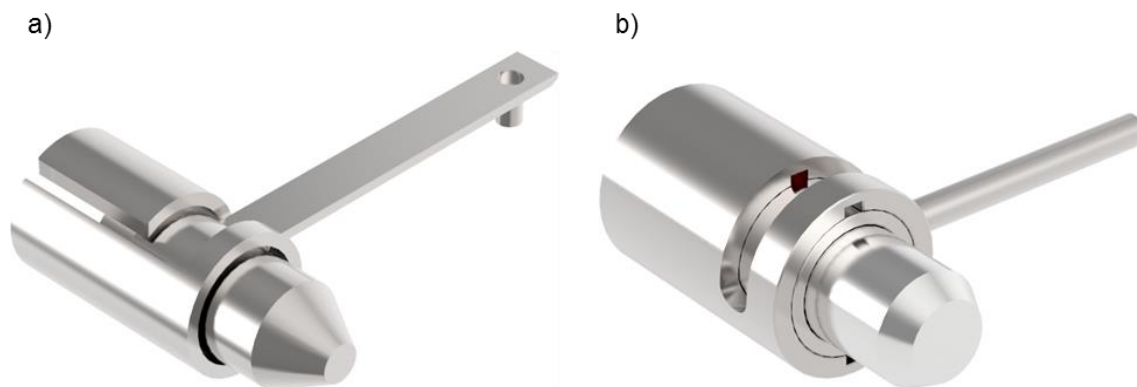


Figure 13: Rotation preventing device: a) DN30 PSP prototype b) DN30 PSP

2.1.4.2.3.2 Justification of the design modification

Practical experience regarding handling of the prototype design of the rotation preventing device during the physical testing of the DN30 package was not considered to be a suitable solution for the series design of the DN30 PSP:

- The design of the welded connection between the lever and the pin was rather weak.
- The shape of the lever was not user-friendly.
- Handling of the rotation preventing device was difficult, especially when wearing gloves.
- There is a discontinuity in the sealing line of the flange of the bottom half so that the ingress of water into the DN30 PSP could not be excluded.

For the series design the following applies:

- The lever is connected to the pin by a robust bolted connection. This connection is secured by a spot weld. In case of a damage to the lever it can be easily exchanged by opening the spot weld and unscrewing the lever.
- The round shape of the lever is user-friendly.
- Handling of the rotation preventing device, even when wearing gloves, is facilitated.
- The continuity of the sealing line of the flange of the bottom half is preserved.
- The overall design of the rotation preventing device is more robust than the prototype design.
- The series design allows lower tolerances between pin and sleeve and thus reduces the relative movement between pin and sleeve during HAC.

2.1.4.2.3.3 Impact on the results of the physical testing

2.1.4.2.3.3.1 Mechanical tests

The prototype design of the rotation preventing device was structurally weaker than the series design:

- The sleeve of the rotation preventing device connecting the device to the bottom half is stronger for the series design than for the prototype design.
- The connection between lever and pin is stronger for the series design than for the prototype design.
- The remaining design modifications only have an impact on the handling of the rotation preventing device.

Hence, a negative impact on the results of the mechanical tests can be excluded.

2.1.4.2.3.3.2 Thermal test

The design modification of the rotation preventing device has no influence on the results of the thermal test.

2.1.4.2.4 Reinforcement plate on the valve side

2.1.4.2.4.1 Description of the design modification

The outer front plate on the valve side of the top half of the prototypes of the DN30 PSP is reinforced by a round steel plate positioned in the middle of the front plate as shown in Figure 14 a). In the modified design used for the series DN30 PSP, the reinforcement plate is extended to a semicircle.

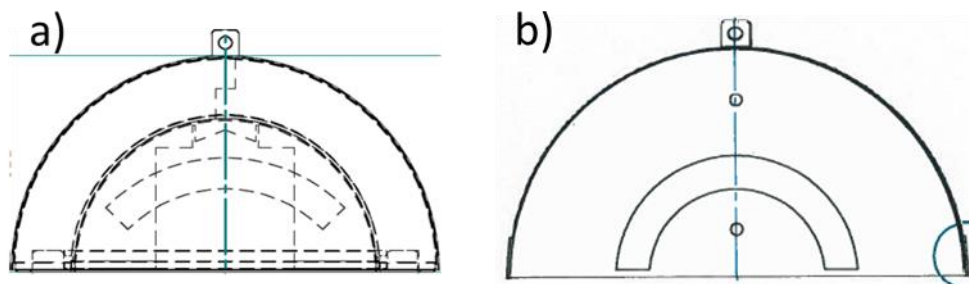


Figure 14: Reinforcement plate: a) DN30 PSP prototype b) DN30 PSP

2.1.4.2.4.2 Justification of the design modification

During manufacturing of the prototypes, it was noticed that the positioning of the reinforcement plate is complicated and requires supervision. Additionally, the welding seams between the front plate and the reinforcement plate affect the appearance of the front plate. Hence, the reinforcement plate is extended to a semicircle so that the welding seams can be placed near the flange.

2.1.4.2.4.3 Impact on the results of the physical testing

2.1.4.2.4.3.1 Mechanical tests

The reinforcement plate was placed at the inner side of the outer shell to avoid puncture of the shell by the bar. It is shown in the drop tests that the front plate with a thickness of the shell of 4 mm is not punctured by the bar, even in areas not covered by the reinforcement plate.

Nevertheless, the reinforcement plate was kept as a design feature to provide additional safety in the valve area.

Neither the 1.2 m drop test simulating NCT nor the 9 m drop test simulating HAC are affected by this design change.

2.1.4.2.4.3.2 Thermal test

The modification of the design of the reinforcement plate has no influence on the results of the thermal test.

2.1.4.2.5 Flange between top and bottom half and its gasket

2.1.4.2.5.1 Description of the design modification

In the design of the prototype of the DN30 PSP, there was no barrier against water ingress into the valve protecting device area.

The design modification is as follows:

- There is a steel bar welded to the bottom half outside the hinges of the valve protecting device, providing a geometrical water barrier.
- There is a gasket attached to the top half that seals the gap between the steel bar and the top half when the DN30 PSP is closed.

2.1.4.2.5.2 Justification of the design modification

The design modification improves the ability of the DN30 PSP to avoid the ingress of water into the cavity.

Remark: the design modification has no influence on the containment system that is solely provided by the 30B cylinder.

2.1.4.2.5.3 Impact on the results of the physical testing

2.1.4.2.5.3.1 Mechanical tests

There is no impact on the results of the mechanical tests as there were no or only minor recorded deformations in that area of the DN30 PSP.

2.1.4.2.5.3.2 Thermal test

The design modification of the sealing line in the valve protecting device area has no influence on the results of the thermal test.

2.1.4.2.6 Layer of MICROTHERM® between RTS 120 foam and inner shell

2.1.4.2.6.1 Description of the design modification

An additional thermal protection is positioned between the inner shell of the DN30 PSP and the RTS 120 foam. This additional protection is comprised of a 10 mm thick layer of

MICROTHERM® OVERSTITCHED 1000R HY. For that, the thickness of the RTS 120 foam is reduced by 10 mm.

2.1.4.2.6.2 Justification of the design modification

In a preliminary thermal test, it was recorded that the maximal temperatures detected near the valve and the plug exceeded the solidus temperature of the thread tinning of 183 °C. This could potentially result in a leakage at the connection between the valve and the 30B cylinder or the plug and the 30B cylinder.

The improved design reduces the maximal temperatures of the valve and the plug well below the solidus temperature of the thread tinning, and below the HAC temperature limit of 131 °C.

2.1.4.2.6.3 Impact on the results of the physical testing

2.1.4.2.6.3.1 Mechanical tests

This influence of the MICROTHERM® layer is analyzed in Appendix 2.2.1.3 (Structural Analysis of the DN30 Package under NCT and HAC) in detail. It is shown, that the modification has no negative influence on the safety of the DN30 package under NCT and HAC.

The MICROTHERM® layer was part of the design of the prototype of the DN30 package used for the thermal test. This prototype was pre-damaged in two full drop test sequences onto the valve corner and onto the plug corner consisting of a 10.2 m drop test and a 1 m drop test onto the bar, respectively. The deformations of the DN30 PSP after these test sequences were similar to the deformations after the drop test sequences without the MICROTHERM® layer.

2.1.4.2.6.3.2 Thermal test

The MICROTHERM® layer was tested in the thermal test.

2.1.4.2.7 Intumescent material

2.1.4.2.7.1 Description of the design modification

An additional thermal protection is glued onto the inner shell of the DN30 PSP. This additional protection is comprised of a 2.6 mm thick intumescent material.

To protect the intumescent material during the loading and unloading of the 30B cylinder protecting rails are welded to the inner shell on both front ends. These rails guide the 30B cylinder and prevent direct contact between the cylinder skirts and the intumescent material during loading or unloading the 30B cylinder.

2.1.4.2.7.2 Justification of the design modification

In a preliminary thermal test, it was detected that hot gases from the decomposition of the PIR foam enter through cracks in the inner shell resulting from mechanical tests into the cavity of the DN30 PSP. These hot gases resulted in a fast increase of the temperature of the 30B cylinder above its design temperature. This could impair the containment system provided by the 30B cylinder and its valve and plug.

The improved design prevents any intrusion of decomposition gases into the cavity and, thus, reduces the heat transfer by convection between the DN30 PSP and the 30B cylinder.

2.1.4.2.7.3 Impact on the results of the physical testing

2.1.4.2.7.3.1 Mechanical tests

The intumescent material has no influence on the results of the mechanical tests:

- The mechanical properties of the DN30 PSP are not affected.
- The thin layer of intumescent material has no measurable influence on the interaction between the 30B cylinder and the DN30 PSP during the drop tests.
- The reduced gap between the 30B cylinder and the DN30 PSP potentially weakens the impact of the 30B cylinder on the inner shells of the DN30 PSP as the relative movement between the 30B cylinder and the DN30 PSP is reduced.
- The protecting rails with a thickness of 4 mm and a width of 15 mm have no influence on the strength of the 10 mm thick front plates.

The intumescent material was part of the design of the prototype of the DN30 package used for the thermal test. This prototype was pre-damaged in two full drop test sequences onto the valve corner and onto the plug corner consisting of a 10.2 m drop test and a 1 m drop test onto the bar, respectively. The deformations of the DN30 PSP after these test sequences were similar to the deformations after the drop test sequences without intumescent material.

2.1.4.2.7.3.2 Thermal test

The intumescent material was tested in the thermal test.

2.1.4.2.8 Housing of the valve protecting device

2.1.4.2.8.1 Description of the design modification

The valve protecting device used in the mechanical tests was shaped like a “U” with open upper side and front side. For the thermal test, a housing made of 1 mm thick stainless-steel sheet was positioned into the U-shape to close the upper and front side. On its inside, the housing is covered with intumescent material.

The housing is moveable in the axial direction of the valve to facilitate loading and unloading of the 30B cylinder into and out of the DN30 PSP, respectively.

2.1.4.2.8.2 Justification of the design modification

In a preliminary thermal test, it was detected that hot gases from the decomposition of the PIR foam enter through cracks in the inner shell resulting from mechanical tests into the cavity of the DN30 PSP. These hot gases resulted in a fast increase of the temperature of the 30B cylinder above its design temperature. This could impair the containment system provided by the 30B cylinder and its valve and plug.

The improved design prevents the transport of hot decomposition gases to the valve as the steel-sheet housing provides a barrier and the intumescent material encloses the valve because of the expansion of the intumescent material at increased temperatures.

2.1.4.2.8.3 Impact on the results of the physical testing

2.1.4.2.8.3.1 Mechanical tests

The housing does not affect the results of the mechanical tests:

- The mechanical properties of the DN30 PSP are not affected.
- The thin steel sheet (1 mm) does not affect the mechanical strength of the valve protecting device.
- The remaining distance between the valve and any part of the valve protecting device was minimally 21 mm under RCT and minimally 5 mm under HAC (see Appendix 2.2.1.3 (Structural Analysis of the DN30 Package under NCT and HAC)). The remaining distances are much greater than the thickness of the steel sheet (1 mm) and the thickness of the intumescent material (2.6 mm). The requirement, that there is no contact between the valve and any other part of the DN30 PSP is still fulfilled.
- The housing was part of the design of the prototype of the DN30 package used for the thermal test. This prototype was pre-damaged in two full drop test sequences onto the valve corner and onto the plug corner consisting of a 10.2 m drop test and a 1 m drop test onto the bar, respectively. There was no contact between the valve or the plug and any other part of the DN30 prototype after the test sequences.

The impact of the design modification is analyzed in detail in Appendix 2.2.1.3 (Structural Analysis of the DN30 Package under NCT and HAC).

2.1.4.2.8.3.2 Thermal test

The housing was part of the design of the prototype of the DN30 package used for the thermal test.

2.1.4.2.9 Thermal plugs

2.1.4.2.9.1 Description of the design modification

The design, position and number of the thermal plugs is modified. The following applies for the series design:

- The thermal plugs are screwed into a cylindrical receptacle that is welded to the outer shell. An EPDM gasket between the thermal plug and the receptacle avoids ingress of water into the foam.
- There are nine thermal plugs in the bottom half and in the top half, respectively.
- The thermal plugs are distributed such that the decomposition gases during the thermal fire test are released to the environment instead of the interior of the DN30 PSP.

2.1.4.2.9.2 Justification of the design modification

In a preliminary thermal test, it was detected that hot gases from the decomposition of the PIR foam enter through cracks in the inner shell into the cavity of the DN30 PSP, which results in a fast increase of the temperature at the 30B cylinder above its design temperature. This could impair the containment system provided by the 30B cylinder and its valve and plug.

The improved design prevents the intrusion of decomposition gases into the cavity through the thermal plugs previously positioned at the inner shell and, thereby, reduces the heat transfer by convection between the DN30 PSP and the 30B cylinder.

2.1.4.2.9.3 Impact on the results of the physical testing

2.1.4.2.9.3.1 Mechanical tests

The thermal plugs have a diameter of 21 mm. Their size is small compared to the dimensions of the DN30 PSP. Additionally, the holes that are introduced in the outer shell of the DN30 PSP to install the thermal plugs are reinforced by a cylindrical receptacle, which is welded to the outer DN30 PSP shell. Consequently, the outer shell is not weakened in the area of the thermal plugs and any influence on the results of the mechanical tests can be excluded.

The new design of the thermal plugs was part of the design of the prototype of the DN30 package used for the thermal test. This prototype was pre-damaged in two full drop test sequences onto the valve corner and onto the plug corner consisting of a 10.2 m drop test and a 1 m drop test onto the bar, respectively. In the area of the thermal plugs, there was no crack initiation in the outer DN30 PSP shell.

2.1.4.2.9.3.2 Thermal test

The design of the thermal plugs was tested in the thermal test.

2.1.4.2.10 Support pads

2.1.4.2.10.1 Description of the design modification

The material of the support pads for the 30B cylinder in the bottom half of the DN30 PSP are made of silicone.

2.1.4.2.10.2 Justification of the design modification

The pads used in the prototype of the DN30 package were made of NBR/SBR. Compared to NBR/SBR, Silicone is more resilient to heat. In contrast to other pad materials, the silicon pads will remain intact during the thermal test as the decomposition temperature of the silicone is not reached.

2.1.4.2.10.3 Impact on the results of the physical testing

2.1.4.2.10.3.1 Mechanical tests

The change in material of the support pads has no influence on the results of the mechanical tests.

2.1.4.2.10.3.2 Thermal test

The change in material of the support pads has no influence on the results of the thermal test.

2.1.4.2.11 Sealing block

2.1.4.2.11.1 Description of the design modification

The DN30 PSP prototypes had a single massive sealing block installed on only one side of the PSP. The serial DN30 PSP has two less massive sealing blocks installed on each side of the PSP.

2.1.4.2.11.2 Justification of the design modification

By using two sealing blocks on both sides of the DN30 PSP, an opening of the DN30 PSP without breaking the seals is prevented.

2.1.4.2.11.3 Impact on the results of the physical testing

2.1.4.2.11.3.1 Mechanical tests

The design modification of the sealing blocks has no influence on the results of the mechanical tests.

2.1.4.2.11.3.2 Thermal test

The design modification of the sealing blocks has no influence on the results of the thermal test.

2.2 TECHNICAL ANALYSES

2.2.1 STRUCTURAL ANALYSIS

In this chapter, the structural design of the DN30 package is analyzed and it is proven that the requirements towards a type B(U)F package are met. With that, also the requirements towards a type IF and a type AF package are met. The following proofs are carried out:

- Static structural analysis for RCT.
- Fatigue analysis for dynamically loaded components.
- Dynamic structural analysis for NCT and HAC.

Fracture analysis at -40 °C is not required for components of austenitic stainless steels according to [SSG-26], para. V.9.

2.2.1.1 Basic assumptions for the calculations

Basic assumptions for the calculations are listed in the following. They include load assumptions for different load situations, the definition of calculation methods and material parameters of the materials used for the proof.

2.2.1.1.1 Load assumptions

Load assumptions are made for the following situations:

- Handling
- RCT
- NCT
- HAC

The individual load assumptions are discussed in the following sections.

2.2.1.1.1.1 Handling

Load assumptions for handling include:

- Temperatures at the package corresponding to an ambient temperature of 38 °C and solar insolation.
- Hoisting coefficients that have to be considered for handling operations.
- Internal and external pressure.

Load assumptions as basis for calculations for handling the package are listed in Table 17.

Table 17: Load assumptions for handling

Load assumption	To be used for component	Value
Temperature	30B cylinder	64 °C
	Lifting lugs at feet	70 °C
	Lifting lugs at top half	100 °C
	Feet	70 °C
Hoisting coefficient	Lifting lugs	2
Pressure	30B cylinder, internal	152 kPa
	30B cylinder, external	100 kPa
Fatigue analysis	Lifting lugs	load cycle number 150000

2.2.1.1.1.2 RCT

Load assumptions for routine conditions of transport include:

- Temperatures at the package corresponding to an ambient temperature of 38 °C and solar insolation (see section 2.2.2.3.4).
- Maximum transport accelerations.
- Vibrations during transport.

Load assumptions as basis for calculations for routine conditions of transport are listed in Table 18.

Table 18: Load assumptions for RCT

Load assumption	To be used for component	Value
Temperature (for ambient temperature of 38 °C, with insolation, see section 2.2.2.3.4)	Outer shell, feet	70 °C
	30B cylinder	64 °C
Temperature (for ambient temperature of -40 °C, without insolation)	Complete packaging	-40 °C
Accelerations <ul style="list-style-type: none"> • axial • lateral • vertical 	Complete packaging	10.0 g 5.0 g 1.0 g down ± 2.0 g
Vibrations	Complete packaging	0.3 g

2.2.1.1.1.3 NCT

Load assumptions for normal conditions of transport include:

- Temperatures at the package corresponding to an ambient temperature of 38 °C and solar insolation (see section 2.2.2.3.4).
- Tests for demonstrating the ability to withstand normal conditions of transport according to [10CFR71] §71.71(a) and [49CFR173] §173.465(a) or [IAEA 2012], para. 719.
- Reduction of ambient pressure.

Load assumptions as basis for calculations for normal conditions of transport are listed in Table 19.

Table 19: Load assumptions for NCT

Load assumption	Individual test	To be used for component	Value
Temperature	Drop test, stacking test, penetration test	DN30 PSP	60 °C
		30B cylinder	64 °C
Tests according to [10CFR71] §71.71(a) or [IAEA 2012], para. 719	Water spray test	Packaging surface	[10CFR71] §71.71(c)(6) and [49CFR173] §173.465(b) or [IAEA 2012], para. 721
	Drop test	Complete package	[10CFR71] §71.71(c)(7) and [49CFR173] §173.465(c) or [IAEA 2012], para. 722 Free drop height 1.2 m
	Stacking test	Complete package	[10CFR71] §71.71(c)(9) and [49CFR173] §173.465(d) or [IAEA 2012], para. 723
	Penetration test	Packaging surface	[10CFR71] §71.71(c)(10) and [49CFR173] §173.465(e) or [IAEA 2012], para. 724
Ambient pressure	-	30B cylinder	[10CFR71] §71.71(c)(3) and [49CFR173] §173.412(f) or [IAEA 2012], para. 645 60 kPa

2.2.1.1.1.4 HAC

Load assumptions for hypothetical accident conditions of transport include:

- Temperatures at the package corresponding to an ambient temperature of 38 °C and solar insolation (see section 2.2.2.3.4).
- Tests for demonstrating the ability to withstand accident conditions of transport according to [10CFR71] §71.73(a) or [IAEA 2012], para. 726.
- Internal and external pressure.

Load assumptions for accident conditions of transport are listed in Table 20.

Table 20: Load assumptions for HAC

Load assumption	Individual test	To be applied for component	Value
Temperature	Drop test I and drop test II	Packaging main body outer shell	60 °C
		30B cylinder	64 °C
Tests according to [10CFR71] §71.73(a) or [IAEA 2012], para. 726	Drop test I	Complete package	[10CFR71] §71.73(c)(1) or [IAEA 2012], para. 727 (a) Free drop height 9 m
	Drop test II	Complete package	[10CFR71] §71.73(c)(3) or [IAEA 2012], para. 727 (b) Free drop height 1 m
	Thermal test	Complete package	[10CFR71] §71.73(c)(4) or [IAEA 2012], para. 728
	Water immersion test	30B cylinder	[10CFR71] §71.73(c)(6) or [IAEA 2012], para. 729 150 kPa, 8 h
Water pressure	Water immersion test for packages containing fissile materials	30B cylinder	[10CFR71] §71.73(c)(5) or [IAEA 2012], para. 731 9 kPa, 8 h
Pressure increase due to max. temperatures during the thermal test	Thermal test	30B cylinder	[10CFR71] §71.73(c)(4) or [IAEA 2012], para. 728 106 kPa (see section 2.2.1.5.3.1)

2.2.1.1.2 Material data

Materials are specified in section 1.4.1. Table 21 to Table 27 contain the material data for all steel materials including their substitutes. The data given in the tables prove that the chosen substitute materials are appropriate choices as all materials have the same characteristics:

- Based on the elongation at fracture, all primary and substitute materials provide a very high ductility;
- The resulting stress-strain curves for all substitute materials are similar to the primary material as the stress-strain curves are determined based on the yield strength and the ultimate strength as well as their corresponding strains;
- The strain-rate behavior is nearly the same, which can be deduced from the similarities in the chemical composition of the primary materials and their substitutes (also compare [ASME BPVC], Section III, Non-mandatory appendix EE, Table EE-1250-1);
- Based on the carbon content, all materials have excellent weldability.

For the static analyses, the data given in Table 22, Table 24, Table 26 and Table 27 is used as these define the lower bounds with regard to the mechanical strength. This ensures that the results obtained in the static analyses bound the results for any of the given material data. For the dynamic analysis, the material data is specified in Appendix 2.2.1.3 (Structural Analysis of the DN30 Package under NCT and HAC).

Table 21: Material data for plates of material No. 1.4301 (Type 304)

Material property	Designation	Temperature	Value	Applicable EU standards	Applicable US standards
Density	ρ	20 °C	7.9 g/cm ³	DIN EN 10088-1	ASME SA-240
0.2 % yield stress	$R_{p0.2}$	20 °C	230 MPa	DIN EN 10088-2	ASME SA-240
		70 °C	184 MPa	DIN EN 10088-2	ASME SA-240
		100 °C	157 MPa	DIN EN 10088-2	ASME SA-240
1.0 % yield stress	$R_{p1.0}$	20 °C	260 MPa	DIN EN 10088-2	ASME SA-240
		70 °C	217 MPa	DIN EN 10088-2	ASME SA-240
		100 °C	191 MPa	DIN EN 10088-2	ASME SA-240
Ultimate tensile strength	R_m	20 °C	540 MPa	DIN EN 10088-2	ASME SA-240
Elastic modulus	E	20 °C	2.00E5 MPa	DIN EN 10088-1	ASME SA-240
		100 °C	1.94E5 MPa	DIN EN 10088-1	ASME SA-240
Poisson's ratio	ν		0.3		
Elongation at fracture	A		45 %	DIN EN 10088-2	ASME SA-240
Linear thermal expansion coefficient	α	20-100 °C	16E-6 K ⁻¹	DIN EN 10088-1	ASME SA-240

Table 22: Material data for plates of material No. 1.4307 (Type 304L)

Material property	Designation	Temperature	Value	Applicable EU standards	Applicable US standards
Density	ρ	20 °C	7.9 g/cm ³	DIN EN 10088-1	ASME SA-240
0.2 % yield stress	R _{p0.2}	20 °C	220 MPa	DIN EN 10088-2	ASME SA-240
		70 °C	175 MPa	DIN EN 10088-2	ASME SA-240
		100 °C	147 MPa	DIN EN 10088-2	ASME SA-240
1.0 % yield stress	R _{p1.0}	20 °C	250 MPa	DIN EN 10088-2	ASME SA-240
		70 °C	207 MPa	DIN EN 10088-2	ASME SA-240
		100 °C	181 MPa	DIN EN 10088-2	ASME SA-240
Ultimate tensile strength	R _m	20 °C	520 MPa	DIN EN 10088-2	ASME SA-240
Elastic modulus	E	20 °C	2.00E5 MPa	DIN EN 10088-1	ASME SA-240
		100 °C	1.94E5 MPa	DIN EN 10088-1	ASME SA-240
Poisson's ratio	ν		0.3		
Elongation at fracture	A		45 %	DIN EN 10088-2	ASME SA-240
Linear thermal expansion coefficient	α	20-100 °C	16E-6 K ⁻¹	DIN EN 10088-1	ASME SA-240

Table 23: Material data for plates of material No. 1.4541 (Type 321)

Material property	Designation	Temperature	Value	Applicable EU standards	Applicable US standards
Density	ρ	20 °C	7.9 g/cm ³	DIN EN 10088-1	ASME SA-240
0.2 % yield stress	R _{p0.2}	20 °C	220 MPa	DIN EN 10088-2	ASME SA-240
		70 °C	193 MPa	DIN EN 10088-2	ASME SA-240
		100 °C	176 MPa	DIN EN 10088-2	ASME SA-240
1.0 % yield stress	R _{p1.0}	20 °C	250 MPa	DIN EN 10088-2	ASME SA-240
		70 °C	224 MPa	DIN EN 10088-2	ASME SA-240
		100 °C	208 MPa	DIN EN 10088-2	ASME SA-240
Ultimate tensile strength	R _m	20 °C	520 MPa	DIN EN 10088-2	ASME SA-240
Elastic modulus	E	20 °C	2.00E5 MPa	DIN EN 10088-1	ASME SA-240
		100 °C	1.94E5 MPa	DIN EN 10088-1	ASME SA-240
Poisson's ratio	ν		0.3		
Elongation at fracture	A		40 %	DIN EN 10088-2	ASME SA-240
Linear thermal expansion coefficient	α	20-100 °C	16E-6 K ⁻¹	DIN EN 10088-1	ASME SA-240

Table 24: Material data for shapes of material No. 1.4541 (Type 321)

Material property	Designation	Temperature	Value	Applicable EU standards	Applicable US standards
Density	ρ	20 °C	7.9 g/cm ³	DIN EN 10088-1	ASME SA-479
0.2 % yield stress	$R_{p0.2}$	20 °C	190 MPa	DIN EN 10088-3	ASME SA-479
		70 °C	180 MPa	DIN EN 10088-3	ASME SA-479
		100 °C	175 MPa	DIN EN 10088-3	ASME SA-479
1.0 % yield stress	$R_{p1.0}$	20 °C	225 MPa	DIN EN 10088-3	ASME SA-479
		70 °C	212 MPa	DIN EN 10088-3	ASME SA-479
		100 °C	205 MPa	DIN EN 10088-3	ASME SA-479
Ultimate tensile strength	R_m	20 °C	500 MPa	DIN EN 10088-3	ASME SA-479
Elastic modulus	E	20 °C	2.00E5 MPa	DIN EN 10088-1	ASME SA-479
		100 °C	1.94E5 MPa	DIN EN 10088-1	ASME SA-479
Poisson's ratio	ν		0.3		
Elongation at fracture	A		40 %	DIN EN 10088-3	ASME SA-479
Linear thermal expansion coefficient	α	20-100 °C	16E-6 K ⁻¹	DIN EN 10088-1	ASME SA-479

Table 25: Material data for shapes of material No. 1.4571 (Type 316Ti)

Material property	Designation	Temperature	Value	Applicable EU standards	Applicable US standards
Density	ρ	20 °C	8.0 g/cm ³	DIN EN 10088-1	ASME SA-479
0.2 % yield stress	$R_{p0.2}$	20 °C	200 MPa	DIN EN 10088-3	ASME SA-479
		70 °C	191 MPa	DIN EN 10088-3	ASME SA-479
		100 °C	185 MPa	DIN EN 10088-3	ASME SA-479
1.0 % yield stress	$R_{p1.0}$	20 °C	235 MPa	DIN EN 10088-3	ASME SA-479
		70 °C	223 MPa	DIN EN 10088-3	ASME SA-479
		100 °C	215 MPa	DIN EN 10088-3	ASME SA-479
Ultimate tensile strength	R_m	20 °C	500 MPa	DIN EN 10088-3	ASME SA-479
Elastic modulus	E	20 °C	2.00E5 MPa	DIN EN 10088-1	ASME SA-479
		100 °C	1.94E5 MPa	DIN EN 10088-1	ASME SA-479
Poisson's ratio	ν		0.3		
Elongation at fracture	A		40 %	DIN EN 10088-3	ASME SA-479
Linear thermal expansion coefficient	α	20-100 °C	16.5E-6 K ⁻¹	DIN EN 10088-1	ASME SA-479

Table 26: Material data for bars of material No. 1.4542 (Type 630)

Material property	Designation	Temperature	Value	Applicable EU standards	Applicable US standards
Density	ρ	20 °C	7.8 g/cm ³	DIN EN 10088-1	ASME SA-564
0.2 % yield stress	$R_{p0.2}$	20 °C	720 MPa	DIN EN 10088-3	ASME SA-564
		100 °C	680 MPa	DIN EN 10088-3	ASME SA-564
Ultimate tensile strength	R_m	20 °C	930 MPa	DIN EN 10088-3	ASME SA-564
Elastic modulus	E	20 °C	2.00E5 MPa	DIN EN 10088-1	ASME SA-564
		100 °C	1.95E5 MPa	DIN EN 10088-1	ASME SA-564
Poisson's ratio	ν		0.3		ASME SA-564
Elongation at fracture	A		16 %	DIN EN 10088-3	ASME SA-564
Linear thermal expansion coefficient	α	20-100 °C	10.9E-6 K ⁻¹	DIN EN 10088-1	ASME SA-564

Table 27: Material data for plates of material No. 1.4462 (Type 2205)

Material property	Designation	Temperature	Value	Applicable EU standards	Applicable US standards
Density	ρ	20 °C	7.8 g/cm ³	DIN EN 10088-1	ASME SA-240
0.2 % yield stress	$R_{p0.2}$	20 °C	460 MPa	DIN EN 10088-2	ASME SA-240
		70 °C	398 MPa	DIN EN 10088-2	ASME SA-240
		100 °C	360 MPa	DIN EN 10088-2	ASME SA-240
Ultimate tensile strength	R_m	20 °C	640 MPa	DIN EN 10088-2	ASME SA-240
Elastic modulus	E	20 °C	2.00E5 MPa	DIN EN 10088-1	ASME SA-240
		100 °C	1.94E5 MPa	DIN EN 10088-1	
Poisson's ratio	ν		0.27		ASME SA-240
Elongation at fracture	A		25 %	DIN EN 10088-2	ASME SA-240
Linear thermal expansion coefficient	α	20-100 °C	13.0E-6 K ⁻¹	DIN EN 10088-1	ASME SA-240

2.2.1.2 Handling

The DN30 packaging is designed for the transport of UF₆. Specified contents are defined in section 1.3.

Strains in the packaging result from the following loads:

- internal pressure
- external pressure
- assembling loads
- handling loads
- temperature gradients in the components

2.2.1.2.1 Internal and external pressure

During handling and transport, the UF₆ content is in solid state. For the analysis of the packaging, it is assumed that the UF₆ and the 30B cylinder have a temperature of 64 °C, which corresponds to the triple point of UF₆. In this condition, the gas pressure above the solid UF₆ is 152 kPa. This value is used for the analytical proof of an internal pressure in the 30B cylinder. For the proof of an external pressure in the 30B cylinder, a pressure difference of 100 kPa is assumed between ambient and internal pressure of the 30B cylinder.

The 30B cylinder is designed according to [ANSI N14.1] and [ISO 7195] for an external pressure of 172 kPa and an internal pressure of 1.38 MPa. Consequently, the requirements concerning the internal and external pressure for the 30B cylinder as well as for the DN30 package are fulfilled.

2.2.1.2.2 Assembling

During assembling, the components of the DN30 packaging are inserted into each other without applying forces. Stresses in the components during assembling are negligible. For tightening the securing bolts of the closure system, tightening torques are defined in handling instruction 0023-HA-2015-001.

2.2.1.2.3 Handling loads

The following handling processes are carried out with the DN30 package:

- Handling of the loaded and empty package by using the lifting lugs at the feet (see Figure 1).
- Handling of the loaded and empty package using a forklift (see Figure 2).
- Handling of the empty package by using slings (see Figure 3).
- Handling of the top half of the DN30 PSP by using the lifting lugs (see Figure 4).

All other operations during handling and loading are carried out manually. The stresses in the respective components are negligible.

2.2.1.2.3.1 Lifting lugs at the feet

2.2.1.2.3.1.1 Static analysis

The DN30 package is lifted with a handling beam. For the analysis of the stresses in the lifting lugs at the feet, the model shown in Figure 15 and Figure 16 is used. Two different lifting cases are investigated:

- the load is distributed over four load attaching points of the DN30 package and
- only two of the four lifting lugs are used in a cross-diagonal pattern.

The angle of the load attaching means to the vertical is assumed to be 30°. For the DN30 package, a mass of 4100 kg is assumed. Hence, considering the hoisting coefficient of 2, the force acting on a single lug is calculated by:

$$F = 2 \cdot \frac{4100 \text{ kg} \cdot 9.81 \frac{\text{m}}{\text{s}^2}}{n_L \cdot \cos 30^\circ} = \frac{92.9 \text{ kN}}{n_L}$$

The minimal thickness of the lug above the hole is:

$$b = 35 \text{ mm} - \frac{25 \text{ mm}}{2} = 22.5 \text{ mm}$$

Conservatively, the cross section for tension failure of the lug (cross section A-A in Figure 16) is calculated assuming the minimal thickness of the lug on both sides of the hole:

$$A_{AA} = 2 \cdot b \cdot t = 2 \cdot 22.5 \text{ mm} \cdot 20 \text{ mm} = 900 \text{ mm}^2$$

Then, the normal stress in the lifting lug is calculated as:

$$S_{zd} = \frac{F}{A_{AA}} = \frac{92.9 \text{ kN}}{n_L \cdot 900 \text{ mm}^2} = \frac{103.2 \text{ MPa}}{n_L}$$

With the yield strength $R_{p0.2}$ at 70 °C of material No. 1.4462 and the compressive strength factor $f_\sigma = 1$ in compliance with [FKM 2012], the stress limit for tensional loads is:

$$S_{SK,zd} = f_\sigma \cdot R_p = 1 \cdot 398 \text{ MPa} = 398 \text{ MPa}$$

The cross section above the hole is (cross section B-B in Figure 16):

$$A_{BB} = b \cdot t = 22.5 \text{ mm} \cdot 20 \text{ mm} = 450 \text{ mm}^2$$

The nominal shear stress for a rectangular profile considering a double shear plane is:

$$T_s = \frac{F}{2 \cdot A_{BB}} = \frac{92.9 \text{ kN}}{n_L \cdot 2 \cdot 450 \text{ mm}^2} = \frac{103.2 \text{ MPa}}{n_L}$$

Given the shear stress factor $f_\tau = 0.577$, the shear stress limit of material No. 1.4462 at 70 °C is (see Table 27):

$$T_{SK,s} = f_\tau \cdot R_p = 0.577 \cdot 398 \text{ MPa} = 230 \text{ MPa}$$

Table 28 lists the resulting safety factors j .

Table 28: Nominal stresses in the lifting lugs at the feet

Number of lifting lugs	$n_L = 2$	$n_L = 4$
Normal stress	$S_{zd} = 51.6 \text{ MPa}$	$S_{zd} = 25.8 \text{ MPa}$
Safety factor (at 70 °C)	$j_{SK,zd} = \left \frac{S_{SK,zd}}{S_{zd}} \right = 7.7$	$j_{SK,zd} = \left \frac{S_{SK,zd}}{S_{zd}} \right = 15.4$
Shear stress	$T_s = 51.6 \text{ MPa}$	$T_s = 25.8 \text{ MPa}$
Safety factor (at 70 °C)	$j_{SK,s} = \left \frac{T_{SK,s}}{T_s} \right = 4.4$	$j_{SK,s} = \left \frac{T_{SK,s}}{T_s} \right = 8.9$

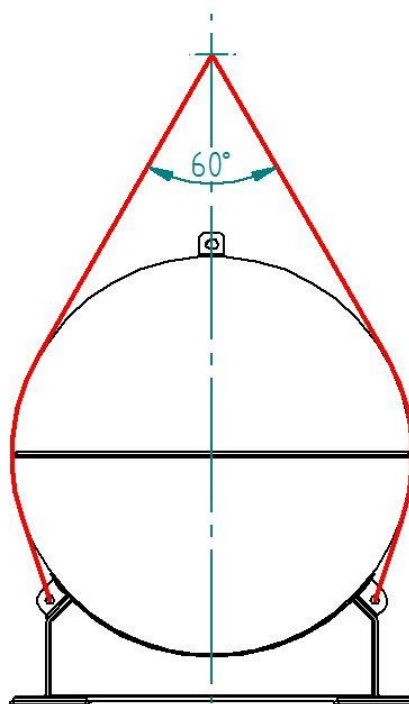


Figure 15: Forces in the handling means of the loaded DN30 package when lifted using the lifting lugs

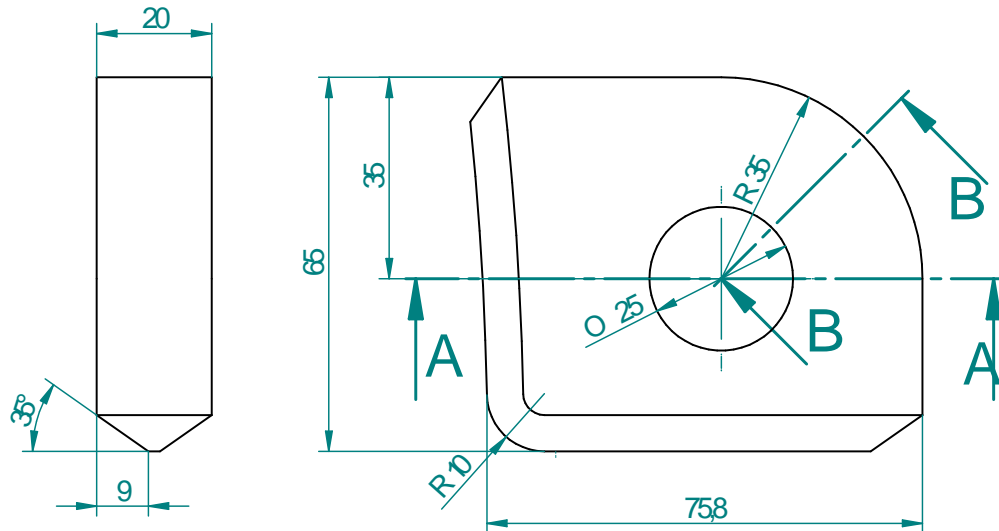


Figure 16: Geometry of the lifting lug for calculation

2.2.1.2.3.1.2 Fatigue analysis of the lifting lugs at the feet

For proof of the fatigue strength, [FKM 2012] is used. The required minimal number of load cycles is assumed to be $\bar{N} = 150000$. This number is higher than the expected number, which corresponds to 50 years in service with 25 transports per year and 100 load cycles for each transport.

The required average force is calculated by

$$F_m = \frac{F_{\max} + F_{\min}}{2} = \frac{F}{2} = \frac{92.8 \text{ kN}}{2 \cdot n_L} = \frac{46.4 \text{ kN}}{n_L}$$

where the minimal force is assumed to be zero. Accordingly, the force amplitude is:

$$F_a = F_{\max} - F_m = F - \frac{F}{2} = \frac{F}{2} = \frac{92.8 \text{ kN}}{2 \cdot n_L} = \frac{46.4 \text{ kN}}{n_L}$$

The corresponding stress amplitude and average stress are:

$$S_{a,zd} = \frac{F_a}{A_{AA}} = \frac{46.4 \text{ kN}}{900 \text{ mm}^2 \cdot n_L} = \frac{51.6 \text{ MPa}}{n_L}$$

$$S_{m,zd} = \frac{F_m}{A_{AA}} = \frac{46.4 \text{ kN}}{900 \text{ mm}^2 \cdot n_L} = \frac{51.6 \text{ MPa}}{n_L}$$

In compliance with [FKM 2012], the fatigue limit for pulsating stress of material No. 1.4462 is chosen to be (see Table 27):

$$\sigma_{W,zd} = f_{W,\sigma} \cdot R_m = 0.4 \cdot 640 \text{ MPa} = 256 \text{ MPa}$$

The stress slope is:

$$G_\sigma(r) = \frac{2.3}{r} = \frac{2.3}{12.5 \text{ mm}} = 0.18 \text{ mm}^{-1}$$

The support number for normal stresses is given by the following formula:

$$n_{\sigma} = 1 + \sqrt{G_{\sigma} \cdot \text{mm}} \cdot 10^{-\left(a_G + \frac{R_m}{b_G \cdot \text{MPa}}\right)}$$

With $a_G = 0.4$ and $b_G = 2400$ the support number is:

$$n_{\sigma} = 1 + \sqrt{0.18 \text{mm}^{-1} \cdot \text{mm}} \cdot 10^{-\left(0.4 + \frac{640 \text{MPa}}{2400 \cdot \text{MPa}}\right)} = 1.09$$

Finally, with the shape factor for flat plates with a hole $K_{t,zd} = 2.25$, the fatigue notch factor is:

$$K_{f,zd} = \frac{K_{t,zd}}{n_{\sigma}} = \frac{2.25}{1.09} = 2.06$$

The fatigue factor considering the surface roughness is calculated with a bounding surface roughness of $R_z = 200 \mu\text{m}$. For steel, the factor $a_{R,\sigma} = 0.22$ and the minimal tensile strength $R_{m,n,\min} = 400 \text{MPa}$ are required.

$$K_{R,\sigma} = 1 - a_{R,\sigma} \cdot \log\left(\frac{R_z}{\mu\text{m}}\right) \cdot \log\left(\frac{2 \cdot R_m}{R_{m,N,\min}}\right) = 1 - 0.22 \cdot \log\left(\frac{200 \mu\text{m}}{\mu\text{m}}\right) \cdot \log\left(\frac{2 \cdot 640 \text{MPa}}{400 \text{MPa}}\right) = 0.74$$

The factors for the edge layer K_V and the protective layer K_S are assumed as 1. The total fatigue factor is hence:

$$K_{WK,zd} = \left(K_{f,zd} + \frac{1}{K_{R,\sigma}} - 1\right) \cdot \frac{1}{K_V \cdot K_S} = 2.06 + \frac{1}{0.74} - 1 = 2.4$$

Then, the fatigue stress limit is:

$$S_{WK,zd} = \frac{\sigma_{W,zd}}{K_{WK,zd}} = \frac{256 \text{MPa}}{2.4} = 107 \text{MPa}$$

The medium stress sensitivity M_{σ} is calculated with $a_M = 0.35$ and $b_M = -0.1$:

$$M_{\sigma} = a_M \cdot 10^{-3} \cdot \frac{R_m}{\text{MPa}} + b_M = 0.35 \cdot 10^{-3} \cdot \frac{640 \text{MPa}}{\text{MPa}} - 0.1 = 0.124$$

Considering the average stress, the factor $K_{AK,zd}$ is then calculated according to [FKM 2012]:

$$K_{AK,zd} = \frac{1}{1 + M_{\sigma} \cdot S_m / S_a} = \frac{1}{1 + 0.124 \cdot 1} = 0.89$$

Hence, the fatigue limit for the stress amplitude is:

$$S_{AK,zd} = K_{AK,zd} \cdot S_{WK,zd} = 0.89 \cdot 107 \text{MPa} = 95 \text{MPa}$$

The resulting fatigue stresses, when two or four lifting lugs are used, are listed in Table 29. The required safety factor is set to $j_D = 1.2$ as the lifting lugs are regularly inspected.

Similarly, the fatigue strength against shear is proven for the cross section above the hole. The corresponding shear stress amplitude and average shear stress are:

$$T_{a,s} = \frac{F_a}{2 \cdot A_{BB}} = \frac{46.4 \text{kN}}{900 \text{mm}^2 \cdot n_L} = \frac{51.6 \text{MPa}}{n_L}$$

$$T_{m,s} = \frac{F_m}{2 \cdot A_{BB}} = \frac{46.4 \text{kN}}{900 \text{mm}^2 \cdot n_L} = \frac{51.6 \text{MPa}}{n_L}$$

The fatigue limit for pulsating shear stress of material No. 1.4462 is:

$$\tau_{W,s} = f_{W,\tau} \cdot \sigma_{W,zd} = 0.577 \cdot 256 \text{ MPa} = 148 \text{ MPa}$$

For the shear stresses no fatigue notch factor is required in the case of a plate with a hole:

$$K_{f,s} = 1$$

The fatigue factor considering the surface roughness $K_{R,\tau}$ is calculated in the same way as the factor $K_{R,\sigma}$.

$$\begin{aligned} K_{R,\tau} &= 1 - f_{W,\tau} \cdot a_{R,\sigma} \cdot \log\left(\frac{R_z}{\mu\text{m}}\right) \cdot \log\left(\frac{2 \cdot R_m}{R_{m,N,\min}}\right) \\ &= 1 - 0.577 \cdot 0.22 \cdot \log\left(\frac{200 \mu\text{m}}{\mu\text{m}}\right) \cdot \log\left(\frac{2 \cdot 640 \text{ MPa}}{400 \text{ MPa}}\right) = 0.85 \end{aligned}$$

Hence, the total fatigue factor in the case of shearing is:

$$K_{WK,s} = \left(K_{f,s} + \frac{1}{K_{R,\tau}} - 1\right) \cdot \frac{1}{K_V \cdot K_S} = 1 + \frac{1}{0.85} - 1 = 1.17$$

The fatigue shear stress limit is:

$$T_{WK,s} = \frac{\tau_{W,s}}{K_{WK,s}} = \frac{148 \text{ MPa}}{1.17} = 126 \text{ MPa}$$

Considering the average shear stress, the factor $K_{AK,s}$ is calculated in compliance with [FKM 2012] with the medium stress sensitivity M_τ :

$$M_\tau = f_{W,\tau} \cdot M_\sigma = 0.577 \cdot 0.124 = 0.074$$

$$K_{AK,s} = \frac{1}{1 + M_\tau \cdot S_m / S_a} = \frac{1}{1 + 0.074 \cdot 1} = 0.933$$

Hence, the fatigue limit for the stress amplitude is:

$$T_{AK,s} = K_{AK,s} \cdot T_{WK,s} = 0.933 \cdot 126 \text{ MPa} = 118 \text{ MPa}$$

The resulting fatigue stresses, when two or four lifting lugs are used, are listed in Table 29. The required safety factor is set to $j_D = 1.2$ as the lifting lugs are regularly inspected.

Table 29: Stress amplitudes in the lifting lugs at the feet

Number of lifting lugs	$n_L = 2$	$n_L = 4$
Normal stress amplitude	$S_{a,zd} = 25.8 \text{ MPa}$	$S_{a,zd} = 12.9 \text{ MPa}$
Safety factor (at 70 °C)	$j_{AK,zd} = \left \frac{S_{AK,zd}}{S_{a,zd}} \right = 3.7$	$j_{AK,zd} = \left \frac{S_{AK,zd}}{S_{a,zd}} \right = 7.3$
Shear stress amplitude	$T_{a,s} = 25.8 \text{ MPa}$	$T_{a,s} = 12.9 \text{ MPa}$
Safety factor (at 70 °C)	$j_{AK,s} = \left \frac{T_{AK,s}}{T_{a,s}} \right = 4.6$	$j_{AK,s} = \left \frac{T_{AK,s}}{T_{a,s}} \right = 9.1$

2.2.1.2.3.1.3 Fatigue analysis of the welding seams at the lifting lugs at the feet

For proof of the fatigue strength of the welding seams between the lifting lugs and the DN30 PSP, the guideline [FKM 2012] is used. To obtain a meaningful distribution of the forces in each double-bevel-groove weld, an FEM analysis is performed in ANSYS Workbench [ANSYS] to calculate the resulting bearing forces.

Geometry

The geometry of the lifting lug used in the FEM analysis is shown in Figure 17.

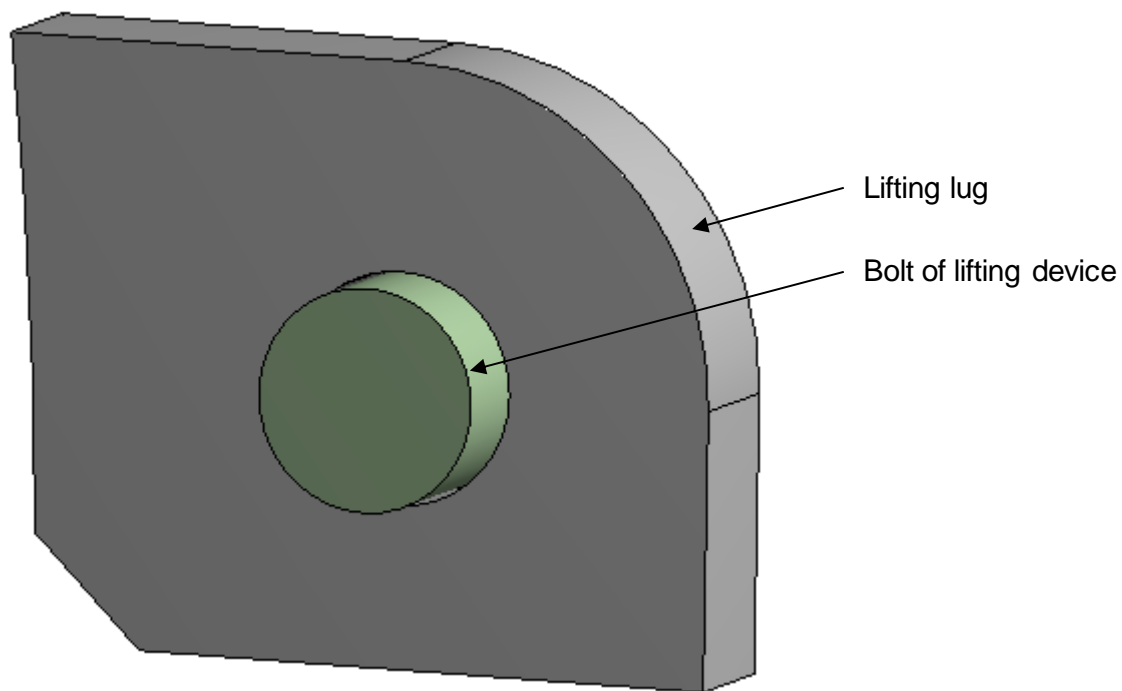


Figure 17: Geometry of the lifting lug for the FEM analysis

Material

For the material of both parts, material No. 1.4307 is used with the material data specified in Table 22. Additionally, the multilinear kinematic hardening model as specified in Table 30 is used. Compared to the DN30 PSP prototype, the lifting lugs of the series DN30 PSP are manufactured of material No. 1.4462. However, the results obtained with material No. 1.4307 are conservative because material No. 1.4462 is stronger than material No. 1.4307.

Table 30: Material 1.4307 for the FEM analysis

Plastic strain [%]	Stress [MPa]	Plastic strain [%]	Stress [MPa]
0	152.8	0.080	370.0
0.001	158.6	0.090	386.4
0.002	164.1	0.100	401.8
0.003	169.3	0.110	416.3
0.004	174.4	0.120	430.3
0.005	179.2	0.130	443.5
0.006	183.8	0.140	456.3
0.007	188.3	0.150	468.5
0.008	192.7	0.160	480.4
0.009	196.9	0.170	491.8
0.010	200.9	0.180	502.8
0.012	208.8	0.190	513.5
0.014	216.2	0.200	523.9
0.016	223.3	0.300	615.0
0.018	230.0	0.400	690.0
0.020	236.5	0.500	754.8
0.030	265.8	0.600	812.6
0.040	291.0	0.700	865.0
0.050	313.5	0.800	913.3
0.060	333.9	0.900	958.2
0.070	352.6	1.000	1000.2

Meshing

The solid element formulation SOLID186 with quadratic shape functions is used for meshing. The mesh shown in Figure 18 consists of 24546 nodes and 5220 elements.

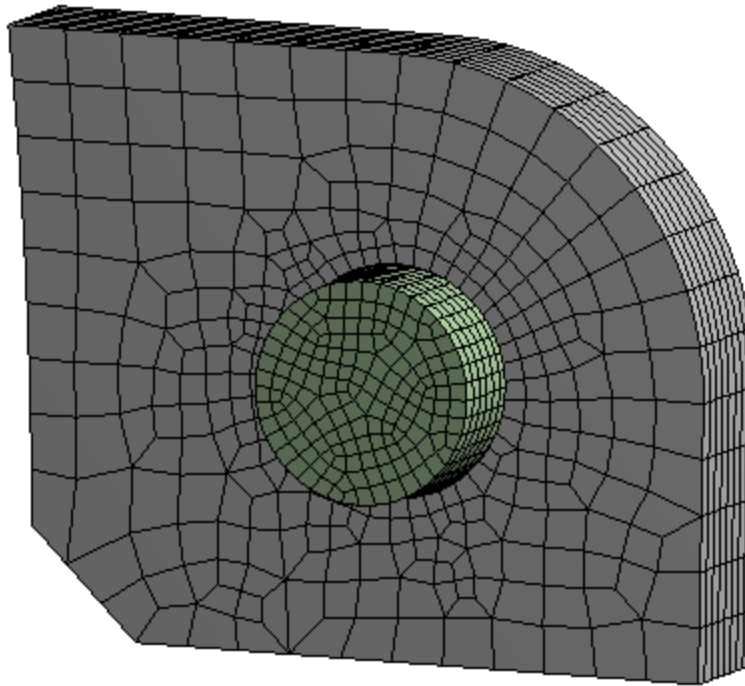


Figure 18: Mesh of the lifting lug used for the FEM analysis

Boundary conditions

The boundary conditions are shown in Figure 19. The force acting on a single lug is displayed on the left, marked in red. For the case that only two of the four lifting lugs are loaded ($n_L = 2$), the force is calculated according to the formula listed at the beginning of section 2.2.1.2.3.1:

$$F = 2 \cdot \frac{4100 \text{ kg} \cdot 9.81 \frac{\text{m}}{\text{s}^2}}{2 \cdot \cos 30^\circ} = 46.4 \text{ kN}$$

The fixed support representing the welded connection is shown on the right side, marked in blue with "A" and "B".

The pin and the lifting lug interact using a frictional contact with a friction coefficient of 0.15.

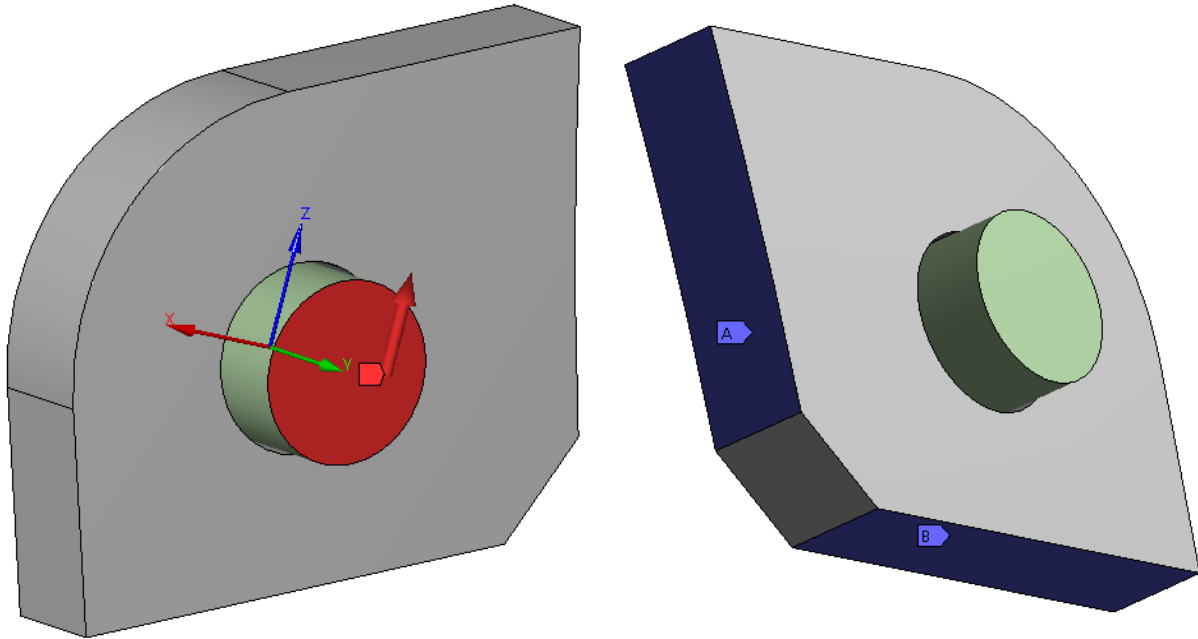


Figure 19: Boundary conditions for the FEM analysis

Results of the analysis

The reaction forces calculated for the welds are listed in Table 31 below.

Table 31: Reaction forces obtained from the FEM analysis

Number of lifting lugs	$n_L = 2$	$n_L = 4$
Left weld	$F_{\max,\perp} = 10282 \text{ N}$	$F_{\max,\perp} = 5141.0 \text{ N}$
	$F_{\max,\parallel} = 14968 \text{ N}$	$F_{\max,\parallel} = 7484.0 \text{ N}$
Lower weld	$F_{\max,\perp} = 28324 \text{ N}$	$F_{\max,\perp} = 14162 \text{ N}$
	$F_{\max,\parallel} = 6537.1 \text{ N}$	$F_{\max,\parallel} = 3268.6 \text{ N}$

For a sensitivity analysis, the element size of the mesh was reduced by 50 %. The resulting difference for the reaction forces are in the range of $\pm 0.25 \%$ of the forces shown in Table 31.

The total length of the left butt weld in Figure 16 is:

$$l_{\text{left}} = 65 \text{ mm}$$

The left and the lower welding seams are double-bevel-groove welds. These are through welded butt welds with a minimal thickness of $a = 20 \text{ mm}$ so that the corresponding welding cross section for the left welding seam is:

$$A_{W,\text{left}} = a \cdot l_{\text{left}} = 1300 \text{ mm}^2$$

In all cases, the minimal force is assumed to be zero. This results in the following nominal tension and shear stress amplitudes and average tension and shear stresses for the left weld:

$$S_{a,\perp,\text{left}} = \frac{F_{a,\perp}}{A_{W,\text{left}}} = \frac{7.91 \text{ MPa}}{n_L}$$

$$S_{m,\perp,\text{left}} = \frac{F_{m,\perp}}{A_{W,\text{left}}} = \frac{7.91 \text{ MPa}}{n_L}$$

$$T_{a,\text{left}} = \frac{F_{a,\parallel}}{A_{W,\text{left}}} = \frac{11.5 \text{ MPa}}{n_L}$$

$$T_{m,\text{left}} = \frac{F_{m,\parallel}}{A_{W,\text{left}}} = \frac{11.5 \text{ MPa}}{n_L}$$

The length of the lower weld in Figure 16 is:

$$l_{\text{lower}} = 75.8 \text{ mm}$$

The corresponding welding cross section is:

$$A_{W,\text{lower}} = a \cdot l_{\text{lower}} = 1516 \text{ mm}^2$$

Again, the minimal force is assumed to be zero. This results in the following nominal tension and shear stress amplitudes and average tension and shear stresses for the lower weld:

$$S_{a,\perp,\text{lower}} = \frac{F_{a,\perp}}{A_{W,\text{lower}}} = \frac{18.7 \text{ MPa}}{n_L}$$

$$S_{m,\perp,\text{lower}} = \frac{F_{m,\perp}}{A_{W,\text{lower}}} = \frac{18.7 \text{ MPa}}{n_L}$$

$$T_{a,\text{lower}} = \frac{F_{a,\parallel}}{A_{W,\text{lower}}} = \frac{4.31 \text{ MPa}}{n_L}$$

$$T_{m,\text{lower}} = \frac{F_{m,\parallel}}{A_{W,\text{lower}}} = \frac{4.31 \text{ MPa}}{n_L}$$

For full penetration welds, the fatigue limit under shearing is considered. In compliance with [FKM 2012], the design factor is FAT 80 in the case of the lifting lugs and the fatigue limit conversion factors equal $f_{\text{FAT},\sigma} = 0.37$ and $f_{\text{FAT},\tau} = 0.23$. The thickness factor f_t , the factor for the edge layer K_V and the constant $K_{\text{NL},E}$ are all equal to 1. Then, the corresponding fatigue limits for tension and shearing are:

$$S_{WK,\perp} = \text{FAT}_{\perp} \cdot f_{\text{FAT},\sigma} \cdot f_t \cdot K_V \cdot K_{\text{NL},E} = 80 \text{ MPa} \cdot 0.37 = 29.6 \text{ MPa}$$

$$T_{WK} = \text{FAT}_{\tau} \cdot f_{\text{FAT},\tau} \cdot f_t \cdot K_V = 80 \text{ MPa} \cdot 0.23 = 18.4 \text{ MPa}$$

With $M_{\sigma} = 0.3$ and $M_{\tau} = 0.17$, the factors for the average stress are calculated as:

$$K_{AK,\perp} = \frac{1}{1 + M_{\sigma} \cdot S_{m,\perp}/S_{a,\perp}} = \frac{1}{1 + 0.30 \cdot 1} = 0.769$$

$$K_{AK,\tau} = \frac{1}{1 + M_{\tau} \cdot T_m/T_a} = \frac{1}{1 + 0.17 \cdot 1} = 0.855$$

The factors for the residual stresses are equal to $K_{E,\sigma} = 1.54$ and $K_{E,\tau} = 1.3$. Overall, the fatigue limit stresses for tension and shearing for both welding seams of the lifting lugs are calculated as:

$$S_{AK,\perp} = K_{AK,\perp} \cdot K_{E,\sigma} \cdot S_{WK,\perp} = 0.769 \cdot 1.54 \cdot 29.6 \text{ MPa} = 35.1 \text{ MPa}$$

$$T_{AK} = K_{AK,\tau} \cdot K_{E,\tau} \cdot T_{WK} = 0.855 \cdot 1.30 \cdot 18.4 \text{ MPa} = 20.4 \text{ MPa}$$

The required safety factor is set to $j_D = 1.2$ as the lifting lugs are regularly inspected.

The resulting stress amplitudes and safety factors in the case of two or four loaded lifting lugs are listed in Table 32 for the left welding seam and in Table 33 for the lower welding seam.

Table 32: Stress amplitudes in the left welding seam of the lifting lugs at the feet

Number of lifting lugs	$n_L = 2$	$n_L = 4$
Normal Stress amplitude	$S_{a,\perp,\text{left}} = 3.95 \text{ MPa}$	$S_{a,\perp,\text{left}} = 1.98 \text{ MPa}$
Safety factor (at 70 °C)	$j_{AK,\perp} = \left \frac{S_{AK,\perp}}{S_{a,\perp,\text{left}}} \right = 8.9$	$j_{AK,\perp} = \left \frac{S_{AK,\perp}}{S_{a,\perp,\text{left}}} \right = 17.7$
Shear stress amplitude	$T_{a,\text{left}} = 5.76 \text{ MPa}$	$T_{a,\text{left}} = 2.88 \text{ MPa}$
Safety factor (at 70 °C)	$j_{AK,\tau} = \left \frac{T_{AK}}{T_{a,\text{left}}} \right = 3.5$	$j_{AK,\tau} = \left \frac{T_{AK}}{T_{a,\text{left}}} \right = 7.1$
Combined safety factor (at 70 °C)	$j_{AK,SN} = \frac{1}{\frac{1}{2} \left(\frac{1}{j_{AK,\perp}} + \sqrt{\left(\frac{1}{j_{AK,\perp}} \right)^2 + 4 \cdot \left(\frac{1}{j_{AK,\tau}} \right)^2} \right)}$ $= 2.9$	$j_{AK,SN} = \frac{1}{\frac{1}{2} \left(\frac{1}{j_{AK,\perp}} + \sqrt{\left(\frac{1}{j_{AK,\perp}} \right)^2 + 4 \cdot \left(\frac{1}{j_{AK,\tau}} \right)^2} \right)}$ $= 5.8$

Table 33: Stress amplitudes in the lower welding seam of the lifting lugs at the feet

Number of lifting lugs	$n_L = 2$	$n_L = 4$
Normal Stress amplitude	$S_{a,\perp,\text{lower}} = 9.34 \text{ MPa}$	$S_{a,\perp,\text{lower}} = 4.67 \text{ MPa}$
Safety factor (at 70 °C)	$j_{AK,\perp} = \left \frac{S_{AK,\perp}}{S_{a,\perp,\text{left}}} \right = 3.7$	$j_{AK,\perp} = \left \frac{S_{AK,\perp}}{S_{a,\perp,\text{left}}} \right = 7.5$
Shear stress amplitude	$T_{a,\text{lower}} = 2.16 \text{ MPa}$	$T_{a,\text{lower}} = 1.08 \text{ MPa}$
Safety factor (at 70 °C)	$j_{AK,\tau} = \left \frac{T_{AK}}{T_{a,\text{left}}} \right = 9.4$	$j_{AK,\tau} = \left \frac{T_{AK}}{T_{a,\text{left}}} \right = 18.8$
Combined safety factor (at 70 °C)	$j_{AK,SN} = \frac{1}{\frac{1}{2} \left(\frac{1}{j_{AK,\perp}} + \sqrt{\left(\frac{1}{j_{AK,\perp}} \right)^2 + 4 \cdot \left(\frac{1}{j_{AK,\tau}} \right)^2} \right)}$ $= 3.3$	$j_{AK,SN} = \frac{1}{\frac{1}{2} \left(\frac{1}{j_{AK,\perp}} + \sqrt{\left(\frac{1}{j_{AK,\perp}} \right)^2 + 4 \cdot \left(\frac{1}{j_{AK,\tau}} \right)^2} \right)}$ $= 6.6$

2.2.1.2.3.2 Forklift pockets

2.2.1.2.3.2.1 Static analysis

Identically to the calculation of the tie-down forces in section 2.2.1.3.1, it is assumed that the forces caused by accelerations are acting in the center of the DN30 package. When the DN30 package is handled by the forklift pockets, it is assumed that 2 g are acting in axial and lateral direction, respectively. A combination of accelerations in axial and lateral direction is not assumed as this is highly unrealistic. Therefore, the axial and lateral forces are:

$$F_a = F_l = m_{\text{DN30}} \cdot 2g = 4100 \text{ kg} \cdot 2 \cdot 9.81 \frac{\text{m}}{\text{s}^2} = 80.4 \text{ kN}$$

The forklift pockets consisting of 3 mm thick steel plates are welded to the connection profile. With the welding thickness $a_W = 3 \text{ mm}$, the minimal welding seam area is at each connection point:

$$A_W = a_W \cdot l_W = 3 \text{ mm} \cdot (2 \cdot 70 \text{ mm} + 216 \text{ mm}) = 1068 \text{ mm}^2$$

First, the case of a load in the axial direction of the DN30 package is investigated. Such a load causes a tilting of the DN30 package that results in tensile stresses in the welding seams. The relevant height of the center of gravity of the package from the connection point is:

$$h = 692 \text{ mm} - 145 \text{ mm} = 547 \text{ mm}$$

The distance between the centers of each forklift pocket is:

$$d_{\text{FLP}} = 700 \text{ mm}$$

If only one connection point is taking the whole load, the force at one connection point caused by the tilting is:

$$F = F_a \cdot \frac{h}{d_{\text{FLP}}} = 80.4 \text{ kN} \cdot \frac{547 \text{ mm}}{700 \text{ mm}} = 62.8 \text{ kN}$$

The tensile stress in the welding seams is:

$$S_{\perp, \text{zd}, a} = \frac{F}{2 \cdot A_W} = \frac{62.8 \text{ kN}}{2 \cdot 1068 \text{ mm}^2} = 29.4 \text{ MPa}$$

Next, tilting in the lateral direction of the DN30 package is investigated. The relevant center distance of the welding seams is:

$$d_{\text{WS}} = 500 \text{ mm}$$

Hence, if only one connection point is taking the whole load, the force at one connection point is:

$$F = F_l \cdot \frac{h}{d_{\text{WS}}} = 80.4 \text{ kN} \cdot \frac{547 \text{ mm}}{500 \text{ mm}} = 88 \text{ kN}$$

The tensile stress in the welding seams is

$$S_{\perp, \text{zd}, l} = \frac{F}{2 \cdot A_W} = \frac{88 \text{ kN}}{2 \cdot 1068 \text{ mm}^2} = 41.2 \text{ MPa}$$

The allowable normal stress for the welding seam is calculated in compliance with [FKM 2012]. Therefore, the yield strength of the base material needs to be applied (material No. 1.4307 at

70 °C in Table 22). Since the welding seams at the connection points are fillet welds, the welding seam factor is conservatively assumed to be $\alpha_W = 0.8$:

$$S_{SK,\perp,zd} = R_{p0,2} \cdot \alpha_W = 140 \text{ MPa}$$

Then, the resulting safety factors for the axial and lateral direction are:

$$j_{SK,\perp,zd,a} = \left| \frac{S_{SK,\perp,zd}}{S_{\perp,zd,a}} \right| = 4.8 \quad j_{SK,\perp,zd,l} = \left| \frac{S_{SK,\perp,zd}}{S_{\perp,zd,l}} \right| = 3.4$$

2.2.1.2.3.2.2 Fatigue analysis

The calculated stresses in the previous section only occur in case of the assumed high accelerations of 2 g in the axial and lateral direction. Small vibrations would not lead to tilting of the DN30 package and, thus, no tensile forces occur at the welding seams. Consequently, a fatigue analysis is neither required for the welding seams nor for the forklift pockets themselves as the DN30 package would be resting safely on the forks of the forklift even without the forklift pockets.

2.2.1.2.3.3 Lifting of the empty DN30 PSP with slings

For the calculation, it is assumed that the DN30 package is a simply supported beam. Conservatively, the supports are assumed to be at each end (distance 2435 mm) and the load is concentrated in the center. For the moment of inertia, only the outer shell of the bottom half of the DN30 is taken into account.

The force is calculated with a hoisting coefficient of $h_c = 2$:

$$F_{\text{Lift}} = h_c \cdot m_{\text{DN30}} \cdot g = 2 \cdot 4100 \text{ kg} \cdot 9.81 \frac{\text{m}}{\text{s}^2} = 80.4 \text{ kN}$$

Hence, the bending moment is:

$$M_b = 2435 \text{ mm} \cdot \frac{F_{\text{Lift}}}{4} = 4.9 \cdot 10^4 \text{ Nm}$$

The moment of inertia about the vertical axis is according to [YOUNG 1998], Table 1, case 22:

$$I = \frac{\pi}{8} \cdot (R^4 - R_i^4) - \frac{8}{9\pi} \cdot \frac{(R^3 - R_i^3)^2}{R^2 - R_i^2}$$

And the largest distance of the neutral axis to the outer fiber is:

$$y_{1b} = \frac{4}{3\pi} \cdot \frac{R^3 - R_i^3}{R^2 - R_i^2}$$

With $R = 553 \text{ mm}$, $R_i = 547 \text{ mm}$, $I = 2.97 \cdot 10^8 \text{ mm}^4$, $y_{1b} = 350 \text{ mm}$ and $W_b = 8.48 \cdot 10^5 \text{ mm}^3$, the bending stress is:

$$S_b = \frac{M_b}{W_b} = \frac{4.9 \cdot 10^4 \text{ Nm}}{8.48 \cdot 10^5 \text{ mm}^3} = 57.7 \text{ MPa} < R_{p0,2} = 175 \text{ MPa at } 70^\circ$$

Safety factor against $R_{p0,2}$ at 70 °C (see Table 22):

$$j_{SK,b} = \frac{R_{p0,2}}{S_b} = 3$$

2.2.1.2.3.4 Lifting lugs at the top half

2.2.1.2.3.4.1 Static analysis

For the analysis of the stresses in the lifting lugs, the model shown in Figure 20 and Figure 21 is used.

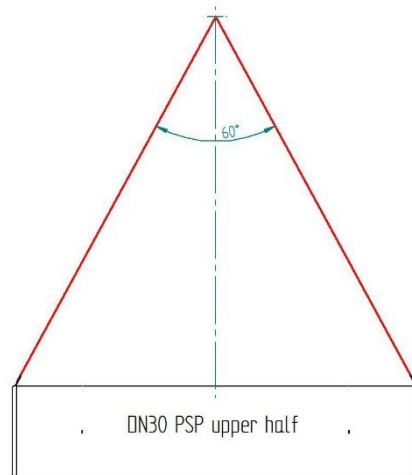


Figure 20: Forces in the handling means when lifting the top half

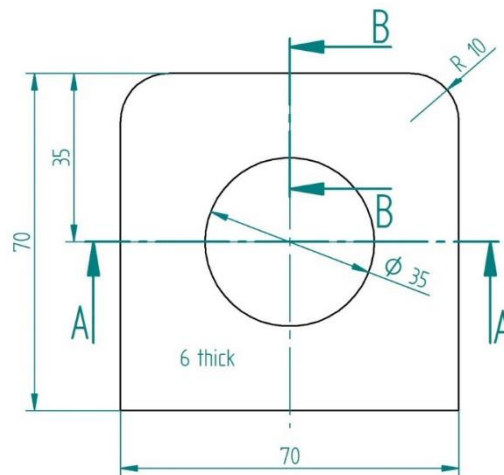


Figure 21: Geometry of the lifting lug for calculation of the handling of the top half

The top half of the DN30 PSP is lifted using the two load attaching points. The angle of the load attaching means to the vertical is assumed to be 30°. For the top half of the DN30 PSP, a mass of 500 kg is assumed. Taking into account a hoisting coefficient of $h_c = 2$, the force acting on one lug is:

$$F = h_c \cdot \frac{m_{\text{top}} \cdot g}{2 \cdot \cos \alpha} = 2 \cdot \frac{500 \text{ kg} \cdot 9.81 \frac{\text{m}}{\text{s}^2}}{2 \cdot \cos 30^\circ} = 5.7 \text{ kN}$$

The cross section across of the hole is (cross section A-A in Figure 21):

$$A_{AA} = (70 \text{ mm} - 35 \text{ mm}) \cdot 6 \text{ mm} = 210 \text{ mm}^2$$

The nominal stress in the lifting lug is:

$$S_{zd} = \frac{F}{A_{AA}} = \frac{5.7 \text{ kN}}{210 \text{ mm}^2} = 27 \text{ MPa} < R_{p0.2} = 147 \text{ MPa (at } 100^\circ \text{C)}$$

The safety factor is:

$$j_{SK,zd} = \frac{R_{p0.2}}{S_{zd}} = 5.5$$

The cross section above the hole is (cross section B-B in Figure 21):

$$A_{BB} = \left(35 \text{ mm} - \frac{35 \text{ mm}}{2} \right) \cdot 6 \text{ mm} = 105 \text{ mm}^2$$

The shear stress for a double shear plane is:

$$T_s = \frac{F}{2 \cdot A_{BB}} = \frac{5.7 \text{ kN}}{210 \text{ mm}^2} = 27.0 \text{ MPa} < \frac{R_{p0.2}}{\sqrt{3}} = 85 \text{ MPa (at } 100^\circ \text{C)}$$

The safety factor is:

$$j_{SK,s} = \frac{R_{p0.2}/\sqrt{3}}{T_s} = 3.1$$

2.2.1.2.3.4.2 Fatigue analysis

For proof of the fatigue strength, [FKM 2012] is used. The required minimal number of load cycles is assumed to be $\bar{N} = 150000$. This number is higher than the expected number that corresponds to 50 years in service with 25 transports per year and 100 load cycles for each transport. The average force and force amplitude are calculated by:

$$F_m = \frac{F_{\max} + F_{\min}}{2} = 2.8 \text{ kN}$$

$$F_a = F_{\max} - F_m = 2.8 \text{ kN}$$

The corresponding stress amplitude and average stress are:

$$S_{a,zd} = \frac{F_a}{A_{AA}} = 13.5 \text{ MPa}$$

$$S_{m,zd} = \frac{F_m}{A_{AA}} = 13.5 \text{ MPa}$$

The fatigue limit for pulsating stress of material No. 1.4307 is:

$$\sigma_{W,\sigma} = f_{W,\sigma} \cdot R_m = 0.4 \cdot 520 \text{ MPa} = 208 \text{ MPa}$$

The stress slope is:

$$\bar{G}_\sigma = \frac{2.3}{r} = \frac{2.3}{17.5 \text{ mm}} = 0.131 \text{ mm}^{-1}$$

The derived support number for normal stresses is:

$$n_{\sigma} = 1 + \sqrt{\bar{G}_{\sigma} \cdot \text{mm} \cdot 10^{-\left(a_G + \frac{R_m}{b_G \cdot \text{MPa}}\right)}}$$

With $a_G = 0.4$ and $b_G = 2400$, this results in:

$$n_{\sigma} = 1 + \sqrt{0.131 \text{ mm}^{-1} \cdot \text{mm} \cdot 10^{-\left(0.4 + \frac{520 \text{ MPa}}{2400 \cdot \text{MPa}}\right)}} = 1.088$$

The shape factor for flat plates with a hole is:

$$K_{t,zd} = 2.15$$

And finally, the fatigue notch factor is:

$$K_{f,zd} = \frac{K_{t,zd}}{n_{\sigma}} = \frac{2.1}{1.104} = 1.98$$

For the fatigue factor considering the surface roughness, a value of $K_{R,\sigma} = 0.79$ is obtained. This leads to the following total fatigue factor:

$$K_{WK,zd} = K_{f,zd} + \frac{1}{K_{R,\sigma}} - 1 = 2.24$$

The resulting fatigue stress limit is:

$$S_{WK,zd} = \frac{\sigma_{W,zd}}{K_{WK,zd}} = \frac{208 \text{ MPa}}{2.2} = 92.8 \text{ MPa}$$

Considering the average stress, the factor $K_{AK,zd}$ is calculated as:

$$K_{AK,zd} = 0.92$$

Hence, the fatigue limit for the stress amplitude is:

$$S_{AK,zd} = K_{AK,zd} \cdot S_{WK,zd} = 85.7 \text{ MPa}$$

The required safety factor is set to 1.2 as the lifting lugs are regularly inspected. The actual safety factor is:

$$j_{AK,zd} = \left| \frac{S_{AK,zd}}{S_{a,zd}} \right| = 6.4 > 1.2$$

The corresponding shear stress amplitude and average shear stress are:

$$T_{a,s} = \frac{F_a}{2 \cdot A_{BB}} = 13.5 \text{ MPa}$$

$$T_{m,s} = \frac{F_m}{2 \cdot A_{BB}} = 13.5 \text{ MPa}$$

The fatigue limit for pulsating stress of material No. 1.4307 is (see Table 22):

$$\tau_{W,s} = f_{W,\tau} \cdot \sigma_{W,zd} = 0.58 \cdot 208 \text{ MPa} = 120 \text{ MPa}$$

The derived fatigue notch factor is:

$$K_{f,s} = \frac{K_{t,s}}{n_\tau} = \frac{2.15}{1} = 2.15$$

For the fatigue factor considering the surface roughness, a value of $K_{R,\tau} = 0.88$ is obtained. This leads to the following total fatigue factor:

$$K_{WK,s} = K_{f,s} + \frac{1}{K_{R,\tau}} - 1 = 2.29$$

The resulting fatigue stress limit is:

$$T_{WK,s} = \frac{\tau_{W,s}}{K_{WK,s}} = \frac{120 \text{ MPa}}{2.2} = 52.5 \text{ MPa}$$

Considering the average shear stress, the factor $K_{AK,s}$ is calculated as $K_{AK,s} = 0.95$. Hence, the fatigue limit for the stress amplitude is:

$$T_{AK,s} = K_{AK,s} \cdot T_{WK,s} = 50.1 \text{ MPa}$$

The required safety factor is set to 1.2 as the lifting lugs are regularly inspected. The actual safety factor is:

$$j_{AK,s} = \left| \frac{T_{AK,s}}{T_{a,s}} \right| = 3.7 > 1.2$$

2.2.1.2.3.4.3 Fatigue analysis of the welding seam

For proof of the fatigue strength of the welding seam between the lifting lug and the DN30 PSP, [FKM 2012] is used. The welding is subjected to tensile and shear loads. The length of the welding seam in Figure 21 is:

$$l = 2 \cdot 70 \text{ mm} + 2 \cdot 6 \text{ mm} = 152 \text{ mm}$$

The effective welding thickness is minimal $a_W = 3 \text{ mm}$. The corresponding welding cross section is:

$$A_W = a_W \cdot l_W = 456 \text{ mm}^2$$

This results in the following nominal stress amplitude and average stress:

$$S_{a,zd} = \frac{F_a \cdot \cos(30^\circ)}{A_W} = 5.4 \text{ MPa}$$

$$S_{m,zd} = \frac{F_m \cdot \cos(30^\circ)}{A_W} = 5.4 \text{ MPa}$$

For welds, the material independent fatigue limit stress $\sigma_{W,zd} = 92 \text{ MPa}$ is considered. The design factor for fillet welds is FAT71 for nominal tension stresses so that the fatigue notch factor is:

$$K_{WK,zd} = \frac{225}{\text{FAT}} = 3.17$$

With $M_\sigma = 0.3$, the factor for the average stress is calculated as:

$$K_{AK,zd} = \frac{1}{1 + M_\sigma \cdot \frac{S_{m,zd}}{S_{a,zd}}} = 0.77$$

The factor for the residual stresses is $K_{E,\sigma} = 1.54$. Overall, the fatigue limit stress for the left weld of the lifting lug is calculated as:

$$S_{AK,zd} = K_{AK,zd} \cdot K_{E,\sigma} \cdot \frac{\sigma_{W,zd}}{K_{WK,zd}} = 34.4 \text{ MPa}$$

The safety factor is:

$$j_{AK,zd} = \left| \frac{S_{AK,zd}}{S_{a,zd}} \right| = 6.4$$

The resulting nominal shear stress amplitude and average shear stress are:

$$T_{a,s} = \frac{F_a \cdot \sin(30^\circ)}{A_W} = 3.1 \text{ MPa}$$

$$T_{m,s} = \frac{F_m \cdot \sin(30^\circ)}{A_W} = 3.1 \text{ MPa}$$

For welds, the material independent fatigue limit shear stress $\tau_{W,s} = 37 \text{ MPa}$ is considered. The design factor for fillet welds is FAT 80 for nominal stresses so that the fatigue notch factor for shear stress is:

$$K_{WK,s} = \frac{145}{\text{FAT}} = 1.81$$

With $M_\tau = 0.17$, the factor for the average stress is calculated as:

$$K_{AK,s} = \frac{1}{1 + M_\tau \cdot \frac{T_{m,s}}{T_{a,s}}} = 0.85$$

The factor for the residual stresses is $K_{E,\tau} = 1.3$. Overall, the fatigue limit stress for the left weld of the lifting lug is calculated as:

$$T_{AK,s} = K_{AK,s} \cdot K_{E,\tau} \cdot \frac{\tau_{W,s}}{K_{WK,s}} = 22.6 \text{ MPa}$$

The safety factor is:

$$j_{AK,s} = \left| \frac{T_{AK,s}}{T_{a,s}} \right| = 7.3$$

The required safety factor is set to 1.2 as the lifting lugs are regularly inspected. Combining the two stress components results in the following total safety factor:

$$j_{AK,SN} = \frac{1}{\sqrt{\frac{1}{j_{AK,zd}^2} + \frac{1}{j_{AK,s}^2}}} = 4.8 > 1.2$$

Hence, the fatigue strength of the lifting lugs at the top half is proven for the welding seam.

2.2.1.3 Ability to withstand RCT

The DN30 package is transported by road, rail or sea. For the transport, dedicated flat racks are used (see Figure 5). The tie-down features are designed such that relative movement between the vehicle and the DN30 package is excluded. Thus, only the maximum acceleration values defined in Table 18 affect the package during transport.

2.2.1.3.1 Static analysis of tie-down features

For the proof, the mass of the DN30 package is assumed to be $m_{\text{DN30}} = 4100 \text{ kg}$.

Vertical loads

In the vertically upwards direction, counteracting gravitation is considered so that the vertical acceleration is $a_v = -1.0g + 2.0g = 1.0g$. The resulting force because of this acceleration is:

$$F_v = m_{\text{DN30}} \cdot a_v = 40.2 \text{ kN}$$

There are four tie-down points securing the DN30 package on the flat rack. Hence, the normal force per tie-down point is:

$$F_{\text{TP},v} = \frac{1}{4} \cdot F_v = 10.1 \text{ kN}$$

Axial loads

Axially, an acceleration factor of $a_a = 10g$ is assumed. The resulting force because of this acceleration is:

$$F_a = m_{\text{DN30}} \cdot a_a = 402.1 \text{ kN}$$

Since the line of action of the acceleration forces points through the center of gravity of the DN30 package, the equilibrium of moments results in an additional normal force at the two tie-down points at point A (see Figure 23):

$$F_{\text{TP},n,a} = \frac{1}{2} \cdot F_a \cdot \frac{692 \text{ mm}}{1016 \text{ mm}} = 136.9 \text{ kN}$$

The transversal force at each of the four tie-down points is:

$$F_{\text{TP},a} = \frac{1}{4} \cdot F_a = 100.5 \text{ kN}$$

Lateral loads

In the lateral direction, the acceleration factor is $a_l = 5g$. The resulting force because of this acceleration is:

$$F_l = m_{\text{DN30}} \cdot a_l = 201 \text{ kN}$$

Since the line of action of the acceleration forces points through the center of gravity of the DN30 package, the equilibrium of moments results in an additional normal force at the two tie-down points at point B (see Figure 24):

$$F_{TP,n,l} = \frac{1}{2} \cdot F_l \cdot \frac{692 \text{ mm}}{1474 \text{ mm}} = 47.2 \text{ kN}$$

The transversal force at each of the four tie-down points is:

$$F_{TP,l} = \frac{1}{4} \cdot F_l = 50.3 \text{ kN}$$

Superposition of all loads

The maximal normal force at a tie-down point is the sum of all forces applied in the normal direction:

$$F_{TP,n} = F_{TP,v} + F_{TP,n,a} + F_{TP,n,l} = 194.2 \text{ kN}$$

To calculate the maximal transversal force at a tie-down point, the dissimilar orientations of the partial transversal forces are considered:

$$F_{TP,t} = \sqrt{F_{TP,a}^2 + F_{TP,l}^2} = 112.4 \text{ kN}$$

2.2.1.3.1.1 Welding seams joining the bottom plate and the vertical plate

The bottom plate and the vertical plate are joined by a two-sided fillet weld (see Figure 25), each having a thickness of $a_W = 6 \text{ mm}$. The length is $l_W = 200 \text{ mm}$ so that the resulting cross section of the welding seams is:

$$A_W = 2 \cdot a_W \cdot l_W = 2400 \text{ mm}^2$$

The tension and the shear stress in the welding seam are:

$$S_{\perp,zd} = \frac{F_{TP,n}}{A_W} = 80.9 \text{ MPa} \quad T_{\parallel} = \frac{F_{TP,t}}{A_W} = 46.8 \text{ MPa}$$

The allowable normal and shear stress in the welding seam is calculated in compliance with [FKM 2012]. Therefore, the yield strength of the base material needs to be applied (material No. 1.4307 at 70 °C in Table 22). Since this is a fillet weld, the welding seam factor is conservatively assumed to be $\alpha_W = 0.8$:

$$S_{SK,\perp,zd} = R_{p0,2} \cdot \alpha_W = 140 \text{ MPa} \quad T_{SK,\parallel} = R_{p0,2} \cdot \alpha_W = 140 \text{ MPa}$$

To fulfill the requirements of 10CFR §71.45(b)(1) the resulting stresses must not exceed the materials yield strength:

$$j_{SK,\perp,zd} = \left| \frac{S_{SK,\perp,zd}}{S_{\perp,zd}} \right| = 1.73 \quad j_{SK,\parallel} = \left| \frac{T_{SK,\parallel}}{T_{\parallel}} \right| = 2.99$$

$$j_{SK,SN} = \frac{1}{\sqrt{\frac{1}{j_{SK,\perp,zd}^2} + \frac{1}{j_{SK,\parallel}^2}}} = 1.5$$

2.2.1.3.1.2 Welding seams joining the feet and the outer shell of the DN30 PSP

The feet and the outer shell of the DN30 PSP are joined by welding seams having a thickness of $a_W = 2$ mm. Because of the curvature of the welding seams, their length is approximated by a straight line between the outer points of the feet. This conservative approach results in a length of approximately 890 mm in the axial direction. The width of the vertical plates is 200 mm. The welding seams between the outer shell and the profiles connecting the two feet have a thickness of 3 mm, but only 2 mm will be considered in the calculations. The profile length is 1294 mm.

The forces are calculated as described in Section 2.2.1.3.1. However, different lengths are used in the momentum balances. In addition, to account for the continuous welding seam between the feet and the outer shell in the axial direction of the transport vehicle, the approach described in Figure 22 is used.

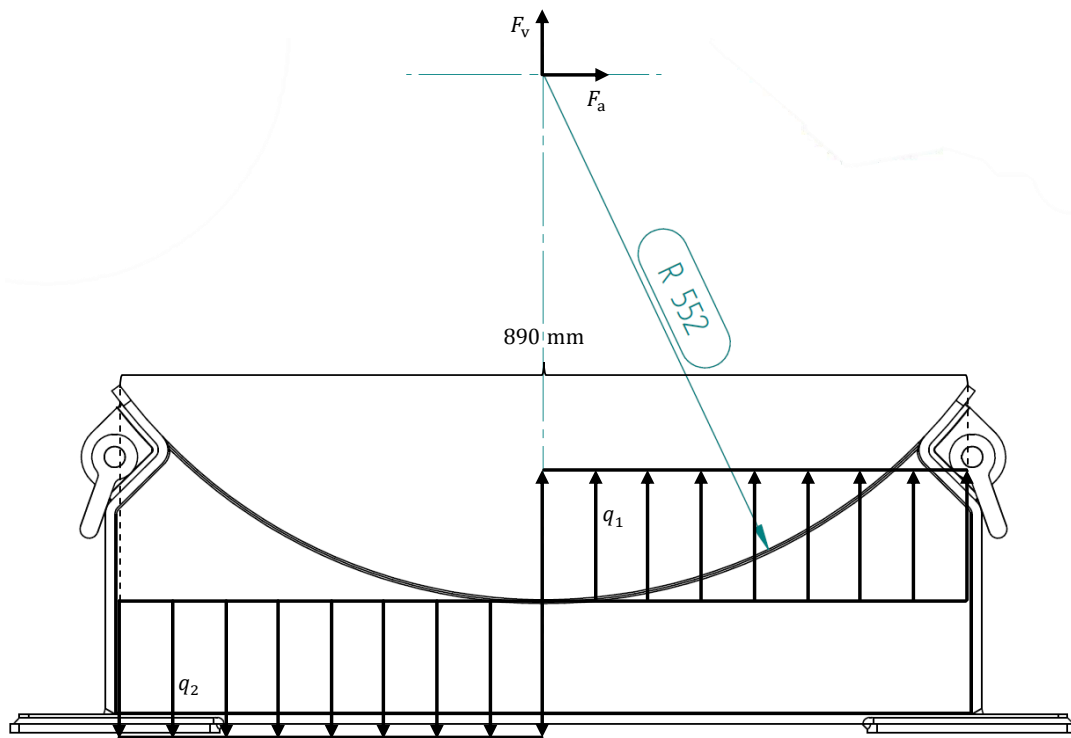


Figure 22: Mechanical model for the welding seams between the feet and the outer shell

Referring to this mechanical model, the equivalent forces of q_1 and q_2 act in the center of these distributed forces, respectively. This leads to the following loads that act on one half of a single foot:

$$F_{TP,n} = \frac{1}{4} \cdot F_v + \frac{1}{2} F_a \cdot \frac{552 \text{ mm}}{890 \text{ mm}} + \frac{1}{2} F_l \cdot \frac{552 \text{ mm}}{\frac{1}{2} \cdot 1474 \text{ mm}} = 210 \text{ kN}$$

$$F_{TP,a} = \frac{1}{4} F_a = 100.5 \text{ kN}$$

$$F_{TP,l} = \frac{1}{4} F_l = 50.3 \text{ kN}$$

In the stress calculations, only those parts of the welding seams being aligned with the applied acceleration force are considered. Since the forces are determined referring only to one half of each of the two feet, the effective length of the welding seams in the axial direction of the transport vehicle is:

$$l_{W,a} = 200 \text{ mm} + 2 \cdot \frac{1}{2} \cdot 1294 \text{ mm} = 1494 \text{ mm}$$

In the lateral direction, only the curved part of the welding seams is considered. With the assumptions made above, the effective length is:

$$l_{W,l} = 2 \cdot \frac{1}{2} \cdot 890 \text{ mm} = 890 \text{ mm}$$

The corresponding cross sections of each part of the welding seams are:

$$A_{W,a} = a_W \cdot l_{W,a} = 1780 \text{ mm}^2$$

$$A_{W,l} = a_W \cdot l_{W,l} = 2988 \text{ mm}^2$$

Stresses because of bending are neglected. In this case, the tensional stress in the welding seams only results from the acceleration force $F_{TP,n}$:

$$S_{\perp} = \frac{F_{TP,n}}{A_{W,a} + A_{W,l}} = 44.0 \text{ MPa}$$

As already mentioned, the shear stress is calculated separately for the axial and the lateral direction. The applied forces are $F_{TP,a}$ and $F_{TP,l}$, respectively:

$$T_{\parallel,a} = \frac{F_{TP,a}}{A_{W,a}} = 56.5 \text{ MPa}$$

$$T_{\parallel,l} = \frac{F_{TP,l}}{A_{W,l}} = 16.8 \text{ MPa}$$

The allowable normal and shear stress for the welding seams are calculated in compliance with [FKM 2012]. Therefore, the yield strength of the base material needs to be applied (material No. 1.4307 at 70 °C in Table 22). Since these are fillet welds, the welding seam factor is conservatively assumed to be $\alpha_W = 0.8$:

$$S_{SK,\perp} = R_{p0,2} \cdot \alpha_W = 140 \text{ MPa}$$

$$T_{SK,\parallel} = R_{p0,2} \cdot \alpha_W = 140 \text{ MPa}$$

To fulfill the requirements of 10CFR §71.45(b)(1) the resulting stresses must not exceed the materials yield strength:

$$j_{SK,\perp} = \left| \frac{S_{SK,\perp}}{S_{\perp}} \right| = 3.2 \quad j_{SK,\parallel,a} = \left| \frac{T_{SK,\parallel}}{T_{\parallel,a}} \right| = 2.5 \quad j_{SK,\parallel,l} = \left| \frac{T_{SK,\parallel}}{T_{\parallel,l}} \right| = 8.3$$

$$j_{SK,SN,a} = \frac{1}{\sqrt{\frac{1}{j_{SK,\perp}^2} + \frac{1}{j_{SK,\parallel,a}^2}}} = 2.0 \quad j_{SK,SN,l} = \frac{1}{\sqrt{\frac{1}{j_{SK,\perp}^2} + \frac{1}{j_{SK,\parallel,l}^2}}} = 3.0$$

2.2.1.3.1.3 Bottom plate

The bottom plate consists of two steel sheets, each having a thickness of 10 mm. The two sheets are joined by welding (see Figure 25) so that the total sheet thickness is $t = 20$ mm.

For the calculation, it is assumed that the reaction forces and moments occur at a distance of 5 mm away from the vertical plate. The forces correspond to the tie-down forces calculated in the beginning of Section 2.2.1.3.1, and the moments are calculated assuming the tie-down forces act in the midplane of the vertical plate of the feet that has a thickness of 10 mm:

$$M_{by} = F_{TP,n} \cdot \left(5 \text{ mm} + \frac{10 \text{ mm}}{2} \right) = 1941.7 \text{ Nm}$$

$$M_{bz} = F_{TP,l} \cdot \left(5 \text{ mm} + \frac{10 \text{ mm}}{2} \right) = 502.6 \text{ Nm}$$

The corresponding section moduli at point A are:

$$W_{by} = \frac{b \cdot h^2}{6} = 13333 \text{ mm}^3$$

$$W_{bz} = \frac{b^2 \cdot h}{6} = 133333 \text{ mm}^3$$

Then, the maximum bending stresses at point A are:

$$S_{by} = \frac{M_{by}}{W_{by}} = 145.6 \text{ MPa}$$

$$S_{bz} = \frac{M_{bz}}{W_{bz}} = 3.8 \text{ MPa}$$

The tie-down forces in the vertical and lateral direction cause shear stresses. The shearing area is in both cases:

$$A_{\tau} = b \cdot t = 4000 \text{ mm}^2$$

The corresponding shear stresses are:

$$T_{sz} = \frac{F_{TP,n}}{A_{\tau}} = 48.5 \text{ MPa}$$

$$T_{sy} = \frac{F_{TP,l}}{A_{\tau}} = 12.6 \text{ MPa}$$

Additionally, the axial tie-down force results in a normal stress. The area is identical to the shearing area so that this stress is calculated as:

$$S_{zd} = \frac{F_{TP,a}}{A_{\tau}} = 25.1 \text{ MPa}$$

To compare the calculated stress components with the allowable stresses, the assembly strength is calculated according to [FKM 2012]. With the plastic support number for bending $n_{pl,b} = 1.5$, the shear factor $f_{\tau} = 0.577$ and the yield strength R_p of material No. 1.4307 at 70 °C (see Table 22), the assembly strengths are:

$$S_{SK,zd} = R_p = 175 \text{ MPa} \quad S_{SK,by} = R_p \cdot n_{pl,by} = 263 \text{ MPa} \quad S_{SK,bz} = R_p \cdot n_{pl,bz} = 263 \text{ MPa}$$

$$T_{SK,sy} = f_{\tau} \cdot R_p = 101 \text{ MPa} \quad T_{SK,sz} = f_{\tau} \cdot R_p = 101 \text{ MPa}$$

Then, the resulting partial safety factors for each stress component are:

$$j_{SK,zd} = \left| \frac{S_{SK,zd}}{S_{zd}} \right| = 7.0 \quad j_{SK,by} = \left| \frac{S_{SK,by}}{S_{by}} \right| = 1.8 \quad j_{SK,bz} = \left| \frac{S_{SK,bz}}{S_{bz}} \right| = 70.0$$

$$j_{SK,sy} = \left| \frac{T_{SK,sy}}{T_{sy}} \right| = 8.0 \quad j_{SK,sz} = \left| \frac{T_{SK,sz}}{T_{sz}} \right| = 2.1$$

The combination of all loads is considered by calculating the equivalent safety factor in accordance with [FKM 2012]:

$$j_{SK,Sv} = \frac{1}{\sqrt{\left(\frac{1}{j_{SK,zd}} + \frac{1}{j_{SK,by}} + \frac{1}{j_{SK,bz}} \right)^2 + \left(\frac{1}{j_{SK,sy}} + \frac{1}{j_{SK,sz}} \right)^2}} = 1.1$$

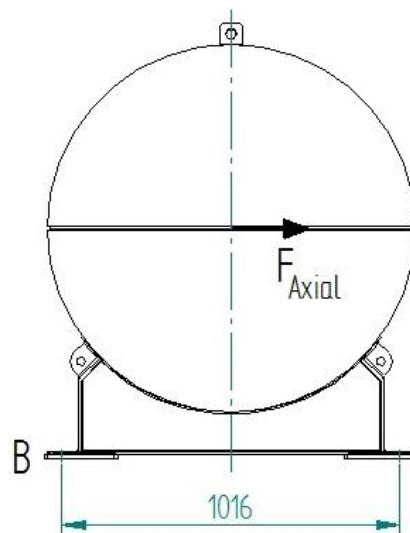


Figure 23: Axial accelerations during RCT

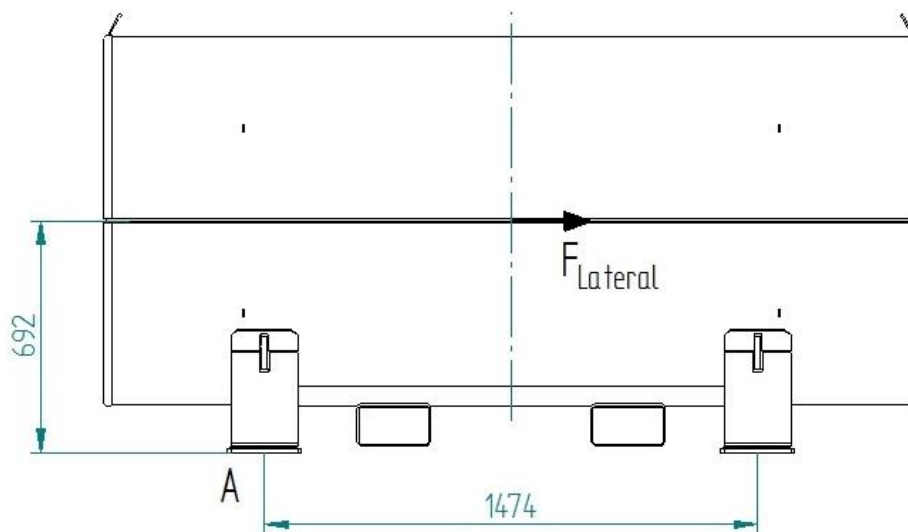


Figure 24: Lateral accelerations during RCT

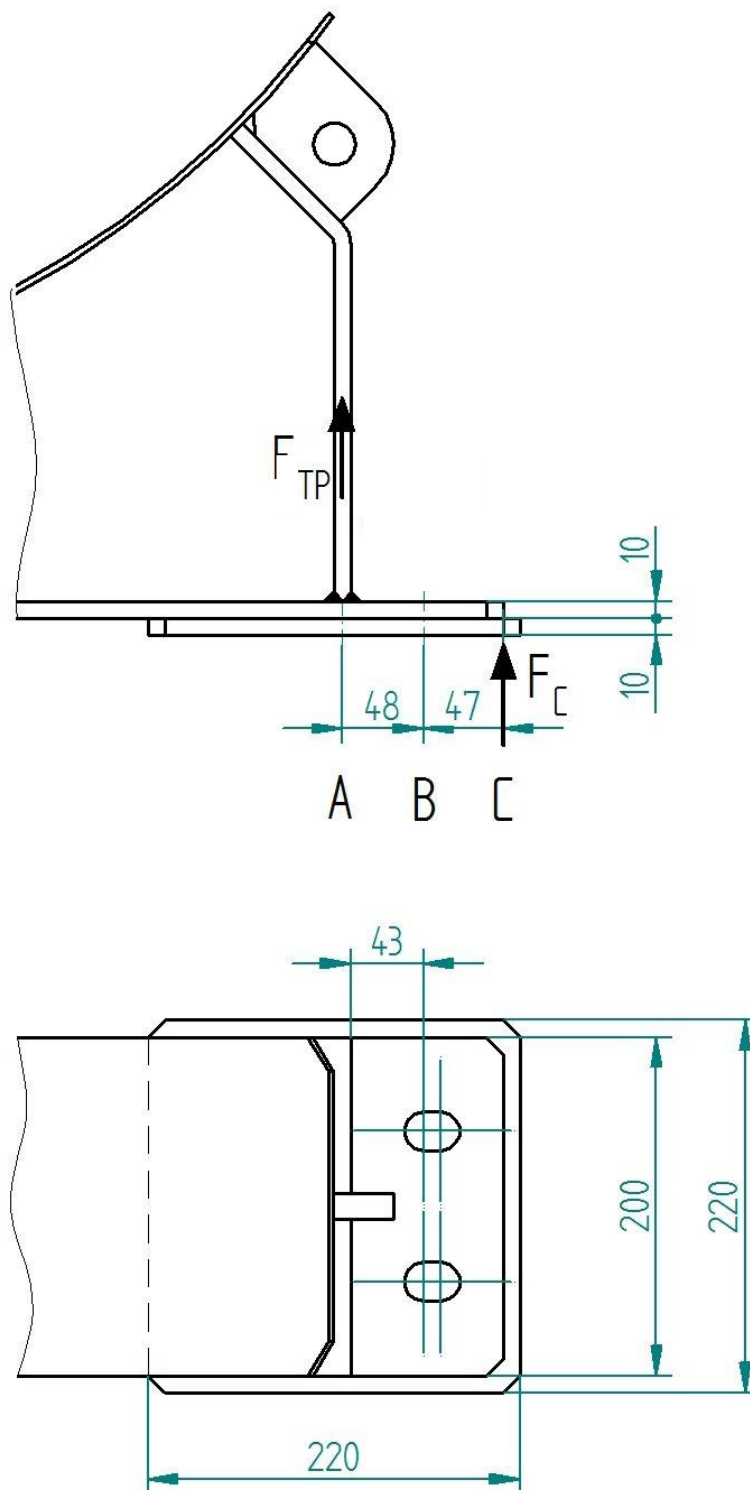


Figure 25: Calculation model of the foot of the DN30 PSP

2.2.1.3.1.4 Bolts

The bolts are not a structural part of the DN30 package. They are part of the external tie-down system.

2.2.1.3.2 Fatigue analysis of tie-down features

For the proof of fatigue strength, the stresses are calculated with the factor of the maximal accelerations because of vibrations as specified in Table 18. Hence, the acceleration forces because of vibrations are in each direction:

$$F_{\text{vib}} = a_{\text{vib}} \cdot m_{\text{DN30}} = 0.3g \cdot 4100 \text{ kg} = 12.1 \text{ kN}$$

For proof of the fatigue strength, [FKM 2012] is used.

2.2.1.3.2.1 Welding seams joining the bottom plate and the vertical plate

Assumptions for the calculation of the cross sections of the welding seams are explained in section 2.2.1.3.1.2. Additional stresses because of bending are neglected. In this case, the tensional and shear stresses in the welding seams only result from the acceleration force F_{vib} :

$$S_{\perp} = \frac{F_{\text{vib}}}{A_{\text{W}}} = 5.0 \text{ MPa} \quad T_{\parallel} = \frac{F_{\text{vib}}}{A_{\text{W}}} = 5.0 \text{ MPa}$$

For fillet welds, the fatigue limits under tension and shearing are considered. In compliance with [FKM 2012], the design factor is FAT 80 and the fatigue limit conversion factors equal $f_{\text{FAT},\sigma} = 0.37$ and $f_{\text{FAT},\tau} = 0.23$. The corresponding fatigue limits for tension and shearing are:

$$S_{\text{WK},\perp} = \text{FAT}_{\sigma} \cdot f_{\text{FAT},\sigma} = 80 \text{ MPa} \cdot 0.37 = 29.6 \text{ MPa}$$

$$T_{\text{WK}} = \text{FAT}_{\tau} \cdot f_{\text{FAT},\tau} = 80 \text{ MPa} \cdot 0.23 = 18.4 \text{ MPa}$$

Considering vibrations, the average stress is assumed to be zero. In this case, the average stress factors are $K_{\text{AK},\perp} = 1$ and $K_{\text{AK},\tau} = 1$.

The factors for the residual stresses are equal to $K_{\text{E},\sigma} = 1.54$ and $K_{\text{E},\tau} = 1.3$. Overall, the fatigue limit stresses for tension and shearing for the welding seams joining the bottom and vertical plate are calculated as:

$$S_{\text{AK},\perp} = K_{\text{AK},\perp} \cdot K_{\text{E},\sigma} \cdot S_{\text{WK},\perp} = 45.6 \text{ MPa}$$

$$T_{\text{AK}} = K_{\text{AK},\tau} \cdot K_{\text{E},\tau} \cdot T_{\text{WK}} = 23.9 \text{ MPa}$$

The required safety factor is set to 1.2 as the welding seams are regularly inspected. Combining the two stress components results in the following total safety factor:

$$j_{\text{AK},\perp} = \left| \frac{S_{\text{AK},\perp}}{S_{\perp}} \right| = 9.1 \quad j_{\text{AK},\parallel} = \left| \frac{T_{\text{AK}}}{T_{\parallel}} \right| = 4.8$$

$$j_{\text{AK},\text{SN}} = \frac{1}{\sqrt{\frac{1}{j_{\text{AK},\perp}^2} + \frac{1}{j_{\text{AK},\parallel}^2}}} = 4.2$$

2.2.1.3.2.2 Welding seams joining the feet and the outer shell of the DN30 PSP

Assumptions for the calculation of the cross sections of the welding seams are explained in section 2.2.1.3.1.2. Additional stresses because of bending are neglected. In this case, the tension stress in the welding seam results from the acceleration force F_{vib} :

$$S_{\perp} = \frac{F_{\text{vib}}}{A_{\text{W},a} + A_{\text{W},l}} = 2.5 \text{ MPa}$$

As already mentioned in section 2.2.1.3.1.2, the shear stress is calculated separately for the axial and the lateral direction. Consequently, the applied force in each direction is F_{vib} , too:

$$T_{\parallel,a} = \frac{F_{\text{vib}}}{A_{W,a}} = 6.8 \text{ MPa}$$

$$T_{\parallel,l} = \frac{F_{\text{vib}}}{A_{W,l}} = 4 \text{ MPa}$$

For fillet welds, the fatigue limits under tension and shearing are considered. In compliance with [FKM 2012], the design factor is FAT 80 and the fatigue limit conversion factors equal $f_{\text{FAT},\sigma} = 0.37$ and $f_{\text{FAT},\tau} = 0.23$. The corresponding fatigue limits for tension and shearing are:

$$S_{WK,\perp} = \text{FAT}_{\sigma} \cdot f_{\text{FAT},\sigma} = 80 \text{ MPa} \cdot 0.37 = 29.6 \text{ MPa}$$

$$T_{WK} = \text{FAT}_{\tau} \cdot f_{\text{FAT},\tau} = 80 \text{ MPa} \cdot 0.23 = 18.4 \text{ MPa}$$

Considering vibrations, the average stress is assumed to be zero. In this case, the average stress factors are $K_{AK,\perp} = 1$ and $K_{AK,\tau} = 1$.

The factors for the residual stresses are equal to $K_{E,\sigma} = 1.54$ and $K_{E,\tau} = 1.3$. Overall, the fatigue limit stresses for tension and shearing for both welding seams of the lifting lugs are calculated as:

$$S_{AK,\perp} = K_{AK,\perp} \cdot K_{E,\sigma} \cdot S_{WK,\perp} = 45.6 \text{ MPa}$$

$$T_{AK} = K_{AK,\tau} \cdot K_{E,\tau} \cdot T_{WK} = 23.9 \text{ MPa}$$

The required safety factor is set to 1.2 as the welding seams are regularly inspected. Combining the stress components results in the following total safety factor:

$$j_{AK,\perp} = \left| \frac{S_{AK,\perp}}{S_{\perp}} \right| = 18.0 \quad j_{AK,\parallel,a} = \left| \frac{T_{AK}}{T_{\parallel,a}} \right| = 3.5 \quad j_{AK,\parallel,l} = \left| \frac{T_{AK}}{T_{\parallel,l}} \right| = 5.9$$

$$j_{AK,SN} = \frac{1}{\sqrt{\frac{1}{j_{AK,\perp}^2} + \frac{1}{j_{AK,\parallel,a}^2}}} = 3.5 \quad j_{AK,SN} = \frac{1}{\sqrt{\frac{1}{j_{AK,\perp}^2} + \frac{1}{j_{AK,\parallel,l}^2}}} = 5.6$$

2.2.1.3.2.3 Bottom plate

FAT = 80 (bending stress and shear stress in the bottom plate)

The fatigue notch factor for tension stress is:

$$K_{WK,N} = \frac{225}{\text{FAT}} = 2.82$$

The fatigue notch factor for shear stress is:

$$K_{WK,S} = \frac{145}{\text{FAT}} = 1.82$$

Hence the fatigue limit tension stress is at point A:

$$\frac{\sigma_{\text{Sch},N}}{K_{WK,N}} = \frac{190 \text{ MPa}}{2.82} = 67.4 \text{ MPa} > 0.15 \cdot \sigma = 0.15 \cdot (111 \text{ MPa} + 10.3 \text{ MPa}) = 18.2 \text{ MPa}$$

And the fatigue limit shear stress is:

$$\frac{\tau_{Sch,S}}{K_{WK,S}} = \frac{120 \text{ MPa}}{1.82} = 65.9 \text{ MPa} > 0.15 \cdot \tau = 0.15 \cdot (14.1 \text{ MPa} + 7.1 \text{ MPa}) = 3.2 \text{ MPa}$$

Von Mises stress:

$$S_{eq} = \sqrt{(18.2 \text{ MPa})^2 + 3 \cdot (3.2 \text{ MPa})^2} = 19.0 \text{ MPa}$$

The safety factor against von Mises stress is:

$$j = \frac{67.4 \text{ MPa}}{19.0 \text{ MPa}} = 3.5 > 1.2$$

2.2.1.3.2.4 Bolts

The bolts are not part of the DN30 package. They are exchanged regularly when the DN30 package is mounted onto the flat racks used for transport. Hence, a fatigue proof is not required.

2.2.1.3.3 Failure-limit for the tie-down features

With respect to the requirement stipulated in [10CFR71] §71.45 and [49CFR173] §173.412(i) or [IAEA 2012] para. 638 it is shown in the following that the tie-down attachment will fail before the ability of the package to meet the requirements for NCT and HAC is impaired. For this proof, the forces are calculated that lead to a failure of the bolts used for tie-down and compared to the forces required to have a failure of the attachment features of the DN30 PSP.

The bolts will fail either when the normal stress in the bolts exceeds the ultimate tensile strength or when the shear stress exceeds the ultimate shear strength.

The stress cross section of a bolt M18 is:

$$A_S = 192.47 \text{ mm}^2$$

Ultimate tensile strength of class 8.8 is:

$$R_m = 800 \text{ MPa}$$

Failure force for normal stress:

$$F_{fail,n} = 192.47 \text{ mm}^2 \cdot 800 \text{ MPa} = 154 \text{ kN}$$

The nominal cross section of a bolt M18 is:

$$A_N = 254.47 \text{ mm}^2$$

Ultimate shear strength of class 8.8 is:

$$R_m = \frac{800 \text{ MPa}}{\sqrt{3}} = 462 \text{ MPa}$$

Failure force for shear stress:

$$F_{fail,s} = 254.47 \text{ mm}^2 \cdot 462 \text{ MPa} = 118 \text{ kN}$$

With these failure forces the stresses in the welding seams between the bottom plate and the vertical plate as shown in Figure 25 are calculated, taking into account two bolts per attachment point.

The cross section has been calculated in section 2.2.1.3.1.1:

$$A_W = 2000 \text{ mm}^2$$

The tensile stress is:

$$S = \frac{2 \cdot F_{\text{fail},n}}{A_W} = \frac{2 \cdot 154 \text{ kN}}{2000 \text{ mm}^2} = 154 \text{ MPa}$$

The shear stress is:

$$T = \frac{2 \cdot F_{\text{fail},s}}{A_W} = \frac{2 \cdot 118 \text{ kN}}{2000 \text{ mm}^2} = 118 \text{ MPa}$$

Von Mises stress:

$$S_{\text{eq}} = \sqrt{(154 \text{ MPa})^2 + 3 \cdot (118 \text{ MPa})^2} = 256 \text{ MPa} > R_{p0,2}$$

Safety factor against R_m of material No. 1.4307 (see Table 22)

$$R_m = 520 \text{ MPa}$$

$$j = \frac{520 \text{ MPa}}{256 \text{ MPa}} = 2$$

The stress in the welding seam exceeds the yield stress, but is well below the ultimate tensile strength when the bolts of the tie-down fail. The plastic deformations to be expected do not result in a rupture of the welding seam and, hence, the ability of the package to meet NCT and HAC is not impaired. In case of higher loads than to be expected during RCT, the bolts will fail, and the DN30 package will be separated from the flat rack used for tie-down.

2.2.1.4 Ability to withstand NCT

2.2.1.4.1 Water spray test

The water spray test as defined in [10CFR71] §71.71(c)(6) and [49CFR173] §173.465(b) or [IAEA 2012] para. 721 requires the simulation of a heavy rainfall of approximately 5 cm for at least an hour.

The outer shell of the DN30 package consists of stainless steel without any openings except for the flange between the top and the bottom half of the DN30 PSP. The flange itself is shaped to prevent the ingress of water during the water spray test. Additionally, it is equipped with a gasket sealing the top half against the bottom half of the DN30 PSP.

There is no influence of this test on either the loss or dispersal of the radioactive contents or on the dose rate at any external surface of the DN30 package with respect to the requirement stipulated in [10CFR71] §71.43(f) and [49CFR173] §173.412(j) or [IAEA 2012] para. 648.

2.2.1.4.2 Free drop test

The free drop test from a height of 1.2 m is analyzed in sequence together with the tests simulating HAC, the 9 m drop test and the 1 m drop test onto the bar. For a better overview and comparison of the deformations after the 1.2 m free drop test and after the 9 m drop test, the results of these sequences are described together in section 2.2.1.5.

In section 2.2.1.5, it is shown that the DN30 package is designed to withstand HAC. Hence, the proof that the DN30 package is designed to withstand NCT is a direct consequence.

In the following, the conditions for proof of [10CFR71] §71.43(f) and [49CFR173] §173.412(j) or [IAEA 2012] para. 648 are established. Preceding corner drops from a height of 0.3 m as required by [49CFR173] §173.465(c)(2) will not have any adverse effect on the DN30 package: the free drop tests from 1.2 m were investigated for every drop angle and only resulted in deformations below 10 % for the steel parts. Accordingly, the impact from preceding 0.3 m corner drops is estimated to be negligible and not investigated in detail.

2.2.1.4.2.1 Conditions to prevent loss or dispersal of the radioactive contents

In section 2.2.1.5, it is shown by analysis that there is no contact between the valve or the plug and any part of the DN30 PSP or any other part of the 30B cylinder other than its initial connection point after the 1.2 m free drop test. Hence, a mechanical damage of the valve or the plug during the 1.2 m drop test can be excluded.

In section 2.2.1.5.1.5, it is shown in real tests that the results of the analysis comply with the real tests. It is confirmed that there is no contact between the valve or the plug and any part of the DN30 PSP or any other part of the 30B cylinder other than its initial connection point even after the cumulative effects of the 1.2 m free drop test, the 9 m drop and the 1 m drop onto the bar.

Furthermore, the leakage rate of the containment system, i.e. the 30B cylinder, was measured and documented after each test sequence. The measurements show that there is no increase of the leakage rate that could lead to a loss or dispersal of the radioactive content.

2.2.1.4.2.2 Conditions to prevent the increase of the maximum external radiation level of more than 20 %

In section 2.2.4.6, it is shown that the maximum dose rate at the surface of the DN30 package is to be expected in radial direction in the center of the side of the package. In section 2.2.1.5,

the deformations to be expected after the 1.2 m free drop tests are analyzed. For the 1.2 m free drop onto the top of the package described in section 2.2.1.5.1.5.6, a reduction of the distance between the inner and the outer shell of the DN30 package of 4 mm was calculated. Conservatively, a distance reduction of 6 mm is assumed for the dose rate analysis.

2.2.1.4.3 Stacking test

The shape of the DN30 PSP effectively prevents stacking. However, according to [10CFR71] §71.71(c)(9), a compression test must be performed for packages weighing up to 5000 kg. The package must be subjected, for a period of 24 hours, to a compressive load applied uniformly to the top and bottom of the package in the position, in which the package would normally be transported. The compressive load must be the greater of the following:

- the equivalent of 5 times the weight of the package or
- the equivalent of 13 kPa multiplied by the vertically projected area of the package.

As shown below, the first requirement results in the larger compressive load in case of the DN30 package. The vertically projected area A_{proj} of the package is calculated using the nominal diameter and length of the package as given in Table 12:

$$F_1 = 5 \cdot m_{DN30} \cdot g = 5 \cdot 4100 \text{ kg} \cdot 9.81 \frac{\text{m}}{\text{s}^2} = 201.1 \text{ kN}$$

$$F_2 = 13 \text{ kPa} \cdot A_{proj} = 13 \text{ kPa} \cdot 1216 \text{ mm} \cdot 2437 \text{ mm} = 38.5 \text{ kN}$$

The structural strength of the DN30 package during the compression test is proven by an FEM simulation with LS-DYNA. The same model as for the safety proof under HAC (see section 2.2.1.5.1.3) is used. However, because of the quasi-static loading of the structure, the implicit LS-DYNA solver is used. This allows for increased time steps, but the demands on the convergence of the simulation are increased. For this reason, the following modifications of this FEM model are made to improve the convergence and to reduce the calculation effort:

- the 30B cylinder and its content are removed;
- the entire foam is removed;
- for tied contacts, only constraint-based types are applied;
- for the automatic-single-surface-contact, the mortar option is applied;
- the element formulations for shell and solid elements are changed to ELFORM=16 and ELFORM=-1, respectively, which both are fully integrated element formulations;
- additional keywords are added to control the implicit solver (see Table 34).

The compressive load F_1 is introduced by a rigid plate that is positioned above the DN30 PSP, and which can only move in the vertical direction. All other degrees of freedom are fixed for the rigid plate. The compressive load is increased linearly over a period of 1 s to reduce dynamic effects. Additional boundary conditions are applied at the bottom plate of the feet using the keyword *BOUNDARY_SPC. For the bottom plates, the displacements and rotational degrees of freedom are fixed in all directions. The geometry of the modified FEM model including the applied boundary conditions is shown in Figure 26.

Because of the negligence of the 30B cylinder and its content as well as the foam, the only remaining material in the FEM model is stainless steel No. 1.4307. To comply with the load assumptions for NCT, a bounding ambient temperature of 70 °C together with the corresponding yield strength of material No. 1.4307 is chosen for this analysis. To this end, the

input for the material model used for this steel is changed to use only the yield stress and the plastic tangent modulus. The plastic tangent modulus E_{tan} is determined based on the yield strength $R_{p0,2}$ at 70 °C, the ultimate strength R_m as well as the elongation at fracture A (see Table 22):

$$E_{\text{tan}} = \frac{R_m - R_{p0,2}}{A - 0.2\%} = \frac{520 \text{ MPa} - 175 \text{ MPa}}{45\% - 0.2\%} = 800 \text{ MPa}$$

This is a very conservative approach to model the actual material behavior. In addition, any rate dependency of the material model is disabled to simulate the static material behavior.

Table 34: Settings for implicit LS-DYNA solver

Keyword	Changed Settings	Comments
*CONTROL_IMPLICIT_GENERAL	IMFLAG=1	Activates implicit solver.
	DT0=0.01	Initial time step
*CONTROL_IMPLICIT_AUTO	IAUTO=1	Provided good convergence behavior.
	DTMIN=0.01	
	DTMAX=0.1	
*CONTROL_IMPLICIT_SOLUTION	NSOLVR=12	Nonlinear BFGS solver with optional arclength
	ECTOL=0.01	Tightened convergence tolerances.
	ABSTOL=1E-20	
	NLNORM=4	Sum of translational and rotational degrees of freedom are considered in convergence criterion instead of translational only.
	LSMTD=5	Same as default, but accounts for residual norm growth to be conservative in step length determination.
*CONTROL_IMPLICIT_DYNAMICS	IMASS=1	Activates dynamic solver.
	TDYDTH=0.5	Death and burial time for application of dynamic terms.
	TDYBUR=0.9	

As shown in Table 34, the dynamic behavior of the system is taken into account. This modelling approach helps to close the initial gap between the outer shell of the DN30 PSP and the rigid plate used for the application of the compressive load. After this contact is well established, rigid body modes are no longer present in the system and the dynamic terms are successively removed by defining a death and burial time in *CONTROL_IMPLICIT_DYNAMICS.

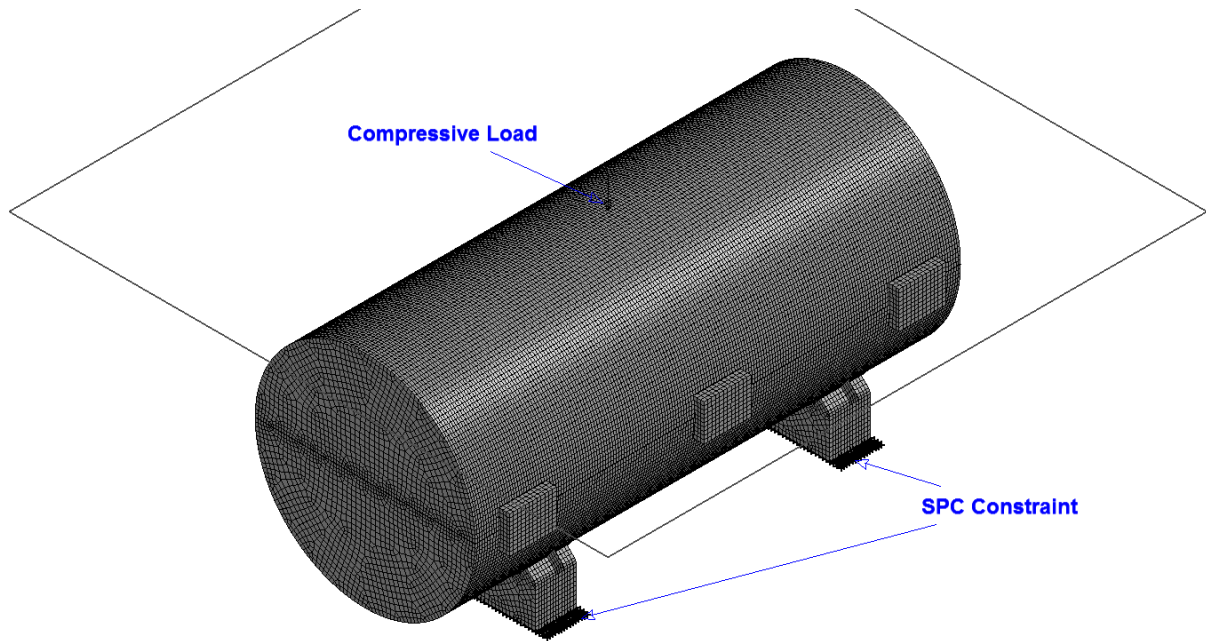
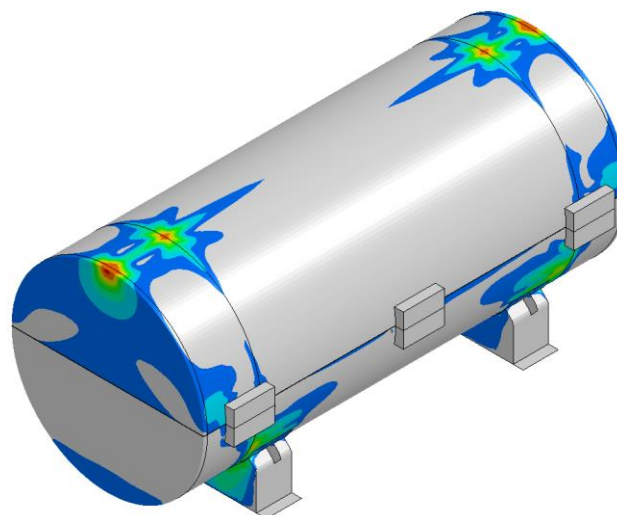


Figure 26: FEM model of the DN30 package for the compression test

The simulation results of the compression test in Figure 27 show that locally stresses above the yield strength of material No.1.4307 at 70 °C occur. These stresses cause plastic strains below 1% as shown in Figure 28. Even though very conservative assumptions have been made by neglecting the entire foam parts as well as regarding the strength of material No. 1.4307, these plastic strains are still one order lower than those observed during the drop tests under NCT. Consequently, the DN30 package passes the compression test without violating any acceptance criteria for NCT.

Time = 1.1
Contours of Effective Stress (v-m)
max IP. value
min=0, at elem# 202797
max=210.423, at elem# 116296



Effective Stress (v-m)

210.423
189.381
168.338
147.296
126.254
105.211
84.169
63.127
42.085
21.042
0.000

Figure 27: Compression test – Results of the von Mises stress

Time = 1.1
Contours of Effective Plastic Strain
max IP. value
min=0, at elem# 36128
max=0.0442165, at elem# 116295

Effective Plastic Strain

0.044
0.040
0.035
0.031
0.027
0.022
0.018
0.013
0.009
0.004
0.000

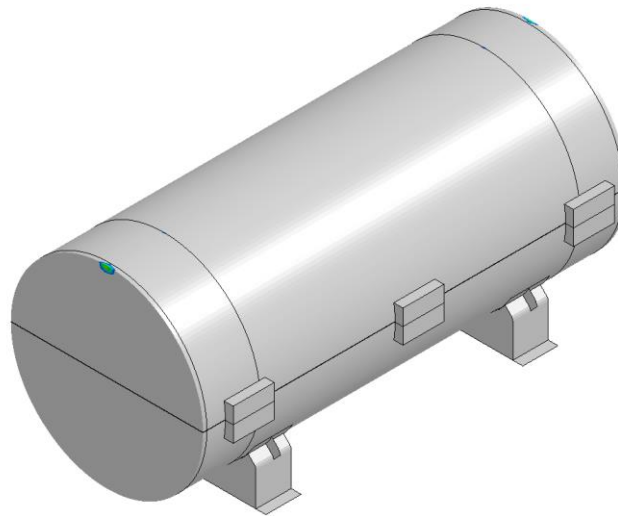


Figure 28: Compression test – Results of the effective plastic strain

2.2.1.4.4 Penetration test

The DN30 package is designed to withstand HAC (see section 2.2.1.5). The drop of the DN30 package with a mass of approx. 4000 kg onto a steel bar from 1 m height is much more severe than the drop of a 6 kg steel bar from 1 m height onto the DN30 package. Hence, the test conditions as defined in [10CFR71] §71.71(c)(10) and [49CFR173] §173.465(e) or [IAEA 2012] para. 724 are covered by the test conditions as defined in [10CFR71] §71.73(c)(3) or [IAEA 2012] para. 727 (b).

There is no influence of this test on the loss or dispersal of the radioactive contents with respect to the requirement stipulated in [10CFR71] §71.43(f) and [49CFR173] §173.412(j) or [IAEA 2012] para. 648 (a).

In comparison to the free drop test from 1.2 m height, the influence of this test on the dose rate at any external surface of the DN30 package with respect to the requirement stipulated in [10CFR71] §71.43(f) and [49CFR173] §173.412(j) or [IAEA 2012] para. 648 (b) is negligible.

2.2.1.4.5 Ambient pressure

The 30B cylinder is designed according to [ANSI N14.1] and [ISO 7195] for an external pressure of 172 kPa and an internal pressure of 1.38 MPa. The MNOP during transport is 152 kPa. Hence, a reduction of the ambient pressure to 60 kPa as specified in [10CFR71] §71.71(c)(3) and [49CFR173] §173.412(f) or [IAEA 2012] para. 645 will not affect the 30B cylinder and the containment system.

2.2.1.5 Ability to withstand HAC

2.2.1.5.1 Structural analysis of NCT and HAC

The structural analysis of the ability of the DN30 package to withstand HAC is documented in several documents provided as appendices to this SAR:

- Appendix 2.2.1.1 (Drop Test Program)
- Appendix 2.2.1.2 (Drop Test Reports)
- Appendix 2.2.1.3 (Structural Analysis of the DN30 Package under NCT and HAC)

In this section, a summary of these reports describes the main points and results of the analyses and real drop tests.

The analysis

- covers the free drop test of NCT, the 9-m drop test and 1-m drop test onto a bar for HAC,
- is valid for all filling ratios from cylinders with heels up to cylinders filled with the maximum amount of UF₆ defined in section 1.3.

The structural analysis of NCT and HAC comprises the analysis of the following tests:

- Test 1:** Analysis of the free drop test defined in [10CFR71] §71.71(c)(7) and [49CFR173] §173.465(c) or [IAEA 2012], para. 722 (1.2 m free drop test)
- Test 2:** Analysis of the mechanical tests defined in [10CFR71] §71.73(c)(1) or [IAEA 2012], para. 727 (a) (drop I, drop height 9 m)
- Test 3:** Analysis of the mechanical test defined in [10CFR71] §71.73(c)(3) or [IAEA 2012], para. 727 (b) (drop II, drop height 1 m onto a bar)

The structural analysis of NCT and HAC was carried out in three major steps:

- Analysis of the behavior of the package by using proven FEM tools and selection of benchmarks.
- Real testing of prototypes by applying the selected benchmark test sequences.
- Comparison and post-analysis of real test results with the calculation results.

2.2.1.5.1.1 Analysis sequences and orientations

In the analysis the following sequences were considered:

- Test 1 – Test 2 – Test 3
- Test 1 – Test 3 – Test 2

The analyses were carried out for all relevant orientations of the package before the tests:

- Flat onto the valve side
- Flat onto the plug side
- Flat onto the closure system

- Flat onto the top side
- Inclined onto the valve side so that the line between center of gravity and point of impact is perpendicular to the target surface
- Inclined onto the plug side so that the line between center of gravity and point of impact is perpendicular to the target surface
- Inclined onto the closure system so that the line between center of gravity and point of impact is perpendicular to the target surface
- Inclined onto the feet (slap-down)
- Inclined onto the top side (slap-down)

2.2.1.5.1.2 Description of the calculation codes

The results of the drop test simulations in this report are obtained by the numerical solving of differential equations, which are based on the finite element method. Due to the highly dynamic nature of this kind of simulations, the FEM solver LS-DYNA (MPP S R8.0.0) [LS-DYNA 2015] of the software developer LSTC is used. The results are analyzed in LS-PrePost [LS-PREPOST].

2.2.1.5.1.3 FEM-Model

The FEM-model deviates from the prototype design in the details listed in Table 35.

Table 35: Deviations of the FEM model from the design of the DN30 package and their justification

Part	Deviation	Justification
Global		
Steel blocks for sealing	Removed	Not required to be modeled because they have no safety relevant function from the mechanical point of view.
Pads (2 mm thick)	Removed	No relevance for the drop test simulations under NCT and HAC because they only cover the interior of the DN30 PSP to protect it against wear and tear due to contact between the 30B cylinder and the inner shell.
Gasket	Removed	The gasket prevents the ingress of water, which is irrelevant for the FEM simulations.
Rounded / beveled edges and boreholes	Removed	Such geometrical details require unreasonably small elements, especially for the evaluation of strains and stresses; they have no influence on the results of the FEM analyses.

Part	Deviation	Justification
Welding seams	Replaced by tied contacts / mesh connections	Every welding seam is removed in the FEM model because the investigation of welding seams requires a very fine mesh in those regions. Moreover, the welding seams of the DN30 PSP have no containment function. They serve as a connection between the individual parts of the DN30 PSP and any failure of the welds is investigated in the real drop tests. Therefore, replacing them by tied contacts or simple mesh connections is sufficient for the FEM simulations. Possible failure of welding seams is accounted for by evaluating the strain in the respective parts.
Closure system	Simplified	Each of the closure devices is modeled as two prismatic bodies instead of the complicated design with four teeth on each block connected by a bolt. This simplification allows a coarser mesh in this area leading to acceptable calculation times. The behavior of the real closure system, including local stresses and possible damage in the teeth or the bolt are then calculated separately from the global stresses and forces in the connection between the two bodies. Furthermore, drop tests with prototypes show that no deformations are to be expected at the closure system which could impair its function.
Bottom half		
Valve protecting device	Hinges removed and foam shrunk	<p>The PIR foam inside the housing of the valve protecting device is scaled down to create a small gap between the foam and the housing. Due to fabrication tolerances, this kind of modeling provides a good representation of the real prototype.</p> <p>The hinges connecting the valve protecting device with the profile of the bottom half of the DN30 PSP are not included in the FEM model but represented by a simple tied contact keeping the valve protecting device in place. The hinges are not meant to withstand the drop tests. Even if they fail, the valve protecting device is pinched between the surrounding elements (30B cylinder, inner shells of the bottom and top half of the DN30 PSP).</p>
Rotation preventing devices	Simplified	The lever has no relevance concerning the mechanical strength of the rotation preventing device. Therefore, it is neglected together with the corresponding slit in the sleeve. Further simplifications concern the bottom part of the flange of the rotation preventing devices. It is removed because the influence on the global deformation behavior is negligible.
Feet	Simplified	Simplifications of the feet mainly concern the replacement of the tongue and groove joints by straight edges.
Top half		
Lifting lugs	Removed	The attachment points are not modeled in the FEM model. These parts are not relevant for the drop tests.

Part	Deviation	Justification
Valve protecting device counterpart	Simplified	Firstly, the bar in the area close to the flange is neglected which allows the whole valve protecting device counterpart to be modeled with shell elements and avoids cumbersome contact modeling between shell and solid elements in this region. Secondly, the roof-like construction is simplified to a single sheet.
Rotation preventing device counterparts	Simplified	Simplified to a square profile.
Content (heavy concrete as surrogate material for UF ₆ in the drop tests)	Debris and cracks in the concrete neglected	In reality, the content is UF ₆ . For the drop tests, a mixture of steel grit and cement (heavy concrete) is used. This mixture is modeled by a homogeneous material model in the FEM calculations. Furthermore, the presence of some loose parts of the UF ₆ in the cylinder is not taken into account. The debris was mainly considered in the real drop tests to investigate the leak-tightness of the 30B cylinder because of a secondary impact of the debris. Since the leak-tightness cannot be investigated with FEM simulations, there is no need to consider the debris in the FEM model.

2.2.1.5.1.3.1 Mesh

The mesh of the FEM model consists of shell and solid elements. Solid elements are used for steel, concrete and foam parts. However, most of the steel parts are modeled using shell elements.

In total the model consists of 137571 shell elements and 112432 solid elements. The mesh statistics are listed in Table 36.

Table 36: Mesh statistics

Parameter	Solid elements		Shell elements		Beam elements
	min	max	min	max	
Characteristic length [mm]	3.99	34.45	2.28	28.6	
Aspect ratio [-]	1.01	5.34	1.0	7.64	
Min. Angle [°]	13.04	89.93	31.9	90.0	
Max. Angle [°]	64.9	173.33	90.0	160.0	
Time step [s]	6.27 · 10 ⁻⁷		4.2 · 10 ⁻⁷		
Number of elements	112432		137571		65
Total number of elements	250068				

The following figures Figure 29 to Figure 33 show the general structure of the mesh. Figure 29 shows the mesh of the outer shell and feet, Figure 30 shows the mesh of the foam parts of the DN30 PSP, Figure 31 shows the mesh of the inner shell of the DN30 PSP, Figure 32 shows the mesh of the 30B cylinder and Figure 33 shows the mesh of the content replacement.

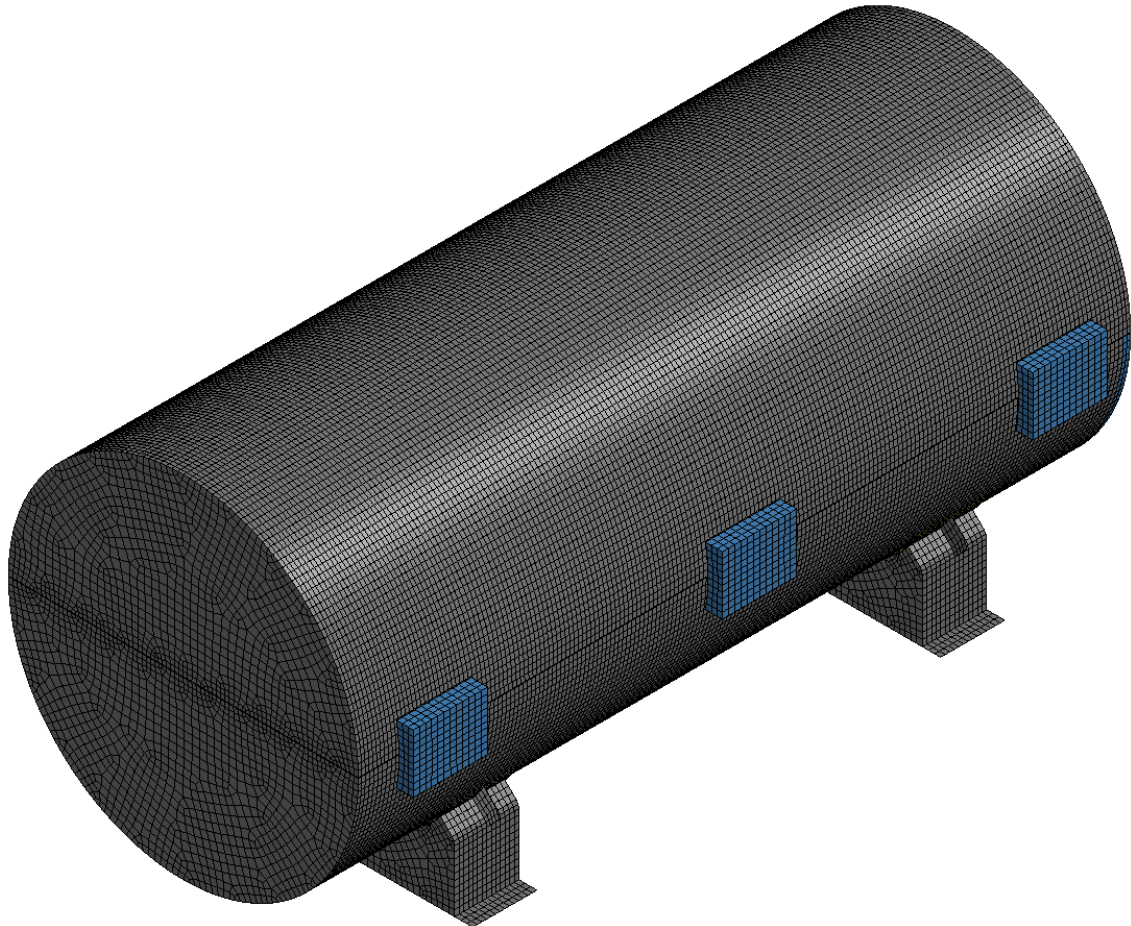


Figure 29: Mesh of the DN30 package, outer shell and feet

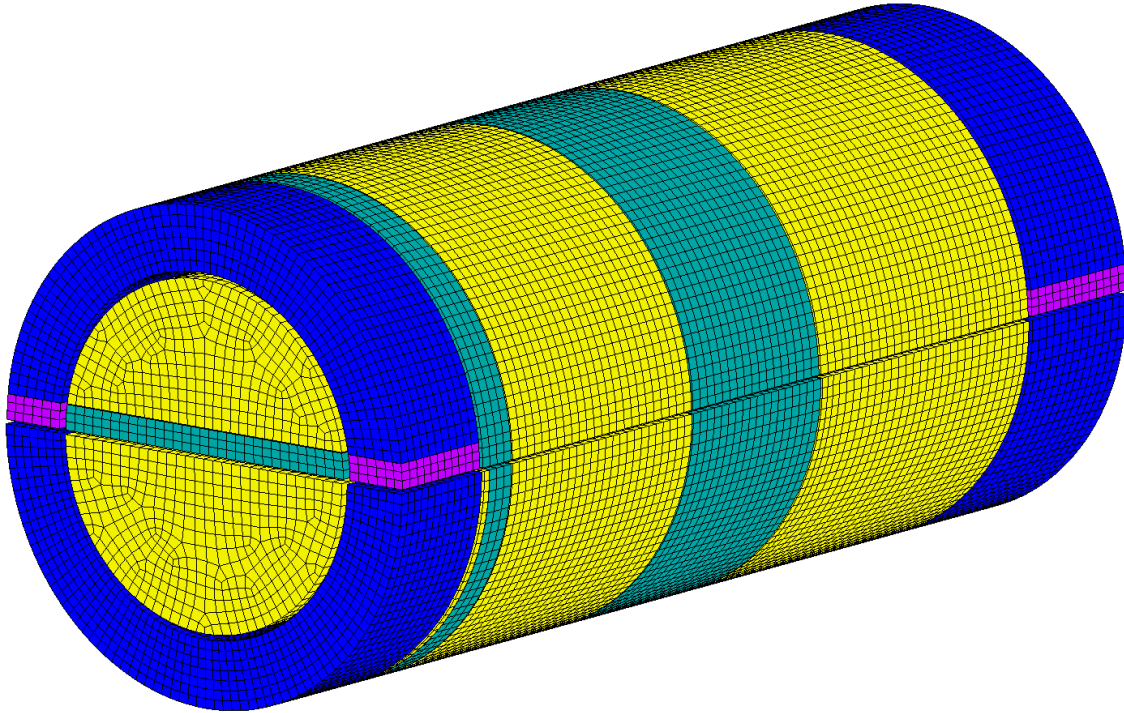


Figure 30: Mesh of the DN30 package, foam parts

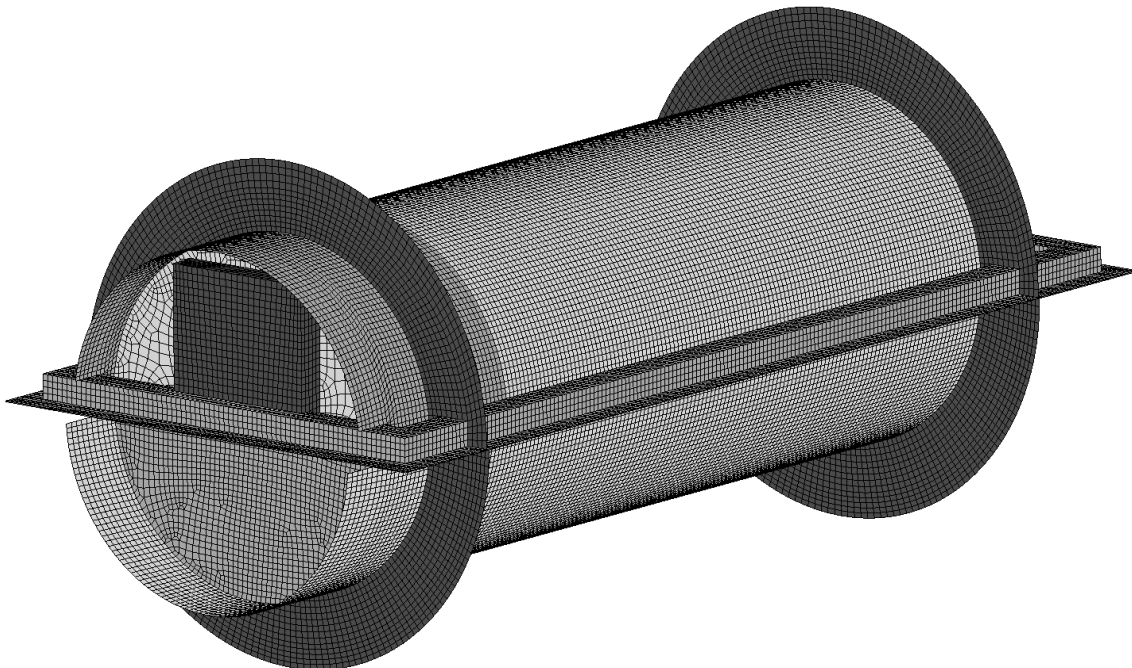


Figure 31: Mesh of the DN30 package, inner shells

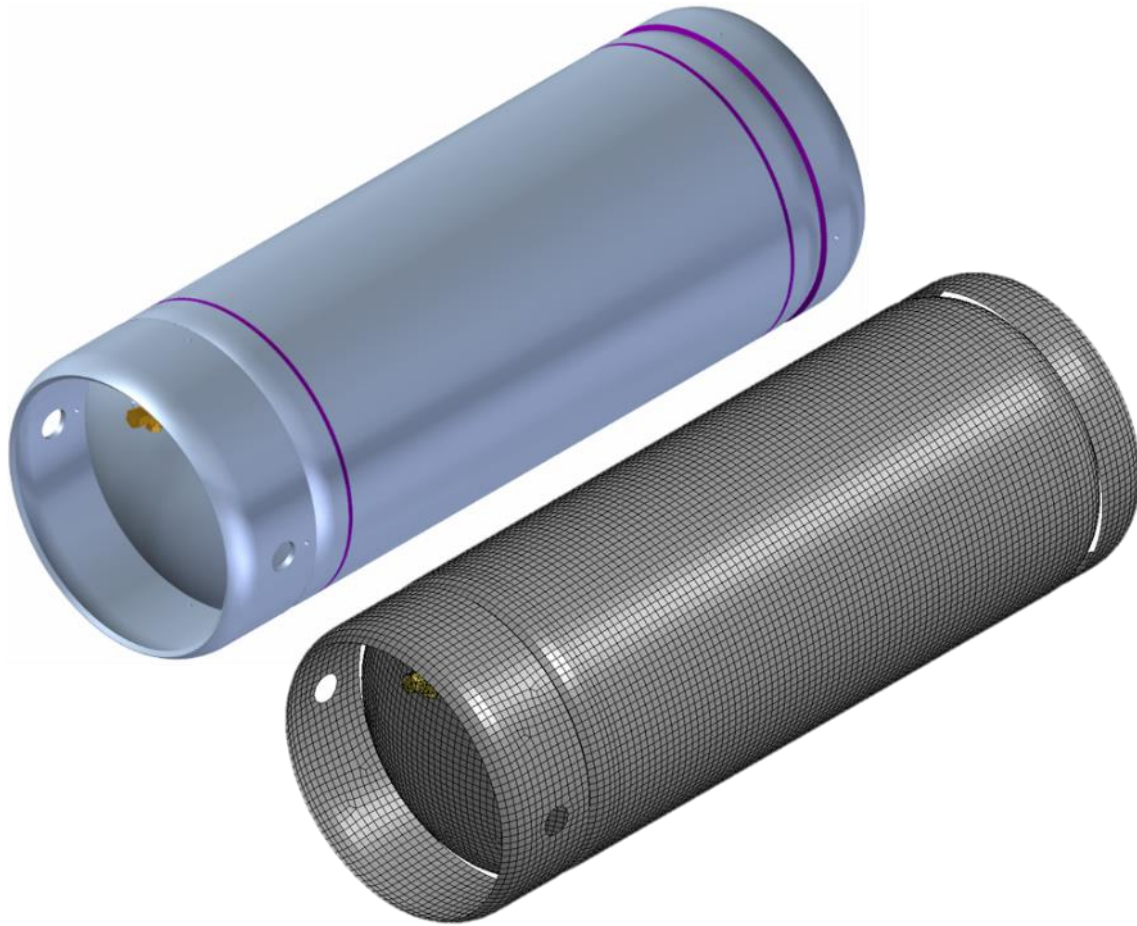


Figure 32: Mesh of the 30B cylinder

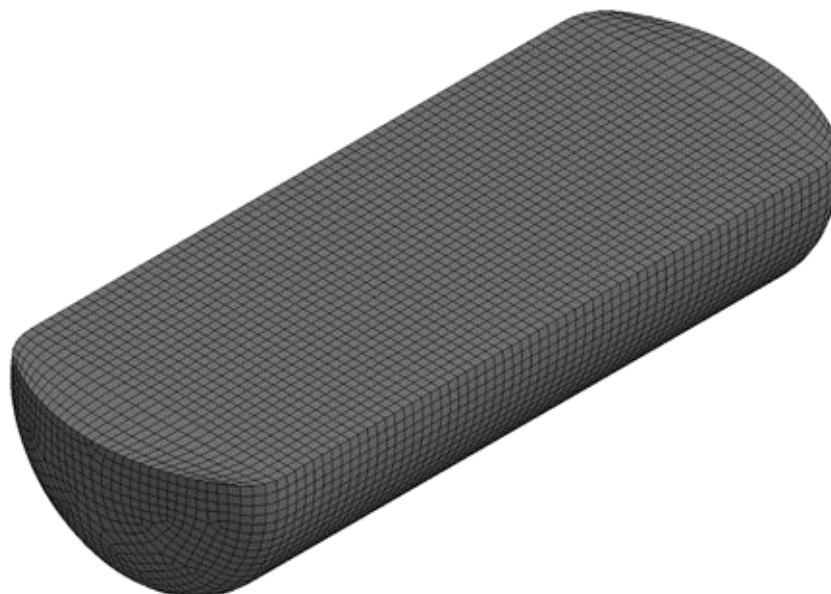


Figure 33: Mesh of the DN30 package, content of the 30B cylinder

2.2.1.5.1.3.2 Boundary conditions

Depending on the simulated drop test, the DN30 package has an initial speed of 4.85 m/s (1.2 m drop), 13.3 m/s (9.0 m drop) and 4.43 m/s (1.0 m drop onto bar). This velocity is orientated vertical downwards onto the target (a flat rigid surface or a rigid bar), which is fixed in all degrees of freedom.

Gravity is not modeled in this calculation because of its expected small influence.

2.2.1.5.1.3.3 Contacts

Welding seams of metal parts are modeled as mesh connections or tied contacts.

A failure criterion is not modeled for the parts of the DN30 package. Possible cracks in the welding seams are detected by determining the strains and stresses in these areas.

If friction is included in the contact, a static and dynamic coefficient as well as a decay constant is provided because the calculation of the friction coefficient is based on an exponential decay curve. Here, the static and dynamic friction coefficients FS and FD are equally set to 0.15 to avoid additional numerical noise in the contact forces and the decay constant is left at the default value.

2.2.1.5.1.3.4 Foam

The material properties of the two types of foam that are used for the DN30 PSP were investigated in Appendix 1.4.2 (Material Data PIR Foam). Best suited for the description of the mechanical behavior of this foam is the material model **MAT_CRUSHABLE_FOAM* of LS-DYNA. The material model that was evaluated in Appendix 2.2.1.3 (Structural Analysis of the DN30 Package under NCT and HAC) is used for the analysis of the drop tests of the DN30 package. The stress-strain relationships for the foam are shown in Figure 34 and Figure 35.

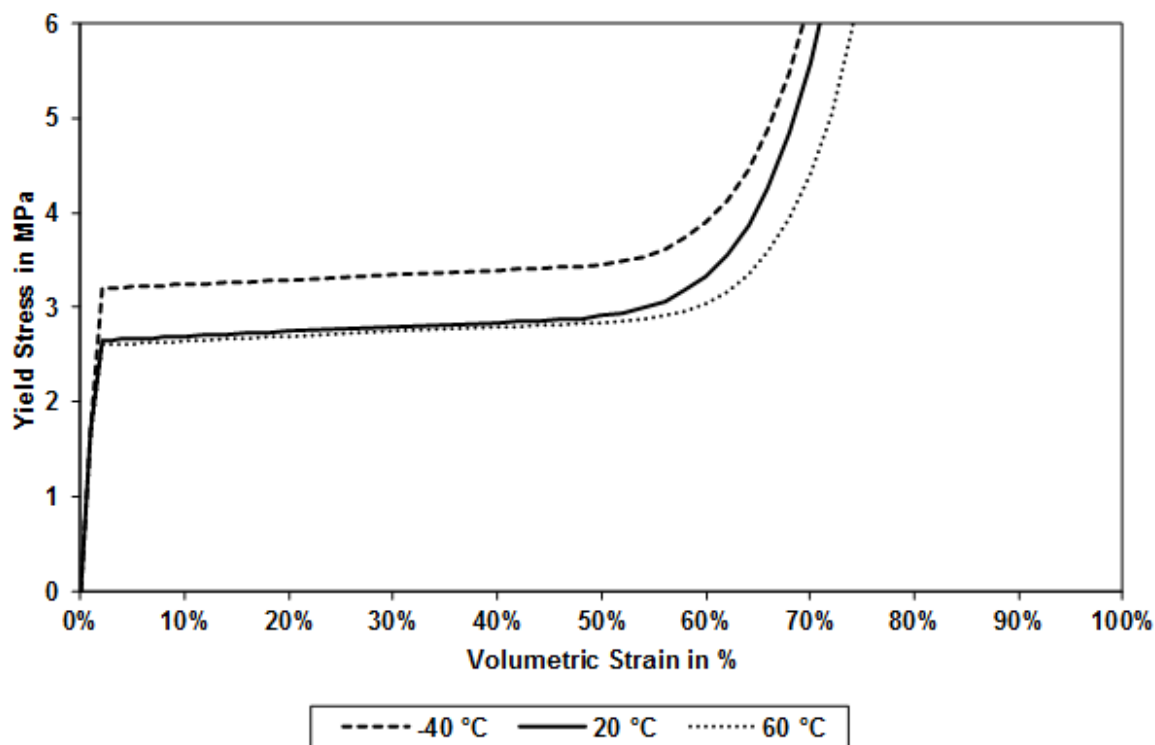


Figure 34: Material properties of PIR foam RTS 120 used for the FEM-model

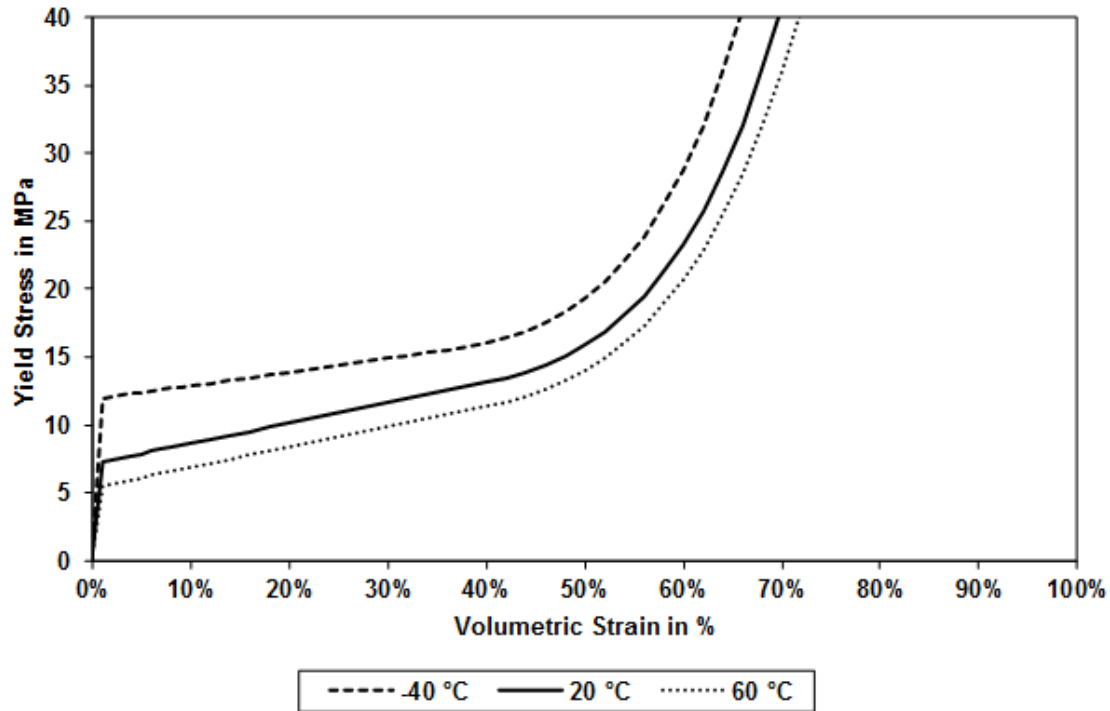


Figure 35: Material properties of PIR foam RTS 320 used for the FEM-model

2.2.1.5.1.3.5 Steel

For all kinds of steel, the same elastic-plastic material model with isotropic linear hardening is used. It is **MAT_MODIFIED_PIECEWISE_LINEAR_PLASTICITY* with the true stress-strain curves defined in Figure 36.

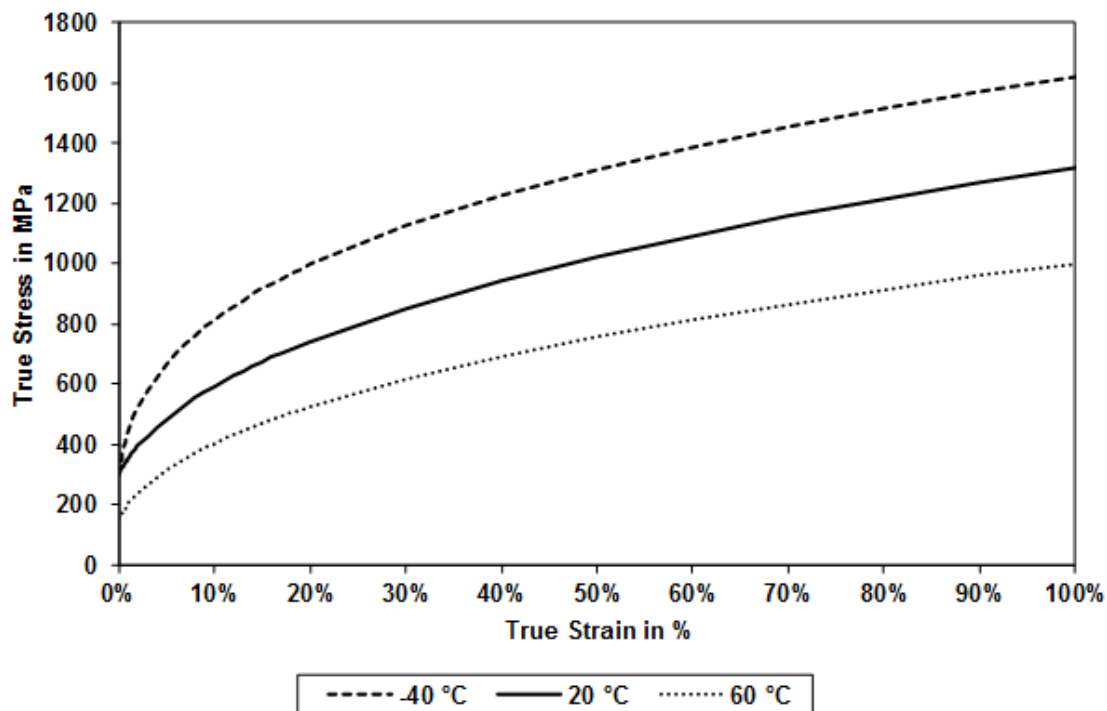


Figure 36: Material properties of stainless steel No. 1.4307 / 1.4301 used for the FE-model

The data given in Figure 36 represent common values for stainless steel in contrary to the minimal values defined in the respective standards. The curves are evaluated with the Swift equation with the input of $R_{p0.2}$, $R_{p1.0}$ and R_m [SWIFT 1952]. Since the yield strength and ultimate tensile strength are determined in quasi static conditions, the resulting steel flow curves are multiplied with a factor taking into account the dynamic stiffening behavior of steel. In the present case, this factor is 1.3. Details are contained in Appendix 2.2.1.3 (Structural Analysis of the DN30 Package under NCT and HAC).

Furthermore, a failure criterion of the steel is not taken into account for the present analysis. So, the strain of steel does not end at approximately 50 % (common value for the elongation at fracture of austenitic stainless steels) but is extended to higher values to achieve a stable calculation. Possible failures and cracks in the steel parts are evaluated by comparing the calculated strains with the elongation at fracture of the material.

In this calculation, there is only one curve for all kinds of stainless steel. Different kinds of steel are used for the DN30 package, but the differences in the stress-strain curves are insignificant for these steels compared to usual manufacturing tolerances for steel.

2.2.1.5.1.3.6 Content of the 30B cylinder

In the FEM simulations, the content of the 30B cylinder (UF_6) is simulated by a block of heavy concrete with a density of 5.1 g/cm^3 . The simulated mass is 2277 kg.

In the real drop tests, the content of the 30B cylinder (UF_6) is simulated by a mixture of steel grit and cement. The density of UF_6 in solid state is 5.1 g/cm^3 . In order to be close to the real content, the simulated content of steel grit and cement has a similar density to UF_6 . The content is modeled as one big block of this mixture positioned at the bottom half of the 30B cylinder and a layer of scraps positioned at the top of this block. The big block as well as the scraps have a density of 5.1 g/cm^3 . The mass of the block is 1977 kg, the scraps have a total weight of approximately 300 kg. While the scraps can move freely during the drop tests, the block remains a solid body during all drop test simulations.

In the FEM simulation, the content of the 30B cylinder (UF_6) is simulated by a single block of heavy concrete with a density of 5.054 g/cm^3 . The simulated mass of 2277 kg corresponds to the maximum allowed net weight of the 30B cylinder. Referring to Eurocode 2, an elastic perfectly plastic material model is used to model the concrete in the safety analysis of the DN30 PSP.

2.2.1.5.1.4 Modeling of the drop test sequence

Each drop test sequence (1.2 m drop – 9.0 m drop – drop onto bar) is modeled in the same way. First the 1.2 m drop is calculated, after that a small restart calculation is performed where the velocity of the entire DN30 package model is set to zero and the target is put in the right position for the next drop test. This is required because of possible rotations of the DN30 package model during the previous drop test. In this restart analysis, all information about internal stresses and strains is retained in the model.

The short time without loads being applied to the DN30 package model is also required for relaxation to reduce internal oscillations. After that, the calculation of the 9.0 m drop is carried out, which is again followed by another relaxation period. Finally, the drop onto the bar is carried out. The order of the drop tests (9.0 m drop followed by drop onto the bar or drop onto the bar followed by 9.0 m drop) is investigated as well. It is demonstrated that the drop order 1.2 m – 9.0 m – bar is more damaging in case of the DN30 package.

The drop test program in Appendix 2.2.1.1 (Drop Test Program) is based on the results of former drop test simulations.

2.2.1.5.1.5 Analysis, results of real drop tests and comparison of analysis and drop tests

2.2.1.5.1.5.1 Corner drop onto the valve side – drop test sequence 1

2.2.1.5.1.5.1.1 General considerations

The valve is the most vulnerable part of the containment system. For the corner drop onto the valve side, maximal deformations of the DN30 PSP in the valve area are expected. The design has to ensure that after the tests simulating HAC:

- There is no contact between valve and any part of the DN30 PSP or any other part of the 30B cylinder except for its initial point of contact (the thread).
- The leakage rate of the containment does not exceed the limit specified in section 2.2.3.

In variation calculations, the angle between the longitudinal axis of the DN30 package and the vertical is determined, which leads to maximum deformation and thus minimum volume of the foam in the valve area. This angle is then used in real drop tests to validate the results of the analysis.

2.2.1.5.1.5.1.2 FEM Analysis

2.2.1.5.1.5.1.2.1 FEM analysis before the drop tests

In the FEM analysis before the real drop testing, different angles from 12° to 42° between the longitudinal axis of the DN30 package and the vertical line through the center of gravity were analyzed for the 1.2 m drop and the 9 m drop onto the corner on the valve side. For the drop from 1 m height onto the bar, the bar is positioned so that the vertical line from the center of gravity touched the valve and the corner of the bar.

The minimal distance between inner and outer shell above the valve was reached for an angle in the range of 12° to 22° and the minimal remaining foam volume in the valve area after the

drop test sequence was reached for an angle in the range of 17° to 27°. Because of these simulations, an angle of 22° has been chosen for the drop tests of sequence 1.

2.2.1.5.1.5.1.2.2 Deformations at -40 °C, RT and +60 °C

In the 1.2 m free drop test at RT, the corner of the DN30 PSP is deformed as shown in Figure 38. There are no deformations of the inner steel plates, the rotation preventing device and the valve protecting device. Furthermore, there are no cracks in the outer shell or the inner shell of the DN30 PSP.

The 9.0 m drop causes larger deformation of the corner of the DN30 PSP, which is shown in Figure 39. The buckling of the outer shell increases, but still without any cracks in the outer surface. There are also deformations visible at the inner steel parts, especially at the front plate, which is in contact with the skirt of the 30B cylinder. The rotation preventing devices are deformed, but their function is still preserved and any rotation of the 30B cylinder is prevented.

Figure 40 shows the deformations during the drop onto the bar. The bar does not penetrate the steel shell of the DN30 PSP and only local deformations occur while the rest of the DN30 package does not undergo further deformations compared to the previous test. Hence, the distance between the valve and the DN30 PSP is still preserved.

The deformations are summarized in Table 37. The definition of the measurement points for the values in Table 37 is shown in Figure 37.

Table 37: Deformation and remaining dimensions calculated for the drop onto the valve corner

Dimension in mm	Drop test at temperature								
	-40 °C			RT			60 °C		
	1.2 m	9.0 m	1 m bar	1.2 m	9.0 m	1 m bar	1.2 m	9.0 m	1 m bar
Largest fold (L1x)	68	148	-	82	156		94	167	-
Largest fold (L1y)	185	401	-	222	422		256	451	-
Weld between head and outer shell (L2x)	49	130	-	64	142		69	153	-
Weld between head and outer shell (L2y)	133	384	-	204	404		214	428	-
Depth of bar penetration (p1)	-	-	7	-	-	32	-	-	49
Depth of bar penetration (p2)	-	-	28	-	-	48	-	-	56

Remark: the values for RT given in Table 37 and Table 39 differ from each other, since different reference nodes of the simulation model were selected for the comparison of the calculated and measured deformations.

The corner drop onto the valve side is the most critical drop orientation concerning the amount of deformations of the DN30 package. Generally, the material response of steel becomes softer with increasing temperature so that even larger deformations are expected at 60 °C. Therefore, sequence 1 is used for the investigation of the deformation behavior of the DN30

package at an ambient temperature of 60 °C. In addition, a simulation at -40 °C is performed to get a general idea of the temperature dependency of the deformation behavior of the DN30 package. In contrast to elevated temperatures, the material response of the austenitic stainless steel becomes stiffer at lower temperatures. Therefore, smaller deformations of the package and higher decelerations in the valve region are expected. Independently of the ambient temperature, the design has to ensure that even after the drop tests simulating HAC, no contact between the valve and any part of the DN30 PSP or the 30B cylinder occurs except for its initial point of contact (the thread).

The deformations of the corner of the DN30 PSP after the free drop test at 60 °C are increased by 15 % compared to the deformations at RT. The displacements of the inner front plate, where the skirt of the 30B cylinder hits the inner shell, are still small with plastic strains up to 15 %. Based on the maximum plastic strain of 35 % occurring in the simulation of the free drop test at 60 °C, there are neither cracks in the outer shell nor the inner shell of the DN30 PSP to be expected. During the 9 m drop, plastic strains up to 48.5 % occur at the inner front plate due to the impact of the 30B cylinder skirt. According to the simulation, cracks are likely to occur in these areas, but there is no contact between the valve and any other part of the DN30 PSP or the 30B cylinder. Additionally, the rotation preventing devices are deformed, but their function is still preserved and any rotation of the 30B cylinder is prevented.

After the free drop test, the deformations at -40 °C of the corner of the DN30 PSP are reduced by 17 % compared to the deformations at RT. Based on the maximum plastic strain of 24 % occurring at the corner of the DN30 PSP in the simulation at -40 °C, there are no cracks expected in the outer shell of the DN30 PSP. The maximum plastic strain at the inner front plate, where the skirt of the 30B cylinder impacts the inner shell, only reaches 7.6 %. Additionally, the rotation preventing devices as well as the valve protecting device remain undeformed so that the valve does not undergo any deformation or contact.

After the 9 m drop, cracks are not expected in the outer surface because the occurring maximal plastic strains are below the elongation at fracture of the austenitic stainless steel. In addition, the deformations at the inner front plate and the profile of the top half are reduced from 40.1 % in the simulation at RT to 36.9 % in the simulation at -40 °C. According to the simulation, cracks are unlikely to occur in these areas at a temperature of -40 °C. The impact of the 30B cylinder skirt causes these deformations.

The above mentioned larger deformations of the inner steel parts have no influence on the valve protecting device, so that the valve is still prevented from getting in contact with other parts. In case of the rotation preventing devices, deformations up to 24 % are observed at the flange. Nevertheless, their function is still preserved and any rotation of the 30B cylinder is prevented.

Neither at -40 °C nor at 60 °C a contact between the valve or the plug and any other part of the DN30 PSP or 30B cylinder occurs except for their initial point of contact (the thread).

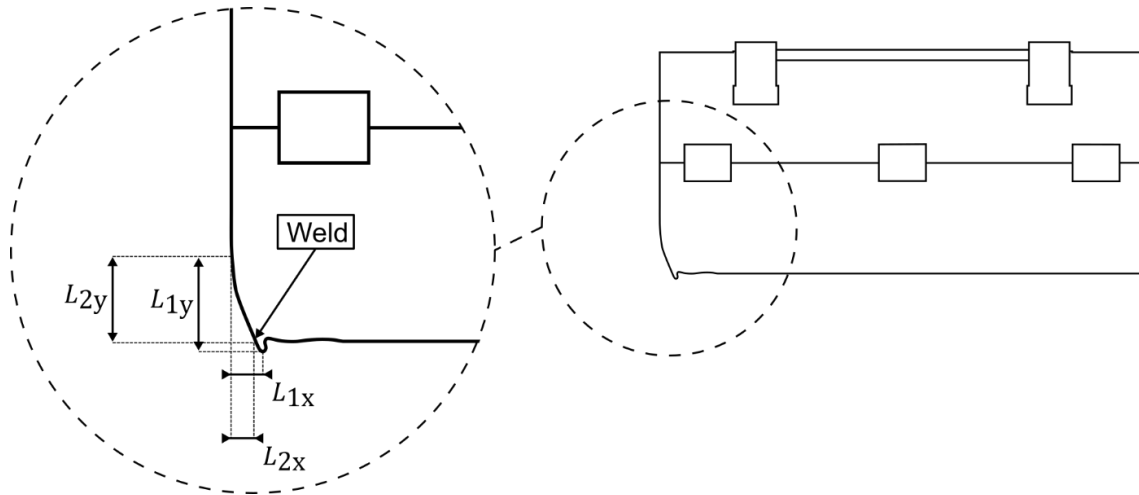


Figure 37: Measured distances in sequence 1

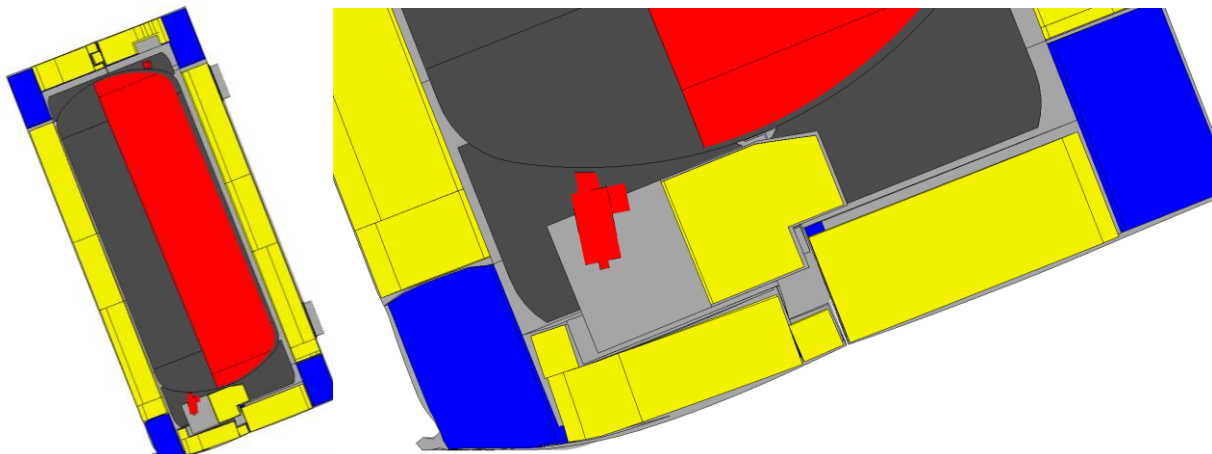


Figure 38: Deformed structure after the 1.2 m free drop test at RT onto the valve corner

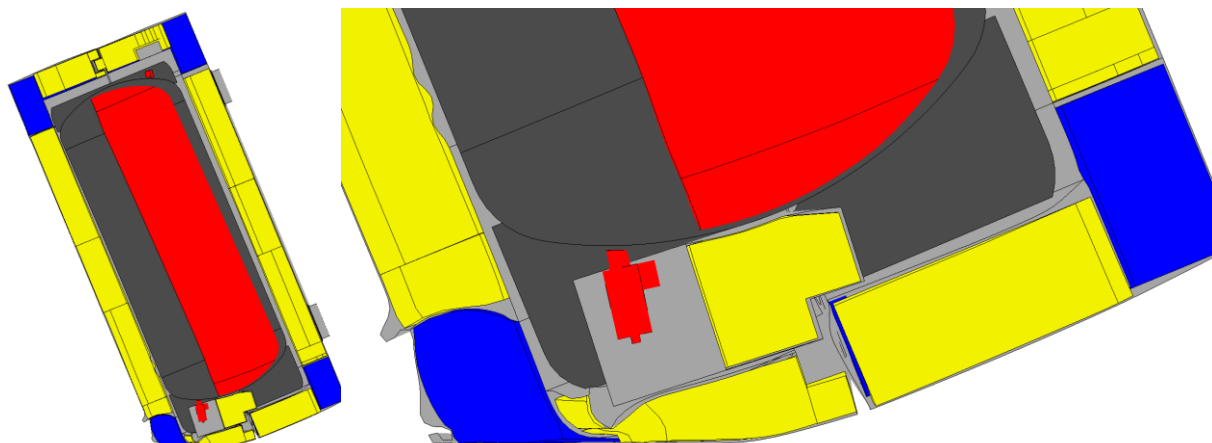


Figure 39: Deformed structure after the 9.0 m drop test at RT onto the valve corner

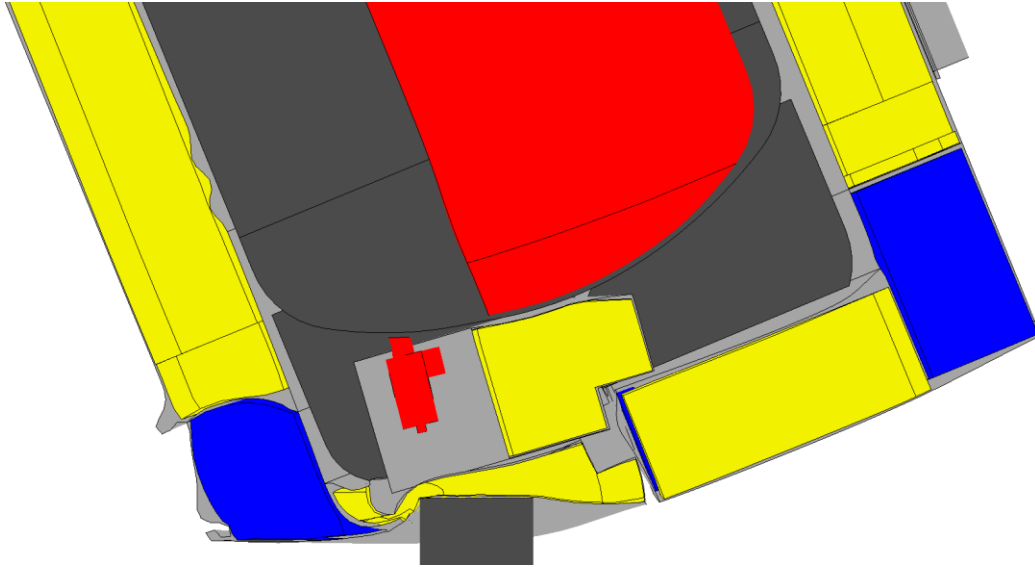


Figure 40: Deformed structure in the valve area after the test sequence at RT onto the valve corner

2.2.1.5.1.5.1.2.3 Decelerations at -40 °C, RT and +60 °C

The measured decelerations in the valve area are filtered with a low-pass SAE filter with a cut-off frequency of 20 Hz and 584 Hz. The comparison of the filtered decelerations at RT and +60 °C is shown in Figure 41 for a cut-off frequency of 20 Hz and in Figure 42 for a cut-off frequency of 584 Hz. The corresponding comparison of the filtered decelerations at RT and -40 °C is shown in Figure 44 and Figure 44.

The deceleration curves at 20 °C and 60 °C are very similar. At a cut-off frequency of 20 Hz, the difference between the two curves is below 5 %. At a cut-off frequency of 584 Hz, the deceleration in the simulation at 60 °C increases earlier than in the simulation at 20 °C. This is attributed to the fact that the 30B cylinder skirt is closer to the inner front plate after the free drop test at 60 °C than after the free drop test at 20 °C. Apart from the initial phase the two deceleration curves are very similar even at a high cut-off frequency of 584 Hz.

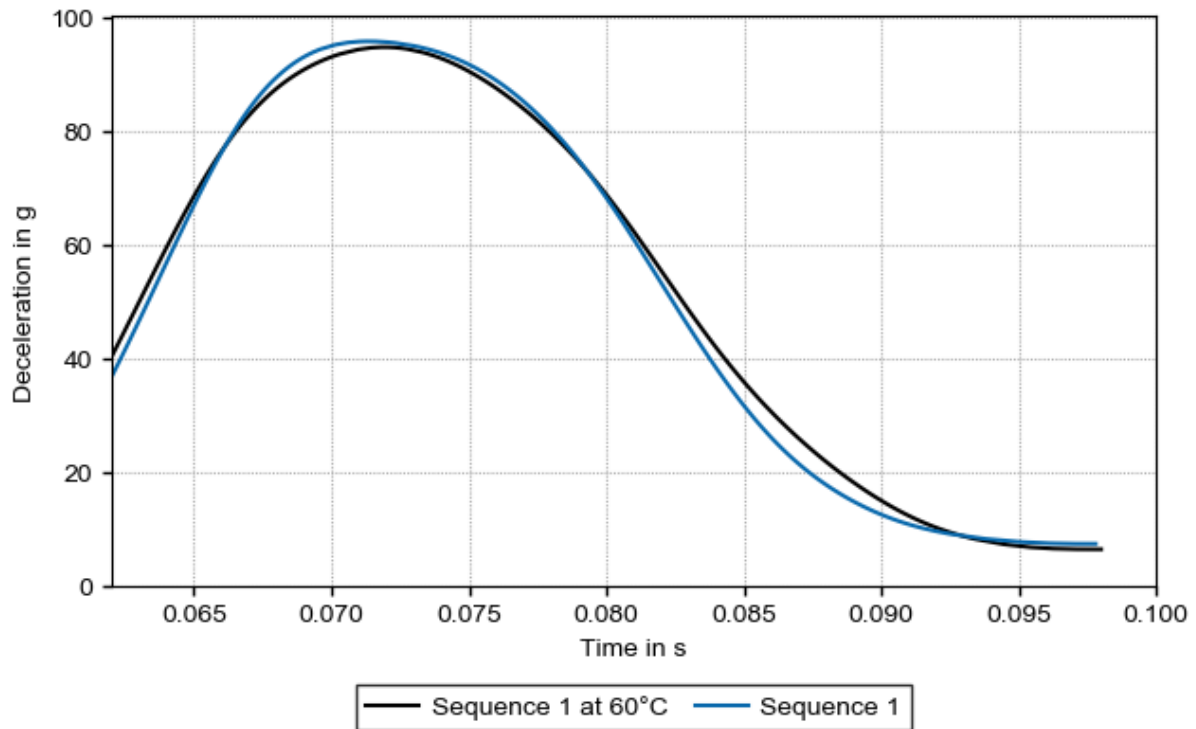


Figure 41: Comparison of the deceleration in the valve area during the 9.0 m drop in sequence 1 at 60 °C and 20 °C – low-pass filtered (SAE, 20 Hz cut-off)

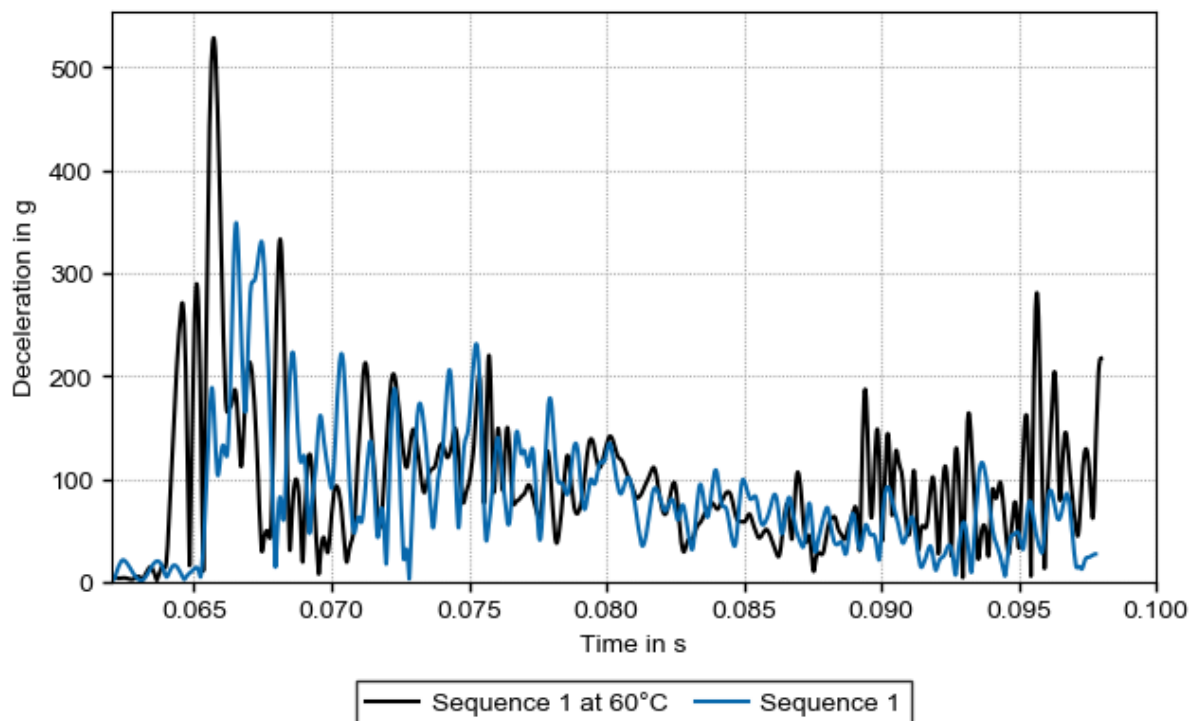


Figure 42: Comparison of the deceleration in the valve area during the 9.0 m drop in sequence 1 at 60 °C and 20 °C – low-pass filtered (SAE, 584 Hz cut-off)

The comparison of the decelerations at -40 °C and 20 °C shows nearly identical curves in height and shape at a cut-off frequency of 20 Hz. Hence, the impact on the decelerations because of the stiffer material behavior at -40 °C is negligible. The impact of the stiffer material behavior on the decelerations becomes only visible at higher cut-off frequencies. At a cut-off frequency of 584 Hz, the deceleration curve of the simulation at -40 °C shows a peak that is about 60% higher than the peak in the deceleration curve of the simulation at 20 °C.

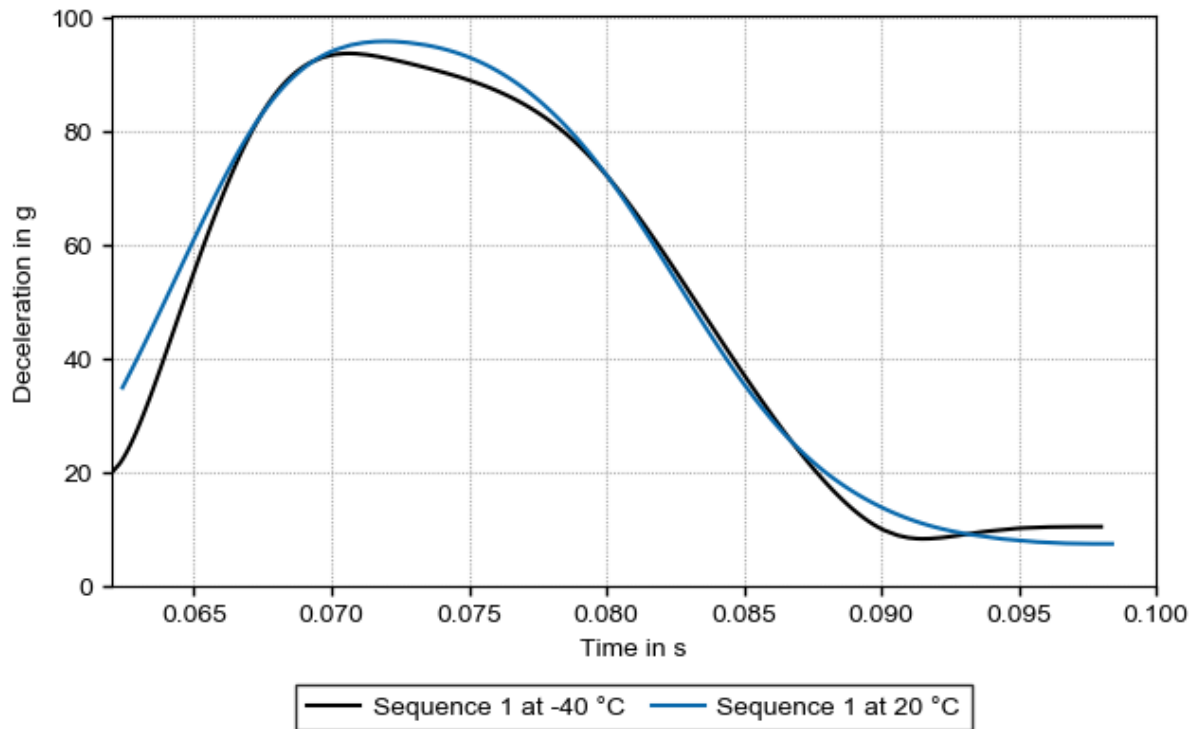


Figure 43: Comparison of the deceleration in the valve area during 9.0 m drop in sequence 1 at -40 °C and 20 °C – low-pass filtered (Butterworth, 584 Hz cut-off)

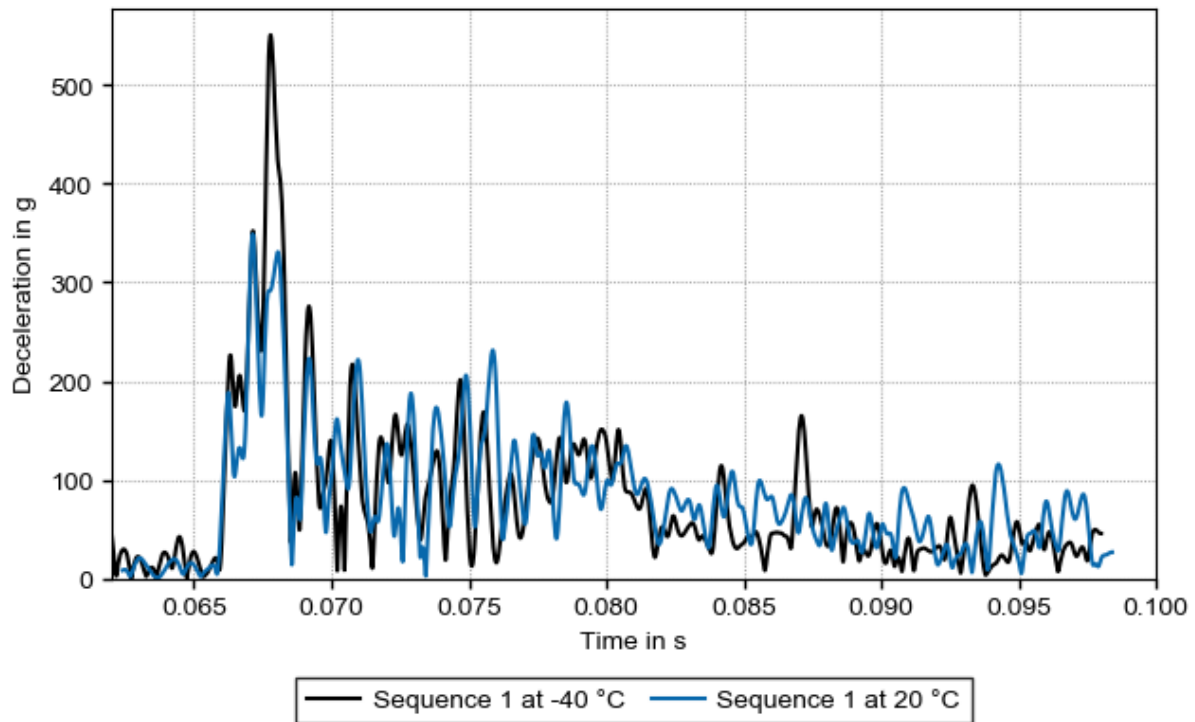


Figure 44: Comparison of the deceleration in the valve area during 9.0 m drop in sequence 1 at -40 °C and 20 °C – low-pass filtered (Butterworth, 584 Hz cut-off)

2.2.1.5.1.5.1.3 Results of drop tests of sequence 1

The drop test sequence onto the corner of the valve side is documented as sequence No. 1 in Appendix 2.2.1.2 (Drop Test Reports).

- Drop No. 1.1 1.2 m corner drop test onto the valve side
- Drop No. 1.2 9 m corner drop test onto the valve side
- Drop No. 1.3 1 m drop onto a bar onto the valve side

2.2.1.5.1.5.1.3.1 Deformations at RT for drop test sequence 1

The 1.2 m drop causes small deformations of the corner of the DN30 package. There is a slight buckling of the outer shell visible (see Figure 45). The 9.0 m drop causes larger deformation of the corner of the DN30 package. The buckling of the outer shell increases, but still without any cracks in the outer surface or outer welding seams (see Figure 46).

The drop onto the bar does not cause a complete penetration of the outer steel shell of the DN30 package, but a crack of the outer shell is visible at the impact area (see Figure 47).



Figure 45: Sequence 1 - Deformation after the 1.2 m drop



Figure 46: Sequence 1 - Deformation after the 9.0 m drop



Figure 47: Sequence 1 - Deformation after the drop onto a bar from 1.0 m

There are also deformations and cracks visible at the inner steel parts, especially at the inner front plate that is in contact with the skirt of the 30B cylinder (see Figure 48). The rotation preventing devices are deformed, but their function is still preserved and any rotation of the 30B cylinder is prevented (see Figure 49).



Figure 48: Sequence 1 – Deformation and cracks of the top half, inner shell

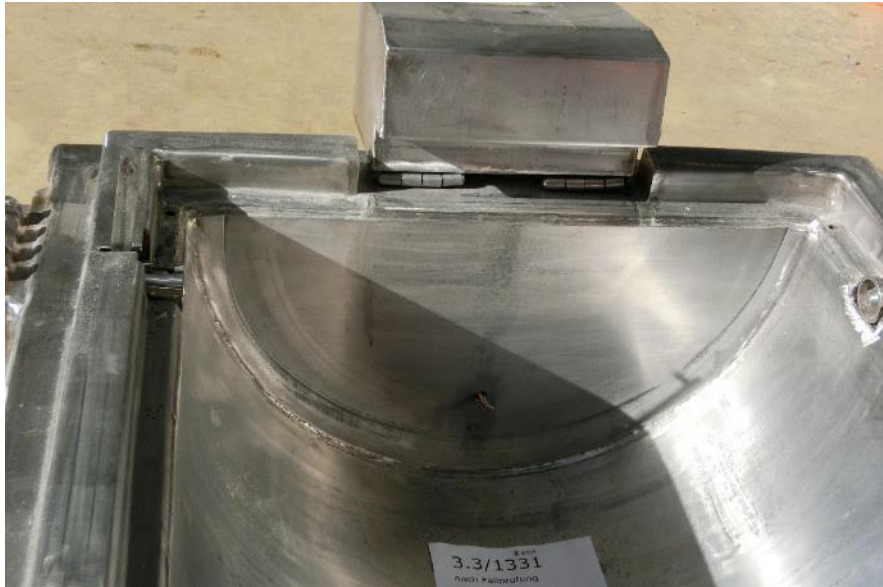


Figure 49: Sequence 1 – Deformation of the bottom half, inner shell

2.2.1.5.1.5.1.3.2 Summary of the drop test results for sequence 1

- The leakage rate after the drop test sequence 1 is $Q_{st} = 5.67 \text{ E-08 Pa} \cdot \text{m}^3/\text{s}$.
- All closure systems are intact.
- The DN30 PSP can be opened without further damaging the DN30 PSP.
- The closure system is still working, and the top half can easily be lifted off the bottom half.
- There was no contact between the valve and any other part of the DN30 PSP or 30B cylinder except for its initial point of contact (the thread).
- There was no contact between the plug and any other part of the DN30 PSP or 30B cylinder except for its initial point of contact (the thread).
- The valve protecting device can still be operated (rotated); the hinges are intact.
- Removal of the 30B cylinder from the bottom half is possible without further damaging the DN30 PSP.
- Loading of a 30B cylinder into the DN30 PSP is still possible.

2.2.1.5.1.5.1.4 Results of drop tests of sequence 7

Another drop test sequence onto the valve corner was carried out to prepare a specimen for the subsequent thermal test. This specimen was equipped with the housing for the valve protecting device and the intumescent material attached to the inner shell. These additional features were added to the specimen before the drop test and were part of the prototype during the drop tests. For the specimen of the thermal test, the two sequences “drop onto the valve corner” and “drop onto the plug corner” were combined. Furthermore, the 1.2 m free drop test was combined with the 9.0 m drop test to a single 10.2 m drop test, which caused larger deformations than the usual drop test sequences 1 and 2.

Drop No. 7.1 10.2 m corner drop tests onto the valve side

Drop No. 7.2 1 m drop onto a bar onto the valve side of the top half of the DN30 PSP

Drop No. 7.3 10.2 m corner drop test onto the plug side

Drop No. 7.4 1 m drop onto a bar onto the plug side of the bottom half of the DN30 PSP

2.2.1.5.1.5.1.4.1 Deformations at RT for drop test sequence 7

The deformations of the outer shell as well as of the inner shell are identical to the deformations documented for sequence 1 (see Figure 50). Table 38 shows the comparison of the deformation measured for drop test sequence 1 with the deformations measured for drop test sequence 7. The measurement points for the values listed are defined in Figure 37.



Figure 50: Deformations of the DN30 PSP after sequence 7

Table 38: Deformations and remaining dimensions measured for the drop onto the valve corner in sequence 1 and sequence 7

Dimension [mm]	Drop					
	1.2 + 9.0 m			1 m bar		
	Seq. 1	Seq. 7	D %	Seq. 1	Seq. 7	D %
Largest fold (L1x)	≈170	≈211	≈24	-	-	-
Largest fold (L1y)	≈490	≈430	≈-12	-	-	-
Weld between head and outer shell (L2x)	-	≈143		-	-	-
Weld between head and outer shell (L2y)	≈460	≈395	≈-14	-	-	-
Depth of bar penetration (p1)	-	-	-	≈32	-	-
Depth of bar penetration (p2)	-	-	-	≈50	≈30	≈-40

2.2.1.5.1.5.1.4.2 Summary of the drop test results for sequence 7

For sequence 7 the results are identical to the results for sequence 1 given in section 2.2.1.5.1.5.1.3. Additionally, the following was recorded regarding the additional features housing for the valve protecting device and intumescent material:

- The housing in the valve protecting device containing the intumescent material remains intact;
- The intumescent material applied to the inner shell of the DN30 PSP as well as the housing and the plug protecting device remains undamaged;
- Removal of the 30B cylinder from the bottom half is possible without further damaging the DN30 PSP;
- Loading of a 30B cylinder into the DN30 PSP is still possible.

2.2.1.5.1.5.1.5 Evaluation of the FEM analysis vs. real drop tests

2.2.1.5.1.5.1.5.1 Deformations at RT

The measured deformations and remaining dimensions are compared to the calculated values in Table 39. The measurement points for the values listed are defined in Figure 37.

Table 39: Deformations and remaining dimensions measured for the drop onto the valve corner (ambient temperature) and comparison with calculated values at RT

Dimension [mm]	Drop								
	1.2 m			9.0 m			1 m bar		
	CV	MV	D %	CV	MV	D %	CV	MV	D %
Largest fold (L1x)	82	90	-9	156	170	-8	-	-	-
Largest fold (L1y)	222	245	-9	422	460	-8	-	-	-
Weld between head and outer shell (L2x)	65	-	-	185	-	-	-	-	-
Weld between head and outer shell (L2y)	204	200	2	421	490	-14	-	-	-
Depth of bar penetration (p1)	-	-	-	-	-	-	32	32	0
Depth of bar penetration (p2)	-	-		-	-	-	48	50	-3

CV = calculated values MV = measured values

D % = deviation of measured values from calculated values in %

The measurement error in the experiment is in the range of 10 % because of the applied measurement technique. Except for L2y, the resulting error between experiment and calculation does not exceed 10 %. Although the calculated distances indicate that the FEM model has a too stiff response, the simulation reproduces the behavior of the prototype observed in the experiment well with most errors below 10 %.

A qualitative comparison of the deformations after the 9.0 m drop between the simulation and the experiment is shown in Figure 51.

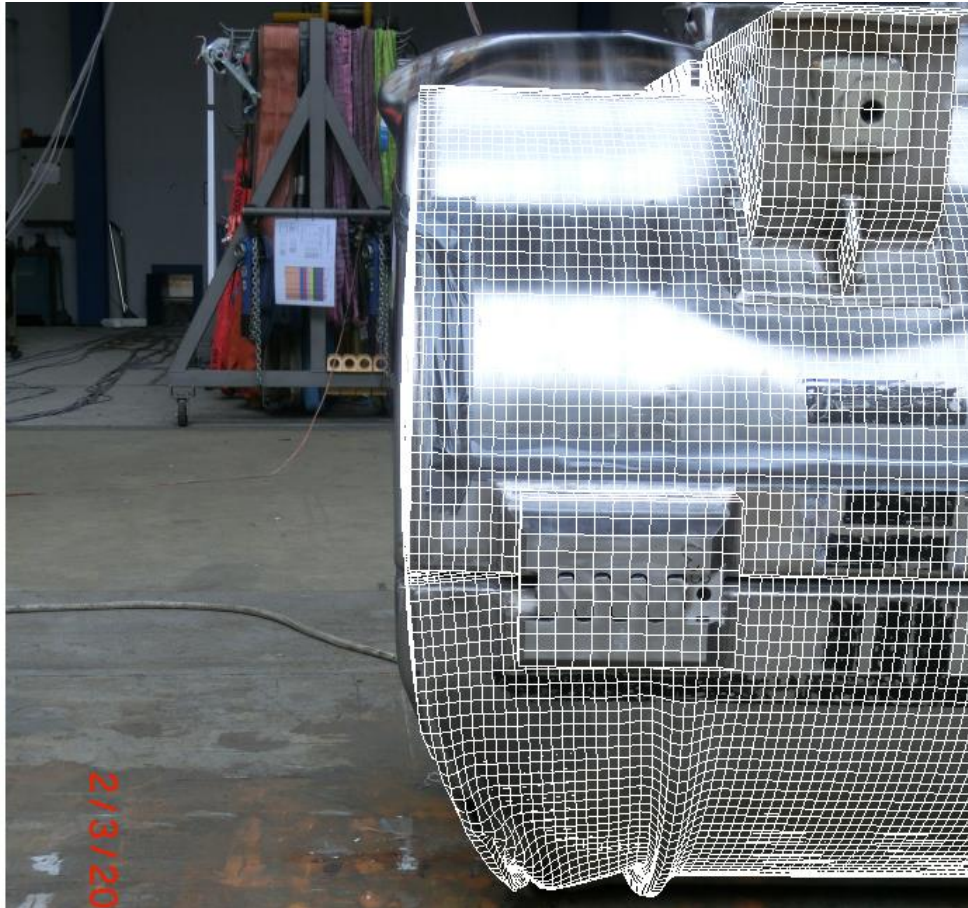


Figure 51: Qualitative comparison of the deformations in simulation and experiment

2.2.1.5.1.5.1.5.2 Decelerations at RT

Figure 52 and Figure 53 show the comparison of the calculated decelerations with the measured decelerations at a cut-off frequency of 20 Hz and 584 Hz. The deceleration curve for the 30B cylinder at a cut-off frequency of 20 Hz maximally differs 15 % from the experiment and, thus, is very similar in height and shape. However, the undefined position of the 30B cylinder at the time of impact may lead to non-deterministic interactions of the 30B cylinder with the DN30 PSP and thus makes it very challenging to accurately predict the deceleration peaks at the higher cut-off frequency of 584 Hz. Nevertheless, the FEM model reproduces the observed behavior from the experimental drop tests very well, especially regarding lower frequency ranges carrying large energy fractions.

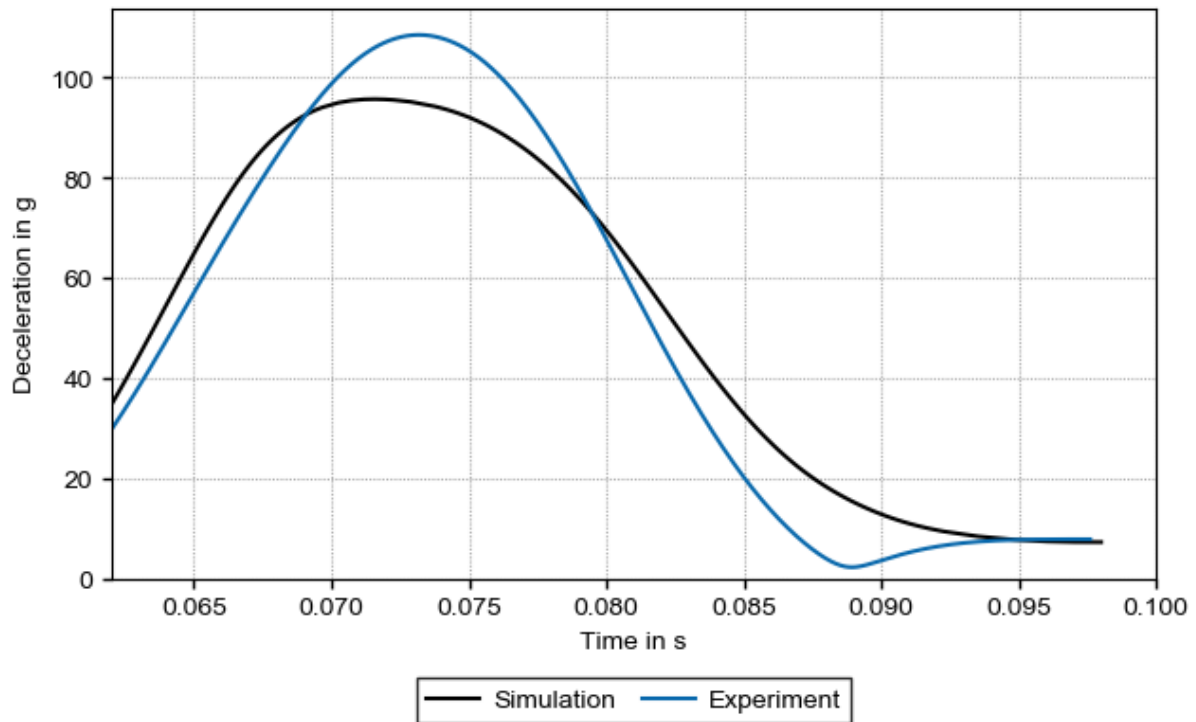


Figure 52: Comparison of simulation and experiment – deceleration in the valve area during 9.0 m drop in sequence 1 – low-pass filtered (SAE, 20 Hz cut-off)

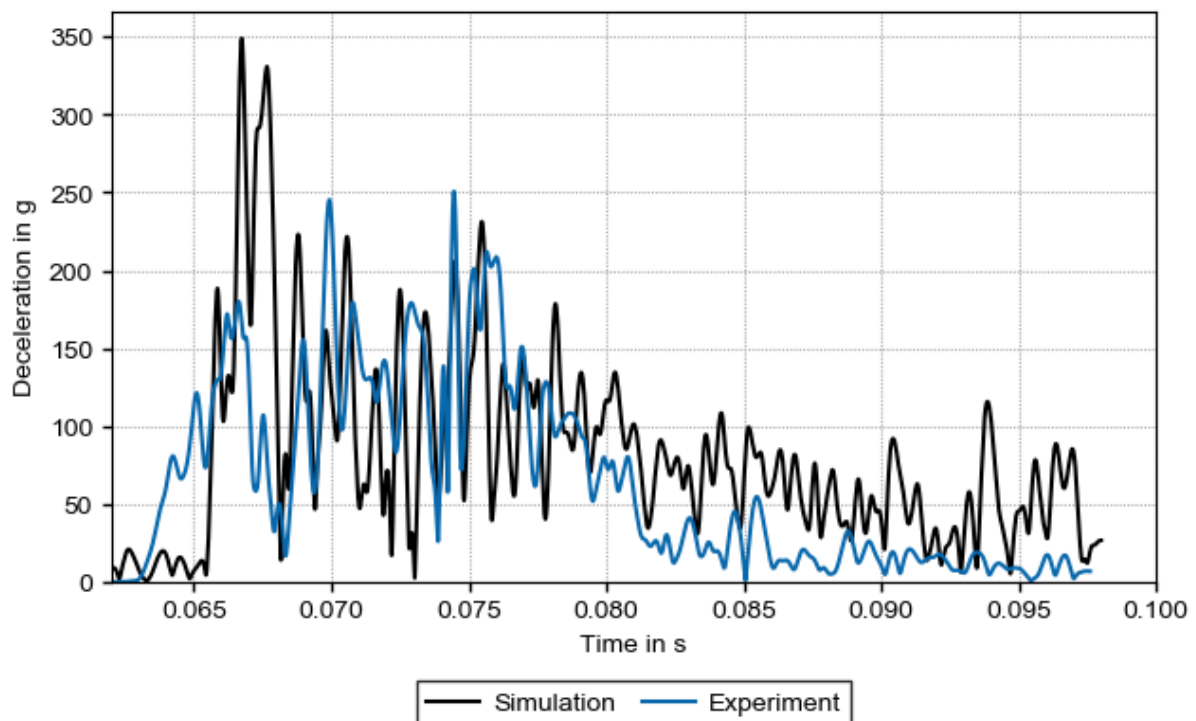


Figure 53: Comparison of simulation and experiment – deceleration in the valve area during 9.0 m drop in sequence 1 – low-pass filtered (SAE, 584 Hz cut-off)

2.2.1.5.1.5.2 Corner drop onto the plug side - drop test sequence 2

2.2.1.5.1.5.2.1 General considerations

Apart from the valve, the plug is the only other opening of the containment system. Maximal deformations of the DN30 PSP in the plug area are expected for the corner drop onto the plug side. The design has to ensure that after the tests simulating HAC:

- There is no contact between plug and any part of the DN30 PSP or any other part of the 30B cylinder except for its initial point of contact (the thread).
- The leakage rate of the containment does not exceed the limit specified in section 2.2.3.

In variation calculations, the angle between the longitudinal axis of the DN30 and the vertical is determined, which leads to maximum deformation and thus minimum volume of the foam in the plug area.

2.2.1.5.1.5.2.2 FEM analysis

2.2.1.5.1.5.2.2.1 *FEM analysis before the drop tests*

In the FEM analysis before the drop tests, different angles from 8° to 38° between the longitudinal axis of the DN30 package and the vertical line through the center of gravity were analyzed for the 1.2 m drop and the 9 m drop onto the corner at the plug side. For the drop from 1 m height onto the bar, the angle was in all cases such as that the vertical line from the center of gravity pointed through the center of the plug protecting device and touched the corner of the bar.

The minimal distance between inner and outer shell above the plug protecting device was reached for an angle in the range of 13° to 23° and the minimal distance between the plug and the plug protecting device was reached for an angle in the range of 8° to 23°. Because of this study, an angle of 23° was selected for the drop tests.

2.2.1.5.1.5.2.2.2 *Deformations at RT*

In the 1.2 m free drop, the corner of the DN30 PSP is deformed as shown in Figure 55. There are no deformations of the inner steel plates, the rotation preventing device and the plug protecting device. Furthermore, there are no cracks in the outer shell or in the inner shell of the DN30 PSP.

During the 9.0 m drop the deformation of the corner of the DN30 PSP continues. The state with the maximal deformation of the corner is shown in Figure 56. There are some deformations visible at the inner steel parts as well, especially at the inner front plate, which is in contact with the skirt of the 30B cylinder. However, the plug protecting device itself remains undamaged so that a contact of the plug with other parts is prevented even at the state with the maximal deformation. Although the foam between the outer shell and the plug protecting device is significantly compressed, it is still present. The rotation preventing devices are deformed, but their function is preserved so that any rotation of the 30B cylinder is prevented.

After the 9.0 m drop, the distance between the outer shell and the inner shell is already small. This leads to further deformation of the inner steel shell and the plug protecting device during the drop onto the bar. There is still a sufficient distance between the plug and the plug protecting device, even at the state with the maximal deformation, which is shown in Figure 57.

Table 40 documents measured deformations for the corner drop onto the plug side. The definition of these measurement points is shown in Figure 54.

Table 40: Deformations and remaining dimensions calculated for the drop onto the plug corner

Dimension [mm]	1.2 m drop	9.0 m drop	Drop onto the bar
Largest fold (L1x)	86	203	-
Largest fold (L1y)	580	609	-
Weld between head and outer shell (L2x)	71	161	-
Weld between head and outer shell (L2y)	559	563	-
Depth of bar penetration (p1)	-	-	20
Depth of bar penetration (p2)	-	-	24

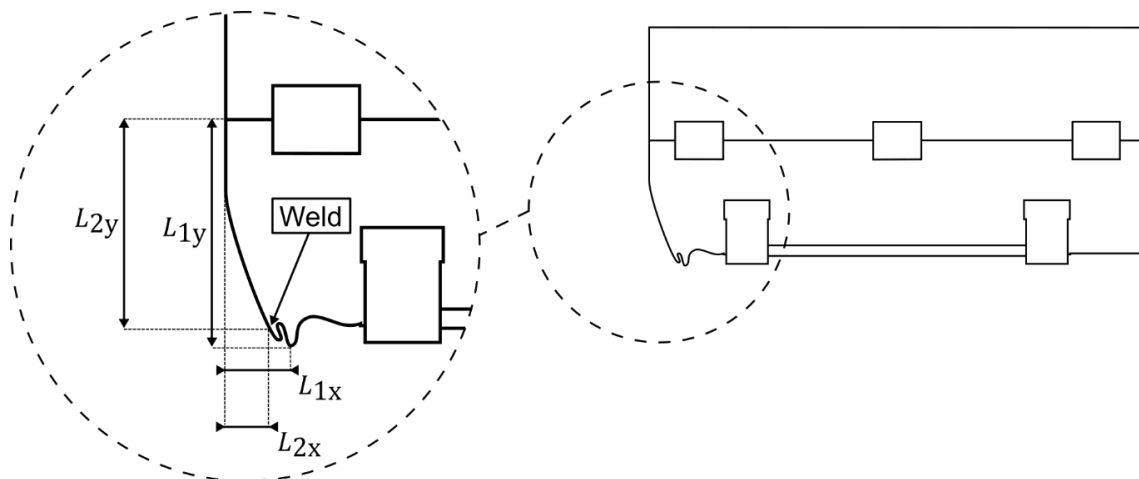


Figure 54: Measured distances in sequence 2

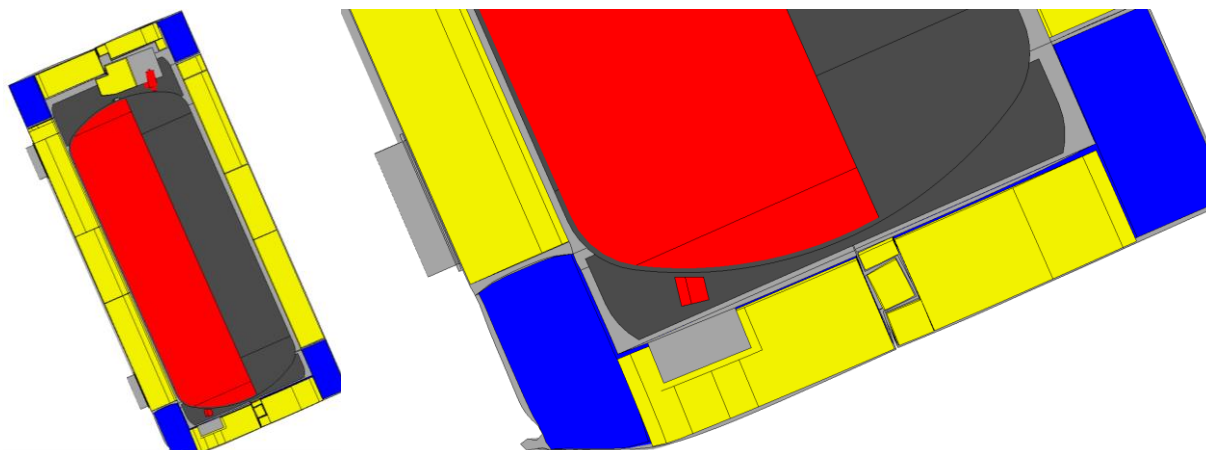


Figure 55: Deformed structure after the 1.2 m free drop onto the plug corner

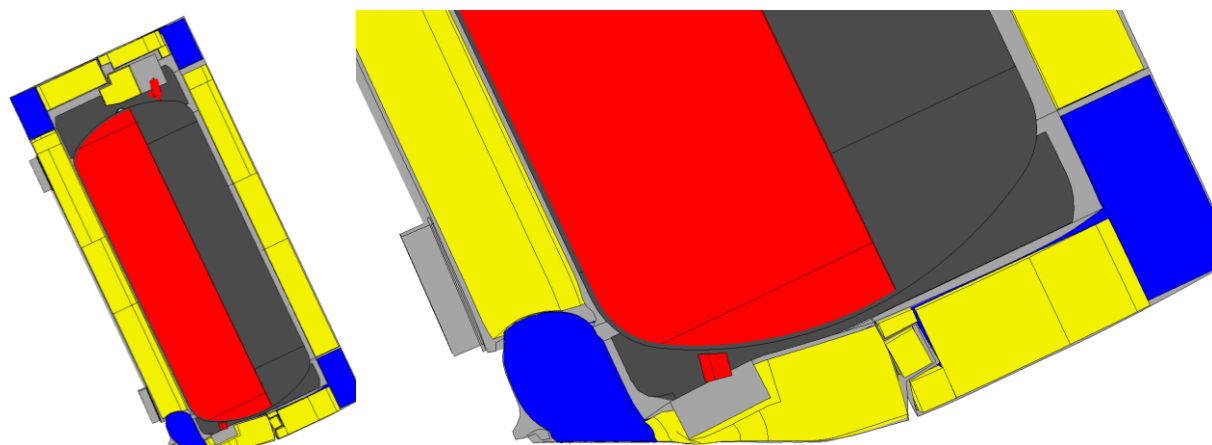


Figure 56: Deformed structure after the 9 m drop onto the plug corner

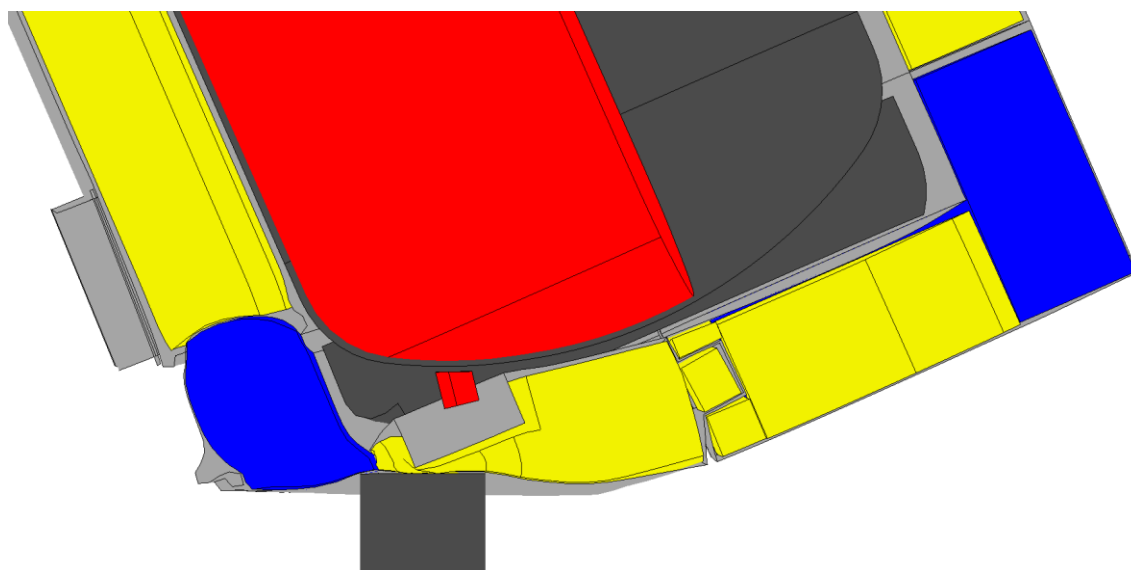


Figure 57: Deformed structure after the test sequence onto the plug corner

2.2.1.5.1.5.2.3 Results of drop tests

The drop test sequence onto the corner of the plug side is documented as sequence No. 2 in Appendix 2.2.1.2 (Drop Test Reports).

- Drop No. 2.1 1.2 m corner drop test onto the plug side
- Drop No. 2.2 9 m corner drop test onto the plug side
- Drop No. 2.3 1 m drop onto a bar onto the plug side

2.2.1.5.1.5.2.3.1 Deformations at RT

The 1.2 m drop causes small deformations of the corner of the DN30 package. A slight buckling is visible (see Figure 58). The 9.0 m drop causes larger deformation of the corner of the DN30 package. The buckling of the outer shell increases, but still without any cracks in the outer surface or outer welds (see Figure 59).

The drop onto the bar does not penetrate the steel shell of the DN30 package (see Figure 60).



Figure 58: Sequence 2 - Deformation after the 1.2 m drop



Figure 59: Sequence 2 - Deformation after the 9.0 m drop



Figure 60: Sequence 2 - Deformation after the drop onto a bar from 1.0 m

There are also deformations and cracks visible at the inner steel parts. The plug protecting device was pushed inside the DN30 PSP due to the impact of the bar (see Figure 61). The rotation preventing devices are deformed, but their function is still preserved and any rotation of the 30B cylinder is prevented.



Figure 61: Sequence 2 – Deformation of the bottom half, inner shell

2.2.1.5.1.5.2.3.2 Summary of the drop test results for sequence 2

- The leakage rate after the drop test sequence 2 is $Q_{st} = 4.15 \text{ E-06 Pa} \cdot \text{m}^3/\text{s}$.
- All closure systems are intact.
- The DN30 PSP can be opened without further damaging the DN30 PSP.
- Operating the closure system and lifting the top half off the bottom half is possible.
- There was no contact between the valve and any other part of the DN30 PSP or 30B cylinder except for its initial point of contact (the thread).
- There was no contact between the plug and any other part of the DN30 PSP or 30B cylinder other except for its initial point of contact (the thread).
- The valve protecting device can still be operated (rotated) and the hinges are intact.
- Removal of the 30B cylinder from the bottom half is possible without further damaging the DN30 PSP.
- Loading of a 30B cylinder into the DN30 PSP is still possible.

2.2.1.5.1.5.2.4 Evaluation of the FEM analysis vs. real drop tests

2.2.1.5.1.5.2.4.1 Deformations at RT

In Table 41, the measured deformations and remaining dimensions are compared to the calculated values. The definition of these measurement points is shown in Figure 54.

Table 41: Deformations and remaining dimensions measured for the drop onto the plug corner (ambient temperature) and comparison to calculated values

Dimension [mm]	Drop								
	1.2 m			9.0 m			1 m bar		
	CV	MV	D %	CV	MV	D %	CV	MV	D %
Largest fold (L1x)	90	90	0	237	251	-6	-	-	-
Largest fold (L1y)	580	577	<1	567	620	-9	-	-	-
Weld between head and outer shell (L2x)	73	79	-8	197	187	6	-	-	-
Weld between head and outer shell (L2y)	560	560	0	533	580	-8	-	-	-
Depth of bar penetration (p1)	-	-	-	-	-	-	17	24	-30
Depth of bar penetration (p2)	-	-	-	-	-	-	22	34	-34

CV = calculated values MV = measured values

D % = deviation of measured values from calculated values in %

The exact measurement error in the experiment is unknown, but in the range of 10 % because of the applied measurement technique. Although the calculated errors indicate that the response of the FEM model is generally stiffer than the DN30 prototype, the simulation reproduces the behavior observed in the experiment well. Except for the depth of bar penetration, the deviations in the measured deformations are below 10 %.

A qualitative comparison of the deformations after the 9.0 m drop between the simulation and the experiment is shown in Figure 62.



Figure 62: Qualitative comparison of the deformations in simulation and experiment

2.2.1.5.1.5.2.4.2 Decelerations at RT

The resulting low-pass filtered decelerations in the plug area for the simulation and the experiment are shown in Figure 63 and Figure 64 for a cut-off frequency of 20 Hz and 584 Hz, respectively.

The deceleration curve for the 30B cylinder at a cut-off frequency of 20 Hz is 6 % higher in the experiment than in the simulation. The undefined position of the 30B cylinder at the time of impact may lead to non-deterministic interactions of the 30B cylinder with the DN30 PSP and, thus, makes it very challenging to accurately predict the deceleration peaks. Nevertheless, the general shape and the height of the deceleration curves is predicted with acceptable accuracy by the FEM model at a higher cut-off frequency of 584 Hz.

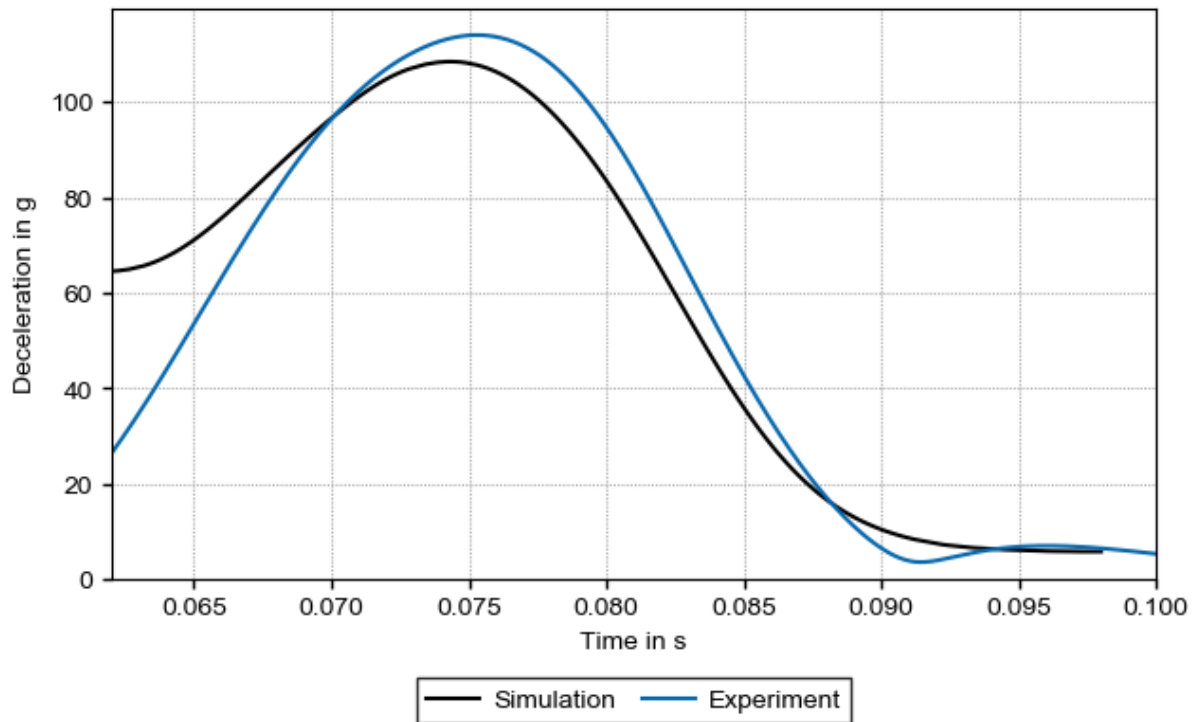


Figure 63: Comparison of simulation and experiment – deceleration in the plug area during 9.0 m drop in sequence 2 – low-pass filtered (SAE, 20 Hz cut-off)

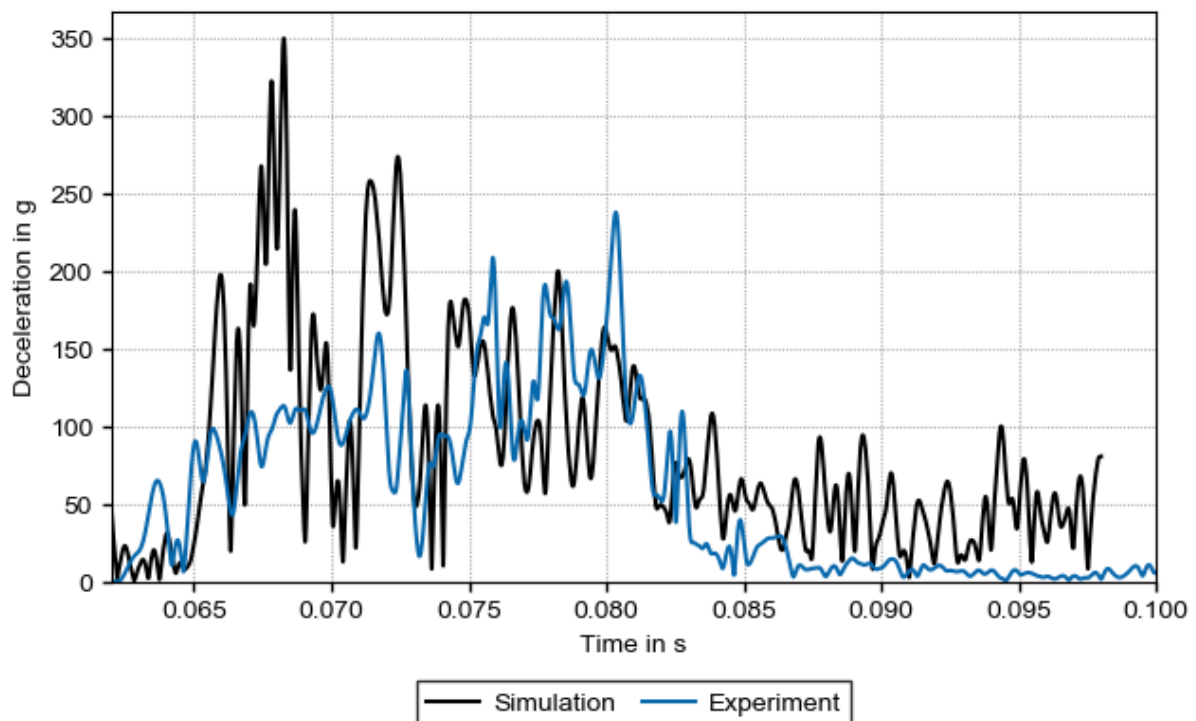


Figure 64: Comparison of simulation and experiment – deceleration in the plug area during 9.0 m drop in sequence 2 – low-pass filtered (SAE, 584 Hz cut-off)

2.2.1.5.1.5.3 Flat drop onto the valve side – drop test sequence 3

2.2.1.5.1.5.3.1 General considerations

With the drop onto the valve corner as described in section 2.2.1.5.1.5.1, maximal deformation is reached in the valve area. In contrast to that, maximal acceleration and, therefore, maximal forces at the valve are expected for the flat drop onto the valve. The design has to ensure that after the tests simulating HAC:

- There is no contact between valve and any part of the DN30 PSP or any other part of the 30B cylinder except for its initial point of contact (the thread).
- The leakage rate of the containment does not exceed the limit specified in section 2.2.3.

The drop orientation is flat onto the valve side for the 1.2 m drop and the 9 m drop. For the drop from 1 m height onto the bar, the bar is positioned so that the vertical line from the center of gravity points through the center of the valve and the center of the top of the bar.

2.2.1.5.1.5.3.2 FEM analysis

2.2.1.5.1.5.3.2.1 *Deformations at -40 °C and RT*

In the 1.2 m drop, almost no deformations occur that are above a few millimeters (see Figure 66). This is true for the rotation preventing devices and the valve protecting device as well. Except for some deformations at the impact zone of the skirt of the 30B cylinder, the inner steel plates remain undamaged and a formation of cracks is expected neither in the outer nor in the inner shell of the DN30 PSP. In addition, the valve undergoes neither any deformation nor contact.

In Figure 67, the state with the maximal deformation during the 9.0 m drop is shown. Compared to the 1.2 m drop, the buckling of the outer shell at the valve side is clearly visible. However, cracks in the outer surface are not expected. The plastic deformations of the inner steel parts have increased from 24.1 % for the 1.2 m drop to 58.5 % for the 9 m drop. Thus, the formation of cracks is very likely in this area. With 13.3 %, the deformations of the valve protecting device are relatively small in the simulation and there is still a sufficient amount of foam left to protect the valve area. In addition, the valve undergoes neither any deformation nor contact.

After the 9.0 m drop, there is a large proportion of foam left between the outer and inner shell of the DN30 PSP. For this reason, further deformations due to the bar impact are very localized with no effect on the inner steel parts of the DN30 PSP. During the drop onto the bar, the distance between valve and DN30 PSP is preserved. The resulting deformed structure is shown in Figure 68.

Table 42 documents measured deformations for the flat drop onto the valve side. The definition of these measurement points is shown in Figure 65.

Table 42: Deformation and remaining dimensions calculated for the flat drop onto the valve side

Dimension [mm]	Drop test at temperature					
	-40 °C			RT		
	1.2 m	9.0 m	1 m bar	1.2 m	9.0 m	1 m bar
L1x	n.m.	2426	-	n.m.	2421	-
Ly	n.m.	1142	-	n.m.	1150	-
L2x	n.m.	2425	-	n.m.	2420	-
Depth of bar penetration (p1)	-	-	41	-	-	44
Depth of bar penetration (p2)	-	-	23	-	-	29

n.m. = not measurable

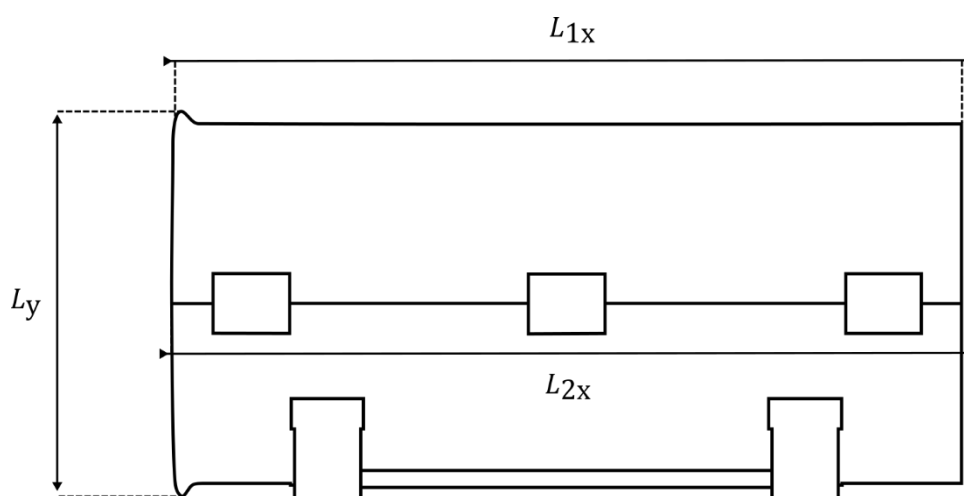


Figure 65: Measured distances in sequence 3

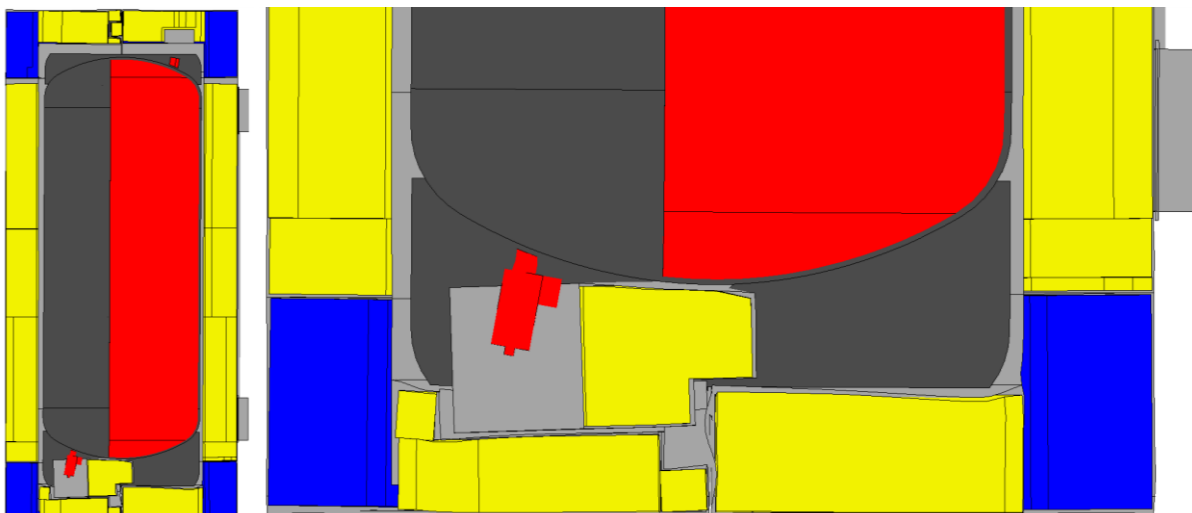


Figure 66: Deformed structure after the 1.2 m free drop flat onto the valve side

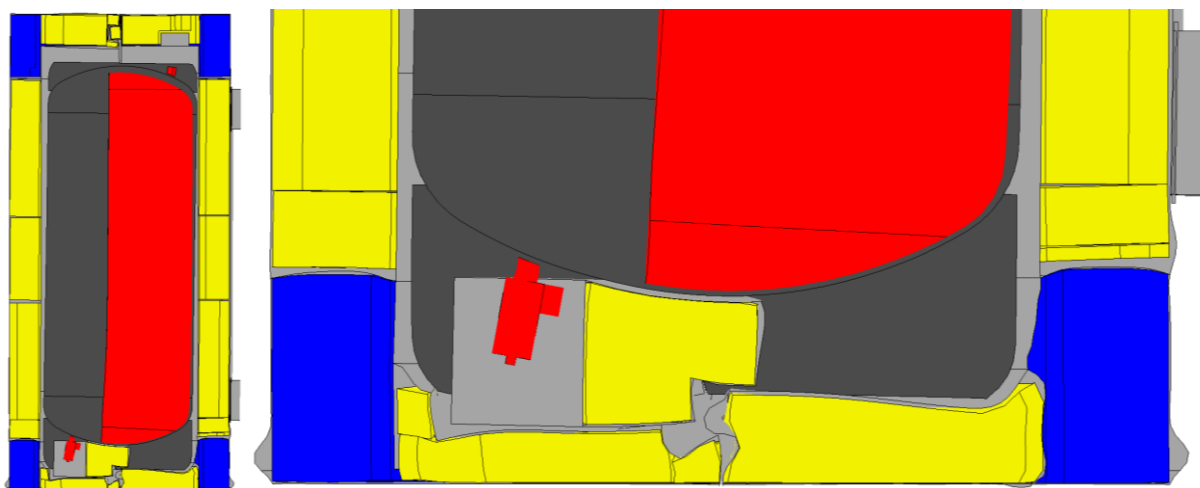


Figure 67: Deformed structure after the 9.0 m drop flat onto the valve side

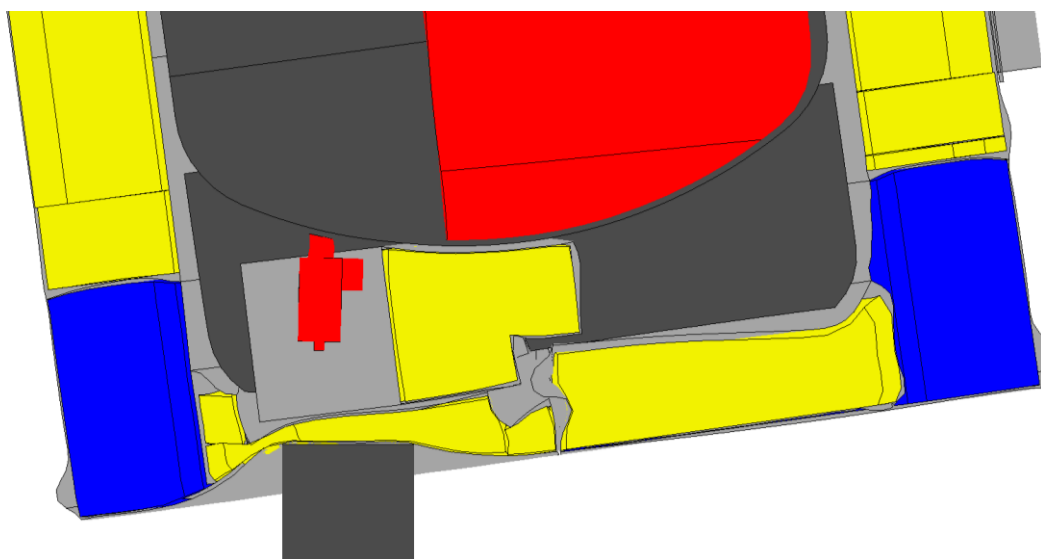


Figure 68: Deformed structure after the test sequence flat onto the valve side

2.2.1.5.1.5.3.2.2 Decelerations at -40 °C and RT

For the flat drop onto the valve side at -40 °C and RT, the resulting low-pass filtered decelerations in the plug area are shown in Figure 69 and Figure 70 for a cut-off frequency of 20 Hz and 584 Hz, respectively. At a cut-off frequency of 20 Hz, both deceleration curves differ by less than 5 % in height. The discrepancy at the beginning between the two simulations refers to the simulation procedure and the applied SAE filter itself. This is explained in more detail in Appendix 2.2.1.3 (Structural Analysis of the DN30 Package under NCT and HAC). The impact of the stiffer material behavior becomes only visible at a higher cut-off frequency of 584 Hz.

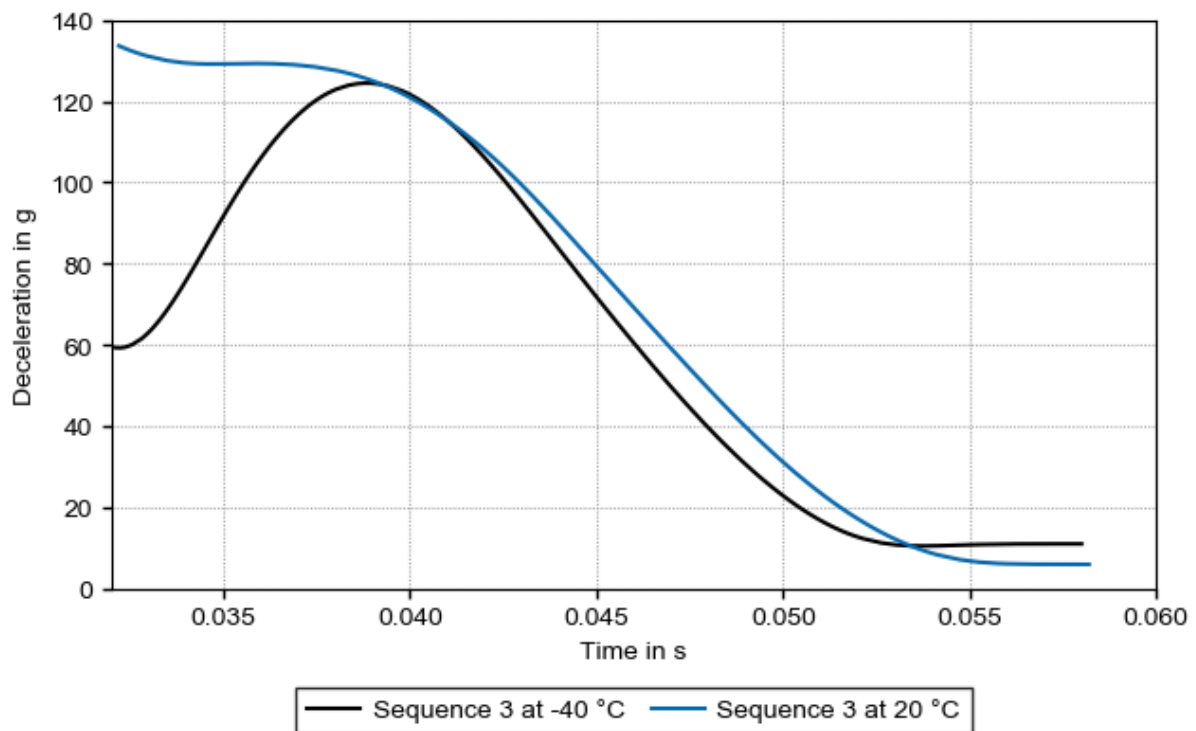


Figure 69: Deceleration in the plug area during 9.0 m drop in Sequence 3 at -40 °C compared to sequence 3 at 20 °C – low-pass filtered (SAE, 20 Hz cut-off)

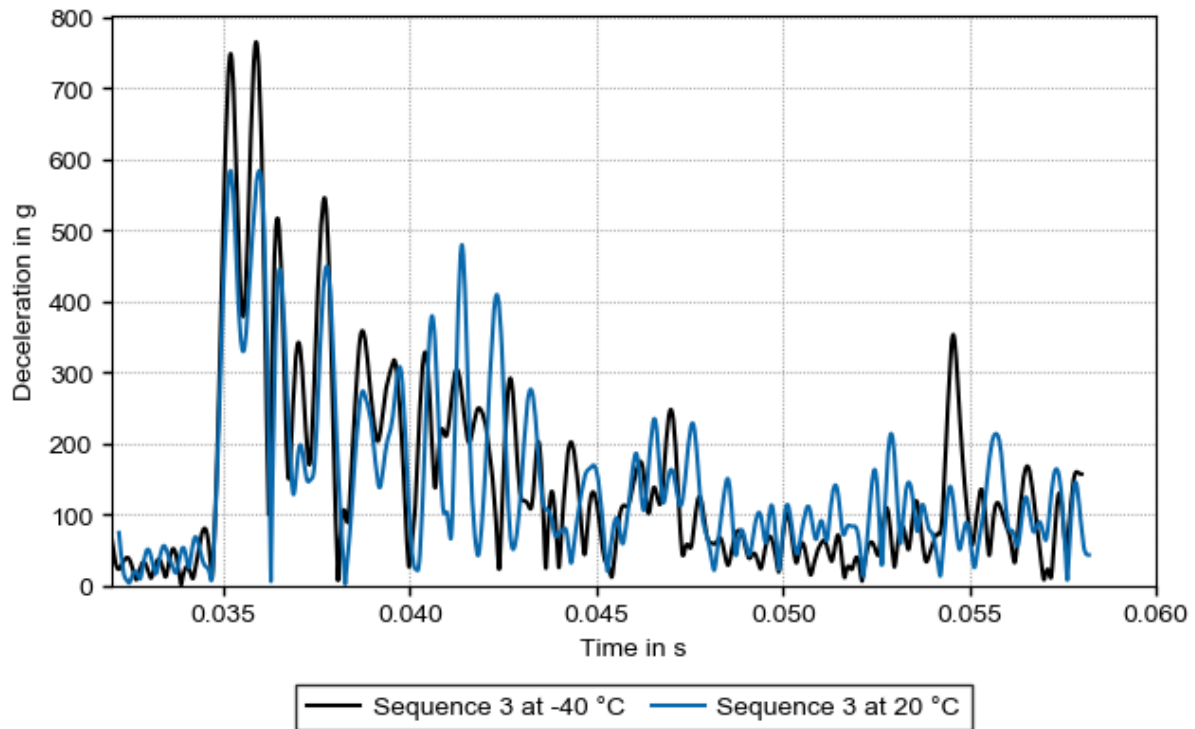


Figure 70: Deceleration in the plug area during 9.0 m drop in Sequence 3 at -40 °C compared to sequence 3 at 20 °C – low-pass filtered (SAE, 584 Hz cut-off)

2.2.1.5.1.5.3.3 Results of drop tests

The drop test sequence flat onto the valve side is documented as sequence No. 3 in Appendix 2.2.1.2 (Drop Test Reports).

- Drop No. 3.1 1.2 m flat drop test onto the valve side
- Drop No. 3.2 9 m flat drop test onto the valve side
- Drop No. 3.3 1 m drop onto a bar onto the valve side

2.2.1.5.1.5.3.3.1 Deformations at RT

The 1.2 m drop causes very small deformations of the DN30 package and there is only a slight buckling of the outer shell (see Figure 71).

The 9.0 m drop causes larger deformation of the DN30 package. The buckling of the outer shell increases, but still without any cracks in the outer surface or outer welds (see Figure 72).

The drop onto the bar does not completely penetrate the steel shell of the DN30 package, but a crack of the outer shell is visible at the impact point (see Figure 73).



Figure 71: Sequence 3 - Deformation after the 1.2 m drop



Figure 72: Sequence 3 - Deformation after the 9.0 m drop



Figure 73: Sequence 3 - Deformation after the drop onto a bar from 1.0 m

There are also deformations and cracks visible at the inner steel parts, especially at the front plate, which is in contact with the skirt of the 30B cylinder. The rotation preventing devices are deformed and damaged, but the rotation of the 30B cylinder was still prevented (see Figure 74).



Figure 74: Sequence 3 – Deformation of the bottom half, inner shell

2.2.1.5.1.5.3.3.2 Summary of the drop test results for sequence 3

- The leakage rate after the drop test sequence 3 is $Q_{st} = 4.91 \text{ E-09 Pa} \cdot \text{m}^3/\text{s}$.
- All closure systems are intact.
- The DN30 PSP could be opened, but cutting the front plate of the DN30 PSP was required.
- Operating the closure system and lifting the top half off the bottom half is possible.
- There was no contact between the valve and any other part of the DN30 PSP or 30B cylinder except for its initial point of contact (the thread).
- There was no contact between the plug and any other part of the DN30 PSP or 30B cylinder except for its initial point of contact (the thread).
- The valve protecting device can still be operated (rotated) and the hinges are intact.
- Removal of the 30B cylinder from the bottom half is possible without further damaging the DN30 PSP.
- Loading of a 30B cylinder into the DN30 PSP is still possible.

2.2.1.5.1.5.3.4 Evaluation of the FEM analysis vs. real drop tests

2.2.1.5.1.5.3.4.1 Deformations at RT

In Table 43, the measured deformations and remaining dimensions are compared to the calculated values. The definition of these measurement points is shown in Figure 65.

Table 43: Deformations and remaining dimensions measured for the flat drop onto the valve side (ambient temperature) and comparison with calculated values

Dimension [mm]	Drop								
	1.2 m			9.0 m			1 m bar		
	CV	MV	D %	CV	MV	D %	CV	MV	D %
Largest fold (L1x)	-	n.m.	-	2421	2410	1	-	-	-
Largest fold (L1y)	-	n.m.	-	1150	1178	-2	-	-	-
Gap between top and bottom half (L2x)	-	n.m.	-	2420	2415	<1	-	-	-
Depth of bar penetration (p1)	-	-	-	-	-	-	29	32	-8
Depth of bar penetration (p2)	-	-	-	-	-	-	44	45	-1

CV = calculated values MV = measured values

D % = deviation of measured values from calculated values in %

n.m. = not measurable

The exact measurement error in the experiment is unknown, but in the range of 10% because of the applied measurement technique. The resulting errors between measurement and simulation do not exceed 2% in all cases, except for the depth of bar penetration. Hence, the simulation reproduces the behavior observed in the experiment very well.

The depth of bar penetration p_2 is maximally 8 % smaller in the simulation than in the experiment. This is probably attributable to the crack that occurred around the bar imprint, but the resulting error is nevertheless acceptable.

A qualitative comparison of the deformations after the 9.0 m drop between the simulation and the experiment is shown in Figure 75.

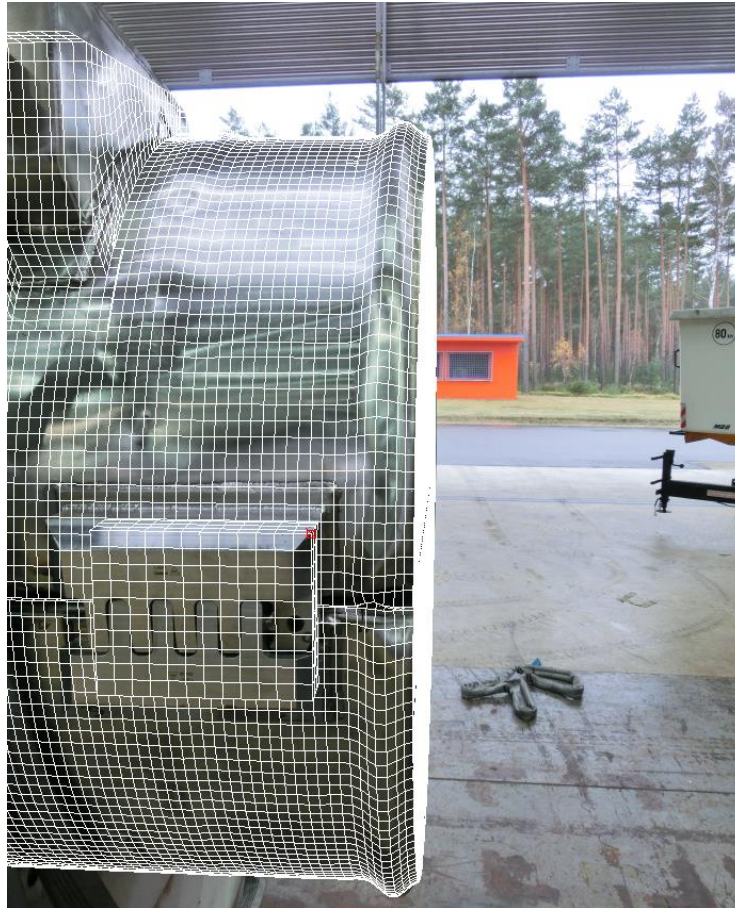


Figure 75: Qualitative comparison of the deformations in simulation and experiment

2.2.1.5.1.5.3.4.2 Decelerations at RT

The resulting low-pass filtered decelerations in the plug area for the simulation and the experiment are shown in Figure 76 and Figure 77 for a cut-off frequency of 20 Hz and 584 Hz, respectively.

At a cut-off frequency of 20 Hz, the deceleration of the 30B cylinder in the simulation is very similar to the experiment. With regard to the maximum decelerations, the two curves differ by less than 3 %. However, at higher cut-off frequencies the shape of the deceleration curves shows more and more fluctuations in the simulation so that the discrepancy between the simulation and the experiment increases. The undefined position of the 30B cylinder at the time of impact may lead to non-deterministic interactions of the 30B cylinder with the DN30 PSP and thus makes it very challenging to accurately predict the deceleration peaks.

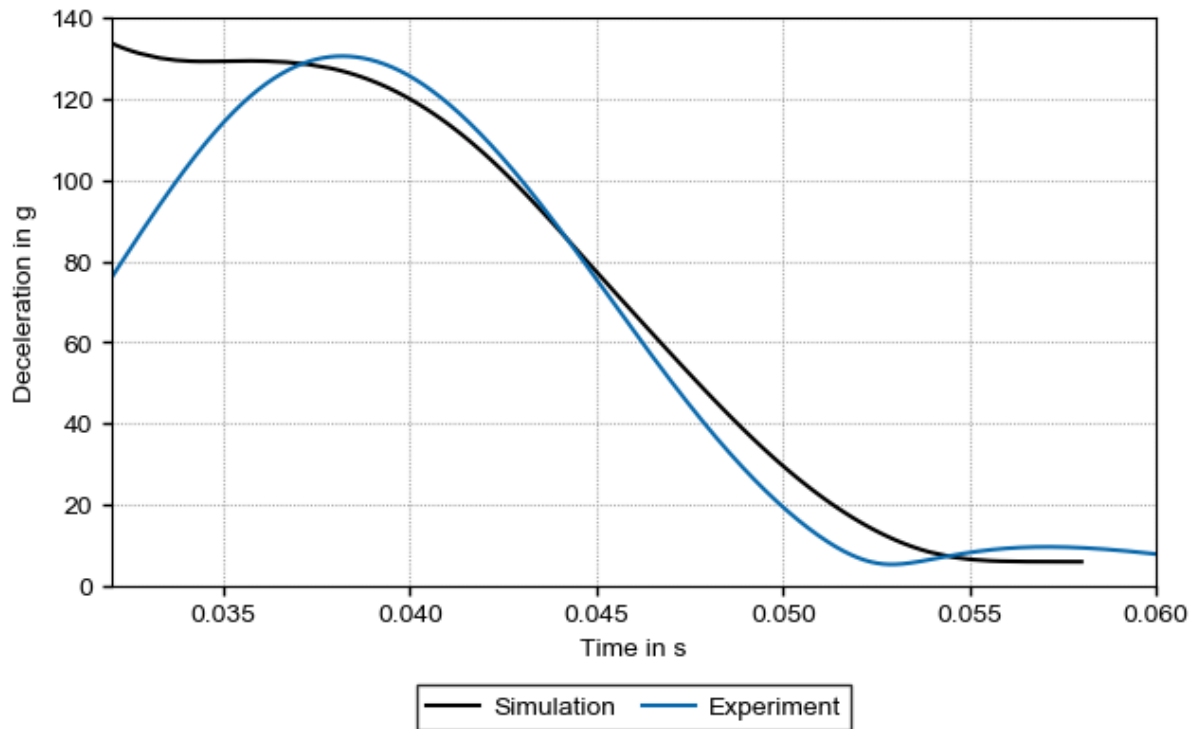


Figure 76: Comparison of simulation and experiment – deceleration in the plug area during 9.0 m drop in sequence 3 – low-pass filtered (SAE, 20 Hz cut-off)

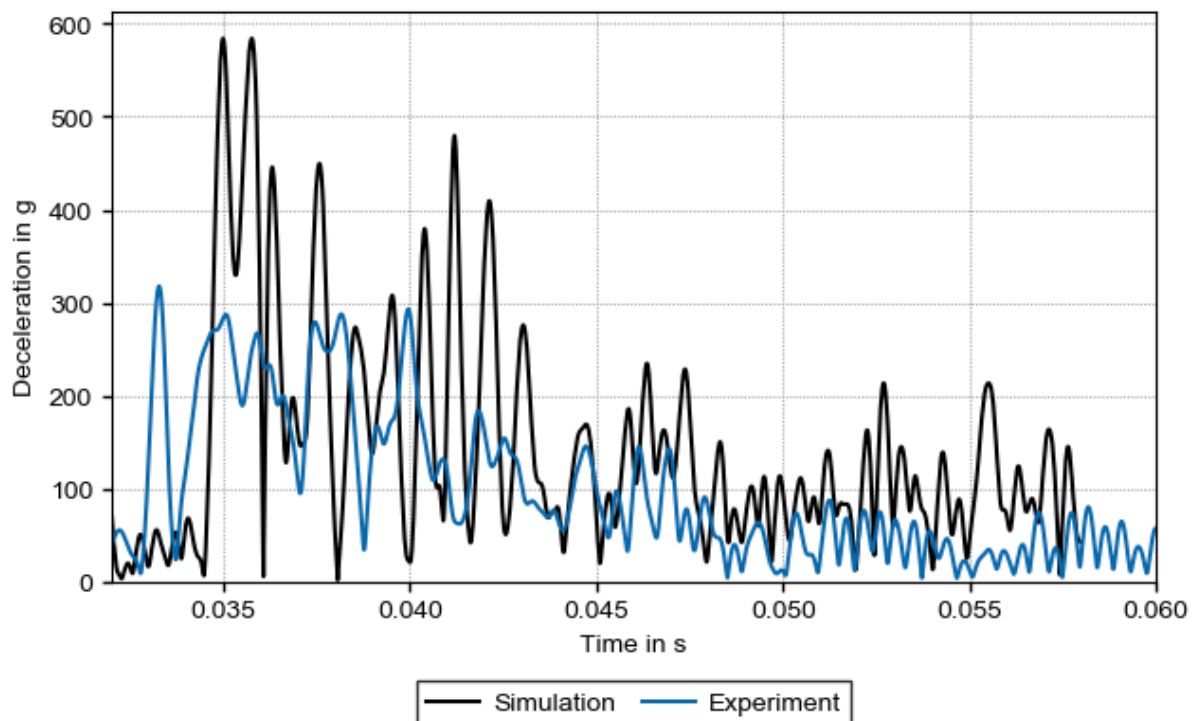


Figure 77: Comparison of simulation and experiment – deceleration in the plug area during 9.0 m drop in sequence 3 – low-pass filtered (SAE, 584 Hz cut-off)

2.2.1.5.1.5.4 Flat drop onto the plug side

2.2.1.5.1.5.4.1 General considerations

The corner drop onto the plug side as described in section 2.2.1.5.1.5.2 causes maximal deformations in the plug area. In contrast to that, maximal accelerations and hence maximal forces at the plug are expected during the flat drop onto the plug side. The design has to ensure that after the tests simulating HAC:

- There is no contact between plug and any part of the DN30 PSP or any other part of the 30B cylinder except for its initial point of contact (the thread).
- The leakage rate of the containment does not exceed the limit specified in section 2.2.3.

The drop orientation is flat onto the plug side for the 1.2 m drop and the 9 m drop. For the drop from 1 m height onto the bar, the bar is positioned so that the vertical line from the center of gravity points through the center of the plug and the center of the top of the bar.

2.2.1.5.1.5.4.2 FEM analysis

As investigated with previous simulations, the response during the drop onto the valve side and the drop onto the plug side is very similar, which is attributed to the similar design of the valve and plug side of the DN30 PSP. The shell thickness on the valve and the plug side of the outer and the inner shell is identical, respectively. In addition, a similar amount of foam of the same type fills the space between the outer and the inner shell.

Naturally, the decelerations of the 30B cylinder are comparable in both drop test sequences. The experimentally measured decelerations during Sequence 3 did not lead to a failure of the containment system. Therefore, this is expected for the flat drop onto the plug side as well, especially because the mass of the plug is lower compared to the mass of the valve.

For these reasons, further analysis of the flat drop onto the plug side with the developed FEM model of the DN30 PSP is not carried out.

2.2.1.5.1.5.4.3 Results of drop tests

With respect to the minor differences in the results of the drop test sequence flat onto the valve side (section 2.2.1.5.1.5.3) to previously obtained results of the flat drop onto the plug side, the drop test flat onto the plug side was not part of the drop test program.

2.2.1.5.1.5.5 Flat drop onto the closure system – drop test sequence 4

2.2.1.5.1.5.5.1 General considerations

During the drop test sequence flat onto the closure system, high tensile and transversal loads are expected. During the 9 m drop test, the closure systems on both sides of the DN30 PSP will experience tensile loads as forces caused by the deceleration of the 30B cylinder act onto the inside of the top and lower shell comparable to an inner pressure. During the 1 m drop test onto the bar impacting the center closure system there are high transversal loads on the closure system.

Furthermore, during the flat drop test sequence onto the closure system maximal forces are expected at the rotation preventing device, because in this orientation the moment caused by the eccentric loading of the 30B cylinder is maximal.

Hence, the design has to ensure that after the tests simulating HAC:

- There is no contact between valve and any part of the DN30 PSP or any other part of the 30B cylinder except for its initial point of contact (the thread).
- The extent of the rotation of the 30B cylinder relative to the DN30 PSP does not affect the function of the valve protecting device or the plug protecting device.
- The leakage rate of the containment does not exceed the limit specified in section 2.2.3.

For the 1.2 m drop as well as the 9 m drop, the drop orientation is flat onto three devices of the closure system. For the drop from 1 m height onto the bar, the bar is positioned so that the vertical line from the center of the central closure device is above the center of the top of the bar.

2.2.1.5.1.5.5.2 FEM analysis

2.2.1.5.1.5.5.2.1 *FEM analysis before the drop tests*

Two different inclinations of the DN30 package to the drop target were analyzed. First, an orientation was investigated where the line across the flange of the DN30 PSP is perpendicular to the drop target. In a second analysis, the line across the flange of the DN30 PSP is inclined by 13.9° so that the impact is predominantly onto the top half of the DN30 PSP. The latter of the two investigated drop orientations has been found to be more damaging and is therefore chosen for drop test sequence 4 (see the initial state of sequence 4 in Figure 78).

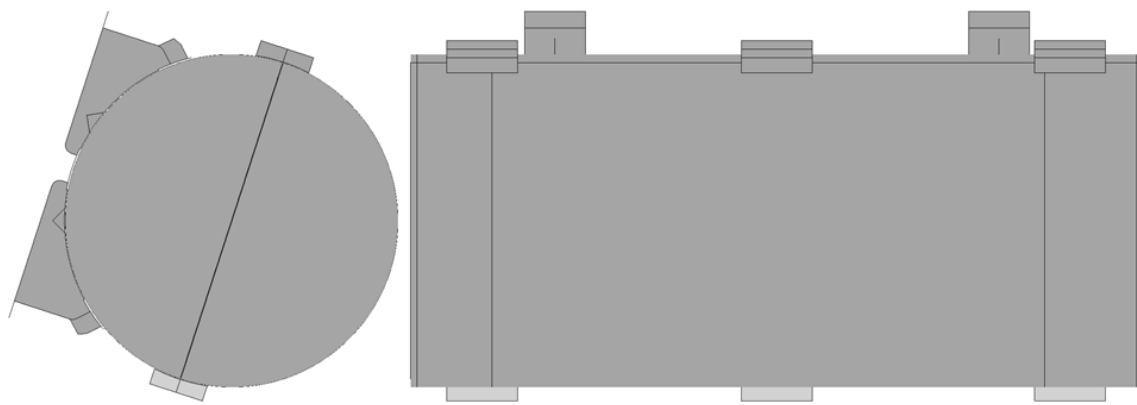


Figure 78: Undeformed initial state of the DN30 package for sequence 4

2.2.1.5.1.5.5.2.2 Deformations at RT

After the 1.2 m drop, the three closure devices on the impact side are deformed and pushed into the outer shell of the DN30 PSP. Only small deformations below 3 % are visible at the rotation preventing devices inside the DN30 PSP. Both rotation preventing devices still work properly and are in the middle of the hole of the 30B cylinder skirt. There are no deformations of the inner steel shell and the valve protecting device. Furthermore, there are no cracks in either the outer shell or inner shell of the DN30 PSP.

After the 9.0 m drop, the three closure devices are pushed inside the outer shell of the DN30 PSP so that the foam is compressed in those areas. There are deformations of up to 10 % at the cylinder skirt at the feedthrough where the lower rotation preventing device is engaged. The rest of the inner steel parts is not deformed that much. The valve and plug protecting devices undergo deformations of up to 6 % equivalent plastic strain.

The deformed structure after the drop onto the bar is basically the same as after the 9.0 m drop. Only directly at the impact zone of the bar some differences are visible because the corresponding closure device is further pushed into the outer shell. Consequently, the foam is being further compressed as well. However, neither the inner steel parts nor the 30B cylinder undergo further deformation compared to the 9.0 m drop.

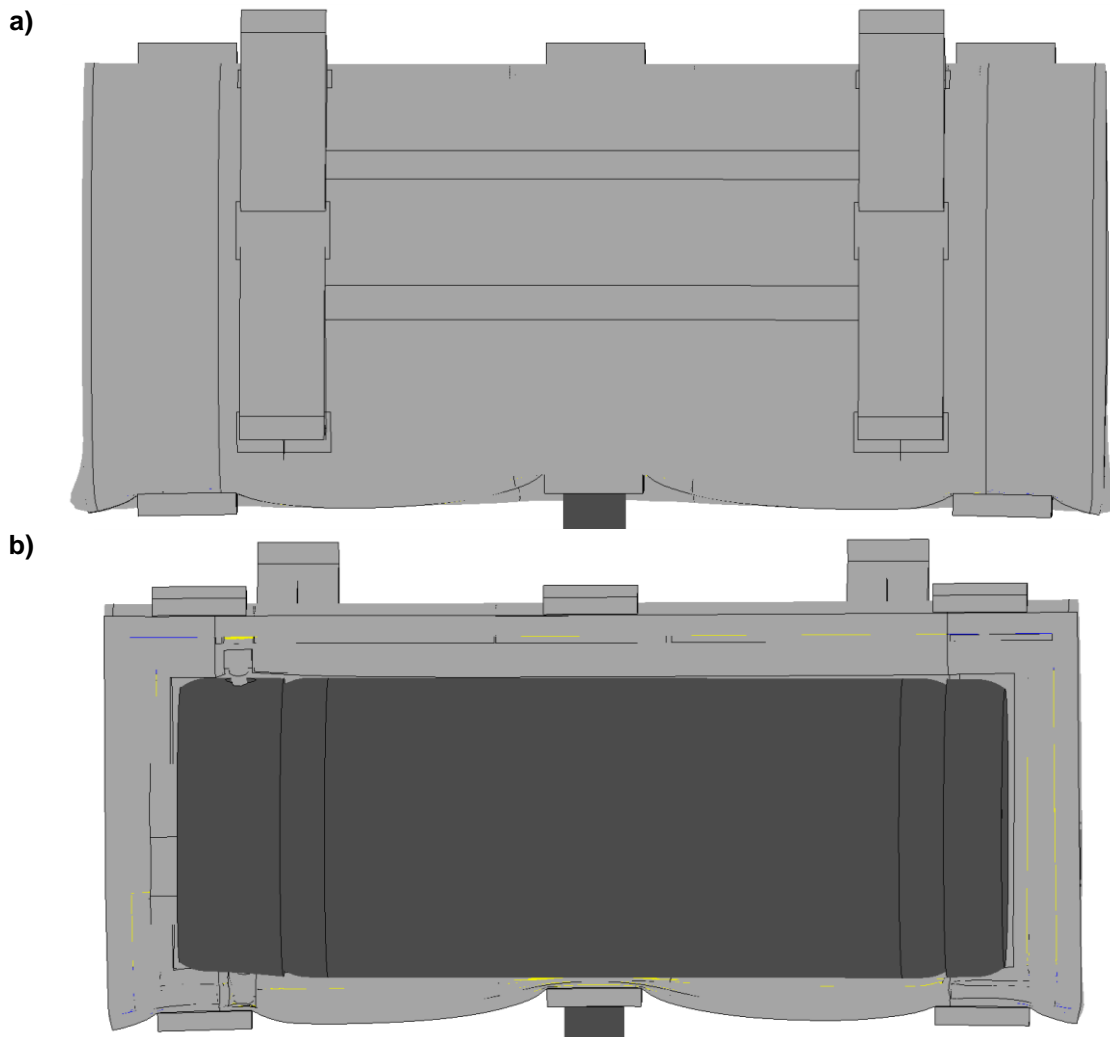


Figure 79: Deformed structure after the test sequence onto the closure system: a) bottom half b) top half (section view)

2.2.1.5.1.5.5.3 Results of drop tests

The drop test sequence flat onto the closure system is documented as sequence No. 4 in Appendix 2.2.1.2 (Drop Test Reports).

- Drop No. 4.1 1.2 m drop flat onto the closure system
- Drop No. 4.2 9 m drop flat onto the closure system
- Drop No. 4.3 1 m drop flat onto the closure system

2.2.1.5.1.5.5.3.1 Deformations at RT

The 1.2 m drop causes small deformations; the three closure systems are pushed inside the outer shell of the DN30 PSP so that the foam is noticeably compressed in those regions. During the 9.0 m drop, the deformations are increased. The penetration of the closure devices in the outer shell continues, but still without any cracks in the outer surface or outer welding seams.



Figure 80: Sequence 4 - Deformation after the 1.2 m drop



Figure 81: Sequence 4 - Deformation after the 9.0 m drop

The drop onto the bar does not damage the closure device itself. The bar impact did not push the closure device into the outer shell entirely. Instead, the closure device buckles due to the rotational degree of freedom about the pin axis.



Figure 82: Sequence 4 - Deformation after the drop onto a bar from 1.0 m

No deformations are visible at the inner shell of the DN30 PSP. The rotation preventing devices are not deformed so that their function is preserved and any rotation of the 30B cylinder is prevented.

2.2.1.5.1.5.5.3.2 Summary of the drop test results for sequence 4

- The leakage rate after the drop test sequence 4 is $Q_{st} = 7.09E-08 \text{ Pa} \cdot \text{m}^3/\text{s}$.
- All closure systems are intact.
- The DN30 PSP could be opened, but small cuts at the DN30 PSP were required.
- Operating the closure system and lifting the top half off the bottom half is still possible.
- There was no contact between the valve and any other part of the DN30 PSP or 30B cylinder except for its initial point of contact (the thread).
- There was no contact between the plug and any other part of the DN30 PSP or 30B cylinder except for its initial point of contact (the thread).
- The valve protecting device can still be operated (rotated) and the hinges are intact.
- Removal of the 30B cylinder from the bottom half is possible without further damaging the DN30 PSP.
- Loading of a 30B cylinder into the DN30 PSP is still possible.

2.2.1.5.1.5.5.4 Evaluation of the FEM analysis vs. real drop tests

2.2.1.5.1.5.5.4.1 Deformations at RT

The measured deformations and remaining dimensions are compared to the calculated values in Table 39. The numbering of the measurement points is described in Figure 83.

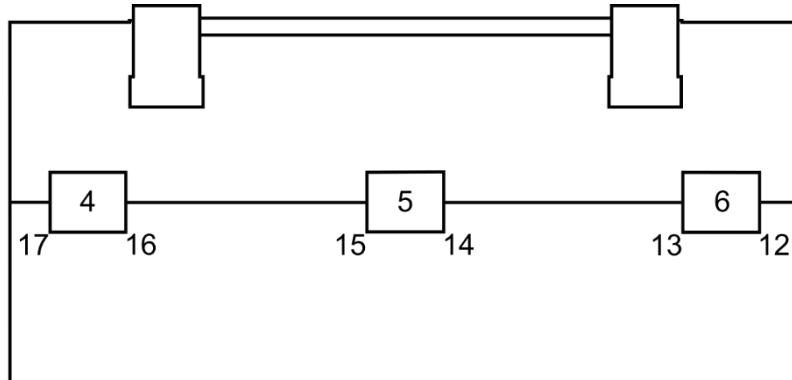


Figure 83: Numbering of the measured depths of impression at the welding seams of the closure devices for the 1.2 m and 9.0 m drop in sequence 4

Table 44: Measured impressions for the flat drop onto the closure system at RT and comparison to calculated values

Dimension [mm]	Drop								
	1.2 m			9.0 m			1 m bar		
	CV	MV	D %	CV	MV	D %	CV	MV	D %
Closure device 4 - 17	25	20	23	45	47	-5	44	44	0
Closure device 4 - 16	23	19	19	46	45	2	45	44	1
Closure device 5 - 15	19	19	-2	48	42	13	67	46	46
Closure device 5 - 14	18	19	-4	48	46	4	68	44	54
Closure device 6 - 13	22	19	18	47	48	-3	45	44	3
Closure device 6 - 12	23	18	27	44	46	-4	43	42	3

CV = calculated values MV = measured values

D % = deviation of measured values from calculated values in %

The applied measurement technique in the experiment was simulated based on photographs to obtain the values in Table 44. However, in the case of closure device 5 the chosen nodes that are necessary for the rebuild are quite subjective. Except for measurement point 15 of closure device 5, the resulting errors for the 9.0 m drop are well below the measurement error of 10 %. Hence, the negligence of the rotational degree of freedom about the pin axis of the closure devices is an acceptable simplification not only for the 1.2 m drop but for the 9.0 m drop as well. Overall, the deformation behavior for drop I of Sequence 4 is accurately reproduced with the developed FEM model.

A qualitative comparison of the deformations after the 9.0 m drop between the simulation and the experiment is shown in Figure 84.



Figure 84: Qualitative comparison of the deformations in simulation and experiment

For the drop onto the bar, the depths of impressions at closure device 4 and 6 are basically identical to the ones after the 9.0 m drop because the impact zone of the bar is too localized to have any noticeable influence in these areas. Consequently, the resulting errors are still small and remain below 3 %. In contrast to that, the depths of impression at closure device 5 are about 50% smaller in the experiment than in the simulation. As expected, the rotational degree of freedom about the pin axis of the closure devices has a measurable influence on the results. If the impact zone is localized at one single closure device, the exact deformation behavior cannot be predicted with this FEM model.

2.2.1.5.1.5.5.4.2 Decelerations at RT

The low-pass filtered decelerations in the valve area for the simulation and the experiment are shown in Figure 85 and Figure 86 for a cut-off frequency of 20 Hz and 584 Hz, respectively.

At a cut-off frequency of 20 Hz, the deceleration curve for the 30B cylinder is in good agreement with the experiment, but the response of the FEM model seems to be too soft as the deceleration peak is about 18 % lower than in the experiment. At a cut-off frequency of 584 Hz the signal becomes noisier in the simulation than in the experiment, but the general shape is still in very good agreement with the experiment.

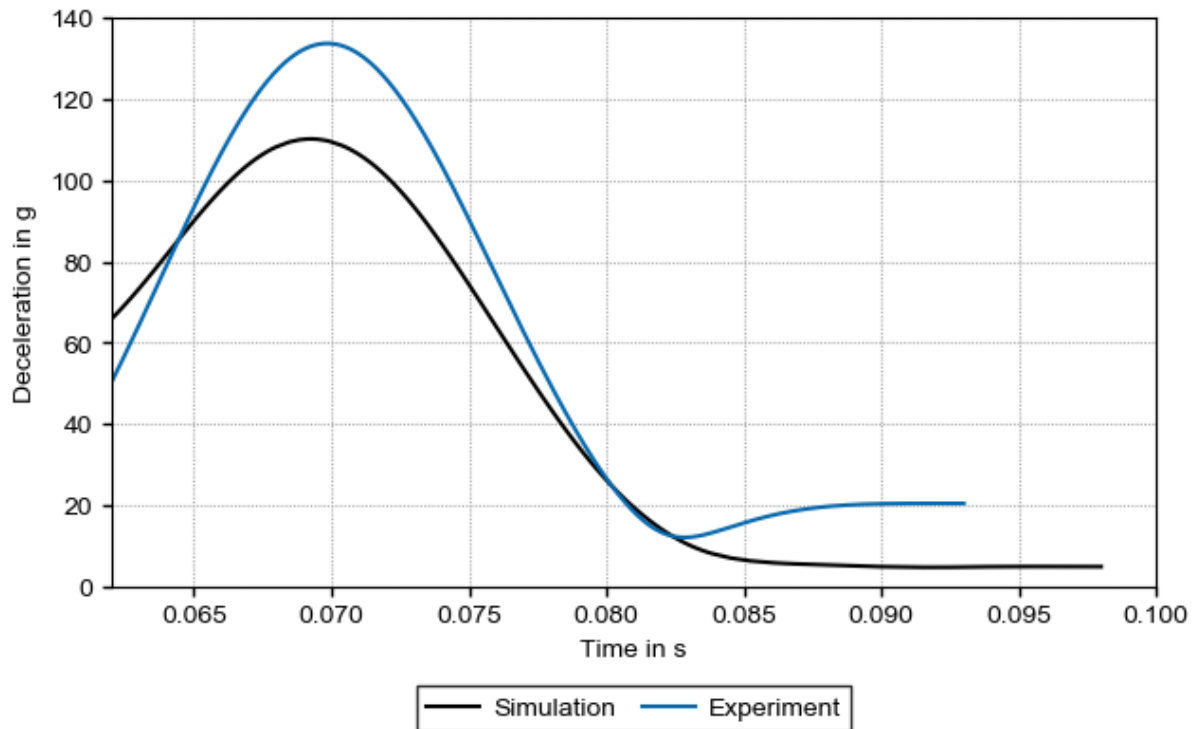


Figure 85: Comparison of simulation and experiment – deceleration in the valve area during drop I in sequence 4 – low-pass filtered (SAE, 20 Hz cut-off)

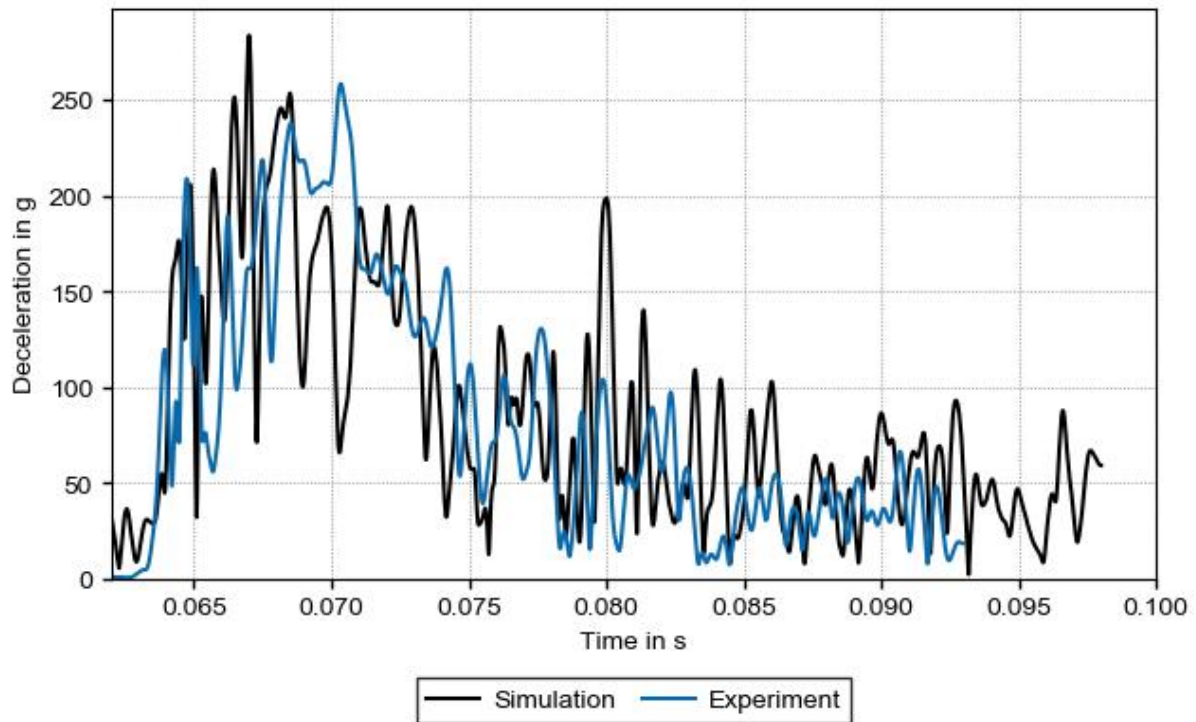


Figure 86: Comparison of simulation and experiment – deceleration in the valve area during drop I in sequence 4 – low-pass filtered (SAE, 584 Hz cut-off)

2.2.1.5.1.5.6 Flat drop onto the top

2.2.1.5.1.5.6.1 General considerations

For the drop test sequence flat onto the top of the DN30 PSP, higher radial deformations are expected than for the flat drop onto the closure system. These deformations are relevant for the determination of the increase in the maximal dose rate after the tests simulating NCT (see section 2.2.4). Additionally, the simulation provides information about the extent of the reduction of the thickness of the DN30 PSP for the thermal calculations in section 2.1.3.2.

The design has to ensure that after the tests simulating HAC:

- There is no contact between valve and any part of the DN30 PSP or any other part of the 30B cylinder except for its initial point of contact (the thread).
- There is no contact between plug and any part of the DN30 PSP or any other part of the 30B cylinder except for its initial point of contact (the thread).
- The extent of the reduction of the thickness of the DN30 PSP after NCT is such that the increase of the dose rate does not exceed the limit specified in section 2.2.4.
- The extent of the reduction of the thickness of the DN30 PSP after HAC is such that the thermal protection properties of the shell DN30 PSP are still sufficient to limit the temperature increase in the thermal tests to the limits specified in section 2.2.1.5.3.1.

The drop orientation is flat onto the top of the DN30 PSP for the 1.2 m drop and the 9 m drop. For the drop from 1 m height onto the bar, the orientation of the DN30 package is flat and the impact of the bar is at the center of the top of the DN30 PSP.

2.2.1.5.1.5.6.2 FEM analysis

2.2.1.5.1.5.6.2.1 *Deformations at RT*

After the 1.2 m drop, noticeable deformations occur only at the impact zone (see Figure 88). The foam is compressed and the separation plate between the two different foam types in the top half of the DN30 PSP buckles. In addition, the valve and the plug side of the outer shell are deformed with plastic strains up to 12 %. The rotation preventing devices, the valve and the plug protecting device do not undergo any deformations. In addition, there is no contact with the valve or the plug during the simulation.

After the 9.0 m drop, the deformations of the plug and the valve side are twice as large as after the free drop test. With regard to the increase in the drop height from 1.2 m to 9 m, the increase in the deformations is small. This is due to the large area of impact. However, in contrast to the 1.2 m free drop test, the inner shell of the DN30 PSP now undergoes small deformations of up to 7 %. The foam and the outer shell of the top half of the DN30 PSP absorb most of the kinetic energy. For that reason, the rotation preventing devices as well as the plug and the valve protecting device undergo deformation of below 3 % so that their function is preserved.

The resulting deformed structure with the deepest penetration of the bar is shown in Figure 89. During the drop from 1 m onto the bar, only the impact zone of the bar is further deformed. Even though the kinetic energy is applied locally, the resulting plastic deformations are below 12 % at the bar impact zone. This is due to the soft response of the DN30 PSP in that area, so that most of the kinetic energy results only in elastic deformations. Therefore, cracks in the outer shell caused by this kind of bar impact are not expected.

The measured deformations are summarized in Table 45. The definition of the corresponding measurement points is shown in Figure 87. Table 45 also includes the time-averaged change of the distance between the inner and outer shell at the center of the DN30 PSP. This change of distance, which amounts to a reduction of 4 mm, is relevant for the determination of the increase in the maximal dose rate after the tests simulating NCT.

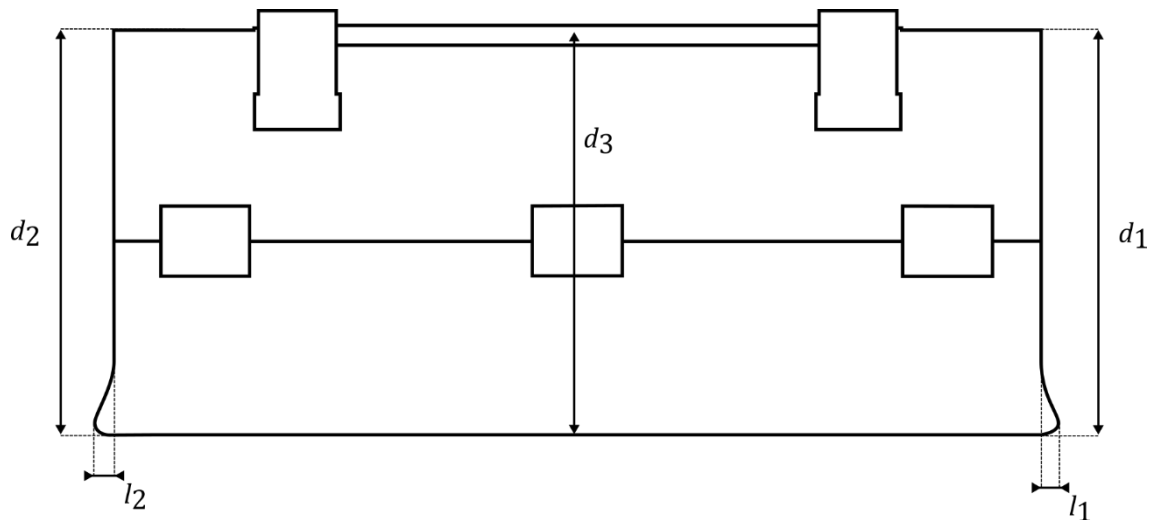


Figure 87: Measured distances for the free drop test and drop I of sequence 8

Table 45: Deformations and remaining dimensions calculated for the flat drop onto the top

Dimension [mm]	1.2 m drop	9.0 m drop	Drop onto the bar
Deformations at the valve corner – l1	18	42	-
Deformations at the valve corner – Ød1	-8	-43	-
Deformations at the plug corner– l2	18	41	-
Deformations at the plug corner – Ød2	-9	-40	-
Deformations at the center – Ød3	-1	-15	-
Distance between inner and outer shell at the center	-4	-	
Depth	-	-	55

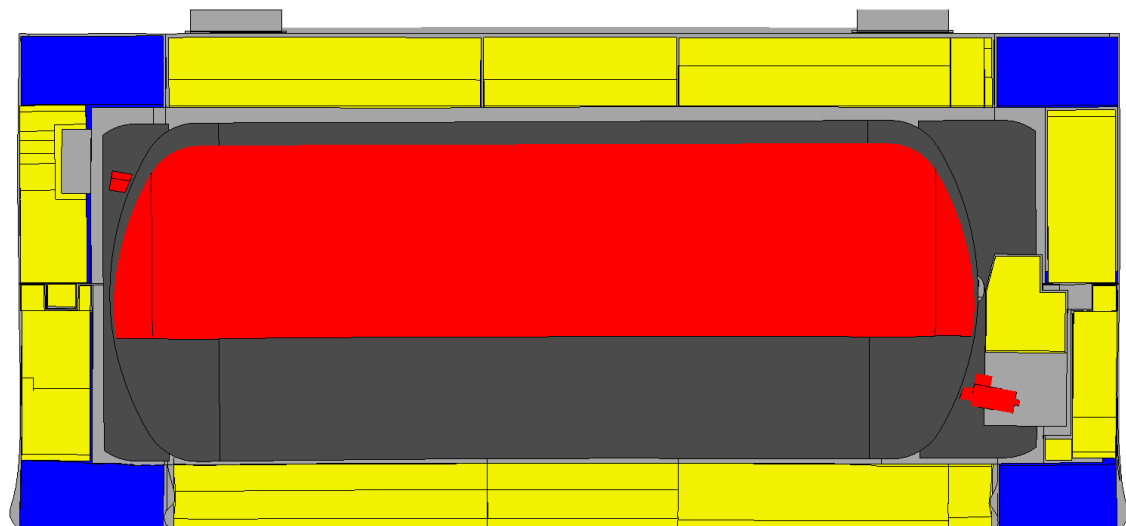


Figure 88: Deformed structure after the 1.2 m free drop flat onto the top

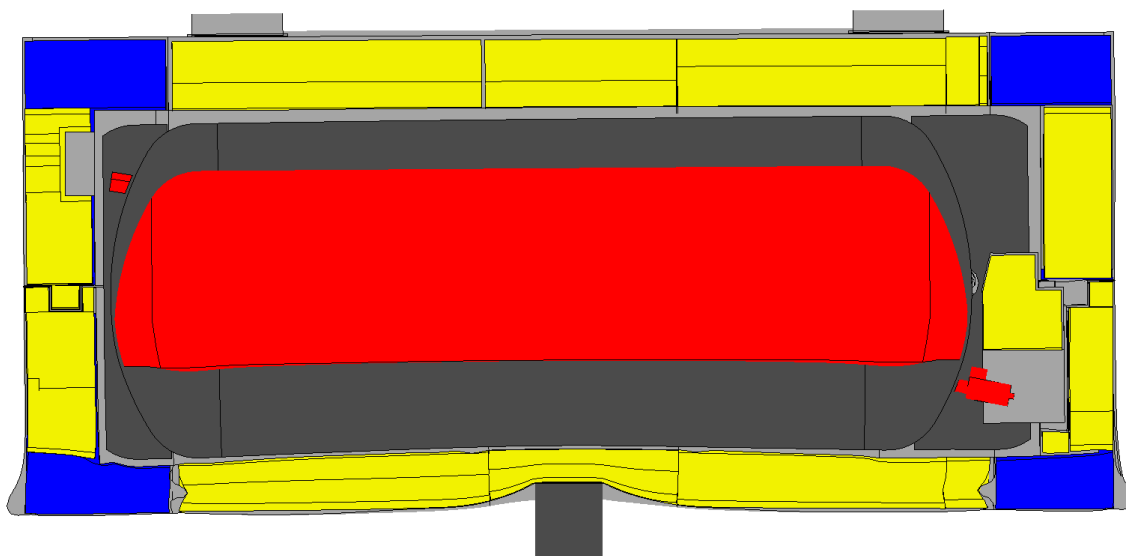


Figure 89: Deformed structure after the drop test sequence flat onto the top

2.2.1.5.1.5.6.2.2 Decelerations at RT

The low-pass filtered decelerations in the valve area for the simulation and the experiment are shown in Figure 90 and Figure 91 for a cut-off frequency of 20 Hz and 584 Hz, respectively.

At a cut-off frequency of 20 Hz, the deceleration is on the same level when compared to the deceleration during the 9 m drop of Sequence 3. At a cut-off frequency of 584 Hz, very high peaks become visible. These peaks result from the non-deterministic interaction between the 30B cylinder and the content. Since the assumption was made that the content is not bonded to the inside of the 30B cylinder pressure envelope, the content begins to move inside the 30B cylinder after the impact of the 30B cylinder on the inner shell of the DN30 PSP during the 1.2 m free drop test. This modelling assumption results in interactions between the 30B cylinder and the content that produce very high peaks. Accordingly, the high deceleration peaks are not expected to occur under real conditions. Therefore, a far better comparison of the level of deceleration with other sequences is achieved at a cut-off frequency of 20 Hz.

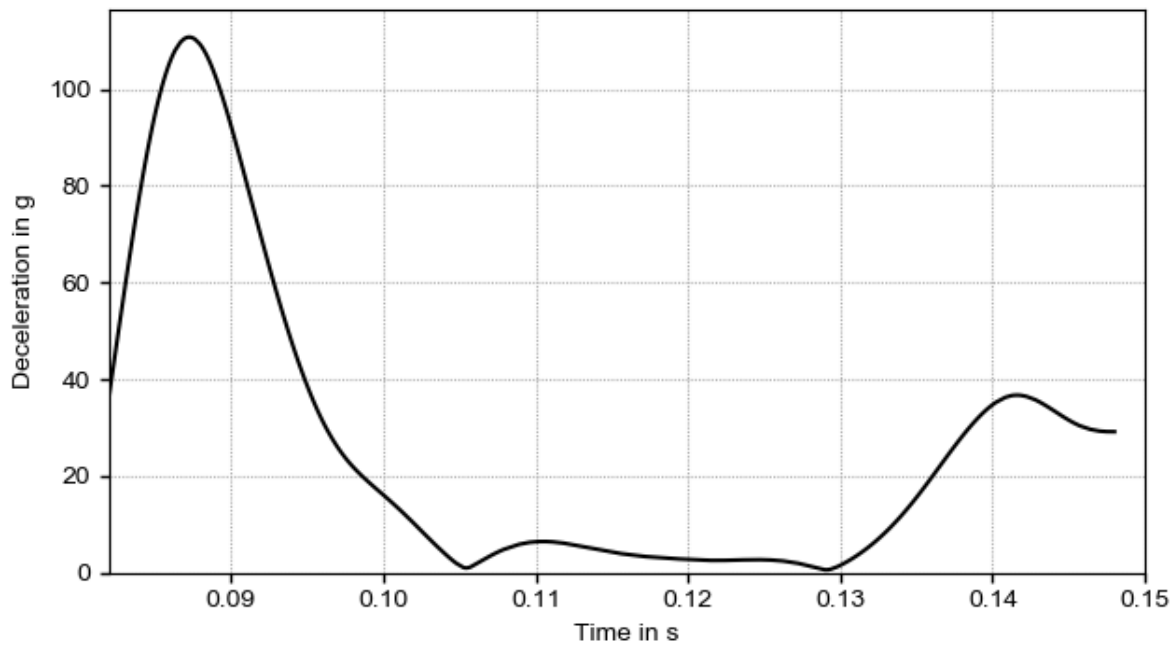


Figure 90: Absolute values of the deceleration in the valve area during the 9.0 m drop test in sequence 8 – low-pass filtered (Butterworth, 584 Hz cut-off)

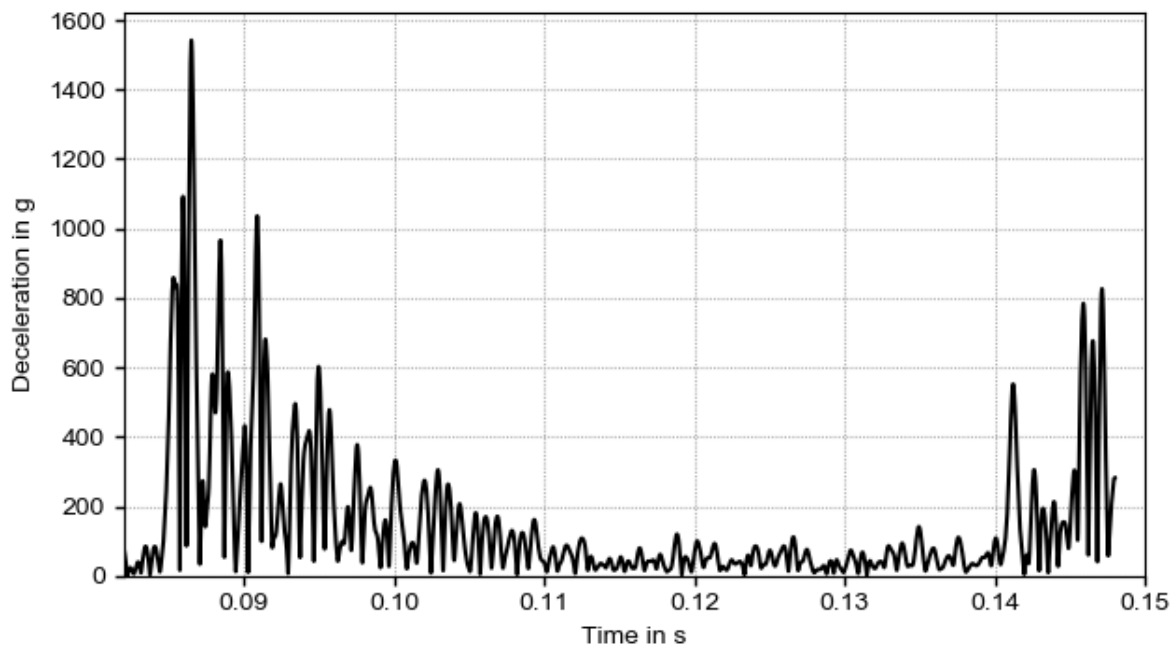


Figure 91: Absolute values of the deceleration in the valve area during the 9.0 m drop test in sequence 8 – low-pass filtered (Butterworth, 584 Hz cut-off)

2.2.1.5.1.5.6.3 Results of drop tests

The drop tests flat onto the top of the DN30 package are covered by the drop tests onto the closure system:

- The drop tests onto the closure system are similar to the drop test flat onto the top line.
- The FEM analysis of the drop tests onto the closure system provided a good benchmark for the analysis of the flat drop onto the top line.
- The closure line is much more vulnerable to loads from HAC due to the closure system connecting the top and bottom half.
- The deformation of the shell of the DN30 package during NCT is much smaller than permissible for meeting the requirement concerning dose rate increase (see section 2.2.4.7.5). Hence, a verification of the results of the FEM analysis can be omitted.

Hence, a real drop test flat onto the topline was not part of the drop test program.

2.2.1.5.1.5.7 Slap-down drop onto the feet – drop test sequence 5

2.2.1.5.1.5.7.1 General considerations

During the slap-down drop onto the feet of the DN30 PSP, the feet are expected to be significantly deformed. In addition, two major impacts onto the plug side corner as well as onto the feet on the valve side are expected. The primary impact onto the plug side of the DN30 PSP should cause less deformation at the plug side compared to the drop test onto the plug corner, because only a fraction of the drop test energy is absorbed during this impact. However, considerably higher deformations caused by the secondary impact are expected at the valve side of the DN30 PSP because the impact velocity at that point is significantly higher than in a flat drop. For the 1 m drop onto the bar, the impact point is selected to be at the top of the DN30 PSP as there are no additional protections like the feet or the forklift pockets.

The design has to ensure that after the tests simulating HAC:

- There is no contact between the valve and any part of the DN30 PSP or any other part of the 30B cylinder except for its initial point of contact (the thread).
- There is no contact between the plug and any part of the DN30 PSP or any other part of the 30B cylinder except for its initial point of contact (the thread).
- The leakage rate of the containment does not exceed the limit specified in section 2.2.3.

2.2.1.5.1.5.7.2 FEM analysis

2.2.1.5.1.5.7.2.1 *FEM analysis before the drop tests*

In the case of the slap-down drop onto the feet, different angles from 5° to 30° between the longitudinal axis of the DN30 package and the horizontal line through the center of gravity were investigated for the free drop test from a height of 1.2 m and the 9 m drop test. The maximal velocity of the valve for the secondary impact was reached for an angle of 15° so that this angle is selected for the analysis. For the drop onto the bar, an angle of 25° between the centerline of the bar and the normal of the outer DN30 PSP shell is chosen because this angle is the most critical one with respect to a penetration of the outer shell.

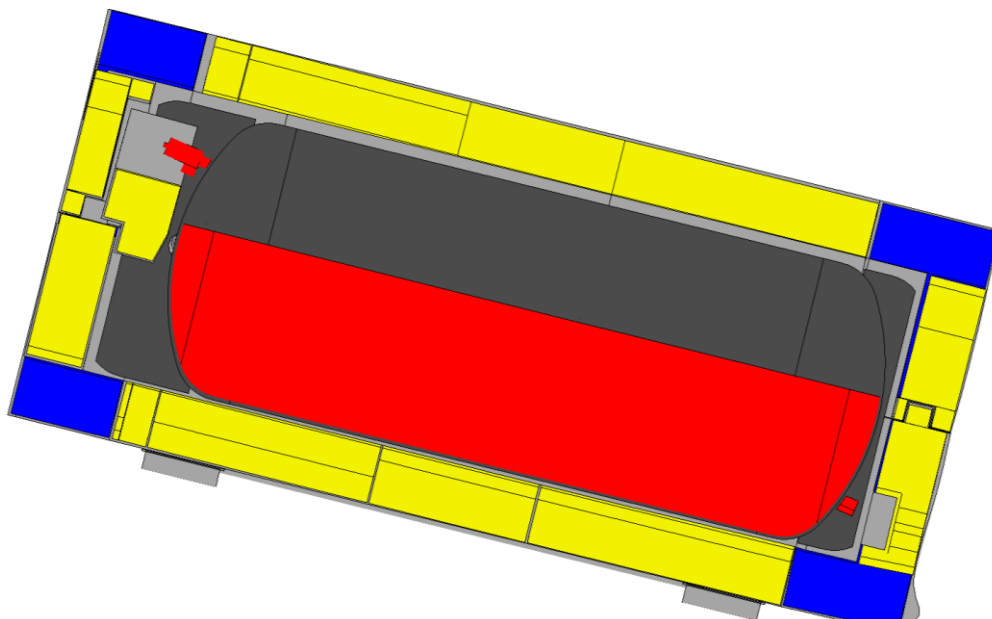
2.2.1.5.1.5.7.2.2 *Deformations at RT*

During the 1.2 m slap-down drop, the plug side of the DN30 PSP is deformed (see Figure 92). Small deformations of about 7 % also occur at the connection of the feet with the outer DN30 PSP shell. Since the valve side does not get in contact with the target, it remains undamaged. In addition, there are no deformations of the inner steel shell, the valve protecting device, the rotation preventing device and the plug protecting device. Overall, the formation of cracks can be ruled out for this drop test. The valve does not get in contact with any other part except for its initial point of contact (the thread).

During the 9.0 m slap-down drop, the feet show severe buckling compared to the 1.2 m drop test. They are pushed into the outer shell of the DN30 PSP, so that the valve side undergoes some deformations as well during the second impact of the slap-down. Cracks in the outer surface of the feet are likely to occur. Nevertheless, the occurring deformations of the inner steel parts remain below 5 % so that the rotation preventing, valve and plug protecting device are nearly undamaged after the 9.0 m slap-down drop.

During the drop onto the bar, further deformation of the DN30 PSP are only visible at the impact zone of the bar (see Figure 93). The inner shell undergoes no deformations because there is enough foam for protection.

a)



b)

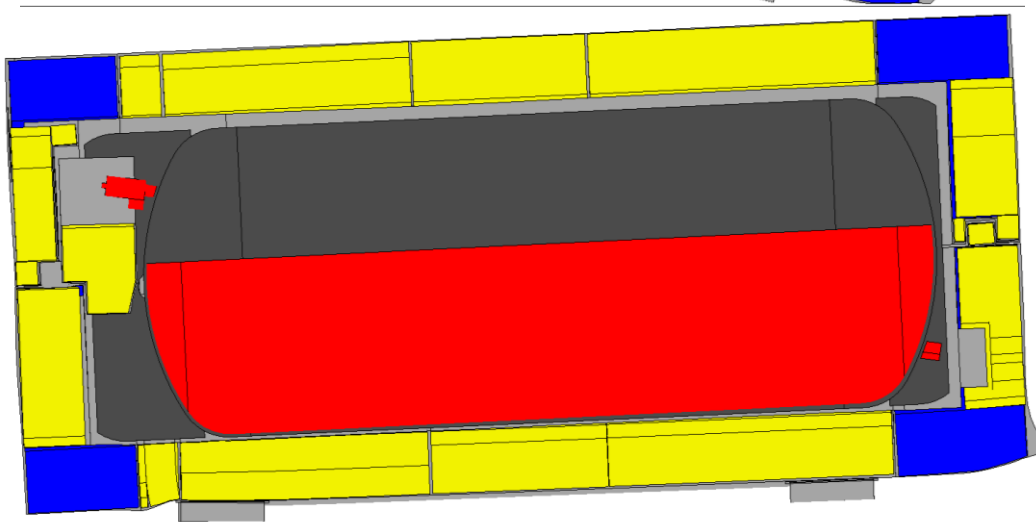


Figure 92: States with maximal deformation of the DN30 package during the free drop test in sequence 5: a) First impact on the plug side b) Secondary impact on the valve side

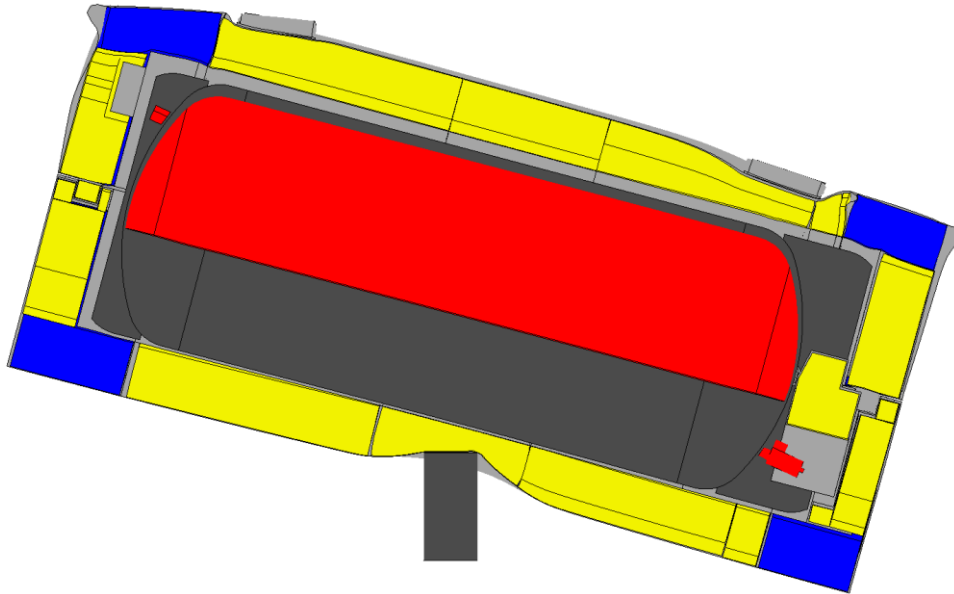


Figure 93: State with the maximal deformation of the DN30 package in sequence 5

2.2.1.5.1.5.7.3 Results of drop tests

The drop test sequence slap-down drop onto the feet is documented as sequence No. 5 in Appendix 2.2.1.2 (Drop Test Reports).

- Drop No. 5.1 1.2 m Slap-down drop onto the feet
- Drop No. 5.2 9 m Slap-down drop onto the feet
- Drop No. 5.3 1 m drop onto the top of the DN30 PSP

2.2.1.5.1.5.7.3.1 Deformations at RT

The 1.2 m drop causes small deformations on the feet, which are pushed into the outer shell of the DN30 PSP (see Figure 94). The 9.0 m slap-down drop causes overall larger deformations. The penetration of the feet into the outer shell continues, but still without any cracks in the outer surface or outer welds (see Figure 95).

The drop onto the bar does lead to a penetration of the outer steel shell of the DN30 package (see Figure 96).



Figure 94: Sequence 5 - Deformation after the 1.2 m drop



Figure 95: Sequence 5 - Deformation after the 9.0 m drop



Figure 96: Sequence 5 - Deformation after the drop onto a bar from 1.0 m

No deformations of the inner shell of the DN30 PSP are visible. The rotation preventing devices are not deformed, so that their function is still preserved and any rotation of the 30B cylinder is prevented.

2.2.1.5.1.5.7.3.2 Summary of the drop test results for sequence 5

- The leakage rate after the drop test sequence 5 is $Q_{st} = 1.37E-08 \text{ Pa} \cdot \text{m}^3/\text{s}$.
- All closure systems are intact.
- The DN30 PSP can be opened without further damaging the DN30 PSP.
- Operating the closure system and lifting the top half off the bottom half is possible.
- There was no contact between the valve and any other part of the DN30 PSP or 30B cylinder except for its initial point of contact (the thread).
- There was no contact between the plug and any other part of the DN30 PSP or 30B cylinder except for its initial point of contact (the thread).
- The valve protecting device can still be operated (rotated) and the hinges are intact.
- Removal of the 30B cylinder from the bottom half is possible without further damaging the DN30 PSP.
- Loading of a 30B cylinder into the DN30 PSP is still possible.

2.2.1.5.1.5.7.4 Evaluation of the FEM analysis vs. real drop tests

2.2.1.5.1.5.7.4.1 Deformations at RT

In Table 46, the measured distances at the feet of the DN30 PSP are compared to the calculated values. The definition of the measurement points is described in Figure 97.

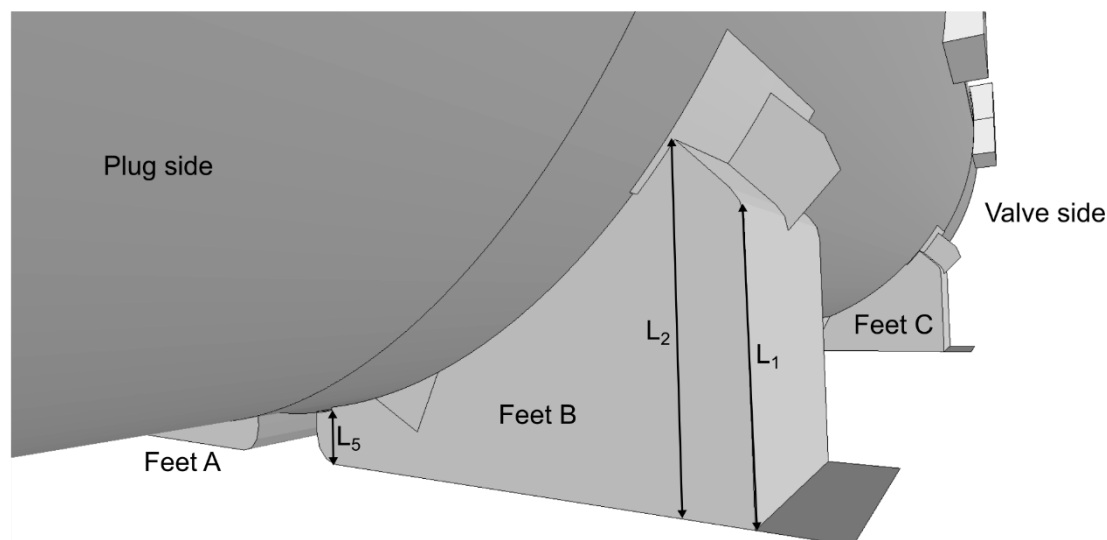


Figure 97: Measurement points in sequence 5

Table 46: Measured distances (penetrations) for the slap-down at RT and comparison to calculated values

Dimension [mm]	Drop								
	1.2 m			9.0 m			1 m bar		
	CV	MV	D %	CV	MV	D %	CV	MV	D %
A L1/L2/L5	196 /239 /40	195 /240 /42	1/-1/-5	189 /216 /29	188 /212 /32	1/2/-10	-	-	-
B L1/L2/L5	196 /239 /40	195 /241 /41	1/-1/-2	187 /218 /29	189 /216 /35	-1/1/-19	-	-	-
C L1/L2/L5	195 /235 /40	195 /236 /40	<1	189 /206 /39	193 /209 /41	-2/-1/-5	-	-	-
D L1/L2/L5	195 /235/ 40	195 /232 /41	0/1/-2	189 /206 /39	194 /206 /41	-3/0/-5	-	-	-
P1	-	-	-	-	-	-	-	130	-

CV = calculated values MV = measured values

D % = deviation of measured values from calculated values in %

The exact measurement error in the experiment is unknown, but in the range of 10 % because of the applied measurement technique. The errors as well as the absolute differences between the measured distances are below 5 % in most cases. In the case of the slap-down, the measured deformations mostly depend on the chosen material parameters and flow curves of the applied material model for the austenitic stainless steel. For this reason, the slap-down provides a good basis for the validation of this specific part of the FEM model, especially concerning the chosen scale factor of the flow curve. The very good agreement shows that the material parameters for the steel are chosen correctly and that the FEM model is capable of reliably reproducing the observed deformation behavior of the slap-down drop.

A qualitative comparison of the deformations after the 9.0 m drop between the simulation and the experiment is shown in Figure 98.



Figure 98: Qualitative comparison of the deformations in simulation and experiment

The comparison of the measured depths of bar penetration in the simulation and experiment is not very meaningful because of a massive crack in the outer shell at the impact zone that occurred during the experimental test.

2.2.1.5.1.5.7.4.2 Decelerations at RT

The low-pass filtered decelerations in the valve area for the simulation and the experiment are shown in Figure 99 and Figure 100 for a cut-off frequency of 20 Hz and 584 Hz, respectively.

At a cut-off frequency of 20 Hz, the deceleration curve for the 30B cylinder is in good agreement to the experiment. The response of the FEM model seems to be too soft, but the shape and height of the deceleration curve is very well predicted by the FEM model with a deviation of 13 % in the peak deceleration. The deceleration signal in the simulation becomes noisier at a higher cut-off frequency of 584 Hz. However, the undefined position of the 30B cylinder at the time of impact may lead to non-deterministic interactions of the 30B cylinder with the DN30 PSP and thus makes it very challenging to accurately predict the deceleration peaks.

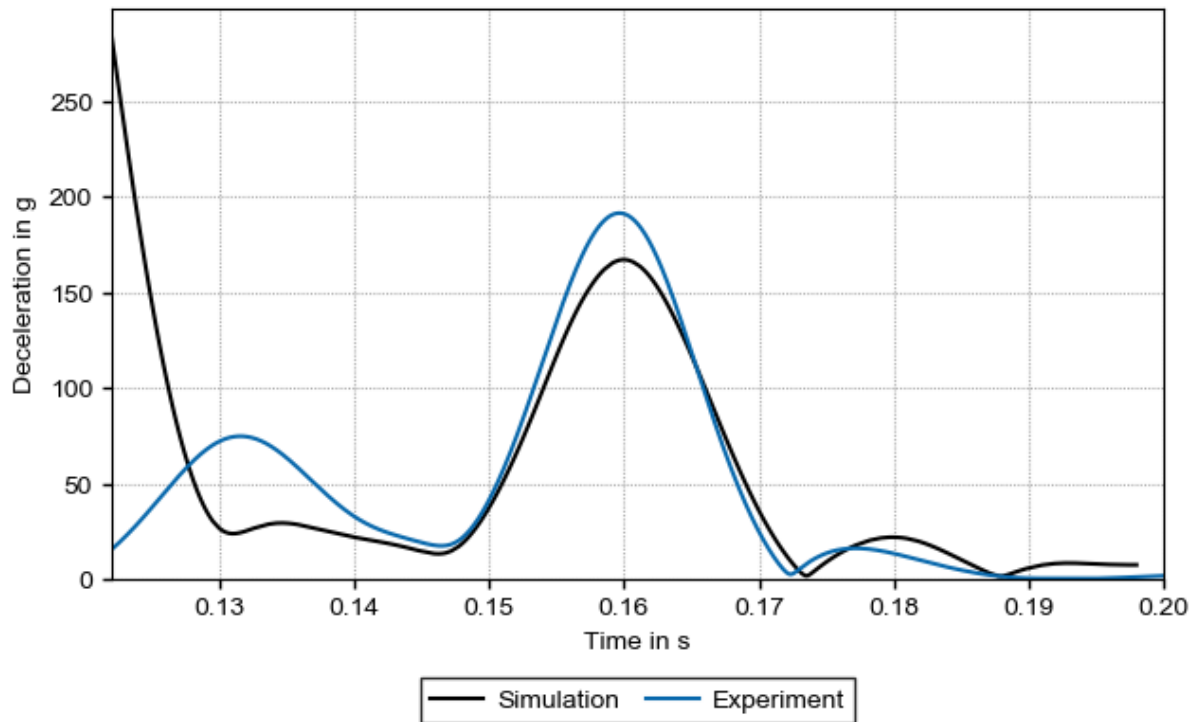


Figure 99: Comparison of simulation and experiment – deceleration in the valve area during the 9.0 m slap down drop in sequence 5 – low-pass filtered (SAE, 20 Hz cut-off)

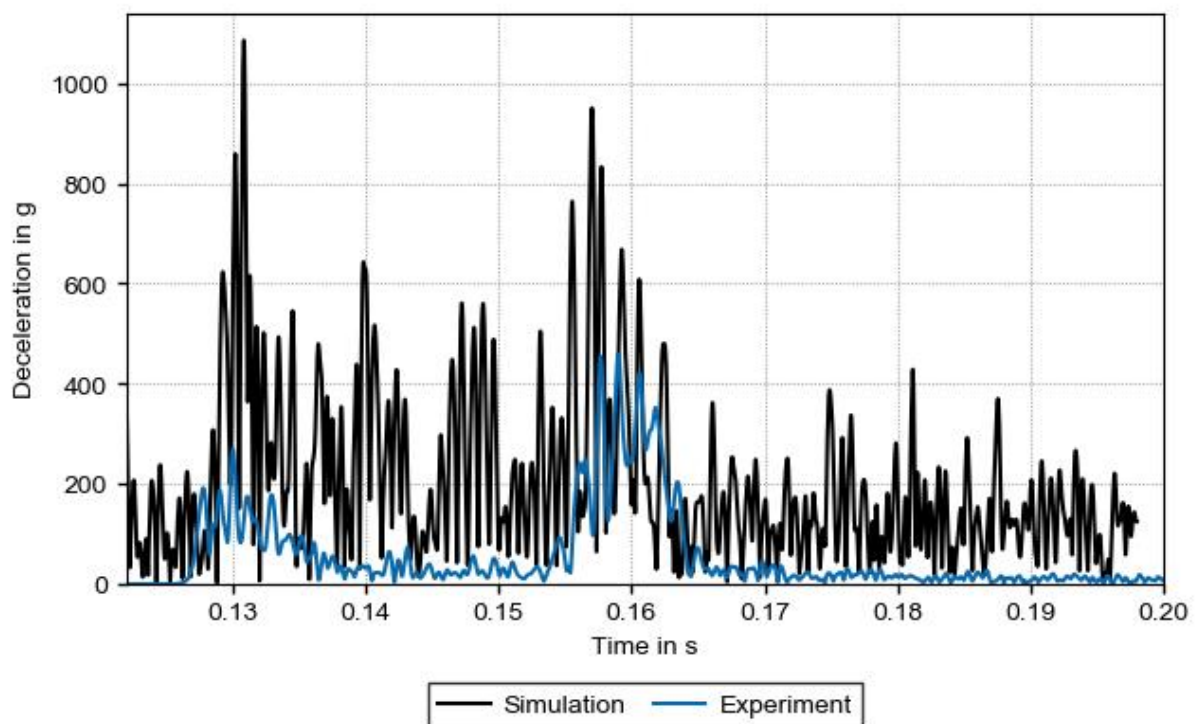


Figure 100: Comparison of simulation and experiment – deceleration in the valve area during the 9.0 m slap down drop in sequence 5 – low-pass filtered (SAE, 584 Hz cut-off)

2.2.1.5.1.5.8 Detailed calculation of the closure system

A detailed model of the closure system is investigated in a static FEM simulation because only a rough representation of this part of the DN30 PSP is represented in the LS-DYNA model for the dynamic FEM simulations of the drops tests.

The only relevant load is a tensile force normal to the section plane between the two main bodies of each closure device. Such a load is observed during the secondary impact on the feet at the valve side of the DN30 PSP in sequence 5 (see section 2.2.1.5.1.5.7).

2.2.1.5.1.5.8.1 FEM model

Figure 101 a) shows one of the six closure devices in comparison to the corresponding FEM model shown in Figure 101 b).

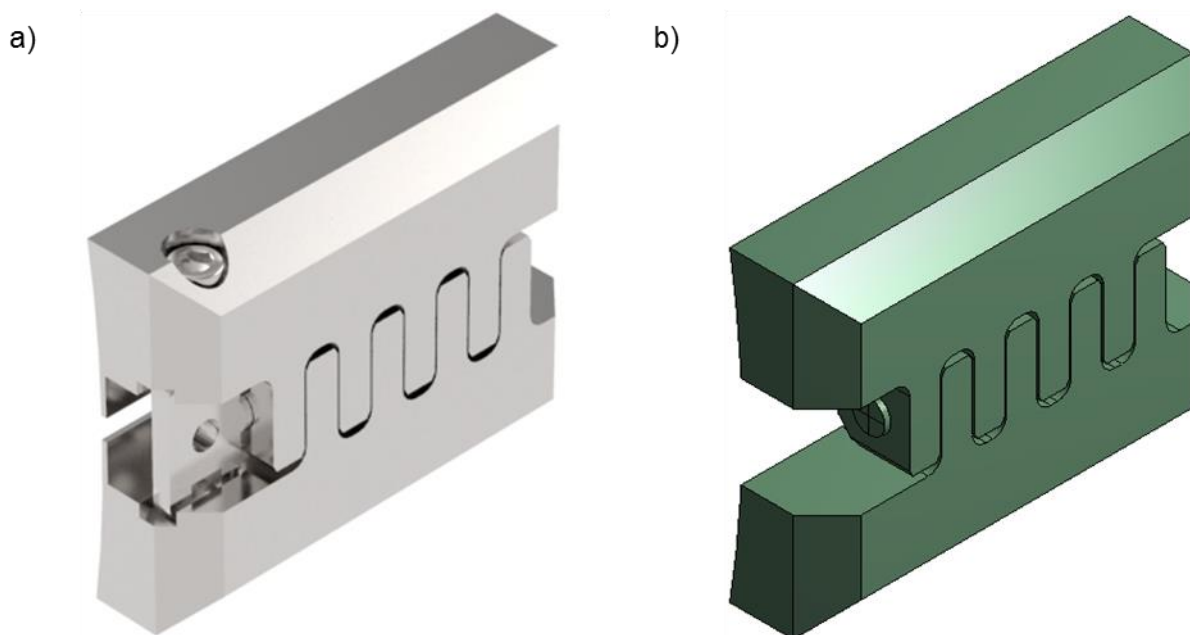


Figure 101: Closure device – comparison between CAD a) and FEM model b)

The design is such that there are no loads acting on the securing bolt and the pin handle. They keep the pin in place so that a representation as boundary conditions for the pin is an acceptable simplification.

In addition, the boreholes for the securing bolt as well as the notches for the pin handle in the lower and upper part of the closure device are removed. Since these areas are far away from the load transmission zones of the mortise joint, no deformations are expected. This is confirmed by the drop tests of Sequence 5.

2.2.1.5.1.5.8.2 Mesh

The generated mesh for each part is shown in Figure 102. Except for the pin, a mesh of tetrahedral elements is chosen for the lower and the upper part of the closure device. For the pin, a mesh of hexahedral elements is generated.

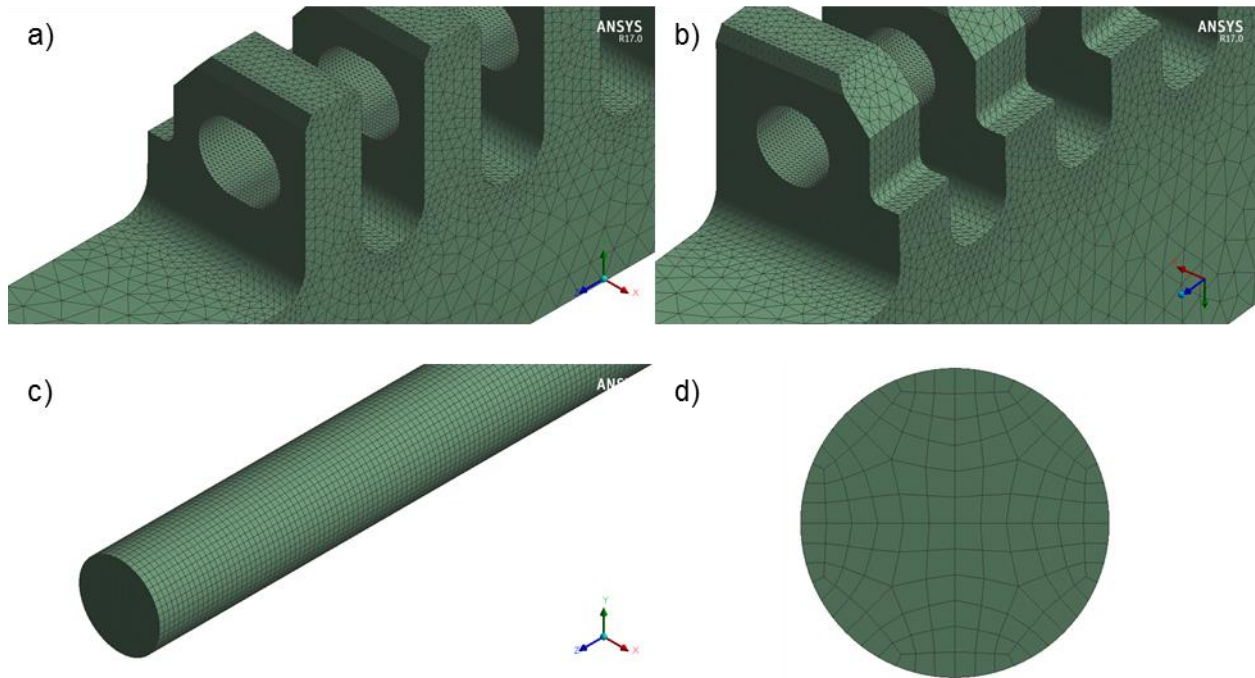


Figure 102: Generated mesh for each part of the closure device: a) Lower part b) Upper part c) Pin d) Pin front view

2.2.1.5.1.5.8.3 Boundary conditions

The static simulation is split into two load steps: the first is displacement-controlled, while the second is force-controlled. During the first load step, the structure is preloaded until the gaps between the pin and the mortise and tenon devices are closed to make sure that the defined frictional contacts are closed before the external force is applied in the second load step. The boundary conditions that are applied in the first and second load step are shown in Figure 103 a) and b), respectively.

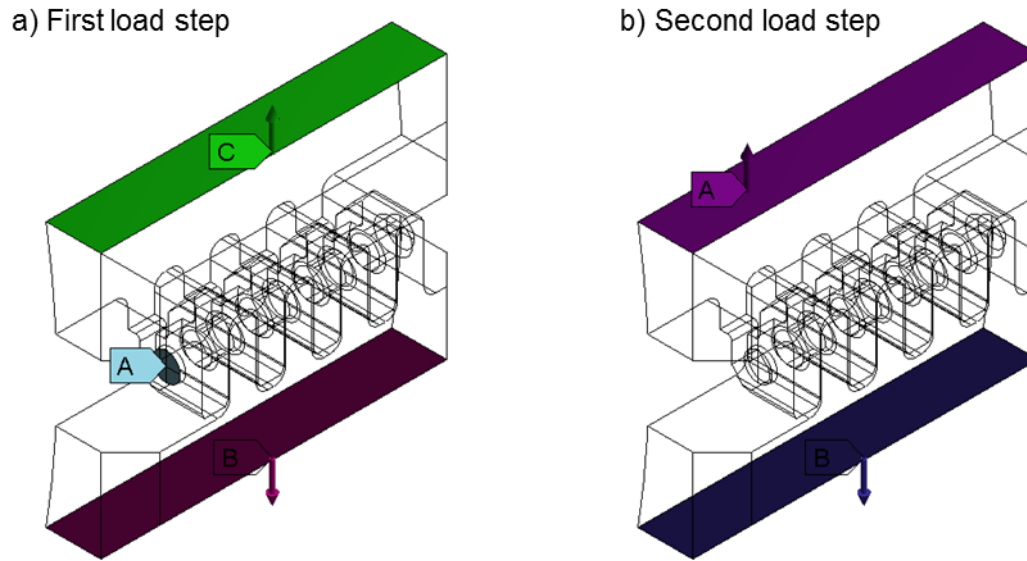


Figure 103: Boundary conditions for the static FEM simulation of the closure device

The value for the applied external force is obtained by calculating the maximal tensile force acting in normal direction onto the section plane between the two main bodies of each closure device during the 9 m-slap-down-drop in sequence 5. To ensure that this is indeed a tensile force, the change in length of a line across the section plane is tracked as well. As explained in Figure 104, a positive value at the corresponding point in time indicates a tensile load. Hence, a maximum of 102 kN occurs during the 9 m-slap-down-drop. Considering the uncertainties in the dynamic calculations, a bounding value of 150 kN is applied for the external force.

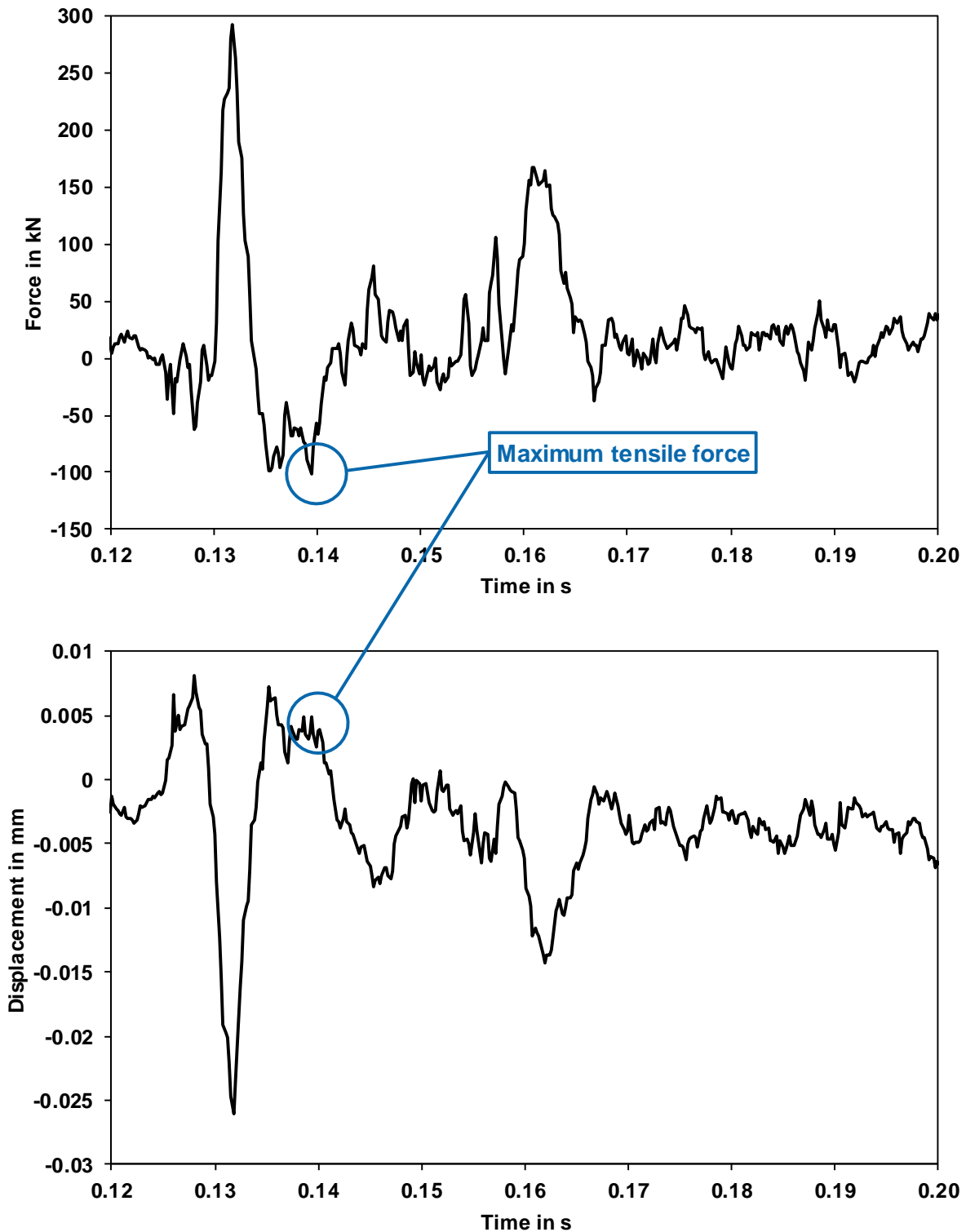


Figure 104: Evaluation of the maximal tensile force at the section plane during the 9 m slap-down drop in Sequence 5

Apart from the boundary condition, two frictional contact interfaces are defined between the pin and each of the mortise and tenon devices. Both contact interfaces are shown in Figure 105.

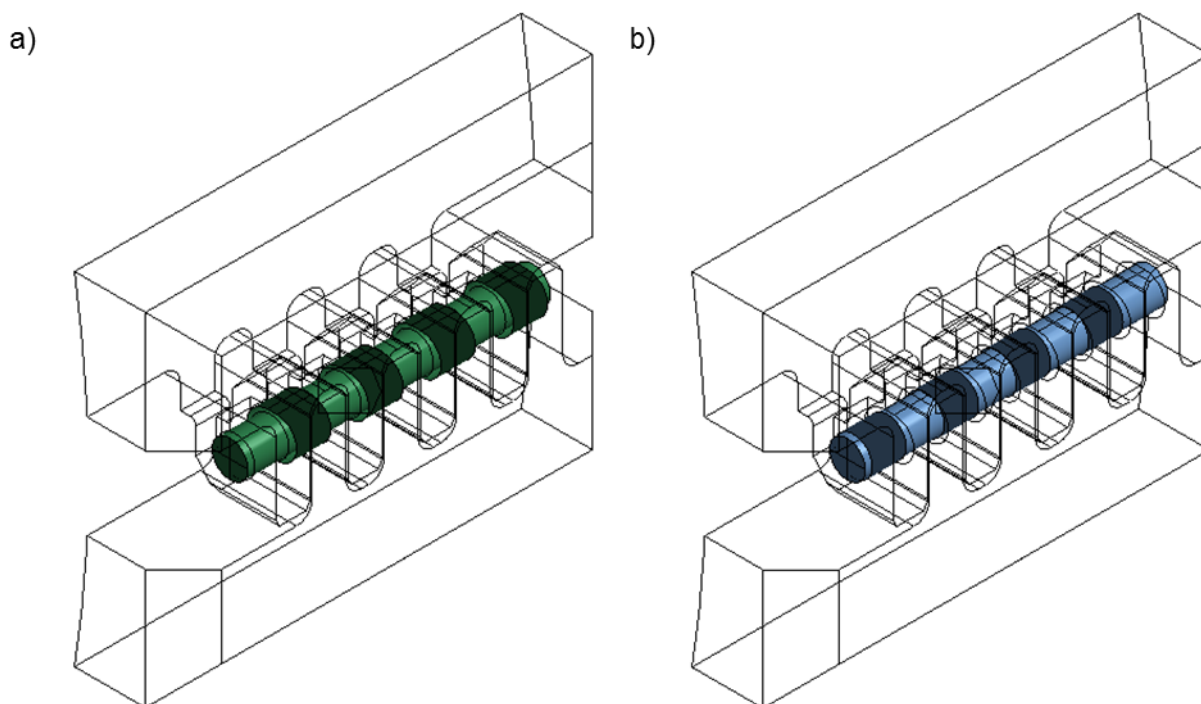


Figure 105: Contact interfaces: a) Between the pin and the lower part b) Between the pin and the upper part

2.2.1.5.1.5.8.4 Materials

Table 47 shows the data for the two different steels used for the closure device. The corresponding material data is listed in Table 24 and Table 26.

Table 47: Material specification of the closure device

Item	Material
Lower part of the closure system	1.4541
Upper part of the closure system	1.4541
Pins of the closure system	1.4542 [+P930]

2.2.1.5.1.5.8.5 Convergence of calculation results

Table 48 compares the corresponding stresses and strains in the most deformed areas of the lower and upper part of the closure device outside the contact zones as well as the plastic strains in the contact zones for a finer and coarser mesh. The comparison shows that convergence is reached as the differences in the stress results for the coarser and finer mesh are below 0.1 %.

Table 48: Convergence study

Mesh	Part	Variable	Min.	Max.
Coarse	Lower Part	Von Mises stress	1.6974 MPa	292.71 MPa
Fine			1.6936 MPa	292.53 MPa
Coarse	Upper Part	Von Mises stress	1.6065 MPa	248.83 MPa
Fine			1.6182 MPa	249.09 MPa
Coarse	Lower Part	Equivalent plastic strain	0.0 %	5.1269%
Fine			0.0 %	5.5318%
Coarse	Upper Part	Equivalent plastic strain	0.0 %	1.3571%
Fine			0.0 %	1.5448%

2.2.1.5.1.5.8.6 Results

The deformed pin is shown in Figure 106 a) and b) at the end of the second load step with the displacements being scaled by a factor of 14. The bending of the pin is attributed to the asymmetrical design of the closure devices, so that the force is not uniformly distributed along the pin. In addition, the pin is exposed to shearing. Nevertheless, only elastic deformations are observed because of the high strength steel that is used as material for the pin (see Figure 106 b)). Consequently, no failure of the pin is expected because of the load occurring in the slap down in sequence 5.

a)

F: Static FEM analysis of the closure system

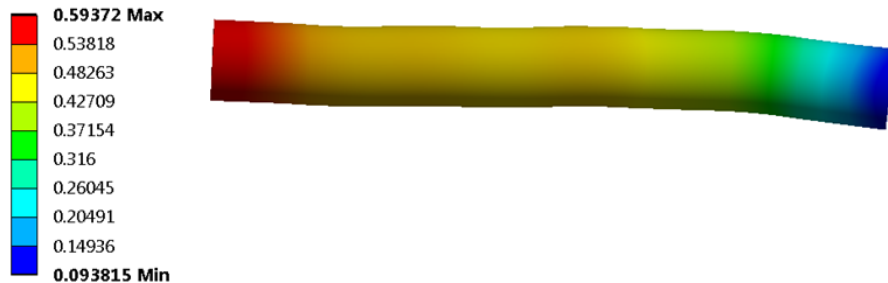
Pin

Type: Total Deformation

Unit: mm

Time: 2

05.12.2016 11:21



b)

F: Static FEM analysis of the closure system

Pin

Type: Equivalent Plastic Strain

Unit: mm/mm

Time: 2

05.12.2016 11:10

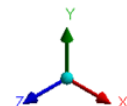
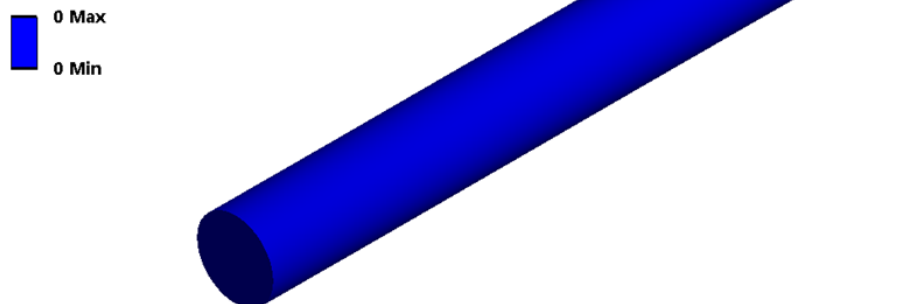


Figure 106: Deformation of the Pin: a) Total deformation (Scale factor 14) b) Equivalent plastic strain

Up to 6 % equivalent plastic strains are observed at the lower part and 2 % in the upper part of the closure device (see Figure 107). However, the austenitic stainless steel 1.4541 is highly ductile having a minimal elongation at fracture of 35 %, so that the occurring plastic strains will not lead to any cracks. Moreover, the maximal values occur in the contact zones of the pin. In these areas, the mean stress is of the compressive type. Thus, even with a crack, there is no crack propagation expected. The critical plastic deformations, which are connected to a tensile load, are located on top of each of the teeth.

Overall, the closure device is able to withstand the occurring loads during the 9 m slap-down drop in sequence 5 and, thus, all HAC scenarios.

a)

F: Static FEM analysis of the closure system

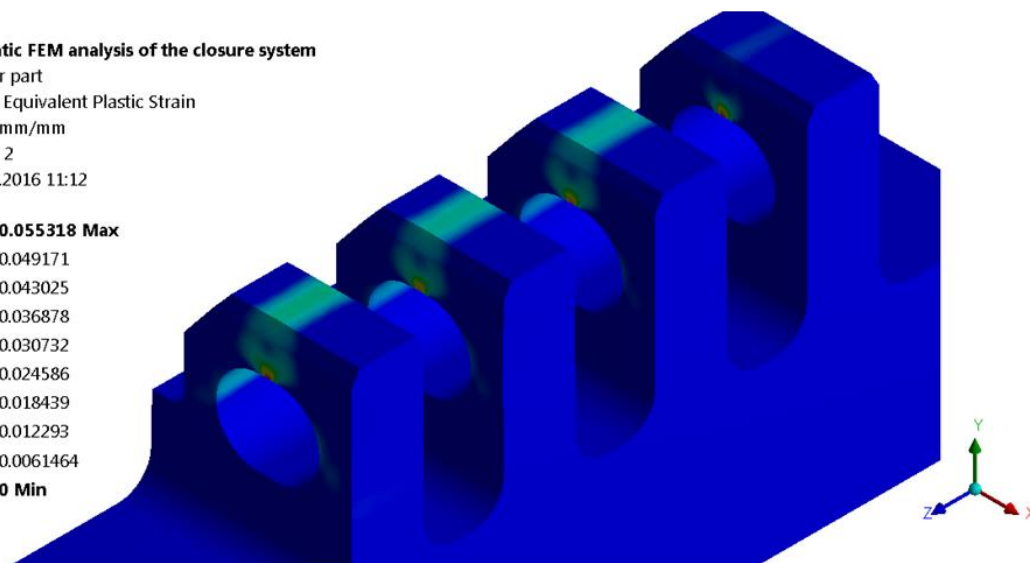
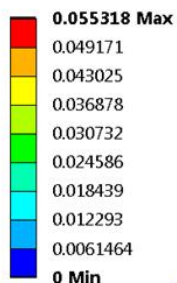
Lower part

Type: Equivalent Plastic Strain

Unit: mm/mm

Time: 2

05.12.2016 11:12



b)

F: Static FEM analysis of the closure system

Upper part

Type: Equivalent Plastic Strain

Unit: mm/mm

Time: 2

05.12.2016 11:15

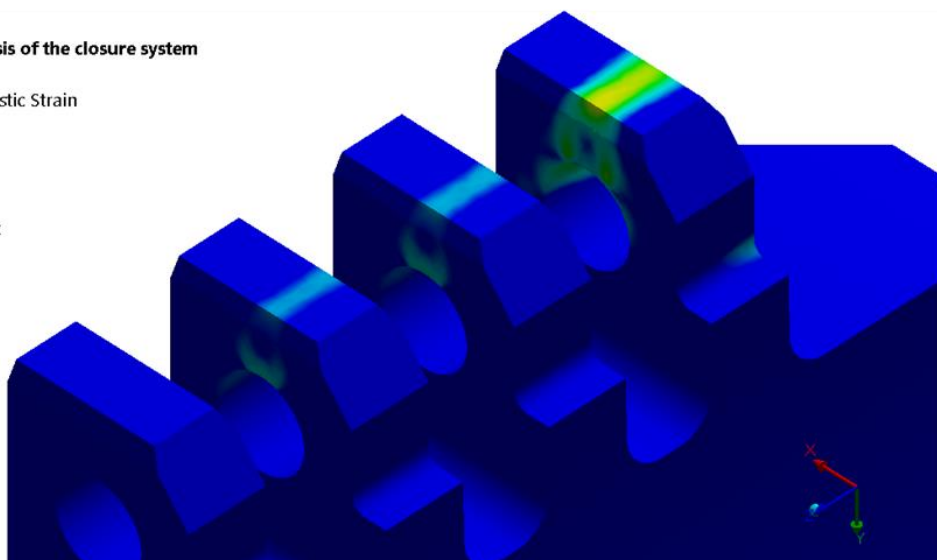
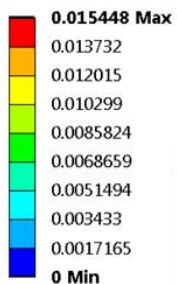


Figure 107: Equivalent plastic strain: a) Lower part b) Upper part

2.2.1.5.1.6 Conclusion

The FEM model is validated based on five drop test sequences with prototypes of the DN30 package. The results of these benchmark analyses are:

- Deformations of the prototype of the DN30 package measured after the real drop test are predicted with good accuracy by the calculation model with deviations remaining mostly below 10 % compared to the experiment. Thus, the deviations of the calculated deformations from the measured deformations are in the range of the measurement error.
- Local effects like rupture of welding seams or puncture of the outer shell of the DN30 PSP can be predicted with sufficient accuracy by evaluating the strains and stresses in the respective parts of the DN30 PSP.
- Decelerations of the 30B cylinder are predicted with the calculation model with sufficient accuracy.
- In some cases, the non-deterministic behavior of the 30B cylinder with respect to the DN30 PSP due to an undefined position of the 30B cylinder at the time of impact leads to deceleration peaks, which cannot be predicted by the calculation model.
- For the drop test sequences 1 and 3 used for the assessment of the deformations and decelerations at -40 °C and at +60 °C, the good agreement of the simulation and the experiment allows for the evaluation of the behavior of the DN30 package in the temperature range of -40 °C to +60 °C.

The analysis of the drop test sequences

- inclined onto the valve side corner
- inclined onto the plug side corner
- flat onto the valve side
- flat onto the plug side
- flat onto the closure system with / without rotation of the DN30 prototype around its axis
- flat onto the top side
- inclined onto the feet (slap-down)

showed, that

- the leakage rate after each of the drop test sequences is less than 1.0E-06 Pa·m³/s.
- all closure systems are intact after each drop test sequence.
- there is no contact between the valve and any other part of the DN30 PSP or 30B cylinder except for its initial point of contact (the thread) in any drop test sequence.
- there is no contact between the plug and any other part of the DN30 PSP or 30B cylinder except for its initial point of contact (the thread) in any drop test sequence.
- the valve protecting device fulfills its function after each drop test sequence.
- the rotation preventing device fulfills its function after each drop test sequence.

- the plug protecting device fulfills its function after each drop test sequence.
- the intumescent material as well as the housing are still present and undamaged after each of the drop test sequences.

For the analysis of sequence 1 at -40 °C and +60 °C and sequence 3 at -40 °C, the following applies:

- the deformations for drop I at +60 °C increase by maximal 8 % compared to RT.
- the deformations for drop I at -40 °C decrease by maximal 9 % compared to RT.
- the decelerations at -40 °C increase by less than 5 % for a cut-off frequency of 20 Hz compared to RT.
- there is no contact between the valve and any other part of the DN30 PSP or 30B cylinder except for its initial point of contact (the thread) neither at -40 °C nor at +60 °C.
- there is no contact between the plug and any other part of the DN30 PSP or 30B cylinder except for its initial point of contact (the thread) neither at -40 °C nor at +60 °C.
- the valve protecting device fulfills its function after each drop test sequence in the whole temperature range.
- the rotation preventing device fulfills its function after each drop test sequence in the whole temperature range.
- the plug protecting device fulfills its function after each drop test sequence in the whole temperature range.

It can be concluded that the DN30 PSP provides the required mechanical protection of the 30B cylinder for the temperature range of -40 °C to +60 °C under RCT; NCT and HAC.

2.2.1.5.2 Water immersion test for packages containing fissile materials

The containment (30B cylinder) is designed according to [ANSI N14.1] and [ISO 7195] for an external pressure of 172 kPa. The water immersion test for packages containing fissile material defined in [10CFR71] §71.73(c)(5) or [IAEA 2012], para. 731 requires the immersion of the specimen under a head of water of at least 0.9 m for a period of not less than 8 h. This is equal to a pressure of 9 kPa. Hence, the design pressure is higher than the test pressure. The DN30 package is designed to withstand the water immersion test.

2.2.1.5.3 Influence of the thermal test on the structural safety of the DN30 package under HAC

2.2.1.5.3.1 Internal pressure

The pressure build-up during the thermal test is investigated in sections 2.2.2.1.4 and 2.2.2.3.5.2. The maximum pressure for the thermal test considering a pressure build-up caused by elevated temperatures and by melted UF₆ contents is below the admissible pressure. Damage of the 30B cylinder, valve or plug and, thus, an influence of the thermal test on the containment system of the DN30 package can be excluded.

2.2.1.5.3.2 Pressure development due to the expansion of the intumescent material

In case of a fire, the intumescent material starts expanding when the expansion temperature is reached. Considering the 30B cylinder, two different situations can occur with increasing expansion of the intumescent material:

- The weight of the 30B cylinder is too high so that the material only expands outside of the contact area between the 30B cylinder and the inner shell of the DN30 PSP.
- In the case of an empty cylinder, the intumescent material also expands below the 30B cylinder and raises the cylinder.

In the first case, the upper gap between the 30B cylinder and the inner shell is at least 23.3 mm. This value is based on the worst combination of the tolerances of the 30B cylinder and the DN30 PSP. Based on experimental tests with the intumescent material detailed in appendix 1.4.3, the maximal pressure load caused by the expansion is about 2.3 kPa for such a large gap. Hence, the actual load being applied to the 30B cylinder is still its own weight, but the resulting stresses in the 30B cylinder envelope reduce because this load is distributed over a larger area after the intumescent material has expanded.

The maximal stresses in the pressure envelope of the 30B cylinder occur in the second case when the intumescent material evenly covers the entire envelope. In this case, the minimal gap is $23.3 \text{ mm} / 2 = 11.7 \text{ mm}$. In the experimental tests with the intumescent material detailed in appendix 1.4.3, the maximal pressure load by the expanding intumescent material was found to be 27 kPa for a gap of 10 mm. This value is well below the external design gauge pressure of 172 kPa for the 30B cylinder according to [ANSI N14.1] and [ISO 7195].

The gaps between the housing of the valve protecting device and the valve itself are in each direction more than 20 mm. In the experimental tests with the intumescent material, the maximal pressure development was 2.3 kPa for a gap of 20 mm and after 60 min at 300 °C there was no pressure at all. Such a small pressure load is unable to cause any damage to the valve.

The distance between the plug and the inner shell is limited by the skirt on the plug side so that the distance is always larger than 13 mm (cf. [ANSI N14.1], [ISO 7195]). Since the plug is a solid structural part that is manufactured from a single piece, even the measured pressure

development of 27 kPa for a gap of 10 mm of the expanding intumescent cannot cause any damage to the plug.

Consequently, neither the 30B cylinder nor the valve or the plug will be damaged by the expansion of the intumescent material.

2.2.1.6 Analysis of stresses caused by temperature influences

Generally, there are only minor and negligible stresses caused by temperature influences for the following reasons:

- The DN30 PSP consists of a welded structure of austenitic stainless steel with the same thermal expansion coefficients in all parts.
- As there is only a very low thermal load from the content, the temperature differences from the heat produced by the content are negligible.
- The possibly different expansions of the top and bottom half of the DN30 PSP because of temperature differences caused by the different insulating conditions on the top and bottom half are small; the gaps between the flanges of the top and bottom half allow enough relative movement to compensate for the different expansions.
- The gaps between the DN30 PSP and the 30B cylinder are sufficient to compensate the different thermal expansions of the DN30 PSP and the 30B cylinder.

Nonetheless, possible stresses caused by the expansion of the 30B cylinder and the expansion of foam are investigated.

2.2.1.6.1 Stresses caused by expansion of the 30B cylinder

In case the DN30 PSP and the 30B cylinder are heated up simultaneously, no stresses can occur because the thermal expansion coefficient of the material of the 30B cylinder is smaller than that of the material of the DN30 PSP shells. The only situation, stresses due to thermal expansion might occur, is when the DN30 PSP cools down much faster than the 30B cylinder after heating. Hence, the following scenario is assumed for the proof:

- The DN30 PSP has a temperature of 100 °C (complying with the outer shell of the top half after 12 hours of solar insolation).
- The 30B cylinder has a temperature of 20 °C (complying with a 30B stored inside before loading).
- Under constant insolation, the 30B cylinder maximally heats up to 58 °C (see Table 64).
- Without insolation, the DN30 PSP cavity minimally cools down to 38 °C (see Table 64).

The length of the 30B cylinder according to [ANSI N14.1] and [ISO 7195] is 2070 ± 13 mm. The minimal length of the cavity (bottom half) is 2084^{+4}_0 mm.

Then, the maximal expansion of the 30B cylinder is:

$$\Delta l_{Cyl} = l_{Cyl,max} \cdot \alpha_{T_{ref}=20\text{ °C}} \cdot \Delta T = (2070 \text{ mm} + 13 \text{ mm}) \cdot \frac{11.5 \cdot 10^{-6}}{\text{°C}} \cdot (58 - 20) \text{ °C} = 0.91 \text{ mm}$$

For the DN30 PSP, the expansion after cooling down is independent of the maximal temperature reached during heating. This results in the following minimal expansion after cooling down:

$$\begin{aligned} \Delta l_{PSP} &= l_{PSP,min} \cdot \alpha_{T_{ref}=20\text{ °C}} \cdot \Delta T = 2084 \text{ mm} \cdot \frac{16.0 \cdot 10^{-6}}{\text{°C}} \cdot [100 - 20 - (100 - 38)] \text{ °C} \\ &= 0.6 \text{ mm} \end{aligned}$$

The total expansion difference is:

$$\Delta l = l_{PSP} + \Delta l_{PSP} - (l_{Cyl} + \Delta l_{Cyl}) = 2084 \text{ mm} + 0.6 \text{ mm} - (2083 \text{ mm} + 0.91 \text{ mm}) = 0.69 \text{ mm}$$

Hence, the gap is wide enough to allow for the dimensional changes due to thermal differences.

2.2.1.6.2 Stresses caused by expansion of foam

The safety analysis for the DN30 package regarding the foam expansion due to heating is based on the following assumptions:

- The linear thermal expansion coefficient for all foam parts is assumed to be $\alpha_{\text{foam}} = 45 \cdot 10^{-6} \text{ K}^{-1}$. This coefficient covers the values for RTS 120 and RTS 320 as documented in the manufacturer specifications (see Appendix 1.4.2 (Material Data PIR Foam)).
- Based on the foam flow curves determined in Appendix 2.2.1.3 (Structural Analysis of the DN30 package under NCT and HAC), the static elasticity modulus of the RTS 120 foam is $E_{\text{foam}} = 170 \text{ MPa}$.
- The entire DN30 PSP is assumed to be heated from 20 °C to a conservative temperature of 70 °C (63 °C were determined at the outer shell during RCT in Appendix 2.2.2.3 (Thermal Analysis), and the temperature of the other components was lower than 63 °C).
- A foam block with a cross section of $A_{\text{foam}} = \frac{1}{2} \cdot \frac{\pi}{4} \cdot d_{\text{shell}}^2$, that corresponds to the upper half of the DN30 package with a diameter $d_{\text{shell}} = 1216 \text{ mm}$ is enclosed in a steel shell with thickness $t_{\text{shell}} = 3 \text{ mm}$.
- The smallest cross section of the steel shell is calculated as: $A_{\text{shell}} = \frac{d_{\text{shell}}}{2} \cdot \pi \cdot t_{\text{shell}}$

Due to the expansion of the foam by the thermal strain $\varepsilon_{\text{therm}} = \alpha_{\text{foam}} \cdot \Delta T$, a force acts on the steel shell. Without taking into account the expansion of the steel shell itself, the equilibrium of forces between the foam and the steel shell leads to the following stress in the steel shell:

$$F_{\text{foam}} = \varepsilon_{\text{therm}} \cdot E_{\text{foam}} \cdot A_{\text{foam}} = \sigma_{\text{shell}} \cdot A_{\text{shell}} = F_{\text{shell}}$$

The stress in the outer shell of the DN30 PSP amounts to:

$$\sigma_{\text{shell}} = \alpha_{\text{foam}} \cdot \Delta T \cdot E_{\text{foam}} \cdot \frac{A_{\text{foam}}}{A_{\text{shell}}} = 39 \text{ MPa} < R_{p,0,2} \text{ at } 70 \text{ °C}$$

Even though very conservative assumptions were taken into account for the geometry of the foam block, the expansion of the steel shell and the expansion coefficient of the foam, the resulting stress in the steel shell reaches only about 22 % of its yield strength. Hence, only elastic deformations are to be expected and damaging of the package can be excluded.

2.2.1.6.3 Stresses caused by temperatures reached during HAC

For HAC, no stresses are to be expected during or after the fire. During the first stages of the fire, the steel shells heat up faster than the foam, increasing the gap between both parts. With the incineration of the foam, the foam is reduced in volume and partly loses its structural integrity (see Figure 129 and Figure 130), so that no stresses are to be expected during cooling down.

2.2.2 THERMAL ANALYSIS

In this chapter, steady state temperatures at the package DN30 which occur under RCT and NCT and transient temperatures which are expected with solar insolation, are presented. Furthermore, transient temperatures for the package DN30 expected under HAC (thermal test) are calculated and analyzed.

For the calculated temperatures, it is proven that they are lower than the admissible temperatures of the used materials and that the objective of proof as laid out in section 2.2.2.1 is met.

The analyses are valid for all filling ratios from heels cylinders up to cylinders filled with the maximum amount of UF₆ defined in section 1.3.

The thermal analysis is described in detail in Appendix 2.2.2.3 (Thermal Analysis).

2.2.2.1 Objective of verification

2.2.2.1.1 Verification for all types of packages

It is verified that the design of the package takes into account ambient temperatures and pressures that are likely to be encountered in RCT ([IAEA 2012] para. 616, there is no adequate rule in [10CFR71] nor in [49CFR173]).

2.2.2.1.2 Verification for packages containing uranium hexafluoride

It is verified that the package can withstand, without rupture of the containment system, the thermal test specified in [10CFR71] §71.73(c)(4) or [IAEA 2012] para. 728.

2.2.2.1.3 Verification for packages containing fissile material

The consequences of the thermal test specified in [10CFR71] §71.73(c)(4) or [IAEA 2012] para. 728 on the package subjected to the mechanical tests specified in [10CFR71] §71.73(a), §71.73(c)(1), §71.73(c)(3) and §71.73(c)(6) or [IAEA 2012] paras 726, 727 (a), 727 (b) and 729 are analyzed to verify the requirements of [10CFR71] §71.55(d), §71.55(e) and §71.59(a)(2) or [IAEA 2012] para. 682 and 685. The verification is contained in section 2.2.5.

2.2.2.1.4 Admissible component temperatures of the DN30 package

For the containment system of the DN30 package, which consists of the 30B cylinder with installed valve and plug as specified in [ANSI N14.1] and [ISO 7195], a covering admissible temperature is calculated that considers the admissible temperatures of the materials with regard to their thermal properties and with regard to a pressure build-up because of melted UF₆ contents according to [USEC 651] and [ASME BPVC].

The materials used for the cylinder shell, the valve and the plug are according to [ANSI N14.1]:

- 30B cylinder shell: the maximum temperature defined in [ASME BPVC] for SA516 steel grade 55/60 is 371.11 °C or 700 °F
- valve/plug body (aluminum bronze UNS C63600): the melting point is 1030 °C, the hot-working temperature is 760 – 875 °C
- valve/plug stem (nickel copper alloy UNS N04400): the melting point is 1300 – 1350 °C, the hot-working temperature is 648 – 1176 °C

- valve/plug solder (tin-lead alloy): the solidus temperature of a tin lead solder compliant with ASTM B32 alloy grade Sn 50 is 183 °C, the liquidus temperature is 216 °C (cf. [Harris Sn50])

For temperatures above the triple point of UF₆ (64 °C) a pressure build-up is investigated for melted UF₆ contents. The following conservative assumptions are used for the calculations:

- The maximum temperature of the UF₆ is assumed to be the average temperature of all UF₆ in the 30B cylinder. Calculations show that only the outmost region of the UF₆ in contact with the 30B cylinder shell will reach that maximum temperature while the core of the UF₆ is still in its solid state; the average temperature calculated for all UF₆ is well below that maximum temperature. For example, for the HAC calculation for a full cylinder (100 % filling), the maximum temperature of more than 50 % of all UF₆ in the 30B cylinder is still below the triple point of 64 °C.
- For the calculation of the pressure build-up, the pressure of the empty 30B cylinder is assumed to be 5 psi instead of 3 psi (cf. [USEC 651] sections 5.3.5 and 8.3).
- The calculations for the pressure build-up are calculated with the safe fill limit of 95 % instead of the minimum volume (cf. [USEC 651]).

The admissible pressure for the 30B cylinder, the valve and the plug for HAC is conservatively set to the test pressure of 2.76 MPa/400 psig as specified in [ANSI N14.1] for these components. The pressure build-up is investigated for filling ratios of 50 % and 100 % for a temperature of 131 °C/267.8 °F.

The vapor pressure data of UF₆ is extracted from [WITT 1960] and listed in Table 49 below.

Table 49: Vapor pressure of UF₆ extracted from [WITT 1960]

Temperature [°C]	Vapor pressure [MPa]
63.88	0.1506 ¹⁾
64.20	0.1527
91.88	0.3395
99.94	0.4174
108.07	0.5091
116.03	0.6129
124.17	0.7349
133.19	0.8892
141.44	1.0517
149.50	1.2300
180.57	2.1313
207.32	3.2436
230.20	4.6103

¹⁾ vapor pressure of the solid, for all other temperatures: vapor pressure for the liquid

The calculation of the total pressure is based on [USEC 651]. The input data for a 30B cylinder is according to [ANSI N14.1]:

$$V_{30B} = 26 \text{ ft}^3$$

$$m_{\text{UF}_6, \text{max}} = 5020 \text{ lb}$$

$$T_1 = 68 \text{ }^\circ\text{F} (20 \text{ }^\circ\text{C})$$

$$T_2 = 267.8 \text{ }^\circ\text{F} (131 \text{ }^\circ\text{C})$$

$$\rho_{\text{UF}_6, 1} = 317.8 \text{ lb/ft}^3 \text{ (solid, at } 20 \text{ }^\circ\text{C}/68 \text{ }^\circ\text{F)}$$

$$\rho_{\text{UF}_6, 2} = 198.6 \text{ lb/ft}^3 \text{ (liquid, at } 131 \text{ }^\circ\text{C}/267.8 \text{ }^\circ\text{F)}$$

The pressure inside an empty 30B cylinder is 5 psi or less according to [USEC 651].

$$p_{\text{Air}, 0} = 5 \text{ psi}$$

The volume of UF_6 and air inside the 30B cylinder for a filling ratio of 50 % are then:

$$V_{\text{UF}_6, 1} = \frac{0.5 \cdot m_{\text{UF}_6, \text{max}}}{\rho_{\text{UF}_6, 1}} = \frac{0.5 \cdot 5020 \text{ lb}}{317.8 \text{ lb/ft}^3} = 7.90 \text{ ft}^3$$

$$V_{\text{Air}, 1} = V_{30B} - V_{\text{UF}_6, 1} = 26 \text{ ft}^3 - 7.90 \text{ ft}^3 = 18.10 \text{ ft}^3$$

The air pressure at 20 °C/68 °F is:

$$p_{\text{Air}, 1} = \frac{p_{\text{Air}, 0} \cdot V_{30B}}{V_{\text{Air}, 1}} = \frac{5 \text{ psi} \cdot 26 \text{ ft}^3}{18.10 \text{ ft}^3} = 7.18 \text{ psi}$$

The vapor pressure of liquid UF_6 at 131 °C/267.8 °F is interpolated linearly from Table 49:

$$p_{\text{UF}_6, 2} = 123.53 \text{ psi}$$

The volume and pressure of the air inside the 30B cylinder at 131 °C/267.8 °F are:

$$V_{\text{Air}, 2} = V_{30B} - \frac{0.5 \cdot m_{\text{UF}_6, \text{max}}}{\rho_{\text{UF}_6, 2}} = 26 \text{ ft}^3 - \frac{0.5 \cdot 5020 \text{ lb}}{198.6 \text{ lb/ft}^3} = 13.36 \text{ ft}^3$$

$$p_{\text{Air}, 2} = p_{\text{Air}, 1} \cdot \frac{V_{\text{Air}, 1} \cdot T_2}{V_{\text{Air}, 2} \cdot T_1} = 7.18 \text{ psi} \cdot \frac{18.10 \text{ ft}^3 \cdot 404.15 \text{ K}}{13.36 \text{ ft}^3 \cdot 293.15 \text{ K}} = 13.42 \text{ psi}$$

The total pressure at 131 °C/267.8 °F is the summation of the partial pressures:

$$p_{\text{Total}, 2} = p_{\text{UF}_6, 2} + p_{\text{Air}, 2} = 123.53 \text{ psi} + 13.42 \text{ psi} = 136.95 \text{ psi} = 0.94 \text{ MPa}$$

The admissible pressure for HAC is the test pressure specified in [ANSI N14.1]. The test pressure of 400 psi/2.76 MPa is applicable for the cylinder itself and for the valves. This testing pressure is then corrected for the elevated temperature of 131 °C/267.8 °F (above the design limit of 121 °C/250 °F) using the strength values for ASME SA516 Grade 55 according to [ASME BPVC]:

$$S_u(200 \text{ }^\circ\text{F}) = S_u(300 \text{ }^\circ\text{F}) = 55.0 \text{ ksi}$$

$$S_y(250 \text{ }^\circ\text{F}) = 27.0 \text{ ksi}$$

$$S_y(300\text{ }^{\circ}\text{F}) = 26.5\text{ ksi}$$

The yield strength at 131 °C/267.8 °F is interpolated linearly:

$$S_y(267.8\text{ }^{\circ}\text{F}) = \frac{(267.8\text{ }^{\circ}\text{F} - 250\text{ }^{\circ}\text{F})}{(300\text{ }^{\circ}\text{F} - 250\text{ }^{\circ}\text{F})} \cdot (26.5\text{ ksi} - 27.0\text{ ksi}) + 27.0\text{ ksi} = 26.82\text{ ksi}$$

The corrected limit for an elevated temperature of 131 °C/267.8 °F is then:

$$p_{\max,267.8\text{ }^{\circ}\text{F}} = 400\text{ psi} \cdot \frac{26.82\text{ ksi}}{27.0\text{ ksi}} = 397.36\text{ psi} = 2.74\text{ MPa}$$

The maximum pressure at 131 °C/267.8 °F is below the corrected admissible pressure of 2.74 MPa/397.36 psi with a safety margin of 2.90 for a filling ratio of 50 %.

The volume of UF₆ and of the air inside the 30B cylinder for a filling ratio of 100 % are:

$$V_{\text{UF}_6,1} = \frac{m_{\text{UF}_6,\max}}{\rho_{\text{UF}_6,1}} = \frac{5020\text{ lb}}{317.8\text{ lb/ft}^3} = 15.80\text{ ft}^3$$

$$V_{\text{Air},1} = V_{30\text{B}} - V_{\text{UF}_6,1} = 26\text{ ft}^3 - 15.80\text{ ft}^3 = 10.20\text{ ft}^3$$

The air pressure at 68 °F is:

$$p_{\text{Air},1} = \frac{p_{\text{Air},0} \cdot V_{30\text{B}}}{V_{\text{Air},1}} = \frac{5\text{ psi} \cdot 26\text{ ft}^3}{10.20\text{ ft}^3} = 12.74\text{ psi}$$

The vapor pressure of liquid UF₆ at 131 °C/267.8 °F is interpolated linearly from Table 49:

$$p_{\text{UF}_6,2} = 123.53\text{ psi}$$

The volume and pressure of the air inside the 30B cylinder at 131 °C/267.8 °F are:

$$V_{\text{Air},2} = V_{30\text{B}} - \frac{m_{\text{UF}_6,\max}}{\rho_{\text{UF}_6,2}} = 26\text{ ft}^3 - \frac{5020\text{ lb}}{198.6\text{ lb/ft}^3} = 0.72\text{ ft}^3$$

$$p_{\text{Air},2} = p_{\text{Air},1} \cdot \frac{V_{\text{Air},1} \cdot T_2}{V_{\text{Air},2} \cdot T_1} = 12.74\text{ psi} \cdot \frac{10.20\text{ ft}^3 \cdot 404.15\text{ K}}{0.72\text{ ft}^3 \cdot 293.15\text{ K}} = 249.40\text{ psi}$$

The total pressure at 131 °C/267.8 °F is the summation of the partial pressures:

$$p_{\text{Total},2} = p_{\text{UF}_6,2} + p_{\text{Air},2} = 123.53\text{ psi} + 249.40\text{ psi} = 372.93\text{ psi} = 2.57\text{ MPa}$$

The maximum pressure at 131 °C/267.8 °F is below the corrected admissible pressure of 2.74 MPa/397.36 psi with a safety margin of 1.07 for a filling ratio of 100 %. As this safety is calculated with the testing pressure specified in [ANSI N14.1], this safety also includes an additional safety margin because the testing pressure only utilizes a maximum of 95 % of the yield strength for primary stresses (cf. [ASME BPVC]).

Additionally, the safety margin for the 30B cylinder is investigated according to ASME Code Section VIII – Division 1 for the maximum internal pressure of 2.57 MPa.

The dimensions of the 30B cylinder are according to [ANSI N14.1]:

$$\text{Outer diameter: } D_o = 30\text{ in} = 762\text{ mm}$$

Nominal shell thickness: $t_{\text{nom}} = 1/2 \text{ in} = 12.7 \text{ mm}$

Minimum shell thickness: $t_{\text{min}} = 5/16 \text{ in} = 7.94 \text{ mm}$

Joint efficiency: $E = 0.85$ (spot RT as a minimum [ANSI N14.1])

Yield Strength at 131 °C $S_{y,131\text{ °C}} = 26.8 \text{ ksi} = 184.93 \text{ MPa}$
(interpolated linearly from [ASME BPVC])

At first, the cylinder itself is investigated. The outside radius R_o , the inside diameter D and the inside radius R are calculated to:

$$R_o = \frac{D_o}{2} = \frac{762 \text{ mm}}{2} = 381 \text{ mm}$$

$$D = D_o - 2 \cdot t_{\text{min}} = 762 \text{ mm} - 2 \cdot 7.94 \text{ mm} = 746.1 \text{ mm}$$

$$R = \frac{D}{2} = \frac{746.1 \text{ mm}}{2} = 373.1 \text{ mm}$$

The required wall thickness is then calculated according to the internal pressure design calculation of cylinders [ASME BPVC]. The formula and results are listed in Table 50:

Table 50: Required wall thickness for the cylinder for internal pressure

	Paragraph/ Appendix	Formula	Required Wall Thickness t_{req}	Safety
I	App. 1-1(1)	$t_{\text{req}} = \frac{p_{\text{max}} \cdot R_o}{S_y \cdot E + 0.4 \cdot p_{\text{max}}}$	6.06 mm	1.31
II	UG-27(1)	$t_{\text{req}} = \frac{p_{\text{max}} \cdot R}{S_y \cdot E - 0.6 \cdot p_{\text{max}}}$	6.16 mm	1.29
III	App. 1-2(1)	$t_{\text{req}} = R_o \left(1 - \exp \left(\frac{p_{\text{max}}}{-S_y \cdot E} \right) \right)$	6.18 mm	1.28
IV	App. 1-2(1)	$t_{\text{req}} = R \left(\exp \left(\frac{p_{\text{max}}}{S_y \cdot E} \right) - 1 \right)$	6.15 mm	1.29

Next, the dished heads are investigated. The inside crown radius L , the outside crown radius L_o , the inside knuckle radius r and the M-Factor are calculated to:

$$D = D_o - 2 \cdot t_{\text{min}} = 762 \text{ mm} - 2 \cdot 7.94 \text{ mm} = 746.1 \text{ mm}$$

$$h = \frac{D}{4} = \frac{746.1 \text{ mm}}{4} = 184.2 \text{ mm}$$

$$K = \frac{1}{6} \cdot \left[2 + \left(\frac{D}{2 \cdot h} \right)^2 \right] = \frac{1}{6} \cdot \left[2 + \left(\frac{746.1 \text{ mm}}{2 \cdot 184.2 \text{ mm}} \right)^2 \right] = 1.02$$

The required wall thickness is calculated according to [ASME BPVC]. The results are listed in Table 51:

Table 51: Required wall thickness for the dished heads for internal pressure

	Paragraph/ Appendix	Formula	Required Wall Thickness t_{req}	Safety
I	App. 1-4(1)	$t_{\text{req}} = \frac{p_{\text{max}} \cdot D_o \cdot K}{2 \cdot S_y \cdot E + p_{\text{max}} \cdot (K - 0.1)}$	6.25 mm	1.27
II	App. 1-4(1)	$t_{\text{req}} = \frac{p_{\text{max}} \cdot D \cdot K}{2 \cdot S_y \cdot E - 0.2 \cdot p_{\text{max}}}$	6.22 mm	1.28

The minimum safety factors calculated according to [ASME BPVC] are 1.28 for the cylinder and 1.27 for the dished heads for a pressure of 2.57 MPa at a temperature of 131 °C/267.8 °F.

Additional calculations are done for the solder connection between the valve and the cylinder. The ultimate tensile strength of the tin-lead-solder at room temperature is 42 MPa/6090 psi. With the conservative assumption, that the tensile strength is 0 MPa at the solidus temperature of 183 °C, the tensile strength at 131 °C is interpolated linearly:

$$S_u(131\text{ °C}) = \frac{(131\text{ °C} - 20\text{ °C})}{(183\text{ °C} - 20\text{ °C})} \cdot (42\text{ MPa} - 0\text{ MPa}) + 0\text{ MPa} = 28.6\text{ MPa}$$

The safety factor for the maximum internal pressure of 2.57 MPa is therefore 11.1 for the solder itself. Next, the solder connection is investigated:

The radius R for the solder connection is calculated as the middle radius at the beginning of the thread (dimensions according to [ANSI N14.1]). The thread roots shall be filled approx. half full, therefore the height h is the height of the solder at that radius:

$$R_i = 0.5 \cdot D_i = 0.5 \cdot 1 \frac{9}{64}\text{ in} = 14.5\text{ mm}$$

$$R_o = 0.5 \cdot D_o = 0.5 \cdot 1 \frac{1}{4}\text{ in} = 15.9\text{ mm}$$

$$R = \frac{R_i + R_o}{2} = \frac{14.5\text{ mm} + 15.9\text{ mm}}{2} = 15.2\text{ mm}$$

$$h = R - R_i = 15.2\text{ mm} - 14.5\text{ mm} = 0.70\text{ mm}$$

With at least 7 inserted threads (cf. [ANSI N14.1]), the thread area is calculated to:

$$A_l = 2 \cdot \pi \cdot R \cdot 7 \cdot h = 2 \cdot \pi \cdot 15.2\text{ mm} \cdot 7 \cdot 0.70\text{ mm} = 463.7\text{ mm}^2$$

The area the internal pressure is acting on is calculated with the outer ($D_{p,o}$) and inner diameter ($D_{p,i}$) of the valve the pressure is acting on:

$$\begin{aligned} A_p &= \frac{\pi}{4} \cdot (D_{p,o}^2 - D_{p,i}^2) = \frac{\pi}{4} \cdot \left(\left(1 \frac{1}{4}\text{ in} \right)^2 - \left(\frac{7}{8}\text{ in} \right)^2 \right) = \frac{\pi}{4} \cdot ((31.8\text{ mm})^2 - (22.2\text{ mm})^2) \\ &= 403.8\text{ mm}^2 \end{aligned}$$

The stress for the solder connection is then:

$$\tau_l = \frac{p_{max} \cdot A_p}{A_l} = \frac{2.57 \text{ MPa} \cdot 403.8 \text{ mm}^2}{463.7 \text{ mm}^2} = 2.24 \text{ MPa}$$

The strength of the solder connection is conservatively assumed to be 20 MPa (cf. [ROLOFF 2017]). The safety factor is then calculated to:

$$S = \frac{\tau_{lB}}{\tau_l} = \frac{20 \text{ MPa}}{2.24 \text{ MPa}} = 8.94$$

The admissible temperatures for the 30B cylinder, the valve and the plug are therefore set to 131 °C/267.8 °F. This admissible temperature is below the maximum temperatures defined in standards, hot-working temperatures and liquidus temperatures/melting points of the used materials and there is no danger of rupture because of a possible pressure build-up caused by elevated temperatures and melted UF₆ contents.

The admissible component temperatures for the package DN30 are summarized in Table 52 for RCT, NCT and HAC.

Table 52: Admissible component temperatures of the package DN30

Component	Material	Admissible temperature [°C]		Remark / Reference
		RCT and NCT	HAC	
Outer shell of the DN30 PSP	Type 304/1.4301	70 / 100 ¹⁾	900 ⁶⁾	70 °C for handling and RCT, 100 °C for the lifting lugs at the top half
Inner shell of the DN30 PSP	Type 304/1.4301	60 ¹⁾	900 ⁶⁾	-
Foam insulation	PIR foam	60 ²⁾	-	Appendix 1.4.2 (Material Data PIR Foam)
Thermal insulation	MICROTHERM®	60 ²⁾	1000	Appendix 1.4.4 (Material Data Microtherm Overstitched 1000R HY)
Intumescent material	Promaseal	150 ³⁾	600	Appendix 1.4.3 (Material Data Intumescent Material)
30B cylinder shell	Pressure vessel steel	64 ⁴⁾	131 ⁵⁾	-
Valve and plug	Body: aluminum bronze Stem: nickel copper alloy Solder: tin lead alloy	64 ⁴⁾	131 ⁵⁾	-

¹⁾ calculation temperature

²⁾ identical to temperature of shells

³⁾ temperature where the expansion of the intumescent material starts

⁴⁾ triple point temperature of UF₆

⁵⁾ covering maximum temperature for the components of the 30B cylinder (see calculation above)

⁶⁾ the hot forming of material Type 304/1.4301 is carried out at temperatures of 950 – 1200 °C. At 900 °C a sufficient strength remains, thus a deformation by own weight is not expected. The strength of the outer shell is neither relevant for the containment system nor for shielding and criticality safety.

2.2.2.2 Results of the thermal tests of specimens and prototypes

To support the thermal analyses conducted with FEM analyses, physical tests with specimens and prototypes of the DN30 package were carried out:

- Thermal tests with specimens of the technical foam used as shock absorbing material and thermal insulation documented in Appendix 1.4.2 (Material Data PIR Foam)
- Thermal tests with specimens of the intumescent material used as thermal insulation documented in Appendix 1.4.3 (Material Data Intumescent Material)
- Two thermal tests with prototypes of the DN30 package loaded with an empty 30B cylinder; one prototype without the Microtherm insulation layer and one fitted with the Microtherm thermal insulation. The DN30 prototypes were damaged at the valve side and the plug side by two consecutive HAC drop test sequences (the tests were carried out with a 30B cylinder loaded with 2277 kg surrogate material). The thermal test is documented in Appendix 2.2.2.1 (Thermal Test Program) and Appendix 2.2.2.2 (Thermal Test Report).

2.2.2.2.1 Preparation of the thermal test

2.2.2.2.1.1 Selection and preparation of the prototype for the thermal test

The thermal test prototypes were selected according to the following criteria:

- The prototype with the largest deformation (minimal remaining foam thickness) on the valve side.
- The prototype with the largest deformation (minimal remaining foam thickness) on the plug side.

The thermal test is carried out with prototypes which have been tested according to sequence 1 followed by testing according to sequence 2 as described in section 2.2.1.5.1.5.1 as drop test sequence 7 (see Figure 108 and Figure 109). This is a rather conservative approach, as these prototypes had therefore to withstand double the drop tests specified in [10CFR71] or [IAEA 2012] before submitted to the thermal test.

Designated “Benchmark 1” is the prototype with the Microtherm insulation layer tested in November 2017, “Benchmark 2” is the prototype without the Microtherm insulation layer tested in September 2016.



Figure 108: Thermal test prototype for Benchmark 2 after drop test sequence 7



Figure 109: Bottom half of the DN30 PSP before the thermal test

2.2.2.2.1.2 Differences between prototypes and series design of the DN30 package

The differences between the prototypes and the series design of the DN30 package were:

- The 30B cylinder was empty and did not contain any surrogate material.
- The fixation of the housing in the valve protecting device was provisional and did not comply with the series design (drawer design); however, size and position of the housing in the prototype complied with the series design.
- The rails protecting the intumescent material from damage in regular service were not present in the prototype.
- The additional bar and the gasket at the hinge of the valve protecting device preventing water ingress into the cavity of the DN30 PSP was not present.
- Due to deformations of the inner shell of the prototype for Benchmark 2 (small folds) the top half could not be installed on the bottom half in such a way that the original pins of the closure system could be inserted. Instead bolts with a smaller diameter than the original bolts had to be used. This problem did not occur for the prototype for Benchmark 1.
- Because of the non-fit of the original pins of the closure system of the prototype for Benchmark 2, the gap between the top half and bottom half was larger than the measured gap after the double drop test sequence 7 thus leading to a conservative simulation of heat transfer through the flange into the cavity. This problem did not occur for the prototype for Benchmark 1.

2.2.2.2.1.3 Temperature sensors

The DN30 prototypes as well as the 30B cylinder were equipped with temperature sensors. These temperature sensors were located:

- On the 30B cylinder body,
- On the valve of the 30B cylinder,
- On the plug of the 30B cylinder,
- On the outer surface of the DN30 PSP,
- At 15 cm from the outer surface of the DN30 PSP,
- At 1 m from the outer surface of the DN30 PSP.

The detailed sensors plan is supplied in Appendix 2.2.2.1 (Thermal Test Program) and in Appendix 2.2.2.2 (Thermal Test Report).

2.2.2.2.1.4 Test conditions of the thermal test compared to the test conditions required by [10CFR71] or [IAEA 2012]

The performance of the thermal test as required by [10CFR71] §71.73(c)(4) and [IAEA 2012] para. 728 is not feasible for the following reasons:

1. The thermal test cannot be performed with a kerosene fire but is carried out with a propane gas fire (environmental issues); this is allowed by [10CFR71] §71.73(c)(4) and [IAEA 2012] as it is shown in the SAR that the propane gas fire provided an equivalent total heat input to the package over a period of 30 minutes.
2. Several solar insolation cycles to reach a constant temperature pattern with the insolation defined in the Regulations cannot be reached under natural conditions; this was compensated by pre-heating the specimen up to 63 °C, which is higher than the temperature reached during several insolation cycles.
3. During the cooling phase, neither the solar insolation nor the ambient temperature of 38 °C can be reached under natural conditions; this condition is not specified in [10CFR71] §71.73(c)(4) but is allowed in [IAEA 2012] para. 728 to be corrected by analysis.

For compensation of the differences some measures are required:

1. The compliance of a propane gas fire must be demonstrated.

The compliance of a propane gas fire with the Regulations was shown in a paper presented at PATRAM 1992 [PATRAM92]. Here it was shown that the thermal flux of both fires is identical, and the thermal load for the propane gas fire is identical to a kerosene fire.

However, an important difference between a kerosene fire and a propane gas fire is the soot produced by the kerosene fire. This soot increases the surface absorptivity of the specimen considerably. [10CFR71] §71.73(c)(4) and [IAEA 2012] para. 728 require a coefficient not less than 0.8. Hence the outer surface of the DN30 prototypes was painted with a black coating satisfying this requirement (see Figure 110). The absorptivity of the black coating is certified to be higher than 0.8.



Figure 110: DN30 prototype for Benchmark 2 coated for the thermal test

2. Pre-heating of the DN30 prototypes before the thermal test to reach NCT conditions.

The preliminary thermal simulations for NCT show that the temperature inside the DN30 package reaches an average of 52 °C for the valve and plug, taking into account 12 h solar insulation/ 12 hour no solar insulation cycles. The maximum temperature calculated for NCT is 63 °C for the outer shell. Therefore, the DN30 prototypes were pre-heated with a heating jacket (see Figure 111 and Figure 112) to a uniform temperature of 63 °C.



Figure 111: DN30 prototype for Benchmark 1 in heating jacket propped up at fire test location



Figure 112: DN30 prototype for Benchmark 2 in heating jacket

3. Prolongation of the fire phase

The ambient temperature in the cooling phase is lower than 38 °C. Furthermore, there could be some wind during the cooling phase increasing the heat transfer from the DN30 prototypes to the environment and hence speeding up cooling down. To compensate for these influences on the thermal test, the duration of the fire phase was increased by 7.5 % from 30 min. to 32 min for the thermal test for Benchmark 2. Considering the average fire temperatures, this prolongation was deemed too conservative and therefore not used for Benchmark 1. However, due to the characteristics of the fire test installation, the actual duration of the fire phase was 32 min at the valve side and 34 min at the plug side.

2.2.2.2.2 Performance of the thermal test

The propane gas fire test was performed at the BAM test facility. Figure 113 shows the fire test and proves that the DN30 prototype is fully engulfed by the flames.



Figure 113: Picture of the fire test showing the full flame engulfment of the DN30 prototype for Benchmark 2

After the fire, the DN30 PSP was naturally cooled down, no artificial means were used. During the cooling phase, there was no rain which could have accelerated cooling-down but wind with a low wind speed accelerating the cool down.

During the cooling phase gases escaped through the openings of the thermal plugs of the DN30 as shown in Figure 114 and Figure 115.



Figure 114: Gases escaping from the DN30 prototype for Benchmark 1 during the cooling phase



Figure 115: Gases escaping from the DN30 prototype for Benchmark 2 during the cooling phase

For the fire test and cooling-down phase, the results are in detail:

- A full engulfment of the specimen;
- Benchmark 1: an average flame temperature of 934 °C, with a maximal temperature of 1085 °C;
- Benchmark 2: an average flame temperature of 977 °C with a maximal temperature of 1095 °C;
- No use of artificial means (like extinguishers) during the cooling phase;
- The thermal plugs behaved as expected; at the beginning of the fire they melted down and were pushed out by the foam decomposition gases. The DN30 prototypes showed no signs of overpressure indicating that the thermal plugs fulfilled their function;
- The temperatures reached inside the DN30 at the end of the fire are listed in Table 53 for Benchmark 1 and Table 54 for Benchmark 2.

Table 53: Temperatures at the 30B cylinder at the end of the fire (Benchmark 1)

Location	Min. Temperature [°C]	Max. Temperature [°C]
30B cylinder	74.3	88.1
Plug	78.4	79.3
Valve	73.3	85.9

Table 54: Temperatures at the 30B cylinder at the end of the fire (Benchmark 2)

Location	Min. Temperature [°C]	Max. Temperature [°C]
30B cylinder	75.2	173.3
Plug	104.2	106.8
Valve	91.8	104.2

2.2.2.2.3 Results of the thermal test

The intumescent material behaved as expected. The gaps between the 30B cylinder and the inner shell of the DN30 PSP were sealed with expanded intumescent material (see Figure 116 through Figure 120). The intumescent material in the valve protecting device expanded considerably and enclosed the valve completely. The intumescent material in the plug protecting device expanded as well considerably and enclosed the plug completely.



Figure 116: 30B cylinder inside the DN30 PSP after the thermal test with expanded intumescent material (Benchmark 1)



Figure 117: 30B cylinder inside the DN30 PSP after the thermal test (Benchmark 2)



Figure 118: Expanded intumescent material inside the plug protecting device (Benchmark 2)



Figure 119: Expanded intumescent material inside the bottom half of the DN30 PSP (Benchmark 2)

Benchmark 1 with the additional Microtherm insulation layer shows lower overall temperatures for the 30B cylinder, valve and plug. These results in less expansion of the intumescent material as seen when comparing the housing of the valve protecting device of the prototype for Benchmark 2 (Figure 119) to the housing of the prototype for Benchmark 1 (Figure 120).



Figure 120: 30B cylinder after the thermal test inside the bottom half (Benchmark 1)

No deformation of the 30B cylinder, the valve and the plug were documented after the thermal test.



Figure 121: 30B cylinder valve after the thermal test (Benchmark 2)

For the thermal test the results are in detail:

- The leakage rate after the thermal test is $Q_{st} = 6.63E-09 \text{ Pa}\cdot\text{m}^3/\text{s}$ (Benchmark 1) and $Q_{st} = 3.40E-05 \text{ Pa}\cdot\text{m}^3/\text{s}$ (Benchmark 2).
- The DN30 PSP could be opened without any further damage; the closure system was still working, and the top half could be easily lifted off the bottom half;
- The 30B cylinder could be removed from the DN30 PSP, the expanded intumescent material does not stick to the 30B cylinder;
- The intumescent material expanded and sealed all the gaps and free spaces in the DN30 prototype for Benchmark 2; for Benchmark 1, the intumescent material extended only slightly near the gap between top and bottom shell because of the lower overall temperatures;
- No deformation of the 30B cylinder, the valve or the plug was documented;
- The maximal temperatures reached inside the DN30 during the fire tests are listed in Table 55 for Benchmark 1 and Table 56 for Benchmark 2.

Table 55: Maximal temperatures at the 30B cylinder in the thermal test (Benchmark 1)

Location	Temperature [°C] at time after the start of the fire [min] (in brackets)
30B cylinder	176.8 (53)
Plug (close to thread)	144.1 (154)
Plug (tip)	144.1 (157)
Valve (close to thread)	130.3 (204)
Valve (tip)	130.9 (205)

Table 56: Maximal temperatures at the 30B cylinder in the thermal test (Benchmark 2)

Location	Temperature [°C] at time after the start of the fire [min] (in brackets)
30B cylinder	283.2 (55)
Plug (close to thread)	204.0 (135)
Plug (tip)	207.2 (123)
Valve (close to thread)	221.1 (119)
Valve (tip)	234.2 (131)

2.2.2.3 Results of the thermal analysis

2.2.2.3.1 Software

The thermal analysis is carried out with ANSYS Workbench 19.0 [ANSYS].

ANSYS Workbench is a software environment for performing linear and non-linear structural, thermal and electromagnetic analysis using the finite element method (FEM). The capabilities of ANSYS Workbench encompass geometry creation or optimization, meshing, setting up the finite element model, solving and reviewing the results. For thermal problems, ANSYS Workbench can solve steady-state as well as transient problems using two- or three-dimensional models. A model may include multiple materials, and the thermal conductivity, density, and specific heat of each material may be temperature-dependent. Materials may undergo change of phase. Thermal properties of materials may be entered as data or may be extracted from a material properties library. The boundary conditions, which may be surface-to-environment or surface-to-surface, may be specified temperatures or any combination of prescribed heat flux, forced convection, natural convection, and radiation. The boundary condition parameters may be time- and/or temperature-dependent. General grey body radiation problems may be modelled with user-defined factors for radiant exchange. Heat-generation rates may be dependent on time and position, and boundary temperatures may be time- and position dependent. Coupled-physics analysis are supported, e.g. structural-thermal, thermal-electric or thermal-diffusion. Additional functions, that are not available via the Workbench user interface can be included in the model using APDL (ANSYS parametric design language) command scripts.

For the validation of the model the results of two real world fire test with DN30 prototypes are used:

- The DN30 prototype is modelled as described below in section 2.2.2.3.2.
- The thermal conductivity of the foam is adjusted so that the temperatures at the 30B cylinder are close to the measured temperatures in the prototype.
- As the foam parts of the prototype burned during the fire test and in the cooling phase it was assumed that the foam acts as a thermal power source during that time. This thermal power is adjusted so that the maximal temperatures reached at the 30B cylinder and its components comply with the measured temperatures in the prototype.

2.2.2.3.2 Calculation model

For the calculation model, an axisymmetric two-dimensional model is used.

The axis of symmetry is the global y-axis which runs along the inner side of the model longitudinally through the center of the cavity. The radial direction is the global x-axis.

The outer diameter, the length over the skirts and the wall thickness of the 30B cylinder are identical to the dimensions specified in [ANSI N14.1] or [ISO 7195]. The cavity volume amounts to 0.736 m³, which is the minimum volume given in [ANSI N14.1] or [ISO 7195].

The inner and outer stainless-steel shells of the DN30 PSP are modelled with their original thickness; they are radial 2 mm and 10 mm for the inner shell, respectively, and 3 mm for the outer shell as well as axial 10 mm for the inner shell, 4 mm for the outer shell and 2 mm for the reinforcements separating the foam parts. The radii of inner and outer shell as well as their inner and outer length comply with the original design, too.

Details of the design such as the flange between top and bottom half or rotation preventing devices are not modelled.

Figure 122 shows the model used in the thermal analysis.

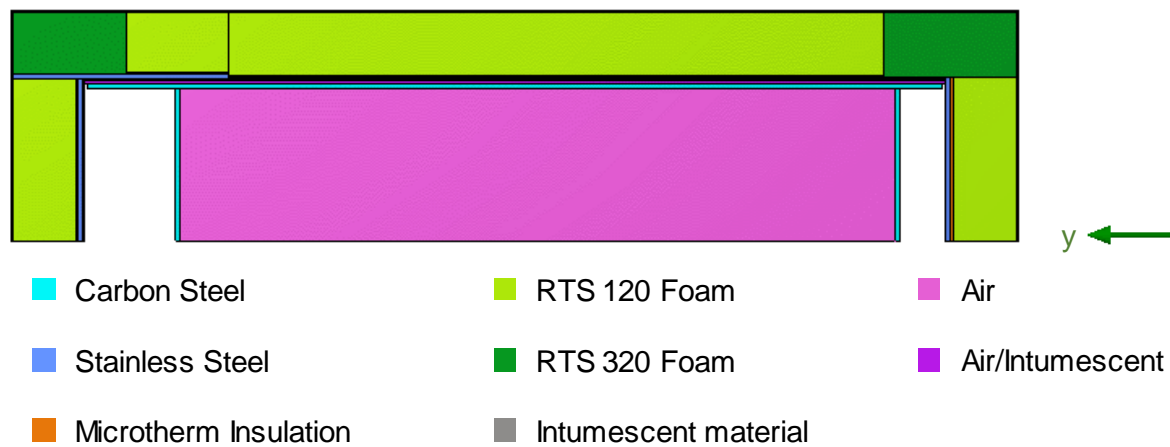


Figure 122: Geometry of the calculation model for the DN30 package, full view

The contacts between different components are modelled using standard bonded contacts, which use a pure penalty formulation, and symmetric behavior. The thermal conductance of the contacts is calculated by the program based on the material properties.

2.2.2.3.2.1 Initial temperatures

The initial temperatures for the steady state and transient calculations for RCT and NCT are uniformly 38 °C.

The initial temperatures for the transient calculations for HAC are:

- For the fire phase: uniformly 63 °C, the maximum temperature calculated for RCT and NCT boundary conditions.
- For the cooling phase: the temperatures at the end of the fire phase.

2.2.2.3.2.2 Heat generation

2.2.2.3.2.2.1 Heat generation of the radioactive content

The thermal power of the content is in all cases 3 W.

It is assumed that the UF₆ completely fills the cavity of the 30B cylinder. The volumetric heat source is hence calculated with a volume of 0.736 m³ (minimal certified volume of a 30B cylinder)

$$Q = \frac{P_{th}}{V_{min}} = \frac{3 \text{ W}}{0.736 \text{ m}^3} = 4.1 \text{ W/m}^3$$

2.2.2.3.2.2.2 Heat generation due to incineration of the foam

During the thermal test with the DN30 prototype incineration of the foam was observed. Hence, for HAC heat generation in the foam parts is included in the calculation model. Flames were visible for half an hour after the end of the fire phase, therefore the heat generation in the foam is active during the fire phase and during the first 30 min of the cooling phase.

To model the incineration front passing through the foam and to account for the loss of already incinerated foam not available for burning any more, a coupled thermal-diffusion analysis is used. The incineration of the foam is modelled using the formula below, which is based on the Arrhenius equation:

$$rate = A \cdot C \cdot e^{-B/T}$$

With

rate = rate constant

A = rate of the reaction

B = activation temperature

C = foam concentration

The heat generation in the foam parts is then calculated with the enthalpy of the reaction ENT:

$$HGen = rate \cdot ENT$$

The rate of foam consumed by incineration is calculated as a negative diffusion generation:

$$DGen = -rate$$

With the benchmark analysis documented in section 2.2.2.2 the heat generation rate of the foam is determined. The best fit to the measured temperature curves is reached for the factors listed in Table 57.

Table 57: Factors used for the calculation of the heat generation of the foam

Factor	Value
A	1.0e-3 s ⁻¹
B	300 °C
ENT	2.0e7 J

2.2.2.3.2.3 Solar insolation

The solar insolation data are specified in Table 58. They comply with [10CFR71] §71.71(c) or [IAEA 2012] para. 657. For the calculation of the initial temperatures for HAC a 12-hour insolation/ no insolation cycle as well as a constant solar insolation with the values listed in Table 58 was investigated.

Table 58: Solar insolation data

Surface orientation	RCT + NCT	Fire phase	Cooling down
Insolation for 12 hours per day [W/m ²]			
Vertical surfaces (valve and plug end)	200	-	200
All other surfaces (cylindrical surfaces)	400		400

2.2.2.3.2.4 Heat transfer to the ambient

2.2.2.3.2.4.1 Ambient temperature

The ambient temperature is defined in Table 59. For RCT, NCT and the cooling phase of HAC the ambient temperature is 38 °C according to [10CFR71] §71.73(a)(4) or [IAEA 2012] para. 656. For the fire phase of HAC the temperature is set to 800 °C according to [10CFR71] §71.73(c)(4) or [IAEA 2012] para. 728.

Table 59: Ambient temperature

RCT + NCT	Fire phase	Cooling down
Ambient temperature [°C]		
38	800	38

2.2.2.3.2.4.2 Radiation

The radiation coefficient of the outer surface of the DN30 package is 0.44 for RCT and NCT (stainless steel, rough surface). During the fire, the surface absorptivity is conservatively set to 1.0; the flame emissivity is set to 0.9 as required by [10CFR71] §71.73(c)(4) and [SSG-26] para. 728.28. The total radiation coefficient for the fire phase therefore is 0.9. In the cooling phase, the radiation coefficient is set to 0.8, as required by [10CFR71] §71.73(c)(4) and [SSG-26] para. 728.29 for soot covered surfaces. The radiation coefficients are listed in Table 60 below.

Table 60: Heat transfer by radiation at the surface of the DN30 package

RCT + NCT	Fire phase	Cooling down
Radiation coefficient [-]		
0.44	0.9	0.8

2.2.2.3.2.4.3 Convection

For the convective heat transfer for RCT and NCT as well as the cooling phase of HAC the formula given in [SSG-26] para. 728.31 is used.

$$Nu = 0.13 \cdot (Pr \cdot Gr)^{1/3}$$

For the convective heat transfer for the fire phase of HAC the formula given in [SSG-26] para. 728.30 is used.

$$Nu = 0.036 \cdot Pr^{1/3} \cdot Re^{0.8}$$

The pool fire gas velocity is assumed with 7.5 m/s, based on recommendations given in [SSG-26] para. 728.30 and [PATRAM86]. The resulting convection coefficients are considerably higher than the coefficient of 10 W/(m²·K) recommended in [SSG-26] para. 728.30 for large packages.

The resulting heat transfer coefficients are listed in Table 61.

Table 61: Heat transfer coefficients for the convective heat transfer

Temperature [°C]	RCT + NCT	Fire phase	Cooling down
	Heat transfer coefficient [W/(m ² ·K)]		
38.1	0.69	28.0	0.69
39	1.50	27.9	1.50
40	1.89	27.9	1.89
50	3.35	27.3	3.35
60	4.02	26.9	4.02
70	4.46	26.4	4.46
80	4.79	25.9	4.79
90	5.04	25.5	5.04
100	5.24	25.1	5.24
150	5.85	23.3	5.85
200	6.13	21.8	6.13
250	6.26	20.7	6.26
300	6.31	19.5	6.31
350	6.32	18.7	6.32
400	6.31	17.8	6.31
450	6.28	17.2	6.28
500	6.24	16.5	6.24
550	6.25	16.1	6.25
600	6.15	15.6	6.15
650	6.09	15.1	6.09
700	6.04	14.5	6.04
750	5.99	14.2	5.99

Temperature [°C]	RCT + NCT	Fire phase	Cooling down
	Heat transfer coefficient [W/(m ² ·K)]		
800	5.93	13.8	5.93
850	5.88	13.4	5.88
900	5.83	13.1	5.83
950	5.77	12.8	5.77
1000	5.72	12.5	5.72

2.2.2.3.3 Benchmark calculations

2.2.2.3.3.1 Benchmark model

For the benchmark calculations, the results of two thermal test with a prototype of the DN30 package are compared with the result of the analysis with ANSYS Workbench used in this report. These calculations are also used to adapt parameters of the model which cannot be derived from standards or literature so that the temperatures at safety relevant parts calculated with the benchmark model comply with measured values. In doing this, also the time-temperature curves of the model are compared with the thermal test results.

The thermal test is described in detail in Appendix 2.2.2.2 of the SAR.

For the benchmark calculations, the ambient conditions of the thermal test are used: the initial temperatures for the benchmark analysis are uniformly 63 °C.

In the benchmark the 30B cylinder is empty and contains only air as in the thermal test. The thermal power is hence zero.

The fire test designated “Benchmark 1” was conducted in November 2017 using a prototype having the same characteristics relevant for the thermal test as the production model with the Microtherm thermal insulation layer. The second prototype fire test, labelled “Benchmark 2” was conducted in September 2016 with a prototype without the Microtherm thermal insulation layer.

2.2.2.3.3.2 Results of the benchmark analysis

The results of the benchmark analysis for Benchmark 1 are shown in Figure 123, Figure 124 and Table 62.

Figure 123 shows an overview of the measured and calculated temperatures at the important temperature positions. The measured data are shown with a dashed line and marked with the initial BM (for benchmark). The calculated values are shown in the same color but with a solid line.

The measured temperature at the surface of the prototype is the average temperature of the four sensors placed at the surface of the prototype at the 0°, 90°, 180° and 270° position. The measured temperatures drop faster to ambient temperatures after the fire phase than the calculated temperatures because the temperature drop is not instant but modelled over a period of 10 s to allow for an easier convergence. The difference during cooling down is caused by the sensor positioning; while the temperature sensors are placed 15 cm from the DN30 package, the calculated temperature of the outer shell is derived directly from the relevant components.

The temperatures at the inner stainless-steel shell of the DN30 PSP were not measured in the thermal test. They are calculated and shown for information purposes.

Figure 124 shows the comparison of the measured and calculated temperatures at the mantle, the valve and the plug of the 30B cylinder. The measured curve of the temperatures of the 30B cylinder surface was used to determine the heat generation rates of the foam in the fire phase and the early cooling phase as well as the heat transfer between the DN30 PSP and the 30B cylinder. While the calculated temperature curves for valve and plug are in good agreement with the measured temperature in the fire test, the difference between the temperatures at the mantle is 5 % bigger. This is due to the different temperatures measured at the 30B mantle. While the bottom sensor at the 180° position reached its maximum of 120 °C after 13080 s, the sensor at the 270° position reached its maximum of 177 °C after 3300 s.

Table 62 shows the maximum temperatures at the important temperature positions as well as the time of their maximum in seconds after the start of the thermal test. The maximum temperatures and the times after which the respective maximum is reached are in very good agreement for the valve and plug of the 30B cylinder.

Figure 125 shows the calculated temperature distribution of the DN30 package at the end of the fire and Figure 126 shows the temperature distribution of the DN30 package around the time of maximum valve temperature.

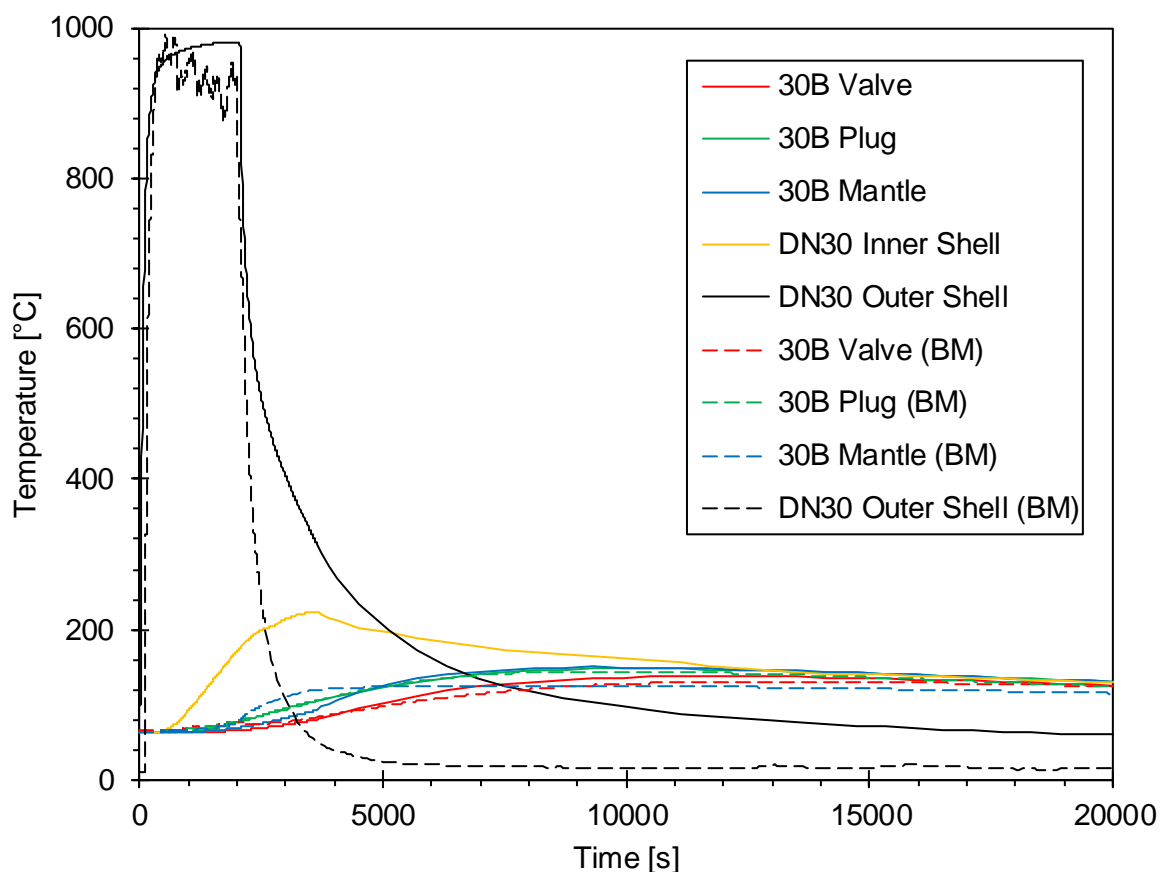


Figure 123: Measured and calculated temperatures at the prototype of the DN30 package for Benchmark 1 – fire phase and 5 hours cooling down

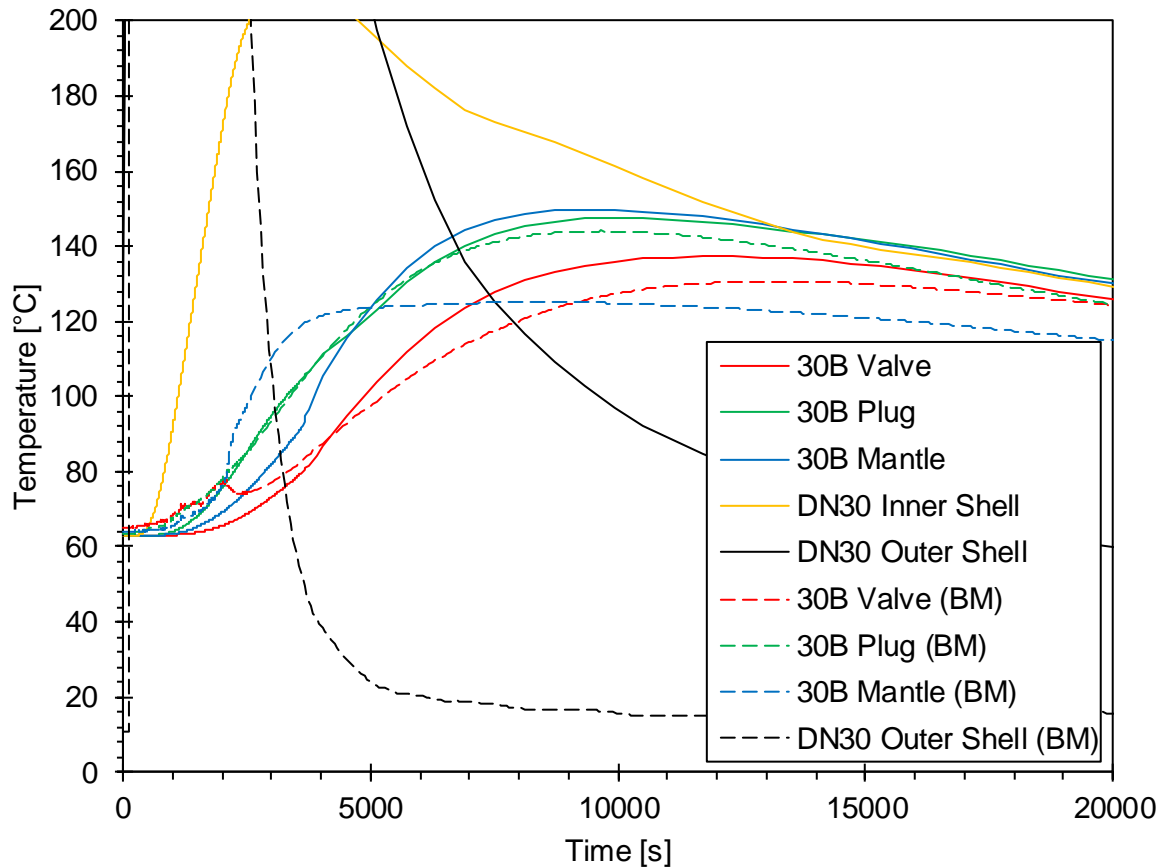


Figure 124: Measured and calculated temperatures at the prototype of the DN30 package for Benchmark 1 – fire phase and 5 hours cooling down; detail view

Table 62: Comparison of measured and calculated maximum temperatures during the test with the prototype of the DN30 package – Benchmark 1

Position	Benchmark calculation		Prototype test	
	Temperature [°C]	Time [s]	Temperature [°C]	Time [s]
Valve	137	12150	131	12680
Plug	148	9920	144	9450
Mantle 30B cylinder	150	9320	143	8505
Inner shell DN30 PSP	223	3630	-	-
Outer shell DN30 PSP	982	1820	992	470

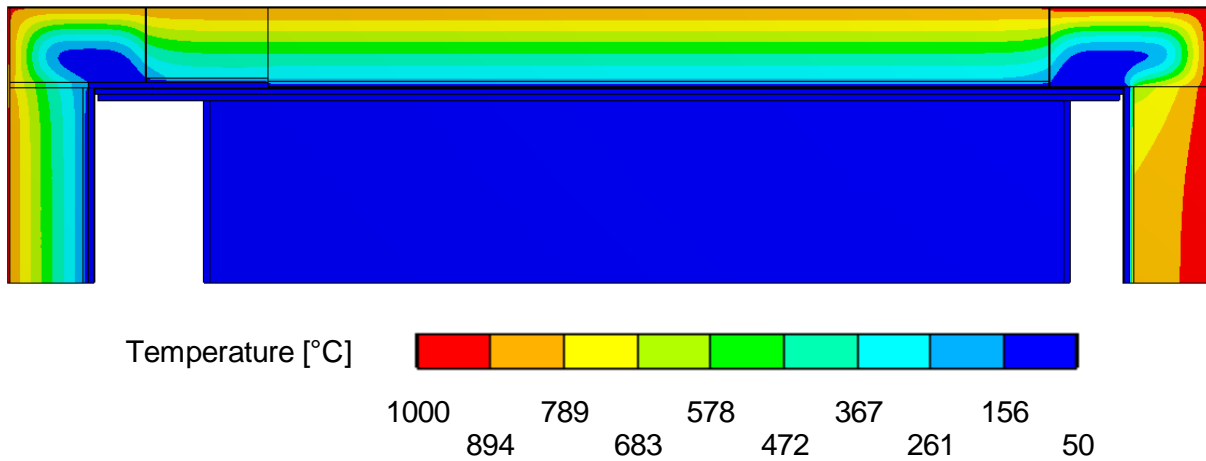


Figure 125: Temperature distribution at the DN30 package for Benchmark 1 at fire end (t = 1810 s)

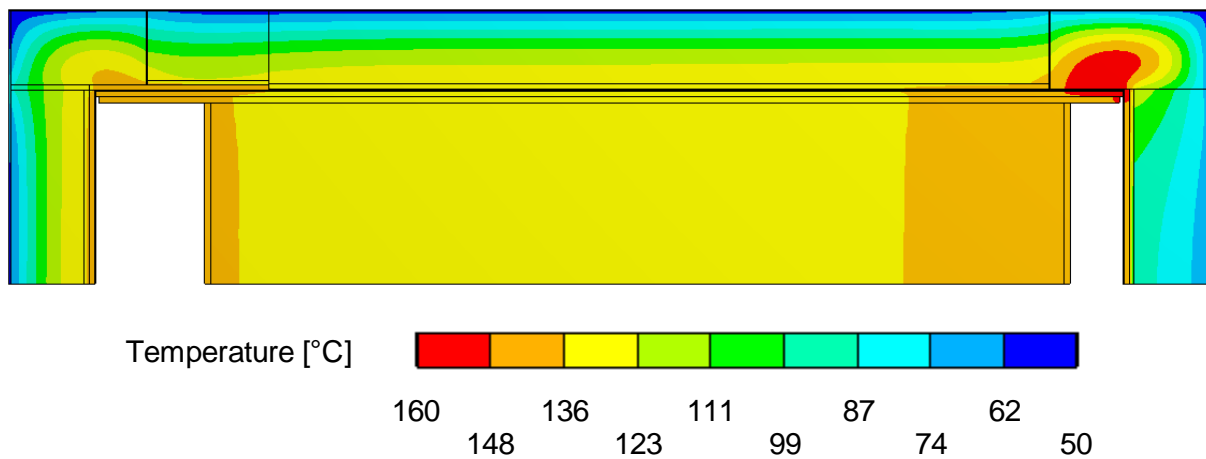


Figure 126: Temperature distribution at the DN30 package for Benchmark 1 around the time of maximal valve temperature (t = 11720 s)

The remaining foam concentration after the fire test is shown in Figure 127 for RTS 120 and in Figure 128 for RTS 320. The remaining concentrations are in relative good agreement with the prototype fire test shown in Figure 129 and Figure 130; the RTS 120 foam parts are burned to a higher degree than the RTS 320 foam parts, which are nearly unburned in some areas.

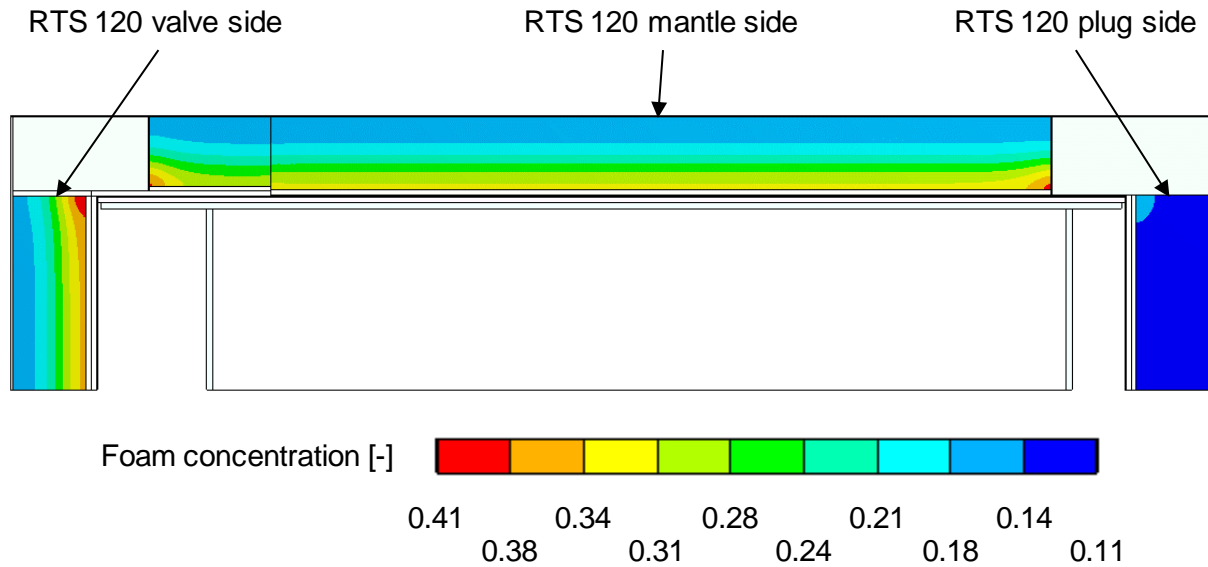


Figure 127: Remaining foam concentration after the fire test for RTS 120 for the Benchmark 1 calculation

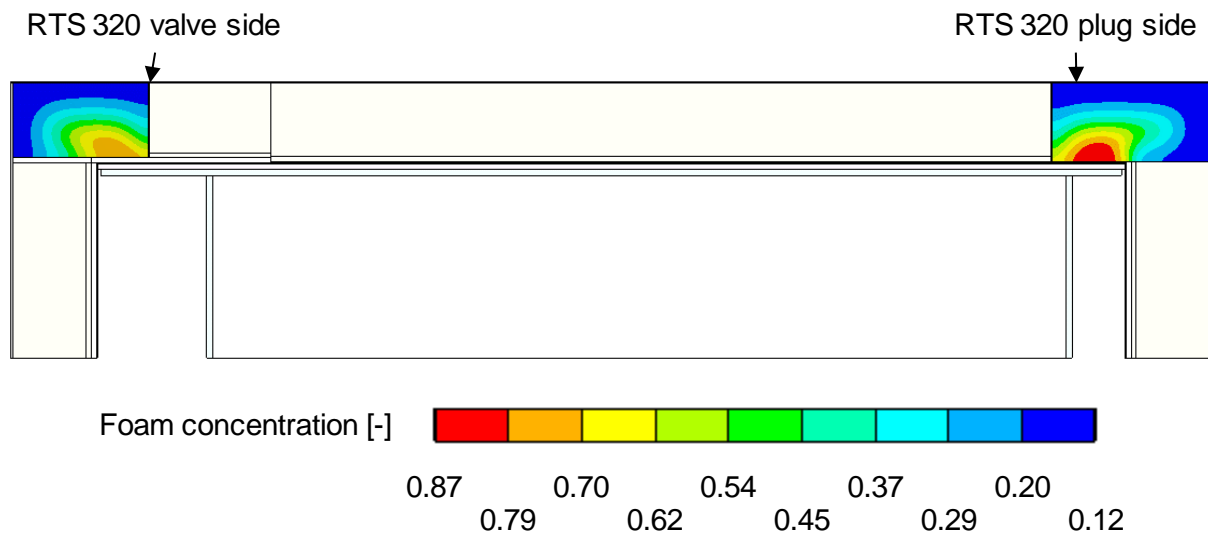


Figure 128: Remaining foam concentration after the fire test for RTS 320 for the Benchmark 1 calculation



Figure 129: Remaining foam after the prototype fire test for Benchmark 1 for RTS 120 mantle side, top shell

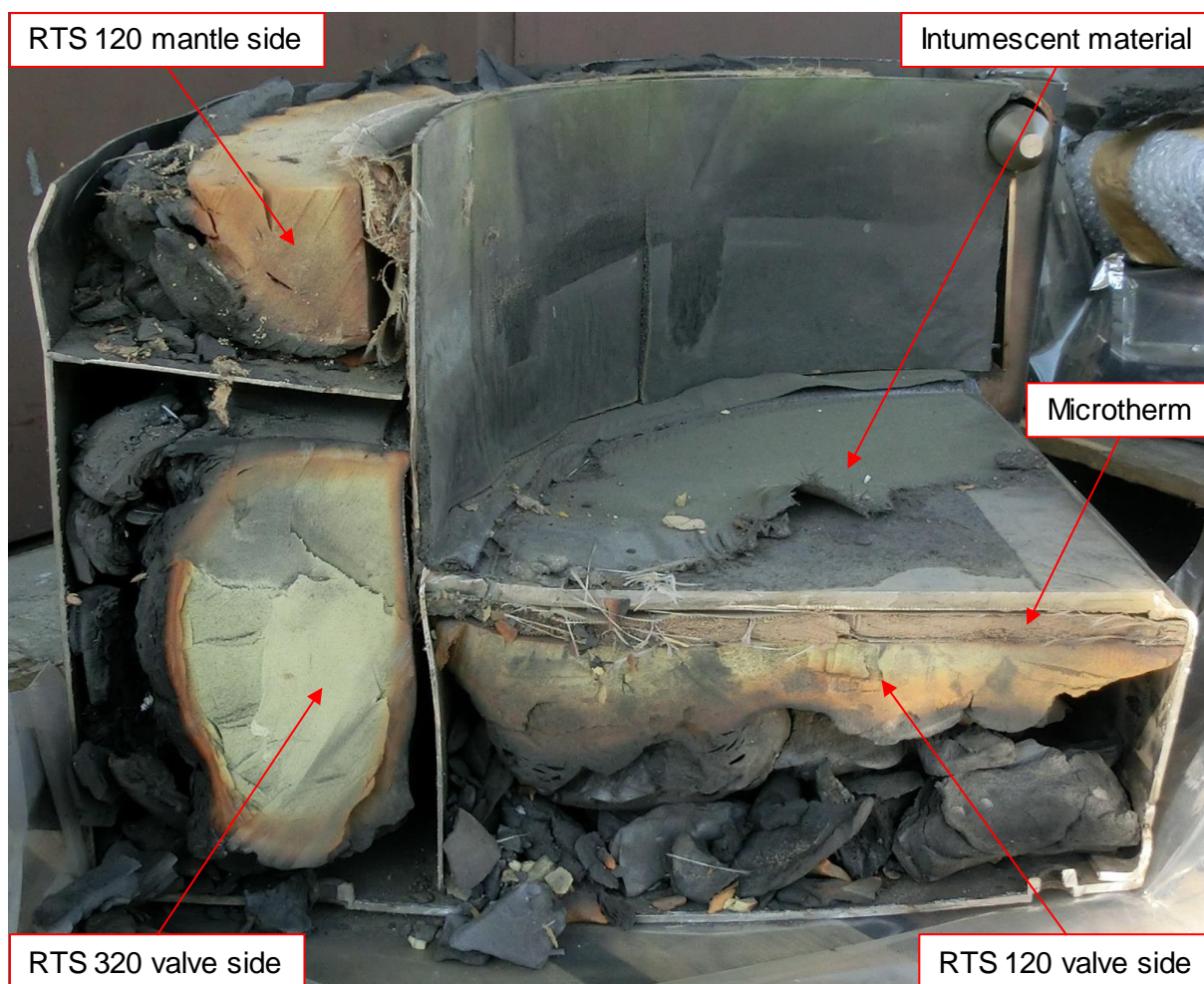


Figure 130: Remaining foam after the prototype fire test for Benchmark 1 for the valve side, bottom shell

The results of the analysis of Benchmark 2, conducted in September 2016, are shown in Figure 131 to Figure 134 and Table 64. The main difference between both benchmark prototype tests is, that the prototype for Benchmark 2 is not outfitted with the Microtherm insulation layer.

Figure 131 shows an overview of the measured and calculated temperatures at the important temperature positions like valve, plug, mantle of the 30B cylinder and DN30 outer shell. The measured data are shown with a dashed line and marked with the initial BM (for benchmark). The calculated values are shown in the same color but with a solid line.

The measured temperature at the surface of the prototype is the average temperature of the four sensors placed at the surface of the prototype at the 0°, 90°, 180° and 270° position. Compared to Benchmark 1, the average temperature of the outer shell is higher in the prototype fire test for Benchmark 2. The measured temperatures drop faster to ambient temperatures after the fire phase than the calculated temperatures because the temperature drop is not instant but modelled over a period of 10 s to allow for an easier convergence. The difference during cooling down is caused by the sensor positioning; while the temperature sensors are placed 15 cm from the DN30 package, the calculated temperature of the outer shell is derived directly from the relevant components.

The temperatures at the inner stainless-steel shell of the DN30 PSP were not measured in the thermal test. They are calculated and shown for information purposes.

Figure 132 shows the comparison of the measured and calculated temperatures at the mantle, the valve and the plug of the 30B cylinder. The measured curve of the temperatures of the 30B cylinder surface was used to determine the heat generation rates of the foam in the fire phase and the early cooling phase as well as the heat transfer between the DN30 PSP and the 30B cylinder. While the calculated temperature curves for valve and plug are in good agreement with the measured temperature in the fire test, the difference between the temperatures at the mantle is significantly bigger. This is due to the different temperatures measured at the 30B mantle. While the bottom sensor at the 180° position reached its maximum of 197 °C after 6240 s, the sensor at the 270° position reached its maximum of 283 °C after 3300 s.

Table 63 shows the maximum temperatures at the important temperature positions as well as the time of their maximum in seconds after start of the thermal test. The maximum temperatures and the times, after the respective maximum is reached are in very good agreement for the valve and plug of the 30B cylinder.

Figure 133 shows the calculated temperature distribution of the DN30 package at the end of the fire and Figure 134 shows the temperature distribution of the DN30 package around the time of maximum valve temperature.

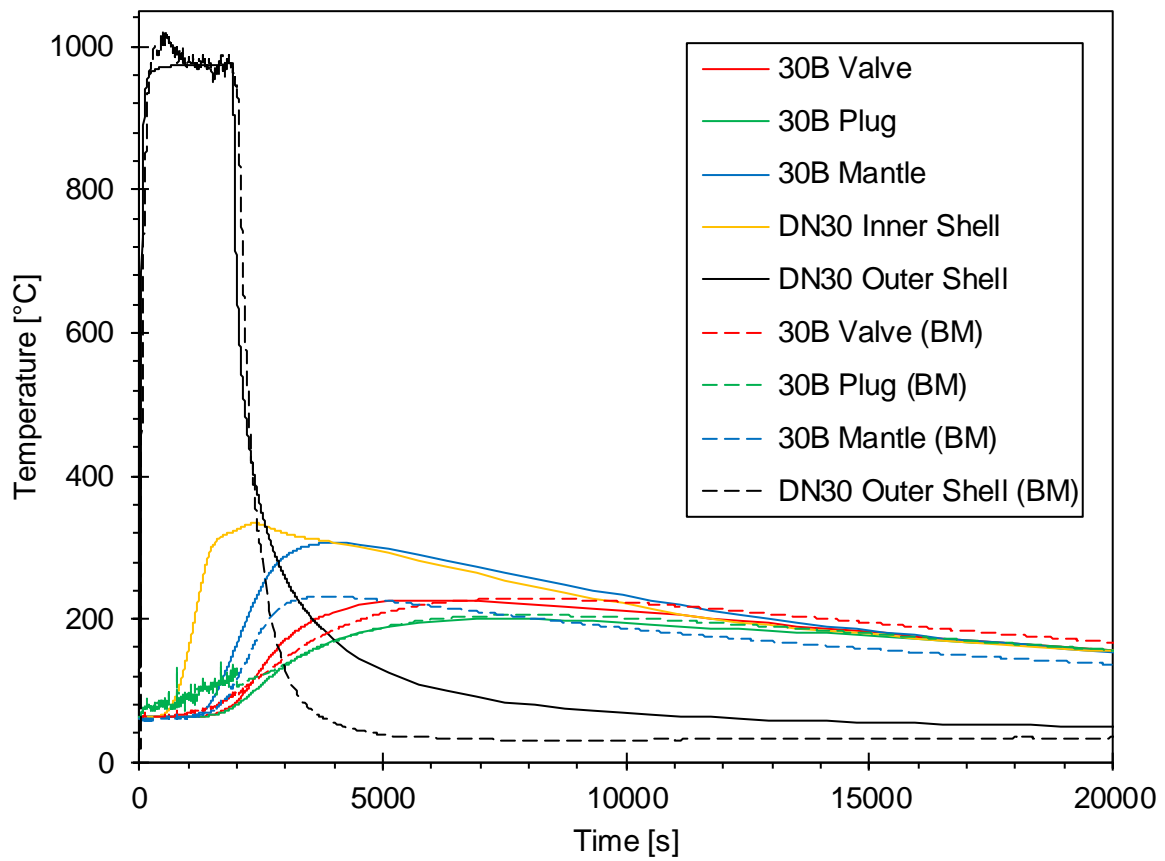


Figure 131: Measured and calculated temperatures at the prototype of the DN30 package for Benchmark 2 – fire phase and 5 hours cooling down

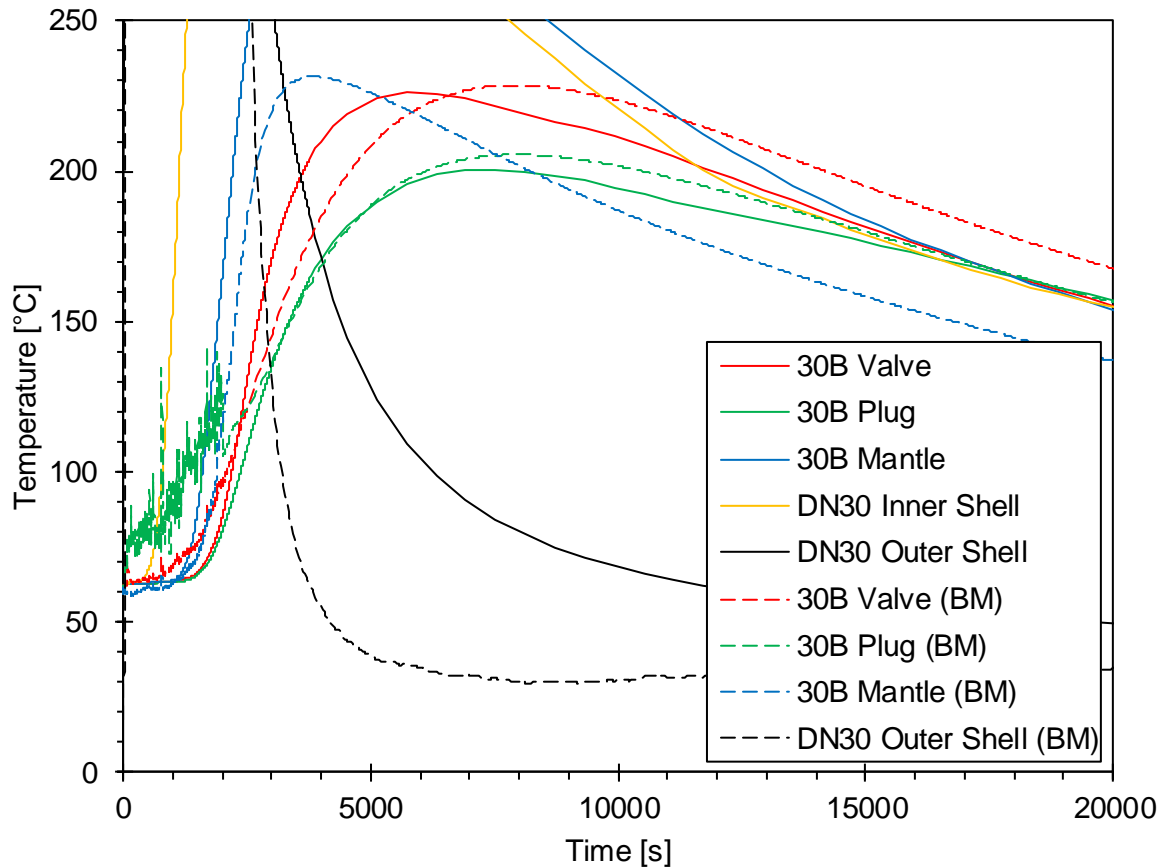


Figure 132: Measured and calculated temperatures at the prototype of the DN30 package for Benchmark 2 – fire phase and 5 hours cooling down; detail view

Table 63: Comparison of measured and calculated maximum temperatures during the test with the prototype of the DN30 package – Benchmark 2

Position	Benchmark calculation		Prototype test	
	Temperature [°C]	Time [s]	Temperature [°C]	Time [s]
Valve	226	5720	229	7740
Plug	200	7520	206	7740
Mantle 30B cylinder	307	3980	238	4050
Inner shell DN30 PSP	334	2350	-	-
Outer shell DN30 PSP	976	1920	1022	470

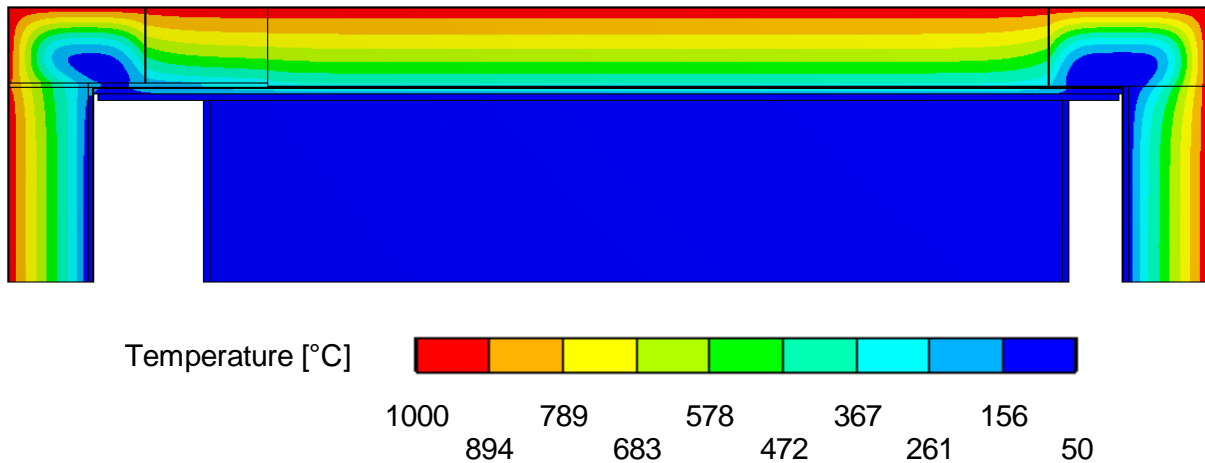


Figure 133: Temperature distribution at the DN30 package for Benchmark 2 at fire end (t = 1930 s)

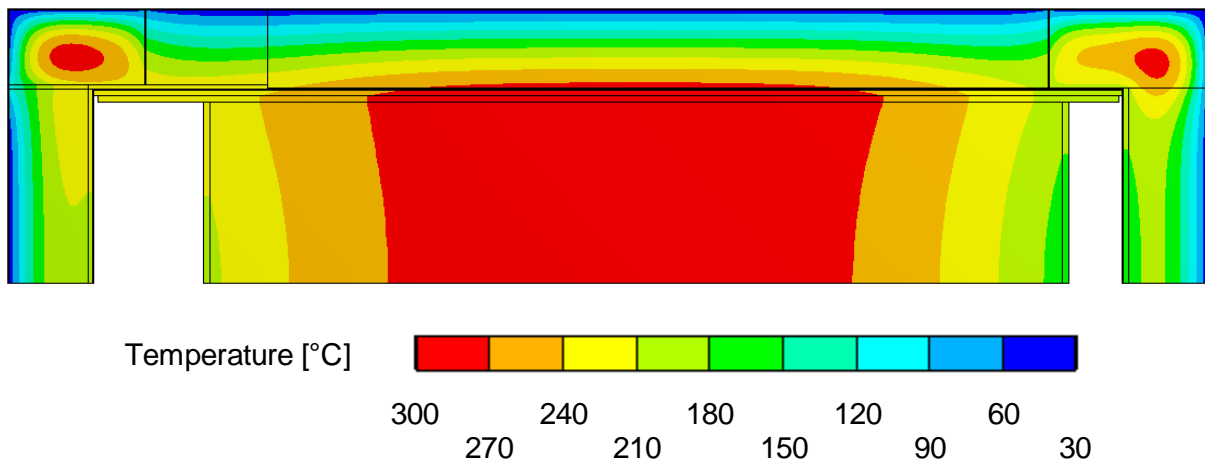


Figure 134: Temperature distribution at the DN30 package for Benchmark 2 around the time of maximal valve temperature (t = 5720 s)

The Benchmark models allow for a very good account of the fire tests. The calculated maximum temperatures in the critical valve and plug area as well as the times after which these maxima are reached are in very good agreement with the measured temperature curves. The calculated temperatures for the critical components are in good agreement with both Benchmark fire tests despite the considerable difference for the maximum temperatures for both tests, e.g. approx. 90 °C for the valve of the 30B cylinder.

The Benchmark models with the adjusted material properties of the foam and the parameters controlling the burning of the foam are therefore well suited for the thermal analyses of the DN30 package.

2.2.2.3.4 Calculations for RCT and NCT

2.2.2.3.4.1 Results without solar insolation

Due to the very low thermal power of the content the temperatures at the DN30 package are without solar insolation only slightly higher than the ambient temperature. The values are given in Table 64.

2.2.2.3.4.2 Results with solar insolation

The results for the cycle of 12 hours with insolation/ 12 hours without insolation according to [10CFR71] §71.71(c)(1) are shown in Table 64. The maximum temperature of 52 °C for a partially or completely filled 30B cylinder and for its components is reached after about 20 days. Hence, it can be assumed that the UF₆ remains solid under RCT and NCT conditions.

The maximum temperature of 63 °C complies with the initial conditions of the thermal test with a prototype.

Table 64: Temperatures at the DN30 package loaded with an empty, a partially filled and a filled 30B cylinder under RCT and NCT

Position	Temperature [°C]					
	Without insolation			12 hours insolation/ no insolation cycles		
	Empty 30B cylinder	Partially filled 30B cylinder (50 %)	Filled 30B cylinder (100 %)	Empty 30B cylinder	Partially filled 30B cylinder (50 %)	Filled 30B cylinder (100 %)
Valve	38	38	38	51	52	52
Plug	38	38	38	51	52	52
Mantle 30B cylinder	38	38	39	53	52	52
Volume 30B cylinder (UF ₆ /Air)	38	38	39	53	52	52
Inner shell DN30 PSP	38	38	38	56	56	56
Outer shell DN30 PSP	38	38	38	63	63	63

2.2.2.3.5 Calculations for HAC

2.2.2.3.5.1 Temperatures at the DN30 package for full and partially filled 30B cylinders

This calculation repeats the benchmark calculation with the ambient temperatures defined in [10CFR71] or [IAEA 2012]. The deviations from the benchmark calculations are

- The fire temperature is set to 800 °C; the duration is 30 min.
- In the cooling phase the ambient temperature is 38 °C with solar insolation as defined in Table 58.

The maximum temperatures are listed in Table 65 below.

Table 65: Maximum temperatures at the DN30 package loaded with an empty, partially filled and filled 30B cylinder

Position	Temperature [°C]		
	Empty 30B cylinder	Partially filled 30B cylinder (50 %)	Filled 30B cylinder (100 %)
Valve	124	115	112
Plug	122	112	108
Mantle 30B cylinder	126	121	120
Inner shell DN30 PSP	191	191	191
Outer shell DN30 PSP	789	789	789

The consequences of temperatures higher than the melting point of UF₆ (64 °C) and of temperatures higher than the design limit for normal operating conditions are investigated in the following section 2.2.2.3.5.2.

2.2.2.3.5.2 Pressure build-up inside the 30B cylinder

The maximum temperatures for the 30B cylinder, its components and the cavity are 126 °C for HAC conditions calculated according to the [10CFR71] and [IAEA 2012] guidelines (see section 2.2.2.3.5.1). As the melting point of UF₆ is 64 °C, melted UF₆ contents can lead to an increase in pressure. The pressure build-up caused by an increasing temperature and by the significant volume expansion of the UF₆ content during the solid-to-liquid phase change was investigated in section 2.2.2.1.4. In this section, the admissible temperature of the containment system was determined as 131 °C. Consequently, the calculated maximum temperature for the containment system during HAC of 126 °C is 5 °C below that admissible temperature.

For a filled (100 %) and partially filled (50 %) cylinder, the maximum temperature calculated for HAC does not exceed the design limit of 121 °C/250 °F specified in [ANSI N14.1] and is at least 10 °C below the admissible temperature of 131 °C (cf. Table 65).

For an empty cylinder and filling ratios up to 50 %, the maximum temperature calculated for HAC is at least 5 °C below the admissible temperature of the containment system of 131 °C.

Therefore, there is no danger of rupture for the maximum temperatures calculated for HAC.

2.2.2.4 Proof for the package DN30 to meet the requirements of [10CFR71]

2.2.2.4.1 Ambient temperatures and pressures

For the analysis an ambient temperature of 38 °C is taken into account (see section 2.2.2.3.2.4.1). Pressures which are likely to be encountered during RCT and NCT have no effect on the results of the thermal analysis. The requirements of [IAEA 2012] para. 616 (there is no equivalent para. neither in [10CFR71] nor [49CFR173]) are met.

2.2.2.4.2 Rupture of the containment system

A possible pressure build-up is investigated in section 2.2.2.1.4 for the calculation of the admissible temperature of the containment system and in section 2.2.2.3.5.2 for the maximum temperatures calculated for HAC. The maximum temperatures are below the admissible temperatures, the internal pressure is below the testing pressure specified in [ANSI N14.1] for the containment system and the wall thickness is above the required wall thickness calculated according to [ASME BPVC]. A possible pressure build-up due to melted UF₆ contents was taken into account. The requirements of [49CFR173] §173.420(a)(3) or [IAEA 2012] para. 632 c) are met.

2.2.2.4.3 Influence of the thermal test on the criticality safety analysis

The analysis in section 2.2.2.3.5 shows that the stainless-steel shells of the DN30 PSP as well as the carbon steel shell of the 30B cylinder are not affected by the thermal test in such a way that their thickness and density is reduced. It is verified in section 2.2.5 that taking into account this result of the thermal analysis criticality safety is ensured. In the criticality safety analysis, a complete loss of the foam is considered.

The requirements of [10CFR71] §71.55(d), §71.55(e) and §71.59(a)(2) or [IAEA 2012] para. 682 and 685 with respect to the thermal test are met.

2.2.2.4.4 Component temperatures of the DN30 package

The maximal component temperatures during RCT and NCT are at their maximum 63 °C for the DN30 PSP and 53 °C for the 30B cylinder and its contents (see section 2.2.2.3.4), and therefore lower than the admissible values specified in Table 52.

The maximum component temperatures of the DN30 PSP during HAC are close to the admissible temperatures defined in Table 52. However, tests with a prototype of the DN30 package showed that these temperatures have no negative effect on the function of the inner and outer shell of the DN30 PSP with respect to shielding or criticality safety.

The maximum temperature of the 30B cylinder shell is below the admissible temperature defined in Table 52. The temperatures of valve and plug thread are below the admissible temperature defined in Table 52, too.

2.2.2.5 Summary

In this report a calculation model for the DN30 package is developed based on the results of two real fire tests with prototypes of the DN30 package. The important parameters in this model are:

- For the foam between inner and outer shell of the DN30 PSP, incineration is modelled to achieve a good agreement with the temperatures of the fire test in the two benchmark analyses.
- The thermal conductivity is increased by a factor of 4 for the RTS 320 foam and by a factor of 5 for the RTS 120 foam at the plug side to achieve a good agreement of the temperature curves of the fire test in the benchmark analysis.

The temperatures calculated with the benchmark models and the temperature curves over time are in good agreement with the results of the fire tests as shown in section 2.2.2.3.3.2.

With this model the temperatures at the DN30 package are calculated with the ambient conditions specified in [10CFR71] or [IAEA 2012]. The maximum temperatures at relevant points of the DN30 package loaded with an empty 30B cylinder for ambient conditions according to [10CFR71] or [IAEA 2012] guidelines are below the maximum temperatures measured at the prototypes during the experimental fire tests. For the DN30 package loaded with a filled or partially filled cylinder, the temperatures are below the temperatures calculated for the empty 30B cylinder.

Sensitivity analyses show that even for a great reduction of the thickness of the Microtherm insulation layer from 10 mm to 2.5 mm, the maximum temperatures of the critical components are well below the temperature limit. If gaps up to double the size of a bar used for the free drop test for HAC are present in the Microtherm insulation layer, the maximum temperatures are below the temperature limit, too. Further sensitivity analyses show that variations in the range of +/-10 % for the thermal properties of the foams above 250 °C or for the parameters controlling the burning of the foam do have only minor impacts on the resulting temperatures.

In section 2.2.2.4 it is demonstrated that the DN30 package fulfils the requirements of [10CFR71] or [IAEA 2012] towards the thermal conditions under RCT, NCT and HAC loaded with a 30B cylinder containing any mass of UF₆ between zero and 2277 kg.

2.2.3 CONTAINMENT DESIGN ANALYSIS

The containment design analysis is valid for enriched uranium from uranium with natural isotopic composition and for all filling ratios from heels cylinders up to cylinders filled with the maximum amount of UF_6 defined in section 1.3. It covers RCT and NCT.

This section provides a summary of the main points and results of the containment analysis, documented in full detail in Appendix 2.2.3.1 (Containment Analysis). That appendix also includes results for contents with reprocessed uranium that are not used here.

2.2.3.1 Objective of verification

It is verified that the package complies with the requirements under NCT according to [10CFR71] §71.43(f) and [49CFR173] §173.412(j) or [IAEA 2012] para. 648 (a) when submitted to the tests according to [10CFR71] §71.71(c)(7) and §71.71(c)(9) and [49CFR173] §173.465(c) and §173.465(d) or [IAEA 2012] para. 722 and 723:

Prevent loss or dispersal of the radioactive content

It is specified in the Advisory Material for the IAEA Regulations for the Transport of Radioactive Material [SSG-26] para. 624.1, which refers to para. 648.2, that a maximum allowable leakage rate for normal transport conditions has never been defined quantitatively. In para. 646.3 it is specified that the intention of para. 622 (a) "is to ensure that under NCT the radioactive contents of the package cannot escape in quantities that may create a radiological hazard".

For type B packages a quantitative maximum allowable leakage rate is defined for NCT in [10CFR71] §71.51 or [IAEA 2012] para. 659 (a). This criterion is used in this report for type A packages. Hence the condition for the activity leakage rate is

$$LA_{NCT} \leq 10^{-6} A_2/h$$

For type A packages, there is no restriction on the radioactivity release under HAC due to the limit of $< 1 A_2$ for the whole content.

2.2.3.2 Calculation method

The containment design analysis is carried out according to [ISO 12807] in following steps:

- Step 1:** Determination of the radioactive inventory (see Appendix 1.3 (Radioactivity))
- Step 2:** Determination of the activity releasable rate
- Step 3:** Specification of the permissible activity release rate
- Step 4:** Determination of the permissible activity release rate due to leakage
- Step 5:** Determination of the activity concentration
- Step 6:** Determination of the maximal volume leakage rate
- Step 7:** Determination of the equivalent capillary diameter
- Step 8:** Evaluation of the permissible standard leakage rate

The package has no elastomeric gaskets; hence there is no permeation activity release rate to be considered.

2.2.3.3 Package data used for the analysis

The package data used for the analysis are listed in Table 66.

Table 66: Package data used for the containment design analysis under NCT

Item	Condition of cylinder	Value
Temperature	filled	64 °C
Free volume of cavity	filled	0.269 m ³
	heels	0.736 m ³
Design standard leakage rate	filled/heels	1.0E-4 Pa·m ³ ·s ⁻¹

2.2.3.4 Radioactive inventory, releasable radioactive inventory and activity concentration in the cavity atmosphere

The radioactive inventory, the derived releasable inventory and the respective activity concentration in the cavity atmosphere are listed in Table 67.

Table 67: Radioactive inventory, releasable radioactive inventory and activity concentration in the cavity atmosphere

Item	Condition of cylinder	Value
Radioactive inventory	filled	1 A ₂
	heels	1 A ₂
Releasable activity	filled	0.0024 A ₂
	heels	1 A ₂
Activity concentration	filled	0.0088 A ₂ /m ³
	heels	1.36 A ₂ /m ³

2.2.3.5 Permissible standard Helium leakage rates

The permissible standard Helium leakage rates are listed in Table 68.

Table 68: Permissible standard Helium leakage rates

Item	Condition of cylinder	Value
Required standard Helium leakage rate	filled	1.6E-01 Pa·m ³ /s
	heels	7.6E-04 Pa·m ³ /s

2.2.3.6 Measured standard Helium leakage rates after the regulatory tests

The standard Helium leakage rates measured after the regulatory tests for HAC are listed in Table 69. They cover the leakage rates expected under NCT.

Table 69: Measured standard Helium leakage rates after the regulatory tests for HAC

Test sequence	Standard helium leakage rate
Drop test sequence onto the valve corner	4.94E-09 Pa·m ³ /s
Drop test sequence onto the plug corner	4.15E-06 Pa·m ³ /s
Drop test sequence flat onto the valve side	4.91E-09 Pa·m ³ /s
Drop test sequence flat onto the closure system	7.09E-08 Pa·m ³ /s
Drop test sequence slap-down onto feet	1.37E-08 Pa·m ³ /s
Thermal test	6.63E-09 Pa·m ³ /s

2.2.3.7 Summary and evaluation of results

2.2.3.7.1 Loss of radioactive content under NCT

The containment design analysis presented in this section shows that the permissible activity release limits for NCT as defined in [10CFR71] and [IAEA 2012] and listed in chapter 2.2.3.1 are met for all contents specified in section 1.3 if the leakage rate of 1.0E-4 Pa·m³·s⁻¹ as specified in [ANSI N14.1] and [ISO 7195] is not exceeded.

Measurements show that leakage rates of the 30B cylinder are far below this limit, even after the regulatory tests for HAC.

2.2.4 EXTERNAL DOSE RATES ANALYSIS

The external dose rate analysis covers the DN30 package loaded with filled cylinders as well as cylinders containing heels under RCT and NCT. The analysis is valid for uranium with an enrichment of max. 5 wt%, commercial grade and covers all contents specified in section 1.3.

This section provides a summary of the main points and results of the external dose rate analysis, which is documented in detail in the full report contained in Appendix 2.2.4 (Dose Rate Analysis). The full report also includes results for contents with reprocessed uranium that are not used here.

2.2.4.1 Objective of verification

2.2.4.1.1 Verification for all types of packages

For DN30 packages loaded with 30B cylinders filled with UF_6 compositions complying with Table 1 or loaded with 30B cylinders containing heels of UF_6 complying with Table 1, it has to be verified that the limit value for RCT specified in [10CFR71] §71.47(a) and [49CFR173] §173.441(a) or [IAEA 2012], para. 526 is not exceeded:

$$TI \leq 10$$

which is equivalent to

$$DL \leq 0.1 \text{ mSv/h at a distance of 1 m from the external surface of the package}$$

It has to be verified that the limit value for RCT specified in [10CFR71] §71.47(a) and [49CFR173] §173.441(a) or [IAEA 2012], para. 527 is not exceeded:

$$DL \leq 2 \text{ mSv/h at cask surface}$$

It has to be verified that the limit values for RCT specified in [10CFR71] §71.47(b) or [IAEA 2012], para. 566 (b) are not exceeded:

$$DL \leq 2 \text{ mSv/h at any point on the external surface of the vehicle,}$$

$$DL \leq 0.1 \text{ mSv/h at any point 2 m from the vertical planes represented by the outer lateral surfaces of the vehicle, or, if the load is transported in an open vehicle, at any point 2 m from the vertical planes projected from the outer edges of the vehicle.}$$

Whenever calculations are performed for the vehicle, it is assumed that the external surface of the package coincides with the external surface of the vehicle. The package might be oriented with its longitudinal axis parallel or perpendicular to the longitudinal axis of the vehicle. In case of parallel orientation, two adjacent packages positioned face to face along their symmetry axis are considered. In case of perpendicular orientation four adjacent packages positioned side by side are considered.

2.2.4.1.2 Verification for type AF packages

It has to be verified that the package complies under NCT with the requirements according to [10CFR71] §71.43(f) and [49CFR173] §173.412(j) or [IAEA 2012] para. 648 (b), when submitted to tests according to [10CFR71] §71.71(a)(6)-(10) and [49CFR173] §173.465(a)-(e) or [IAEA 2012] para. 719 – 724:

$$\Delta DL \leq 20 \%,$$

where ΔDL is the increase in the maximal radiation level at any external surface of the package.

2.2.4.2 Assumptions for the calculations

The calculations of dose rates at the DN30 package and at the vehicle are based on the following assumptions:

2.2.4.2.1 Assumptions valid for all calculations

The following assumptions are valid for all calculations carried out throughout this report:

- The treated contents comply with the content description given in chapter 1.3.
- Based on [ANSI N14.1] / [ISO 7195], maximal dimensions are assumed for the modeled 30B cylinders. A conservative wall thickness of 1.1 cm is considered.
- Axial and radial dimensions of the 30B cylinder are identical under RCT and NCT.
- The skirts of the considered 30B cylinders, on the valve and the plug side respectively, are neglected. All 30B cylinders are assumed to have flat axial faces.
- The DN30 PSP is taken into account in the calculations, unless unshielded material is analyzed. In this case, neither the DN30 PSP nor the 30B cylinder is considered.

2.2.4.2.2 Assumptions for routine conditions of transport (RCT)

- For the polyisocyanurate rigid foam (PIC foam) a conservative density of 0.1 g/cm³ is assumed for all calculations. In fact, the PIC foam fitted in all parts of the DN30 PSP has a density higher than 0.1 g/cm³.

2.2.4.2.3 Assumptions for normal conditions of transport (NCT)

For NCT, taking into account the tests mentioned in [10CFR71] §71.71(a)(6)-(10) and [49CFR173] §173.465(a)-(e) or [IAEA 2012] para. 719 – 724, the following assumptions are made:

- Neither the shape of UF₆ inside the 30B cylinder nor the dimensions of the 30B cylinder are affected by the tests.
- A maximum admissible deformation is assessed for the PSP, up to which the dose rate increase remains within the admissible limit value.

2.2.4.3 Calculation method, its verification and validation

The calculation of dose rates at the DN30 package is carried out by means of the program system SCALE 6.1 [SCALE 2011]. The gamma and neutron source terms are determined by means of the depletion analysis sequence ORIGEN-ARP in the v7-27n-19g energy-group structure [SCALE 2011]. The dose rates are calculated by means of the analysis sequence MAVRIC.

Statistical errors, verification and validation are described in Appendix 2.2.4 (Dose Rate Analysis).

2.2.4.4 Gamma and neutron source terms

The gamma and neutron source terms needed for subsequent dose rate calculations are determined over a period of up to 10 years. This specific period is considered due to the source intensity of U-232 and its decay products reaching their maximum over this period of time. This way, arbitrary time periods are covered by the analysis.

Table 70 provides a list of the considered nuclides, as well as the contribution of their daughter nuclides.

2.2.4.4.1 Gamma source

The performed decay calculations of the nuclides of interest specified in Table 70 result in the gamma source terms needed for subsequent dose rate calculations. The gamma source intensities and the gamma energy release rates, given as a function of time, as well as the gamma spectra, are included in Appendix 2.2.4 (Dose Rate Analysis).

The total gamma energy release rate of U-235 increases slightly over the first 10 days before keeping a constant level over the rest of the considered time period. A similar behavior is observed for U-238: The total gamma energy release rate increases over the first 6 months approx. by a factor of 23, and then keeps a constant level. For U-232 an increase by a factor of approx. 620 is observed over the first 10 years. After this period of time the total gamma energy release rate decreases slowly. The total energy release rate of U-234 is constant over the considered time of 10 years. However, the contribution of the energy groups differs as time elapses and influences the dose rate of this nuclide.

The fission product Tc-99 has a nearly constant total gamma energy release rate over a period of 10 years.

Figure 135 shows the double logarithmic plot of the total gamma energy release rates as a function of the decay time over a period of 10 years.

Table 70: Nuclides and associated daughter nuclides considered for the determination of the source intensities

Nuclide	Daughter nuclides
Uranium nuclides	
U-232	Th-228 Ra-224 Rn-220 Po-216 Pb-212 Bi-212 Po-212 Pb-208 Tl-208
U-234	Th-230 Ra-226 Rn-222 Po-218 At-218 Rn-218 Pb-214 Bi-214 Po-214 Bi-210 Pb-210 Tl-210 Po-210 Pb-209 Bi-209 Pb-206 Tl-206 Hg-206
U-235	Pa-231 Th-231 Ac-227 Th-227 Ra-223 Fr-223 Rn-219 Po-215 Pb-211 Bi-211 Po-211 Pb-207 Tl-207
U-236	Th-232 Ra-228 Th-228 Ac-228 Ra-224 Rn-220 Po-216 Pb-212 Po-212 Bi-212 Tl-208 Pb-208
U-238	U-234 Th-234 Pa-234m Pa-234 Th-230 Ra-226 Rn-222 At-218 Po-218 Po-214 Pb-214 Bi-214 Pb-210 Po-210 Bi-210 Pb-206 Tl-210 Bi-209
Fission products	
Tc-99	Ru-99

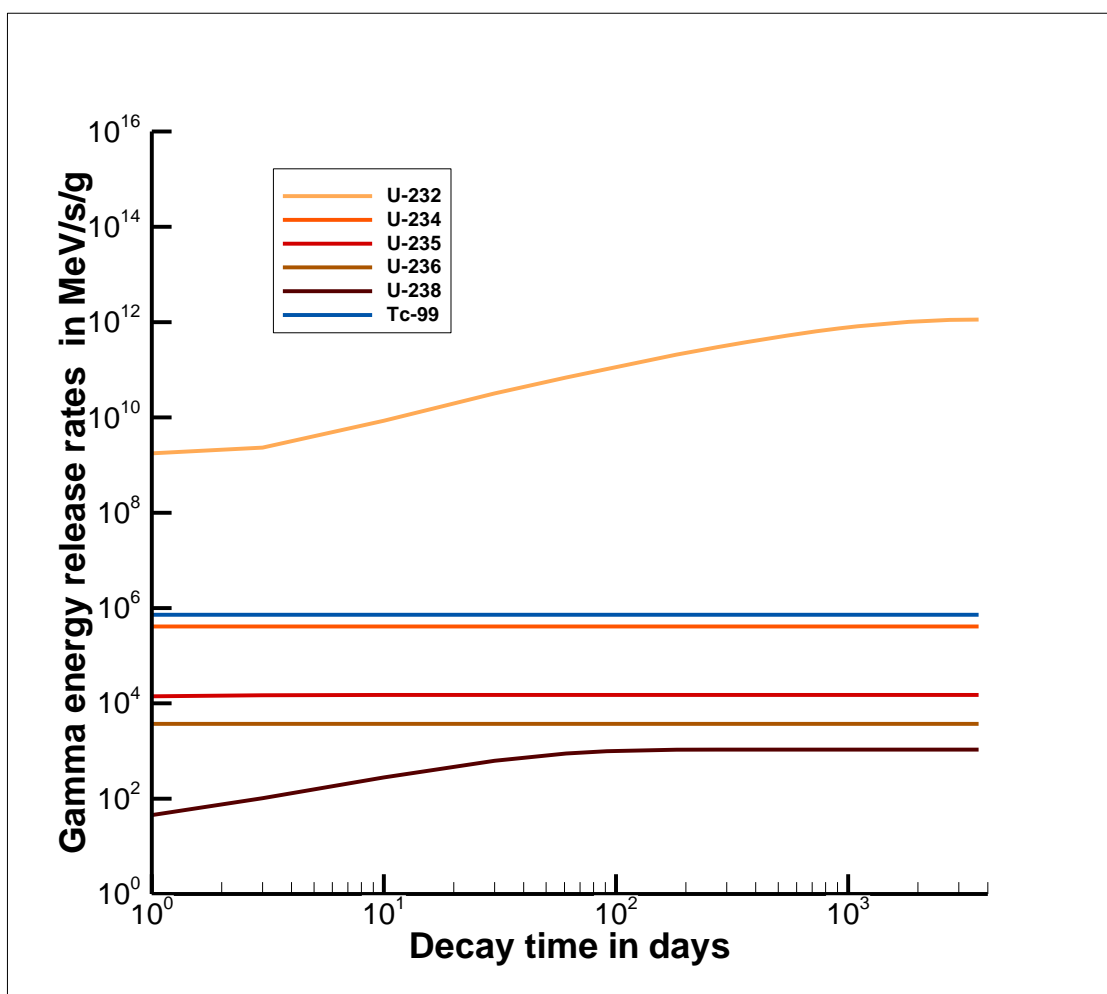


Figure 135: Total gamma energy release rates for initially 1 g of the uranium isotopes U-232, U-234, U-235, U-236, U-238 and the fission product Tc-99 in MeV/s over a period of 10 years

2.2.4.4.2 Neutron source

The uranium isotopes U-234, U-236 and U-238 have practically constant neutron source intensities over a period of 10 years. The neutron source intensity of U-235 increases slightly, for U-232 it increases constantly. Tc-99 does not have decays involving neutron production or release.

Figure 136 shows the double logarithmic plot of the total neutron intensities as a function of the decay time for the uranium isotopes over a period of 10 years.

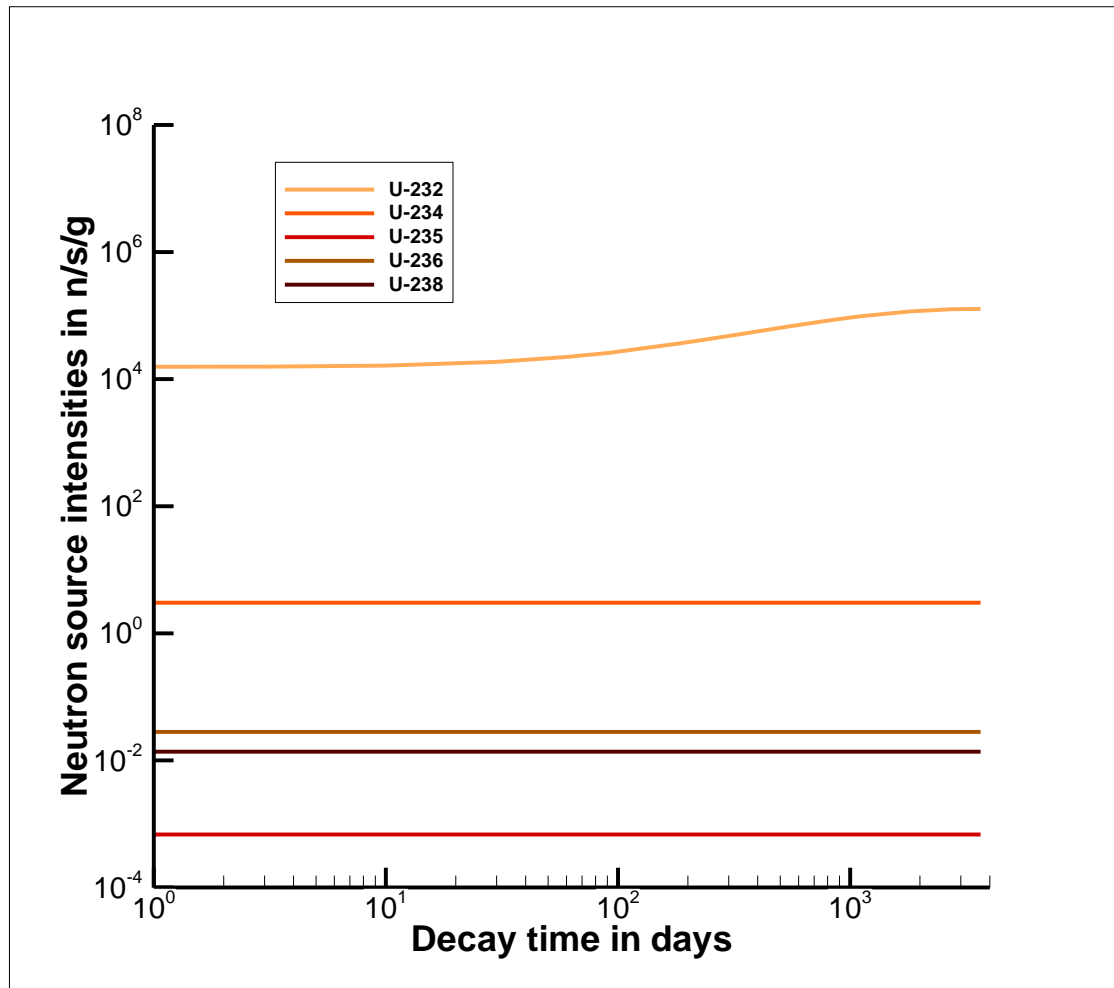


Figure 136: Total neutron source intensities for initially 1 g of the uranium isotopes U-232, U-234, U-235, U-236, U-238 in n/s over a period of 10 years

2.2.4.5 Model Specification

2.2.4.5.1 Geometrical models for the DN30 packaging

2.2.4.5.1.1 30B cylinder

Based on the dimensions of the 30B cylinder as specified in [ANSI N14.1] and [ISO 7195], a conservative 30B cylinder has been considered throughout the external dose rate analysis of the DN30 package. The 30B cylinder is simplified to a cylinder with flat heads. The modeled 30B cylinder is in compliance with the maximal dimensions specified in [ANSI N14.1] and [ISO 7195]. The skirts, valve, plug and nameplate are completely neglected.

2.2.4.5.1.2 DN30 PSP

The DN30 PSP has been modeled as simplified as possible. For this reason, neither the feet nor the six closure devices have been modeled even though they are made up of stainless steel and contribute to the attenuation of gamma radiation. Based on the condition of transport to be modeled, three types of DN30 PSPs have been considered throughout the external dose rate analysis of the DN30 package:

- RCT: In this case, the DN30 PSP is composed of two cylindrical shells of stainless steel with the full thickness of the foam insulation in between.
- NCT: Similar to for RCT; however, a reduction of the thickness of foam insulation by 5 cm is assumed so that the outer diameter is also reduced by 5 cm. The density of the foam is conservatively kept unchanged.

2.2.4.5.2 Geometrical models for the content

2.2.4.5.2.1 Dose rate at unshielded material

For the calculation of the dose rate at the unshielded material, a cylindrical shape of the UF₆ is considered. The source is homogeneously distributed within the UF₆.

2.2.4.5.2.2 Filled cylinder under RCT and NCT

The calculation model used for the filled cylinder under RCT and NCT is a completely filled 30B cylinder without any void at the top of the UF₆. The source is homogeneously distributed within the UF₆.

2.2.4.5.2.3 Cylinder containing heels under RCT and NCT

For heels, three models were investigated:

- 1) The heels material distributed over the whole inner surface of the cylinder as a thin layer.
- 2) The heels material accumulated in the form of a 0.1 cm thick puddle at the bottom of the cylinder.
- 3) The heels material distributed over the inner surface of a front side of the cylinder.

2.2.4.6 Dose rate profiles

In order to assess the maximum dose rates at the DN30 package, dose rate profiles were calculated showing the levels of dose rate around the package.

Figure 137 shows the dose rate profile for a single DN30 package. This profile shows that the maximum radiation level is to be expected at the center of the side of the package. The axial dose rate is about a factor of 3 lower than the radial dose rate.

Figure 138 shows the dose rate profile of a possible transport configuration with two packages arranged face to face, and Figure 139 shows the dose rate profile for the standard transport configuration four packages on a flat-rack side by side. From the profile it can be seen that the dose rate at the surface of the vehicle (equivalent to the surface of the DN30 packages) is not affected by the adjacent packages and hence identical to the dose rate at the surface of a single package.

However, the dose rate in 2 m distance from the vehicle is higher than the dose rate in 2 m distance from the single package. The maximal dose rate in 2 m distance from the vehicle is for the face to face configuration about the factor 1.5 higher than for the single package. For the configuration of four packages side by side, the factor is about 3.1. However, it must be noted that the radial dose rate for the face to face configuration of two packages is still higher than the axial dose rate for the side by side configuration of four packages.

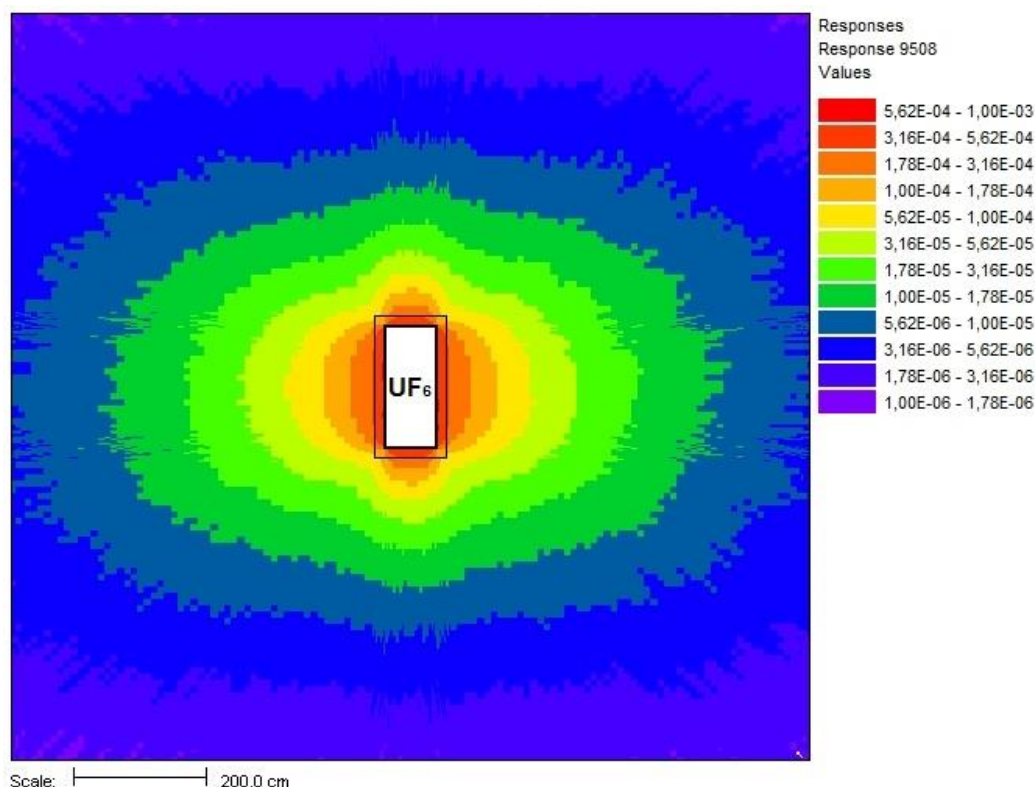


Figure 137: Gamma dose rate profile for the package DN30 loaded with a 30B cylinder completely filled with UF₆ (normalized source strength)

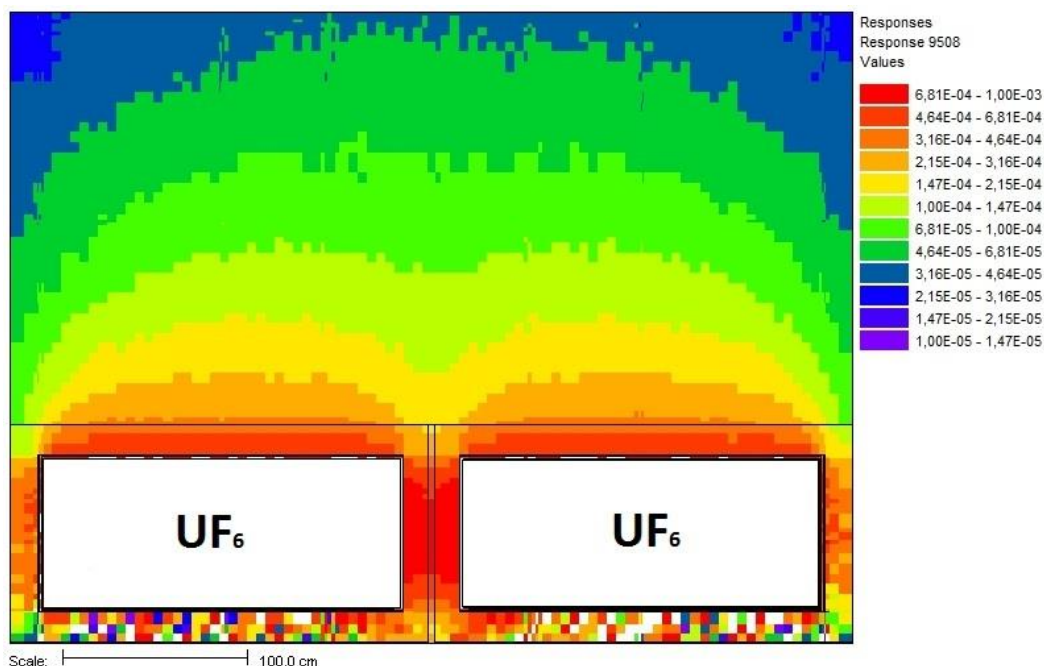


Figure 138: Axial gamma dose rates for two packages DN30 positioned face to face (normalized source strength) – possible transport configuration

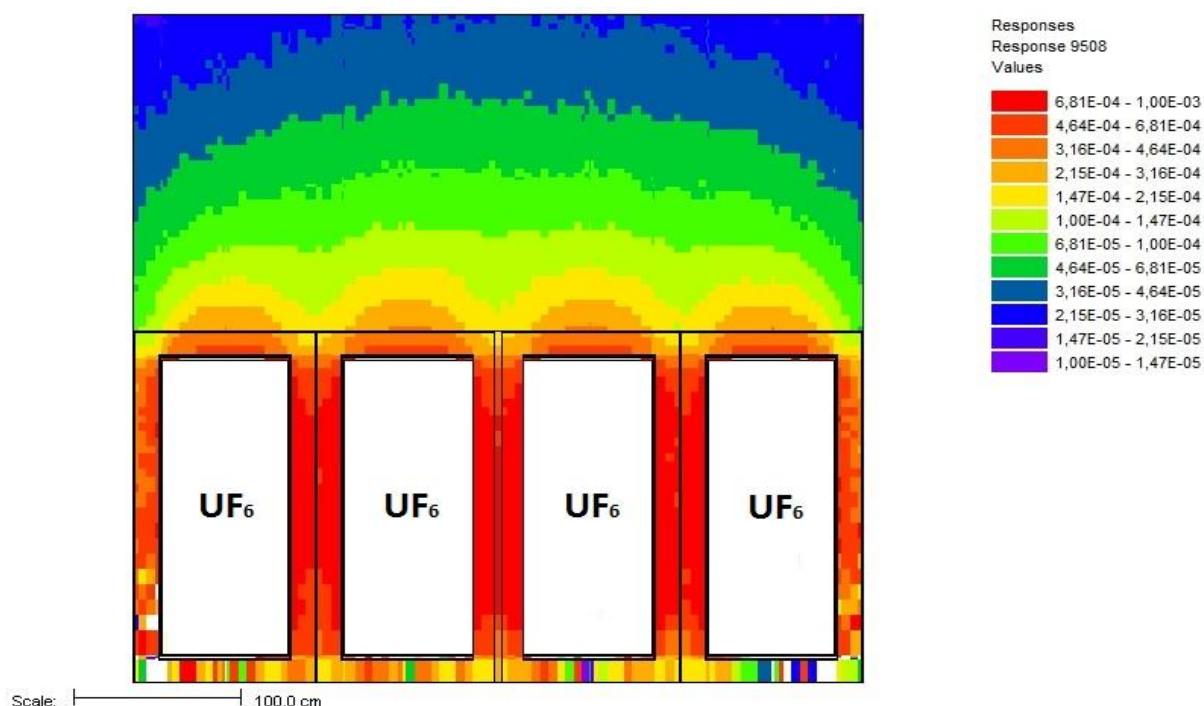


Figure 139: Axial gamma dose rates for four packages DN30 positioned side by side (normalized source strength) – standard transport configuration

2.2.4.7 Verification of compliance with the dose rate limits

2.2.4.7.1 General results of the dose rate calculations

- Maximal dose rates are dominated by the gamma contribution; the contribution from neutrons amounts to less than 4 % of the total dose rates.
- Both for filled 30B cylinders and for 30B cylinders containing heels, all objectives of verification are met with large safety margins.

2.2.4.7.2 Verification of the dose rates according to [10CFR71] §71.47(a) and [49CFR173] §173.441(a) or [IAEA 2012], para. 526

The maximal total dose rates at a distance of 1 m from the surface of the DN30 package loaded with a 30B cylinder filled with UF₆ or heels of UF₆ complying with Table 1 are listed in Table 71.

For the DN30 package loaded with a filled 30B cylinder, the transport index is equal to 0.3 and the transport of the DN30 package loaded with a 30B cylinder containing UF₆ complying with Table 1 may be carried out under non-exclusive use.

For the DN30 package loaded with a 30B cylinder containing heels, the transport index is equal to 3.6 and the transport of the DN30 package loaded with a 30B cylinder containing heels of UF₆ complying with Table 1 may be carried out under non-exclusive use.

Table 71: Maximal dose rates at 1 m distance from the external surface of the DN30 package under RCT loaded with a 30B cylinder containing UF₆

UF ₆ Composition	Total dose rate [μSv/h]
Table 1	2.9
Heels of compositions Table 1	36
Limit value (for non-exclusive use)	100

2.2.4.7.3 Verification of the dose rates according to [10CFR71] §71.47(a) and [49CFR173] §173.441(a) or [IAEA 2012], para. 527

The maximal total dose rates at the surface of the DN30 package loaded with a 30B cylinder filled with UF₆ or heels of UF₆ complying with Table 1 are listed in Table 72.

The calculated dose rates are below the limit value. The objective of verification is met.

Table 72: Maximal total dose rates at the surface of the DN30 package loaded with a 30B cylinder containing UF₆ or heels of UF₆

UF ₆ Composition	Total dose rate [μSv/h]
Table 1	12.4
Heels of compositions Table 1	311
Limit value (for non-exclusive use)	2000

2.2.4.7.4 Verification of the dose rates according to [10CFR71] §71.47(b) or [IAEA 2012], para. 566 (b)

Maximal total dose rates at the external surface of the vehicle (equivalent to the dose rate at the external package surface) loaded with DN30 packages each loaded with a 30B cylinders filled with UF₆ or containing heels of UF₆ are listed in Table 73.

The dose rates are below the limit of 2000 µSv/h; the objective of verification is met.

Table 73: Maximal total dose rates at the external surface of a vehicle loaded with DN30 packages loaded each with 30B cylinders containing UF₆ or heels of UF₆

UF ₆ Composition	Total dose rate [µSv/h]
Table 1	12.4
Heels of compositions Table 1	311
Limit value	2000

Maximal total dose rates at 2 m distance from the external surface of the vehicle loaded with four DN30 packages loaded each with a 30B cylinder filled with UF₆ or containing heels of UF₆ are given in Table 74.

The dose rates are below the limit of 100 µSv/h. The objective of verification is met.

Table 74: Maximal total dose rates at 2 m distance from the external surface of a vehicle loaded with DN30 packages loaded each with 30B cylinders containing UF₆ or heels of UF₆

UF ₆ Composition	Total dose rate [µSv/h]
Table 1	1.3
Heels of compositions Table 1	19
Limit value	100

2.2.4.7.5 Verification according to [10CFR71] §71.43(f) and [49CFR173] §173.412(i) or [IAEA 2012], para. 648 (b)

The increase of the dose rate after the tests simulating normal conditions of transport is evaluated under two scenarios:

1. In scenario 1 a filled cylinder is analyzed under the conservative assumption of a deformation of the outer shell of 50 mm and thus a reduction of the distance of the envelope of the UF_6 to the surface of this amount. The calculated increase of the total dose rate is in this case 16.7 %.

The maximum possible gap between 30B cylinder and inner shell of the DN30 PSP is 33 mm. Hence, even under the assumption of a deformation and a movement of the 30B cylinder of 33 mm the resulting reduction of the distance of the envelope of the UF_6 to the surface of the DN30 package would be with 39 mm smaller than the value of 50 mm used in the assessment. It can hence be concluded that the increase of the maximal dose rate can be expected to be less than the admissible limit of 20 %.

2. In scenario 2 a 30B cylinder containing heels is analyzed considering highly conservative assumptions:
 - The heels quantity is concentrated in a puddle so that the radioactivity is as close as possible to the outer surface of the 30B cylinder. For the 30B cylinder the minimum diameter taking into account the tolerances specified in [ANSI N14.1] and [ISO 7195] is considered.
 - It is assumed that the 30B cylinder is oriented under RCT in such a way, that the distance of the radioactive puddle to the closest point on the outer surface of the DN30 PSP is maximized. This is achieved when the puddle is at 12 o'clock position and the 30B cylinder is in contact with the inner shell of the DN30 PSP at 6 o'clock position (ref. Figure 140 - left side).
 - It is assumed that under NCT the drop orientation is such that the impact is at 12 o'clock position and the distance between the radioactive puddle and the surface of the DN30 PSP is reduced by
 - The relative movement of the 30B cylinder with respect to the inner shell of the DN30 PSP from 6 o'clock to 12 o'clock position allowed by the gap between the DN30 PSP and the 30B cylinder (ref. Figure 140 - right side),
 - The deformation of 6 mm of the outer shell of the DN30 PSP caused by the 1.2 m free drop distance. In the structural analysis, a maximal reduction of the distance between inner and outer shell of the package of 4 mm was calculated (see section 2.2.1.4.2.2). Conservatively, a distance reduction of 6 mm is assumed for the dose rate analysis.

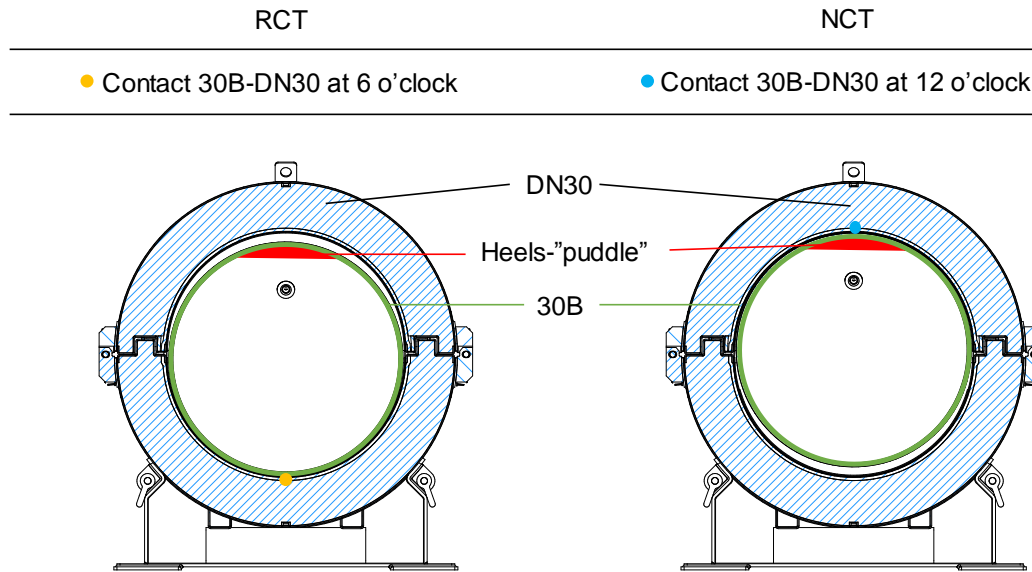


Figure 140: Comparison between DN30 package loaded with 30B cylinders containing heels, contact with the inner shell at 6 o'clock position (left side) and at 12 o'clock position (right side)

This hypothetical calculation model results in an increase of the dose rate at the surface of the DN30 package of 19.7 %, hence the increase of the dose rate is also for this model less than the admissible limit of 20 %.

2.2.4.8 Summary and evaluation of results

The analysis performed in this section shows that the dose rate limits as defined in [10CFR71] and [49CFR173] or [IAEA 2012] and listed in section 2.2.4.1 are complied with for all contents specified in chapter 1.3.

The calculated dose rates at the DN30 package containing full cylinders or cylinders containing heels are always less than the dose rate limits. The assessment covers also multiple refilling of cylinders containing heels with new product.

2.2.5 CRITICALITY SAFETY ANALYSIS

The criticality safety analysis is documented in the full report in Appendix 2.2.5 (Criticality Safety Analysis). In this section a summary of this report describes the main points and results of the analysis.

The analysis

- covers RCT, NCT and HAC taking into account a maximal enrichment of 5 wt. % U-235 in uranium,
- is valid for enriched uranium from uranium with natural isotopic composition,
- is valid for UF₆ containing up to 0.5 wt.% volatile impurities (HF) and additional hydrogenated uranium residues from the reaction of humidity with UF₆ accumulated during the time period between recertifications,
- is valid for all filling ratios from heels cylinders up to cylinders filled with the maximum amount of UF₆ defined in section 1.3.

2.2.5.1 Objective of verification

The criticality safety of the package DN30 is proved according to [10CFR71] §71.55 and §71.59 or [IAEA 2012], para. 673. For RCT, NCT and HAC following criticality safety criterion is complied with:

$$k_{\text{eff}} + 3 \sigma + \Delta k \leq 0.95$$

For the proof of criticality safety, systematical deviations Δk of the calculation method have to be considered [DIN 25478]. The systematical deviations are determined in [DAHER 2019-2] by comparison of calculation results with benchmark experiments. This analysis, summarized in section 2.2.5.3, results in a systematical deviation of $\Delta k = 0.0129$. Accordingly, the safety criterion can be expressed as:

$$k_{\text{eff}} + 3 \sigma \leq 0.9371$$

It is shown that taking into account credible and hypothetical conditions of the arrangement of the UF₆ in the cylinder, the composition and density of UF₆ and the distribution of hydrogenated uranium residues:

- The DN30 package fulfills the criticality safety criterion for a 30B cylinder with a wall thickness down to a minimal value of 7.94 mm.

2.2.5.2 Assumptions for the proof of criticality safety

The proof of criticality safety for the DN30 package is based on following assumptions:

2.2.5.2.1 Assumptions valid for all calculations

The following assumptions are valid for all calculations carried out in the following chapters:

- The admissible number is $N = \text{infinite}$.
- The content is enriched UF₆ with an enrichment of maximal 5 wt.% U-235 in Uranium.
- Volatile impurities in the UF₆ are defined in [ASTM C996] with maximal 0.5 wt.%; these impurities are considered to consist only of HF.

- Other impurities created during the filing and extracting operations, i. e. hydrogenated uranium residues (HUR) are also determined and considered (see section 2.2.5.4.2.3).
- The 30B cylinder might be completely or partially filled with UF_6 . For the partially filled 30B cylinder, there might be a void on top of the UF_6 . A cylindrical void at the center of UF_6 is also considered.
- The density is varied between 3.1 g/cm^3 (equivalent to a cylinder having a certified minimal volume of 0.736 m^3 completely filled with 2277 kg UF_6) and a theoretical density of 5.5 g/cm^3 extrapolated from given data at different temperatures to $-40 \text{ }^\circ\text{C}$.
- Axial and radial dimensions of the 30B cylinder are the same under RCT, NCT and HAC.
- The skirts of the cylinder on the valve and plug side are neglected for the simplified calculation model. In this model the cylinder is assumed to have flat axial faces.
- For heterogeneous distributions of impurities, the shape of the cylinder heads is modeled closer to reality and the skirts are modeled.
- The valve and plug as well as the name plate are neglected in all calculation models.
- In case the DN30 PSP is taken into account, water might penetrate freely into the gap between the cylinder and the PSP or into the foam of the PSP.

2.2.5.2.2 Assumptions for the analysis of the single package under RCT, NCT and HAC

The proof for the package under RCT, NCT and HAC is carried out for the dry, fully reflected package.

The following assumptions are valid for the single package in isolation:

- The 30B cylinder or DN30 package is surrounded by a 20 cm water reflector.
- There is no water ingress into the 30B cylinder under RCT and NCT.
- Ingress of water in larger volumes into the cavity of the 30B cylinder is not assumed as the mechanical analysis shows that [10CFR71] §71.55(b) and §71.55(g) or [IAEA 2012] para. 680 (b) (i) is met.

Based on the standard leakage rate of $10^{-4} \text{ Pa}\cdot\text{m}^3/\text{s}$ for 30B cylinders and immersion under a head of 15 m water for 8 hours, a maximal amount of water ingress of 3 g is calculated. Compared to the homogeneous impurities of 11385 g HF (0.5% of 2277 kg UF_6) and 3908.3 g HUR considered throughout the criticality analysis, this is negligible and was, accordingly, not further taken into account.

2.2.5.2.3 Assumptions for 5 x N packages under NCT

The proof is carried out for an infinite number of packages under HAC according to section 2.2.5.2.4. The proof for 5 x N = infinite number of packages under NCT is covered by the proof for 2 x N = infinite number of packages under HAC.

2.2.5.2.4 Assumptions for 2 x N packages under HAC

The proof is carried out for 2 x N = infinite number of packages under HAC. The proof is based on the conditions of the packages after the tests required to demonstrate their ability to withstand HAC.

The following assumptions are made for HAC, taking into account the tests mentioned in [10CFR71] §71.59(a)(2) or [IAEA 2012], para. 685 (b):

- The shape of the UF₆ inside the 30B cylinder may change arbitrarily.
- The dimensions of the 30B cylinder are not affected by the tests.
- The thickness of the inner and outer steel shells of the DN30 PSP remain unchanged, however the PIC foam is completely neglected and the inner and outer shell are collapsed to a single shell. The position of this collapsed shell is varied (contact to the surface of the 30B cylinder or gap between surface and shell).
- Water ingress due to the immersion under a head of 15 m water for 8 hours according to [10CFR71] §71.73(c)(6) or [IAEA 2012] para. 729 (covering [10CFR71] §71.73(c)(5) or [IAEA 2012] para. 733).

2.2.5.3 Calculation method, verification and validation

All criticality safety calculations are performed by means of the sequence CSAS6 of the criticality safety code KENO VI which are both part of the SCALE software package. Both versions SCALE 6.0 [SCALE 2009] and SCALE 6.1.1 [SCALE 2011] are used for the analyses.

The most recent libraries based on ENDB/BVII data are used for the criticality safety calculations for the DN30 package. This includes the library v7-238 being used for energy multi-group cross sections.

2.2.5.3.1 Verification

The verification consists of the installation verification and of functional verification of the used modules of the SCALE 6 / SCALE 6.1.1 program systems. The functional verification is carried out by the editor of program systems on the basis of the appropriate verification plan. For the individual user the verification of program system SCALE 6 / SCALE 6.1.1 consists of the installation verification on the basis of case studies delivered by the editor. The case studies were calculated successfully and compared with the likewise delivered reference output files. There were no differences in the output files which exceeded the range of admissible deviations mentioned in the installation guide accompanying the code package. Thus, successful installation verification is given.

2.2.5.3.2 Validation

The calculation method (code and cross-section data) used to establish criticality safety must be validated against measured data (e.g. criticality benchmark experiments) that can be applicable to the package design characteristics. The validation process provides a basis for the reliability of the calculation method and should justify that the calculated k_{eff} plus bias and uncertainties (if necessary) for the actual package conditions will ensure the compliance with the criticality safety criterion.

[NEA 2008] contains a large number of evaluated criticality safety benchmark experiments which can be used for validation purposes. The most suitable criticality safety benchmark experiments for UF₆ arrangements available in [NEA 2008] are described in LEU-COMP-THERM-033. In Appendix 2.2.5, the 52 cases associated with the benchmark experiment LEU-COMP-THERM-033, involving cases of reflected and unreflected assemblies of 2 and 3 %-enriched Uranium fluoride in paraffin, are modeled for computational verification purposes by means of both codes SCALE 6.0 and SCALE 6.1.1. The two SCALE versions are used in association with the multi-group libraries v7-238 to prove criticality safety. Their calculation abilities are validated for the actual package criticality characteristics using the same libraries.

Additional validation calculations documented in [DAHER 2019-2] investigate the trending of k_{eff} calculation results with ^{235}U enrichment and the energy of the average lethargy of fission, using more benchmark experiments with uranium fluoride compounds. The results show the applicability of the benchmark series LCT-033. A determination of the calculational bias, taking into account the bias uncertainty, results in a bias of

$$\Delta k = 0.0129$$

2.2.5.4 Model Specification

2.2.5.4.1.1 Geometrical properties

2.2.5.4.1.2 30B cylinder

Two models of the 30B cylinder are considered for the criticality safety analysis of the DN30 package:

- **A simplified 30B cylinder model:** The 30B cylinder is simplified to a cylinder with flat ends. The outer diameter is varied between 75.6 cm and 76.8 cm and the outer length is varied between 191.7 cm and 193.5 cm. The wall thickness is varied between 1.3 cm and 0.794 cm (minimum wall thickness according to [ANSI N14.1] and [ISO 7195]). The skirts, the valve, plug and nameplate are neglected. The maximal possible UF_6 volume of the model is hence between 0.791 m^3 and 0.853 m^3 .
- **Detailed 30B cylinder model:** The ends of the 30B cylinder are of a spherical shape similar to the original cylinder heads, and both skirts are taken into consideration. Maximal dimensions specified in [ANSI N14.1] and [ISO 7195] are used for the 30B cylinder; the outer diameter is 76.8 cm and the outer length 207.5 cm over the skirts and 193.5 cm over the ends. Each cylinder end is modeled as part of a spherical shell with an outer radius of 62.3 cm. The centers of the two spherical shells of both 30B cylinder ends are at a distance of 68.9 cm to each other and are located on the symmetry axis. In deviation to the dimensions given in [ANSI N14.1] and [ISO 7195] the plug end is modeled in such a way that the outer surface of the bended end is in line with the end of the skirt, i. e. moved 1.3 cm to the end of the cylinder. The valve, plug and nameplate are neglected. The wall thickness is varied between 1.3 cm and 0.794 cm (minimum wall thickness). The maximal possible UF_6 volume of the model is between 0.773 m^3 and 0.7907 m^3 .

2.2.5.4.1.3 DN30 PSP

Two models of the DN30 PSP are considered for the criticality safety analysis of the DN30 package.

- **DN30 PSP model as designed:** The PSP is composed of two concentric shells of stainless steel in the form of a cylinder enclosing the insulating foam. In radial direction from inside to outside there is 0.2 cm stainless steel, 15 cm insulation and 0.3 cm stainless steel modeled. In axial direction from inside to outside 1.0 cm stainless steel, 15 cm insulation and 0.4 cm stainless steel is modeled.
- **Damaged DN30 PSP model:** The shells of the DN30 PSP are compressed to a single shell; the thickness of the shells is kept. The insulating foam is completely neglected. This compressed shell has a thickness of 0.5 cm in radial and of 1.4 cm in axial direction.

2.2.5.4.2 Material compositions

2.2.5.4.2.1 UF₆

For the UF₆ the following compositions are considered:

- Pure UF₆ with a density between 3.1 g/cm³ and 5.5 g/cm³.
- UF₆ with a purity of 99.5 wt. % UF₆ containing 0.5 wt. % HF at a density of 5.5 g/cm³.
- UF₆ with a purity of 99.5 wt. % UF₆ with 0.5 wt.% HF and additional HUR.
- The enrichment is in all cases 5.0 wt. % U-235 in uranium. For the criticality assessment, it is considered that apart from U-235 only U-238 is present with 95 wt. %. The very small amounts of the nuclides U-232, U-234 and U-236 have no significant influence on reactivity. They are therefore neglected.

2.2.5.4.2.2 HF

For pure HF acid, the standard material “hfacid” of the SCALE library with a theoretical density of 1.15 g/cm³ is used. For UF₆ containing impurities in form of HF (homogeneously mixed), the density of UF₆ is used for the mixture.

2.2.5.4.2.3 Hydrogenated uranium residues

In Appendix 2.2.5 (Criticality Safety Analysis) the credible accumulation of hydrogenated uranium residues is evaluated. This evaluation is based on recent work to assess the composition and amount of HUR.

The creation of hydrogenated uranium residues has been investigated in [MILIN 2016], [CONNOR 2013], [BEGUE 2013] and [REZGUI 2013].

In [MILIN 2016] it is shown that the envelope composition of HUR is UO₂F₂-2H₂O-2HF with a H/U ratio of 6. The mass of HUR is assumed to be equivalent to the maximal allowable mass of heels in the 30B cylinder of 11.4 kg.

In [CONNOR 2013] and [REZGUI 2013] the composition of HUR was assumed to be UO₂F₂-5.5H₂O with a H/U ratio of 11. [CONNOR 2013] assumed a mass of 12 kg and [REZGUI 2013] a mass of 3.91 kg HUR.

[BEGUE 2013] showed the influence of the mass of HUR and the H/U ratio on reactivity.

For the proof of criticality safety for the DN30 package in this report two approaches are considered.

In a first approach based on a usage period of 5 years under the assumption that the 30B cylinder is filled each year four times, an amount of 3.9083 kg of UO₂F₂*5.5H₂O is calculated at the end of the 5 year period between recertification. This amount of HUR can be mixed homogeneously in the total amount or a small portion of the UF₆.

In a second approach it is assumed that a maximum of 11.4 kg of HUR in the form of UO₂F₂*3H₂O is present as lump in the UF₆.

2.2.5.4.2.4 Carbon steel (30B cylinder)

For the carbon steel of the 30B cylinder, the standard material “carbonsteel” of the SCALE library at a density of 7.8212 g/cm³ is used.

2.2.5.4.2.5 Stainless steel (DN30 PSP)

For stainless steel the standard material “ss304” of the SCALE library with a density of 7.94 g/cm^3 is used.

2.2.5.4.2.6 Polyisocyanurate rigid foam (DN30 PSP)

Polyisocyanurate rigid foam is used for the DN30 PSP. For the variation calculations different densities with the same composition were used. The results of the variation calculations show that maximal reactivity does not depend on the foam density, so that foam densities of less than 0.2 g/cm^3 and more than 0.375 g/cm^3 as well as any intermediate value are covered by the calculations as well. The chemical composition of the foam is given in Table 75.

Table 75: Composition of the polyisocyanurate rigid foam

Element	Weight %
H	5.41
C	68.27
N	7.42
O	18.9

2.2.5.5 Proof of criticality safety

2.2.5.5.1 Proof according to [10CFR71] §71.55(d) and §71.55(e) or [IAEA 2012], para. 682 for the single package in isolation under RCT, NCT and HAC

2.2.5.5.1.1 Performed calculations

The maximum effective neutron multiplication factor k_{eff} for the single package in isolation is determined for RCT, NCT and HAC. Variation calculations are performed to determine the most reactive arrangements. This includes:

- the variation of geometrical parameters of the 30B cylinder and the DN30 PSP such as the variation of the outer dimensions and the wall thickness of a 30B cylinder according to the tolerances specified in [ANSI N14.1] and [ISO 7195],
- the consideration or neglecting of the DN30 PSP,
- the variation of the foam density of the DN30 PSP,
- the consideration of an intact or damaged DN30 PSP for HAC (steel shells compressed together to a single layer),
- variation of the thickness of a water layer between the 30B cylinder and the DN30 PSP.

Parameters related to the fissile material are varied:

- density of the modeled UF_6 ,
- composition of the modeled UF_6 (impurities),

- different arrangements of the UF₆ like a central hole and partial fill conditions.

2.2.5.5.1.2 Results of the calculations

The results of the calculations are:

- The 30B cylinder with maximal outer dimensions and hence maximal mass of UF₆ results in maximal k_{eff} .
- The 30B cylinder with minimal wall thickness results in maximal k_{eff} .
- Reactivity increases with increasing UF₆ density. Maximal k_{eff} is reached for a theoretical density of 5.5 g/cm³ (value for -40 °C).
- Homogeneous UF₆ with 0.5 wt. % HF impurity results in maximal k_{eff} .
- A completely filled cylinder results in maximal k_{eff} .
- The bare cylinder has a higher reactivity than the DN30 package (30B cylinder in the DN30 PSP).

2.2.5.5.1.3 Proof according to [10CFR71] §71.55(d) and §71.55(e) or [IAEA 2012], para. 682 for RCT and NCT

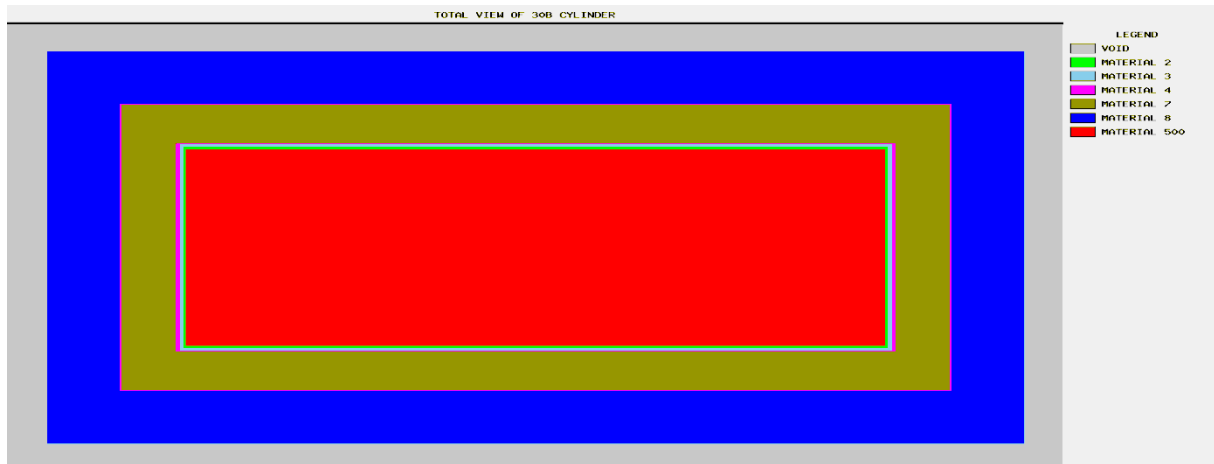
For the single package under RCT and NCT maximal reactivity is reached for the calculation model shown in Figure 141 and Figure 142:

$$k_{\text{eff}} + 3 \sigma = 0.5734$$

This value is reached by taking into account the following conservative assumptions:

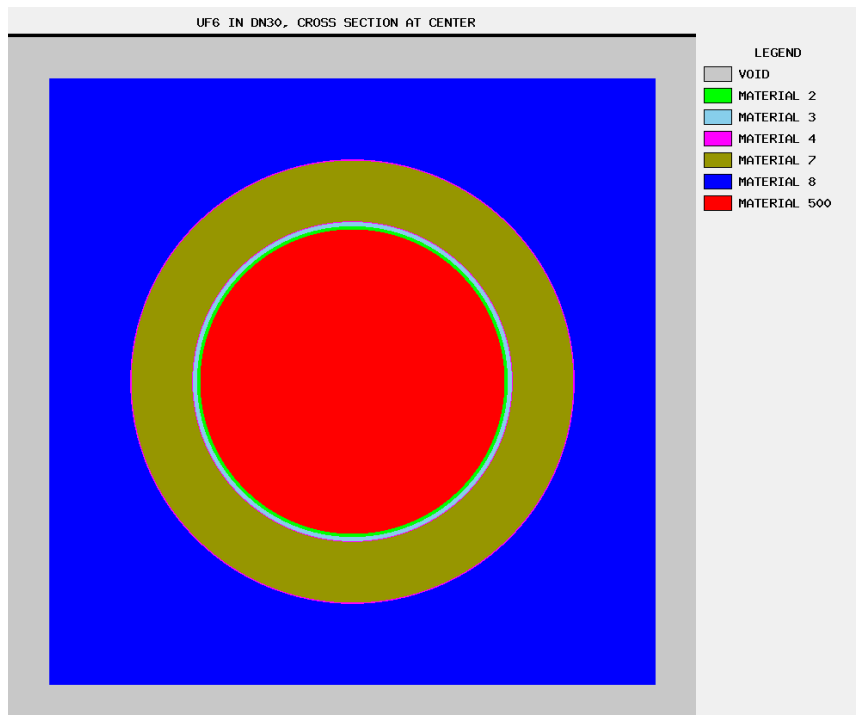
1. Minimal wall thickness of the 30B cylinder of 0.794 cm
2. Maximal UF₆ density of 5.5 g/cm³
3. Maximal cylinder dimensions
4. Completely filled cylinder
5. 0.5 wt.% impurities as HF

The criticality safety criterion is complied with.



red = UF₆, green = carbon steel, magenta = stainless steel, dark blue = water layer,
brown = foam

Figure 141: Longitudinal section of the calculation model used for RCT and NCT



red = UF₆, green = carbon steel, magenta = stainless steel, dark blue = water layer,
brown = foam)

Figure 142: Cross section of the calculation model used for RCT and NCT

2.2.5.5.1.4 Proof according to [10CFR71] §71.55(d) and §71.55(e) or [IAEA 2012], para. 682 for HAC

For the single package under HAC maximal reactivity is reached for the calculation model shown in Figure 143:

$$k_{\text{eff}} + 3 \sigma = 0.6101$$

This value is reached by taking into account following conservative assumptions:

1. Minimal wall thickness of the 30B cylinder 0.794 cm
2. Maximal UF₆ density of 5.5 g/cm³
3. Maximal cylinder dimensions
4. Completely filled cylinder
5. 0.5 wt.% impurities as HF
6. The DN30 PSP is completely neglected.

The criticality safety criterion is complied with.

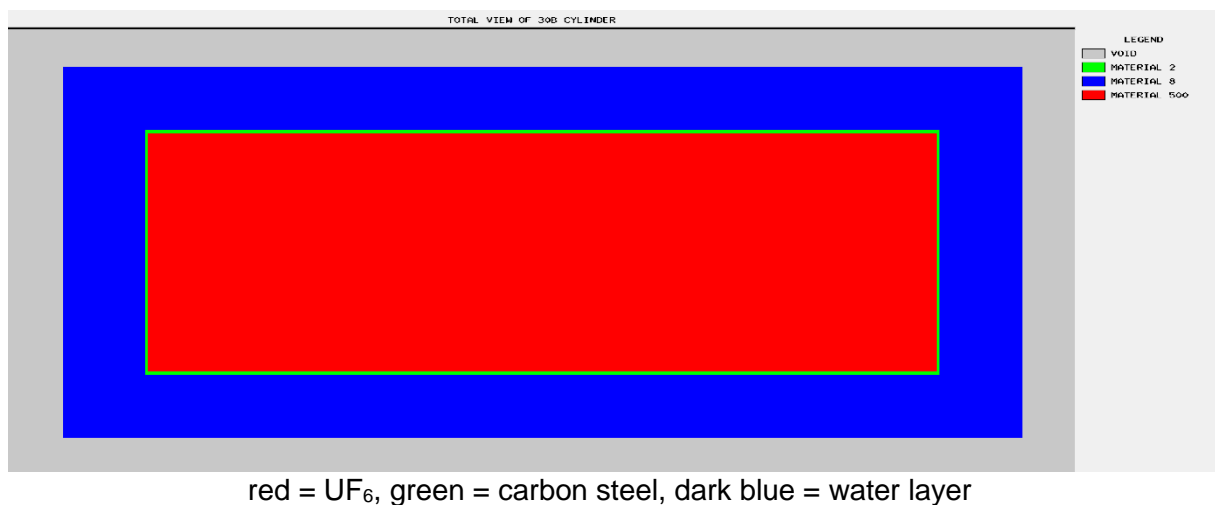


Figure 143: Longitudinal section of the calculation model used for HAC

2.2.5.5.2 Proof according to [10CFR71] §71.59(a)(1) or [IAEA 2012], para. 684 for an array of packages under NCT

The criticality safety index for the package DN30 is CSI = 0. Thus, an infinite number of packages under NCT and under HAC have to be analyzed. Calculation assumptions for the proof of the array of packages under HAC are more restrictive than assumptions for NCT. Thus, proof for the array of packages under NCT is covered by the proof in the following section 2.2.5.5.3.

2.2.5.5.3 Proof according to [10CFR71] §71.59(a)(2) or [IAEA 2012], para. 685 for an array of packages under HAC

2.2.5.5.3.1 Performed calculations

For the array of packages the condition of the packages under HAC is assumed. The conservative assumptions are:

Complete loss of the thermal insulation: Conservatively, for all calculations a complete loss of the thermal insulation (PIC foam) is assumed.

Neglect of the steel shells of the DN30 PSP: For most of the analyses the steel shells of the DN30 PSP are completely neglected and only the bare cylinder is assumed to be present. When required for the proof the influence of the steel shells on reactivity is assessed.

Compaction of the steel shells to a single layer of steel: In all cases where the steel shells of the DN30 PSP are considered a compaction of these steel shells to a single stainless steel layer is assumed. The gap between this single steel shell, the 30B cylinder and adjacent DN30 packages is varied. Hence, rather compact arrangements of packages are taken into account for the proof.

For the array of DN30 packages following variation calculations are performed

- Consideration of quadratic and hexagonal arrays.
- Variation of the gap size between adjacent cylinders for the cylinder completely filled with UF_6 for the different array models.
- Variation of the water density and the gap size between adjacent cylinders for the cylinder completely filled with UF_6 for the different array models.
- Variation of the water density in the gap and gussets between adjacent cylinders for the cylinder completely filled with UF_6 for the hexagonal array model.
- Variation of the UF_6 composition (impurities) for the hexagonal array model.
- Variation of the fill level and the size of a central void for the hexagonal array model.
- Variation of the wall thickness of the 30B cylinder for the hexagonal array model.
- Consideration of the stainless steel shells of the DN30 PSP and variation of the gap between shells and cylinder.
- Consideration of possible and realistic inhomogeneous distributions of the impurities.
 - The assumption of a grain structure consisting of UF_6 cubes surrounded by an impurity layer and the variation of the cube dimensions.
 - The assumption of a grain structure consisting of UF_6 cubes surrounded by an impurity layer, a central void in the UF_6 and variation of the dimensions of this central void.
- Consideration of possible but unrealistic inhomogeneous distributions of the impurities.
 - The assumption of a central void in the UF_6 , concentration of the impurities in a layer at the inside of the UF_6 layer and the variation of the dimensions of the central void.

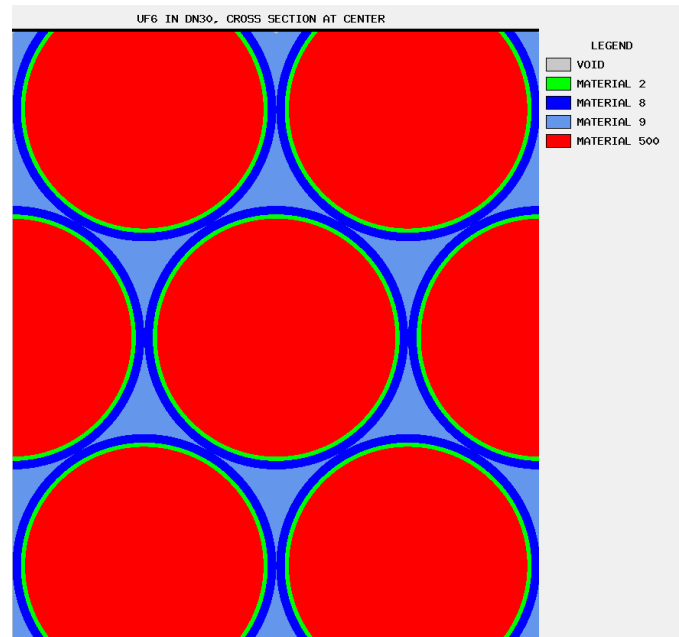
- Concentration of the impurities in an impurity sphere and the variation of its size, composition and position in the 30B cylinder.
- Consideration of hypothetical and unrealistic inhomogeneous distributions of the impurities.
 - Arrangement of the impurities concentrated in a spherical impurity shell and the variation of its size, composition and position in the 30B cylinder.
 - Arrangement of one composition of impurities in a sphere, surrounded by a shell of UF_6 and further surrounded by a spherical shell of another composition of impurities and variation of the size, composition and position of this arrangement in the 30B cylinder.

Water ingress due to the water immersion test [10CFR71] §71.73(c)(6) and §71.73(c)(5) or [IAEA 2012], para. 729, 733 is not considered as it was shown in Appendix 2.2.5 (Criticality Safety Analysis) that the amount of water to be expected to leak into the cylinder is negligible compared to the assumed amount of volatile hydrogenous material and HUR.

2.2.5.5.3.2 Results of the calculations

The general results of the calculations are:

- Hexagonal infinite arrays lead to a higher k_{eff} than quadratic arrays. Highest reactivity is reached for an infinite hexagonal array composed of hexagonal prisms, in which the package (depending on the scenario, only a 30B cylinder or a 30B cylinder accommodated in the compressed steel shells of the DN30 PSP) is surrounded by a water layer. The apothem of the hexagonal prism is equal to the outer radius of the cylinder and package plus the thickness of the surrounding water layer, respectively. Highest reactivity is reached if the gussets between hexagon and water layer are void (see Figure 144).
- Calculation models with homogeneously modeled impurities are less reactive than those with inhomogeneous concentrations of impurities.



red = UF₆, green = carbon steel, dark blue = water layer, light blue = gussets

Figure 144: Cross section of calculation model for the hexagonal array for HAC

2.2.5.5.3.3 Proof according to [10CFR71] §71.59(a)(2) or [IAEA 2012], para. 685 for an array of DN30 packages

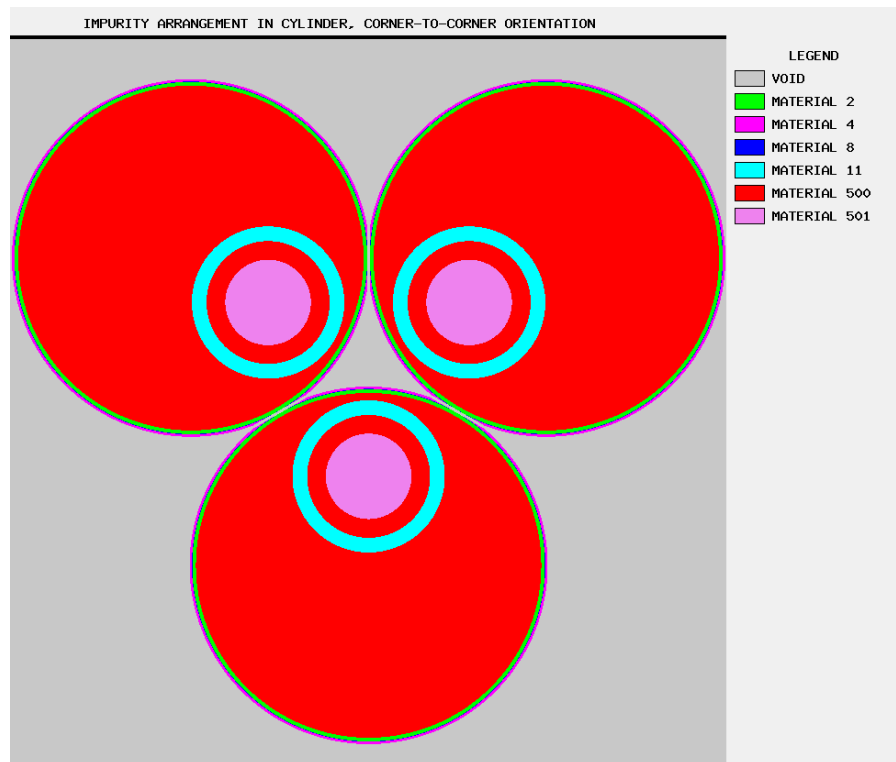
For the array of packages under HAC maximal reactivity is reached for the calculation model shown in Figure 145 and Figure 146:

$$k_{\text{eff}} + 3 \sigma = 0.9351$$

This value is reached by taking into account following conservative assumptions:

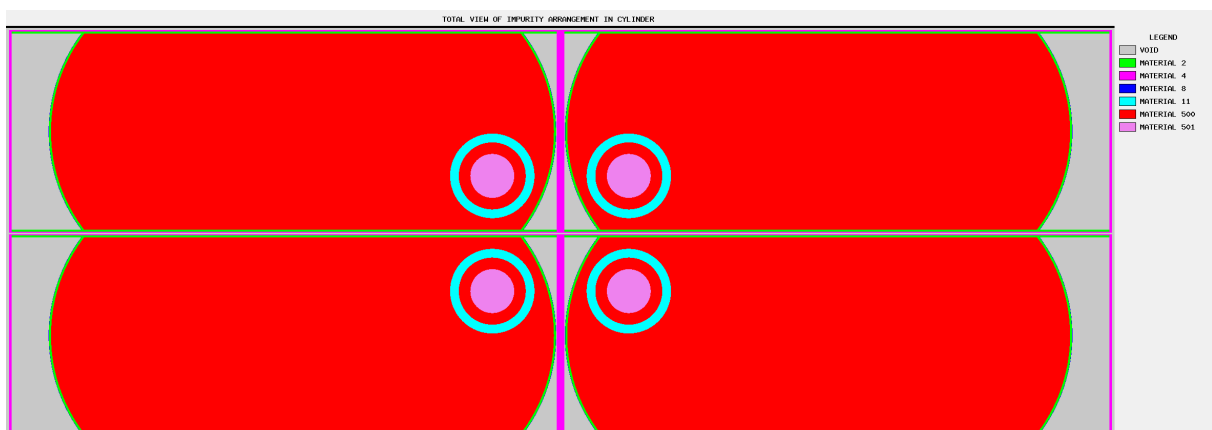
1. Minimal wall thickness of 7.94 mm
2. Maximal UF₆ density of 5.5 g/cm³
3. Maximal cylinder dimensions
4. Completely filled cylinder
5. Hypothetical impurity arrangement consisting of a central impurity sphere consisting of HUR and UF₆ surrounded by a shell of UF₆ surrounded by a shell of HF

The criticality safety criterion is complied with.



red = UF₆, pink = HUR, light blue = HF, green = carbon steel, dark blue = water layer, magenta = stainless steel

Figure 145: Cross section of the arrangement of two cylinders with impurity sphere for corner-to-corner orientation (plane through center of spherical arrangements)



red = UF₆, pink = HUR, light blue = HF, green = carbon steel, dark blue = water layer, magenta = stainless steel

Figure 146: Longitudinal section of the arrangement of two cylinders with impurity sphere for corner-to-corner orientation (plane through center of spherical arrangements)

2.2.5.5.3.4 Proof according to [10CFR71] §71.59(a)(2) or [IAEA 2012], para. 685 for an array of bare 30B cylinder

For an array of bare 30B cylinders under HAC maximal reactivity is reached for the calculation model shown in Figure 145 and Figure 146:

$$k_{eff} + 3 \sigma = 0.9493$$

This value is reached by taking into account following conservative assumptions:

1. Minimal wall thickness of 1.1 cm
2. Maximal UF_6 density of 5.5 g/cm^3
3. Maximal cylinder dimensions
4. Completely filled cylinder
5. Hypothetical impurity arrangement consisting of a central impurity sphere consisting of HUR and UF_6 surrounded by a shell of UF_6 surrounded by a shell of HF

For the infinite array of bare 30B cylinders, the criticality safety criterion is slightly exceeded, but since this result mainly has an illustrative purpose, this has no impact on the safety assessment of the DN30 package.

APPENDIX 1.1 (LIST OF APPLICABLE DOCUMENTS)

Applicable Documents, List Ref. 0023-LST-2016-001

Proprietary Information

Not to be published

APPENDIX 1.3 (RADIOACTIVITY)

Analysis of the total radioactivity of the contents specified for the packaging DN30

Proprietary Information

Not to be published

APPENDIX 1.4.1 (DRAWINGS)

Drawing Parts List No. 0023-STL-1000-000

Proprietary Information

Not to be published

APPENDIX 1.4.2 (MATERIAL DATA PIR FOAM)

Material Report, PIR Foam of company DUNA CORRADINI

Proprietary Information

Not to be published

APPENDIX 1.4.3 (MATERIAL DATA INTUMESCENT MATERIAL)

Material Report, PROMASEAL-PL® of company PROMAT

Proprietary Information

Not to be published

APPENDIX 1.4.4 (MATERIAL DATA MICROTHERM OVERSTITCHED 1000R HY)

Material Data Sheet, MICROTHERM OVERSTITCHED 1000R HY

Proprietary Information

Not to be published

APPENDIX 1.4.5 (ABSENCE OF HALOGEN IN INTUMESCENT MATERIAL)

Letter from ETEX Building Performance GmbH, 13.06.2018

Safety Data Sheet PROMASEAL®-PL, Version 1.2

Proprietary Information

Not to be published

APPENDIX 1.7.1 (HANDLING INSTRUCTION)

Use and Handling of the DN30 Package, Handling Instruction No. 0023-HA-2015-001

APPENDIX 1.7.2 (CONTAMINATION AND DOSE RATE MEASUREMENTS)

Contamination and Dose Rate Measurement at the DN30 package, Test Instruction No. 0023-PA-2015-017

Proprietary Information

Not to be published

APPENDIX 1.8.1 (PERIODICAL INSPECTIONS)

Periodical Inspections of the DN30 PSP, Test Instruction No. 0023-PA-2015-015

Inspection of DN30 PSP, 0023-PA-2015-015-Checklist DN30 CH-0596

APPENDIX 1.8.2 (INSPECTION CRITERIA)

Inspection Criteria for Regular and Periodical Inspections of the DN30 Package,
Test Instruction No. 0023-PA-2015-016

APPENDIX 1.9.1 (IMS)

- 1) Quality Management Handbook of company DAHER Nuclear Technology GmbH
- 2) DIN EN ISO 9001
- 3) Confirmation on quality assurance according to nuclear standard KTA 1401
- 4) Confirmation of the Qualification for the development, manufacturing and operation of packagings of packages requiring approval for the transport of radioactive material

Proprietary Information

Not to be published

APPENDIX 1.9.2 (MANUFACTURING SPECIFICATION)

Specification DN30 PSP, Specification No. 0023-SPZ-2016-001

Manufacturing Test Sequence Plan No. 0023-BPP-2016-001

Material Test Sheet No. 0023-WPB-2016-001

Proprietary Information

Not to be published

APPENDIX 1.9.3 (QUALITY ASSURANCE PROGRAM)

U.S. NRC Quality Assurance Program Approval #0951, Rev. 1, July 6 2018

Quality Assurance Program Description 0023-QAP-2017-001

Proprietary Information

Not to be published

APPENDIX 2.2.1.1 (DROP TEST PROGRAM)

Drop Tests Specification, No. 0023-BDI-2015-002

Proprietary Information

Not to be published

APPENDIX 2.2.1.2 (DROP TEST REPORTS)

Drop Test Report No. 3.3/11627

Proprietary Information

Not to be published

APPENDIX 2.2.1.3 (STRUCTURAL ANALYSIS OF THE DN30 PACKAGE UNDER NCT AND HAC)

Structural Analysis of the DN30 package under NCT and HAC

Proprietary Information

Not to be published

APPENDIX 2.2.2.1 (THERMAL TEST PROGRAM)

Thermal test of the DN30 Overpack, No. 0023-BDI-2014-001

Proprietary Information

Not to be published

APPENDIX 2.2.2.2 (THERMAL TEST REPORT)

Fire Test Report No. 3.2/816010

Fire Test Report No. 3.2/817026

Proprietary Information

Not to be published

APPENDIX 2.2.2.3 (THERMAL ANALYSIS)

Thermal Analysis of the DN30 Package for the Transport of Uranium Hexafluoride

Proprietary Information

Not to be published

APPENDIX 2.2.3.1 (CONTAINMENT ANALYSIS)

Containment Analysis for the DN30 Package for the Transport of Uranium Hexafluoride

Proprietary Information

Not to be published

APPENDIX 2.2.3.2 (URANIUM HEXAFLUORIDE DEWITT 1960)

Uranium Hexafluoride: A Survey of the Physico-Chemical Properties, Goodyear Atomic Corporation, Portsmouth, Ohio, GAT-280 Chemistry General, 1960

APPENDIX 2.2.4 (DOSE RATE ANALYSIS)

Dose Rate Calculations for the DN30 Package for the Transport of Uranium Hexafluoride

Proprietary Information

Not to be published

APPENDIX 2.2.5 (CRITICALITY SAFETY ANALYSIS)

Criticality Analysis of the DN30 Package for the Transport of Uranium Hexafluoride

Proprietary Information

Not to be published